ISSN 2587-6066

СИБИРСКИЙ ЖУРНАЛ НАУКИ И ТЕХНОЛОГИЙ

SIBERIAN JOURNAL OF SCIENCE AND TECHNOLOGY

Том
Vol. 20, № 1

КРАСНОЯРСК 2019

СИБИРСКИЙ ЖУРНАЛ НАУКИ И ТЕХНОЛОГИЙ

Том 20, № 1

Красноярск 2019

СИБИРСКИЙ ЖУРНАЛ НАУКИ И ТЕХНОЛОГИЙ

Том 20, № 1

SIBERIAN JOURNAL OF SCIENCE AND TECHNOLOGY

Vol. 20, No 1

К СВЕДЕНИЮ ЧИТАТЕЛЕЙ

«Сибирский журнал науки и технологий» является научным, производственно-практическим рецензируемым изданием. Свидетельство о регистрации средства массовой информации ПИ № ФС 77-70577 от 03.08.2017 г. выдано Федеральной службой по надзору в сфере связи, информационных технологий и массовых коммуникаций (Роскомнадзор).

ISSN 2587-6066.

Подписной индекс в каталоге «Пресса России» – 39263.

Зарегистрирован в Российском индексе научного цитирования (РИНЦ).

Включен в базу данных Ulrich's Periodicals Directory американского издательства Bowker.

Входит в перечень журналов ВАК по следующим группам научных специальностей:

05.02.00 – машиностроение и машиноведение;
05.07.00 – авиационная и ракетно-космическая техника;
05.13.00 – информатика, вычислительная техника и управление.

Выпускается с 2000 года. До 2002 года журнал носил название «Вестник Сибирской аэрокосмической академии имени академика М. Ф. Решетнева» («Вестник САА»), до мая 2017 года – «Вестник Сибирского государственного аэрокосмического университета имени академика М. Ф. Решетнева».

Каждый выпуск журнала включает три раздела:

1 раздел. Информатика, вычислительная техника и управление.
2 раздел. Авиационная и ракетно-космическая техника.
3 раздел. Технологические процессы и материалы.

Статьи публикуются бесплатно после обязательного рецензирования и при оформлении их в соответствии с требованиями редакции (www.vestnik.sibsau.ru). Журнал выходит 4 раза в год.

Электронная версия журнала представлена на сайте Научной электронной библиотеки (http://www.elibrary.ru) и сайте журнала (www.vestnik.sibsau.ru)

Учредитель и издатель

ФГБОУ ВО «Сибирский государственный университет науки и технологий имени академика М. Ф. Решетнева» (СибГУ им. М. Ф. Решетнева)

АДРЕС РЕДАКЦИИ, УЧРЕДИТЕЛЯ И ИЗДАТЕЛЯ:
Сибирский государственный университет науки и технологий имени академика М. Ф. Решетнева,
Российская Федерация, 660037, г. Красноярск,
проспект имени газеты «Красноярский рабочий», 31,
П-416. Тел./ факс (391)291-90-19
E-mail: vestnik@sibsau.ru

INFORMATION FOR AUTHORS AND SUBSCRIBERS

Siberian Journal of Science and Technology is a research, production and practical peer-reviewed journal. Included by the Higher Attestation Commission of the Russian Federation in the Index of Leading Russian Peer-Reviewed Journals and Periodicals, in which significant scientific dissertation results should be published when applying for a Dr.Sc. degree.
The journal is the official periodical of Reshetnev Siberian State University of Science and Technology.

Certificate of Registration as a Mass Media Resource. Certificate: PI No. FC 77-50577, dated 03 August 2017, given by Federal Supervision Agency for Information Technology, Communications and Mass Media.

The Journal is included in the following subscription catalogue 39263 – Pressa Rossii.

The journal is registered in the Russian Science Citation Index (RSCI).
The journal is indexed in the database of Ulrich's Periodicals Directory.

The journal was first published in 2000. Prior to 2002 it had the title *Vestnik Sibirskoi aerokosmicheskoi akademii imeni academika M. F. Reshetneva (Vestnik SAA)*, prior to may 2017 it had the title *Vestnik Sibirskogo gosudarstvennogo aerokosmicheskogo universiteta imeni akademika M. F. Reshetneva (Vestnik SibGAU)*.

The Journal is recommended for publishing the main results of research when applying for Cand. Sc. degree and Dr. Sc. degree upon the following specialties:

05.02.00 – machine engineering and science of mechanics;
05.07.00 – aviation and spacecraft engineering;
05.13.00 – informatics, computer technology and management.

Each issue consists of three parts:

Part 1. Informatics, computer technology and management.
Part 2. Aviation and Spacecraft Engineering.
Part 3. Technological Processes and Material Science.

Papers prepared in accordance with the editorial guidelines (www.vestnik.sibsau.ru) are published free of charge after being peer reviewed.

The journal is published four times a year.

An online version can been viewed at http://www.elibrary.ru

Siberian Journal of Science and Technology should be cited when reprinting or citing materials from the journal.

CONTACTS. Website: www.vestnik.sibsau.ru
Address: Reshetnev Siberian State University of Science and Technology.
31, Krasnoyarsky Rabochy Av., Krasnoyarsk, 660037, Russian Federation.
Tel./ fax (391)291-90-19; e-mail: vestnik@sibsau.ru

Редактор Н. Н. Голоскокова
Ответственный редактор английского текста М. В. Савельева
Оригинал-макет и верстка М. А. Светлаковой
Подписано в печать 25.03.2019. Формат 70×108/16.
Бумага офсетная. Печать плоская. Усл. печ. л. 14,7.
Уч.-изд. л. 19,6. Тираж 1000 экз. Заказ 2827. С 103/19.
Редакционно-издательский отдел СибГУ им. М.Ф. Решетнева.
Отпечатано в редакционно-издательском центре СибГУ им. М. Ф. Решетнева.
Российская Федерация, 660037, г. Красноярск, просп. им. газ. «Красноярский рабочий», 31.
Дата выхода в свет: 22.04.2019. Свободная цена

Editor N. N. Goloskokova
Executive editor (*English Language*) M. V. Savelyeva
Layout original M. A. Svetlakova
Signed (for printing): 25.03.2019. Format 70×108/16.
Offset Paper. Print flat. 14.7. Published sheets 19.6.
1000 copies. Order 2827. C 103/19.
Printing and Publication Department Reshetnev University.
Printed in the Department of copying and duplicating equipment Reshetnev University.
31, Krasnoyarsky Rabochy Av., Krasnoyarsk, 660037, Russian Federation.
Date of publication: 22.04.2019. Free price

CONTENTS

СОДЕРЖАНИЕ

РАЗДЕЛ 1. ИНФОРМАТИКА, ВЫЧИСЛИТЕЛЬНАЯ ТЕХНИКА И УПРАВЛЕНИЕ

РАЗДЕЛ 2. АВИАЦИОННАЯ И РАКЕТНО-КОСМИЧЕСКАЯ ТЕХНИКА

РАЗДЕЛ 3. ТЕХНОЛОГИЧЕСКИЕ ПРОЦЕССЫ И МАТЕРИАЛЫ

Раздел
Part
1

ИНФОРМАТИКА, ВЫЧИСЛИТЕЛЬНАЯ ТЕХНИКА И УПРАВЛЕНИЕ

INFORMATICS, COMPUTER TECHNOLOGY AND MANAGEMENT

UDC 53.08, 53.06, 528.8
Doi: 10.31772/2587-6066-2019-20-1-8-19

For citation: Makarov D. S., Kharlamov D. V., Sorokin A. V. [Using signals of navigation satellites in the monitoring of the earth covers]. *Siberian Journal of Science and Technology.* 2019, Vol. 20, No. 1, P. 8–19. Doi: 10.31772/2587-6066-2019-20-1-8-19

Для цитирования: Макаров Д. С., Сорокин А. В., Харламов Д. В. Использование сигналов навигационных спутников в мониторинге земных покровов // Сибирский журнал науки и технологий. 2019. Т. 20, № 1. С. 8–19. Doi: 10.31772/2587-6066-2019-20-1-8-19

USING SIGNALS OF NAVIGATION SATELLITES IN THE MONITORING OF THE EARTH COVERS

D. S. Makarov[1*], D. V. Kharlamov[1], A. V. Sorokin[1,2]

[1]Federal Research Center "Krasnoyarsk Scientific Center of the SB RAS"
50, Akademgorodok, Krasnoyarsk, 660036, Russian Federation
[2]Reshetnev Siberian State University of Science and Technology
31, Krasnoyarsky Rabochy Av., Krasnoyarsk, 660037, Russian Federation
[*]E-mail: ikivt@yandex.ru

The features and capabilities of remote sensing of earth covers by means of signals of navigation satellites are presented. The methods of reflectometry of the surfaces of earth covers and radioscopy of forest canopy are described. The options for using the signals of GLONASS, GPS systems are considered. Test measurements of interference diagrams were carried out on 5 test platforms from heterogeneous soil surfaces: salt marshes and asphalt; water surfaces of saline and freshwater bodies in summer, including ice cover of small thickness in the period of autumn freeze-up. The method of radioscopy helped obtain the data on the spatial and temporal characteristics of attenuated signals of the GLONASS and GPS satellites in the pine forest. Estimates of the linear attenuation coefficients of the signals passing through a forest canopy with a coordinate reference were made. The results obtained are the basis for the development of methods and technologies for continuous monitoring of the characteristics and state of earth covers by means of signals of navigation satellites for solving a wide range of applied tasks.

Keywords: signals of navigation satellites, attenuation and reflection, remote sensing of the Earth, earth covers.

ИСПОЛЬЗОВАНИЕ СИГНАЛОВ НАВИГАЦИОННЫХ СПУТНИКОВ В МОНИТОРИНГЕ ЗЕМНЫХ ПОКРОВОВ

Д. С. Макаров[1], Д. В. Харламов[1], А. В. Сорокин[1, 2]

[1]Федеральный исследовательский центр «Красноярский научный центр СО РАН»
Российская Федерация, 660036, г. Красноярск, Академгородок, 50
[2]Сибирский государственный университет науки и технологий имени академика М. Ф. Решетнева
Российская Федерация, 660037, г. Красноярск, просп. им. газ. «Красноярский рабочий», 31
[*]E-mail: ikivt@yandex.ru

Представлены особенности и возможности дистанционного зондирования земных покровов с помощью сигналов навигационных спутников. Описаны методы рефлектометрии поверхностей земных покровов и радиопросвечивания лесного полога. Рассмотрены варианты использования сигналов систем ГЛОНАСС, GPS. Проведены тестовые измерения интерференционных диаграмм на 5 тестовых площадках от гетерогенных почвенных поверхностей: солончаки и асфальт, водные поверхности соленых и пресных водоемов в летний период, включая ледовое покрытие малой толщины в период осеннего ледостава. Методом радиопросвечивания получены данные о пространственно-временных характеристиках ослабленных сигналов спутников ГЛОНАСС и GPS в сосновом лесу. Сделаны оценки значений коэффициентов погонного ослабления проходящих через лесной полог сигналов с координатной привязкой. Полученные результаты являются основой развития методов и технологий непрерывного мониторинга характеристик и состояния земных покровов с использованием сигналов навигационных спутников для решения широкого спектра прикладных задач.

Ключевые слова: сигналы навигационных спутников, ослабление и отражение, дистанционное зондирование Земли, земные покровы.

Introduction. Signals of the global navigation satellite systems (GNSS) are hi-tech and allow in a continuous wave mode to recover electrophysical parameters of environments which they interact with during propagation, along with coordinate measurements, almost in a real time. The GNSS have a significant resource for monitoring earth covers – the coherent and polarized pulse radio signals of multifrequencies passing the near-earth space of the ionosphere and atmosphere reflected and scattered by the surface of earth covers. The radiometry of changes of the signal characteristics transformed by environments allows recovering these environments' electrophysical characteristics significant for practice. They are coefficients of reflection from the boundary line of earth surfaces, phase delays and transmission coefficients of volume environments – ionosphere, atmosphere, vegetation, snow and ice covers [1–3].

Actually navigation satellite systems allow implementing the global radiometer at operating frequencies of the functioning and completely deployed GPS and GLONASS groupings. The periods of revolution of the GLONASS and GPS satellites make up to 11 h 16 min. and 11 h 57 min. accordingly. The receiving equipment registers about 10 scanning series of the signals transformed by the studied object within one hour. The frequency of registered changes of the parameters is 1 Hz [4]. The recovery of temporary changes of environment characteristics of earth covers is theoretically possible in time intervals with discreteness of 1 second. Space localization of these changes is limited by the accuracy of coordinate measurements of the functioning navigation systems.

The specifics of interaction of GNSS signals with the objects of sounding is defined by the parameters of probing radiation and electrophysical characteristics of earth covers. This fact requires the development of both special receivers and methods of processing of experimental data, and models of interaction of a pulse coherent radio emission with various environments of earth covers.

GNSS – reflectometry. The method works as a bistatic radar device: a system where a transmitter and a receiver are spaced-apart by a considerable distance. This definition can be expanded to a system where one receiver can monitor simultaneously the diversity of bistatically scattered signals from a set of different transmitting sources. The scheme of formation of an interferential signal is presented in fig. 1. The signals registered by the receiver from different devices with angular data of lateral angle φ and elevation angle above the horizon θ create an interferential field in the receiving point:

$$E^2 = E_0^2\left[1 + r^2 + 2r\cos\left(\frac{4\pi h \sin\theta}{\lambda}\right)\right], \qquad (1)$$

where h is the height of the antenna; θ is an arrival angle of the electromagnetic wave coming from the navigation satellite; r is a reflection coefficient (for linear and circular polarization).

The interferential field in the receiving point is created by forward signals from the navigation satellite transmitter and reflected from soil, water and snow-and-ice surfaces.

The information on a variation of characteristics of GNSS forward signals on the channel of the transmitter and receiver in an empty space, depending on the time, angle of altitude and azimuth is necessary for processing the primary data about scattered and reflected signals by the earth surface. The changes in the state of GNSS signals polarization and amplitude which occur during the interaction with environments surface and volume as well as considering the variations of forward signals characteristics allow to recover correctly effective values of a number of parameters, significant for monitoring. They are reflection coefficients of earth surfaces to determine the thickness and terrain of snow and ice covers, humidity of soil and grassland vegetation [2; 5–12].

Test measurements and platforms. A series of test measurements of the interferential diagrams (IDs) is carried out for earth covers: soils, saline and freshwater bodies, ice. There is a platform ("an antenna field") on the territory of the hospital of Krasnoyarsk Scientific Center (KSC) where the surface of the soil is with small variations of a terrain and sites with essential distinctions in composition and reflective characteristics of navigation satellites signals within the range of L1, fig. 2.

The scene of carrying out the measurements is presented in fig. 2, *a*. The use of GLONASS satellites demonstrated on the polar diagram of fig. 2, *b* would allow receiving IDs of the area of effective scanning with various sites: the soil with grassland vegetation, the soil covered with asphalt and the compacted motor road ground.

The test registration of IDs was carried out on this platform for the purpose of identification of selective opportunities of the GNSS-scatterometry method in diagnostics of characteristics of surface soil and vegetation state. The receiving dipolar antenna focused vertically was located at a distance of 6 meters from the asphalt platform and a traffic-compacted motor road. The elevation of the antenna phase center was 4.2 m. The coordinates of the receiving antenna were 54°29'36.1" N, 90°08'29.8" E, the absolute altitude (the Baltic Sea level altitude) was 398 m. The registration was carried out by MRK-32 receiver. The session duration was 2 h. 23 min. Moderate rain was registered within 20 minutes at the closing stage.

The IDs, created by GLONASS navigation satellites 9, 10 and 11 are presented in fig. 3. These IDs contain the characteristic sites connected with reflection from the horizontal asphalt platform, the traffic-compacted road and a natural soil with grassland vegetation. The rehabilitation of the soil humidity and its characteristics are possible on the basis of specialized dielectric models.

Amplitude characteristics are registered on IDs with a frequency of 1 Hz and are followed by the record of angular coordinates of the navigation satellite. These data allow determining coordinates of the platform which reflects a signal and local reflective characteristics of the soil surface. The values of reflection coefficients are connected with granulometric and mineral composition of the soil, humidity and existence of vegetation.

There was held a registration session of IDs of salt Lake Shira surface and waterside soil. The antenna was located on the shore in the vicinity of the water surface. The lakeshore has a flat terrain with a grade of about 10°,

with rare grassland and shrub vegetation. The soil type is saline. The registration scene of IDs and the polar diagram of satellites trajectories of sequential scanning of water and soil surface are presented in fig. 4.

The dipolar antenna focused vertically was used. It was located at the distance of 3.2 meters from the border of the water surface. The elevation of the antenna phase center was 4.5 m from water level. The coordinates of the receiving antenna were 54°30'22.9" N, 90°08'55.9" E, the absolute altitude was 338 m. The registration was carried out by MRK-32 receiver. The session duration was 3 h. 10 min. Fig. 5 presents IDs containing characteristic sites connected with the reflection from the surface of water and waterside soil.

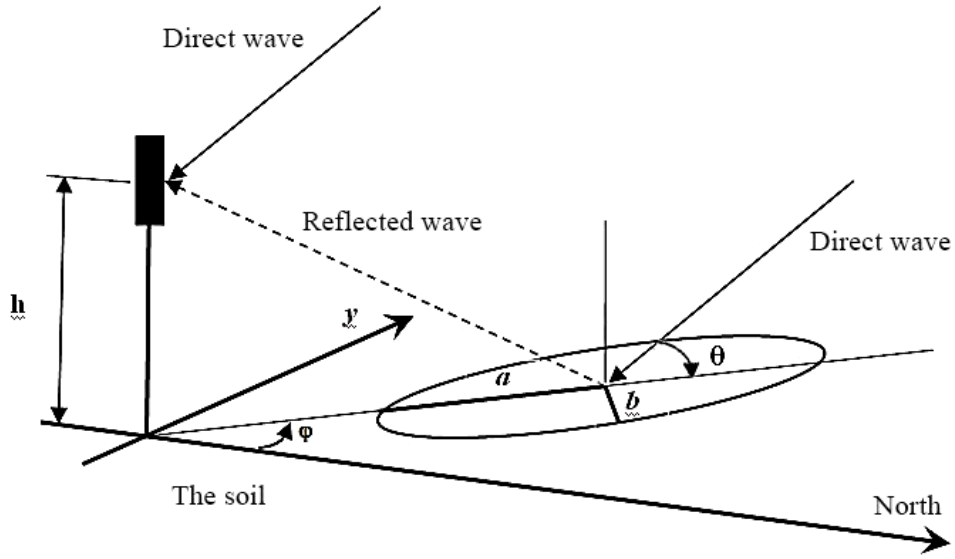

Fig. 1. The scheme of formation of the interferential signal at the receiving antenna

Рис. 1. Схема формирования интерференционного сигнала на приемной антенне

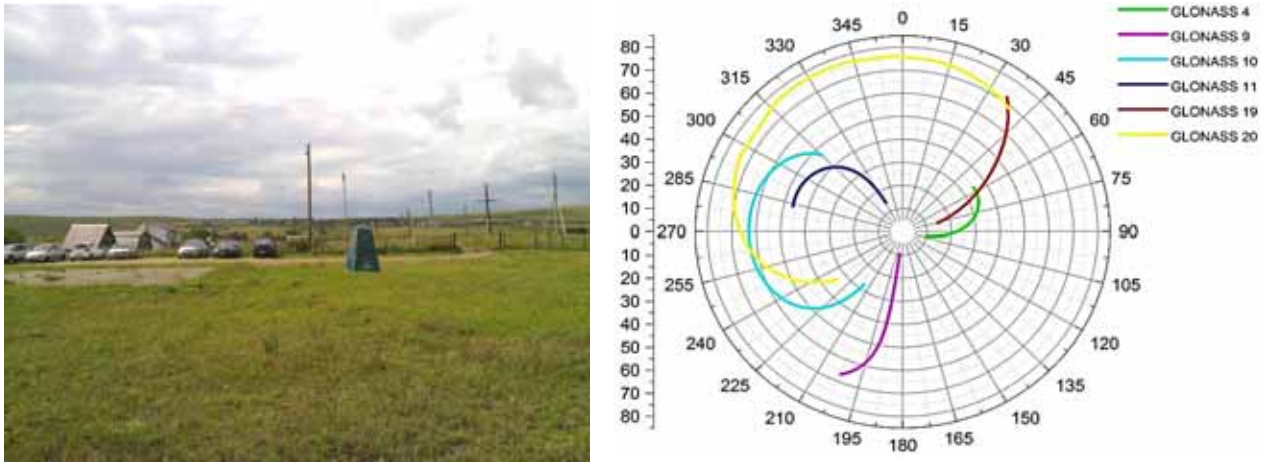

a *b*

Fig. 2. Experimental platform of "antenna field":
a – is an Interferential diagrams (ID) measuring scene on the test platform of the soil of the KSC hospital; *b* – is a polar diagram of the angular coordinates of effective scanning satellites of the "antenna field" test platform

Рис. 2. Экспериментальная площадка «антенное поле»:
а – сцена измерений интерференционной диаграммы (ИД) на тестовой площадке почвы стационара ФИЦ КНЦ; *б* – полярная диаграмма угловых координат спутников эффективного сканирования тестовой площадки «антенное поле»

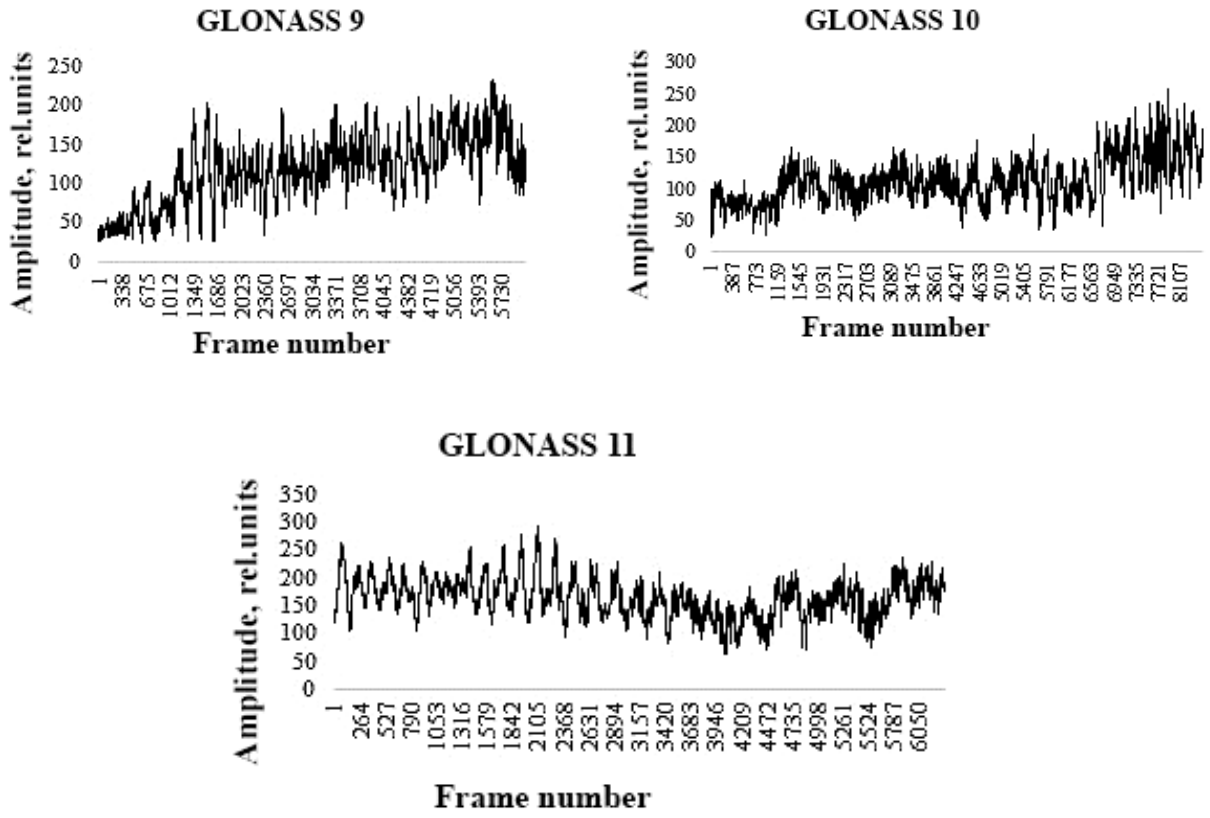

Fig. 3. ID of the test soil platform, soil sites:
GLONASS 9 – mostly horizontal asphalt platform; GLONASS 10 – mostly grassy soil with a rough terrain;
GLONASS 11 – equivalent parts of the road and soil with a rough terrain

Рис. 3. ИД тестовой площадки почвы, участки почвы:
ГЛОНАСС 9 – преимущественно горизонтальная асфальтовая площадка; ГЛОНАСС 10 – преимущественно травянистая почва с шероховатым рельефом; ГЛОНАСС 11 – эквивалентные части дороги и почвы с шероховатым рельефом

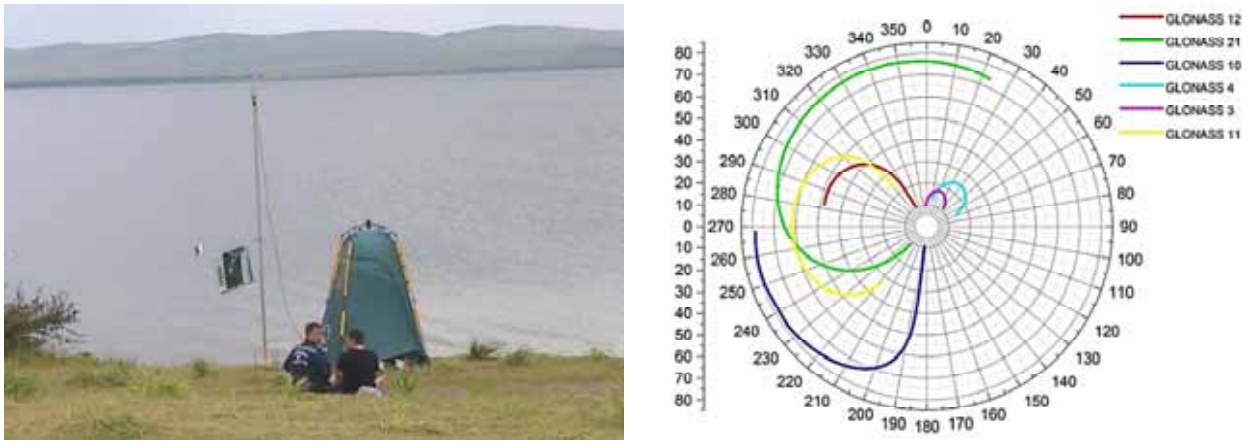

a *b*

Fig. 4. Test platform “Lake Shira”:
a – is a registration scene of IDs on the shore of salt Lake Shira; *b* – is a polar diagram of the angular coordinates of GLONASS satellites of the test platform of “Lake Shira”

Рис. 4. Тестовая площадка «оз. Шира»:
а – сцена регистрации ИД на берегу соленого озера Шира; *б* – полярная диаграмма угловых координат спутников ГЛОНАСС тестовой площадки «оз. Шира»

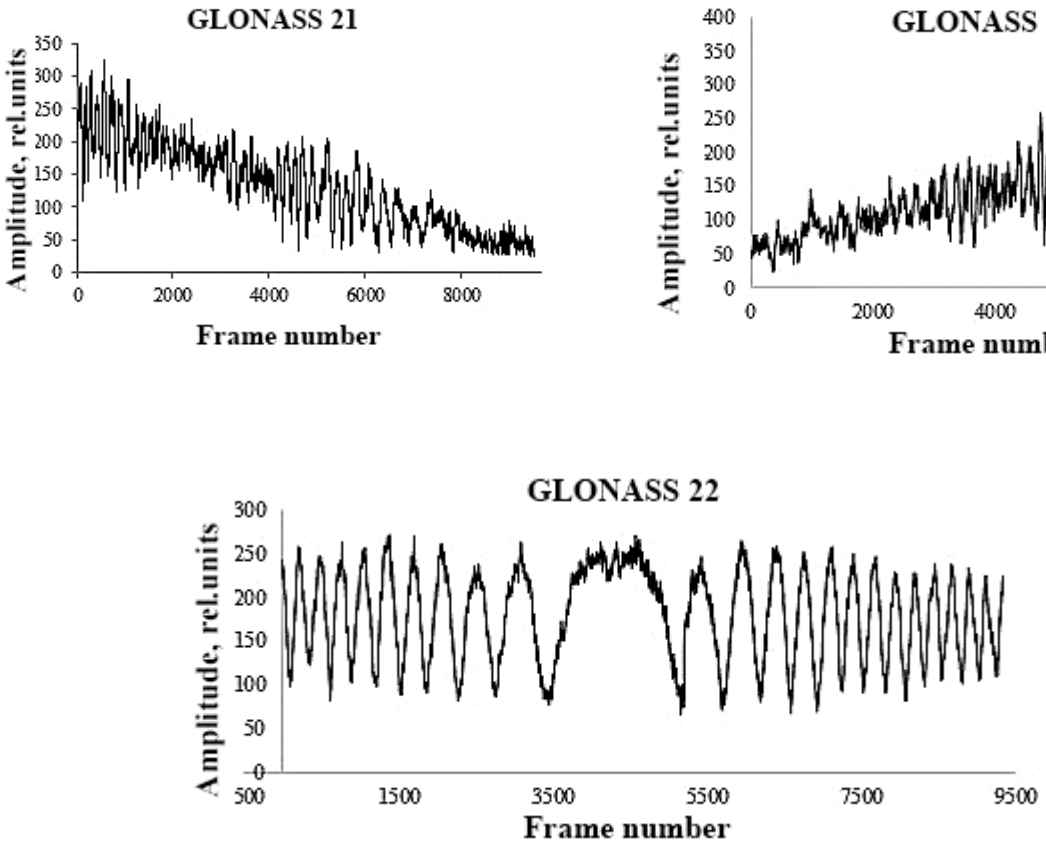

Fig. 5. IDs of the test platform:
GLONASS 21 – water site and shore; GLONASS 22 – mainly water surface;
GLONASS 10 – soil with a rough terrain and reasonable gradient

Рис. 5. ИД тестовой площадки:
ГЛОНАСС 21 – участок воды и берег; ГЛОНАСС 22 – преимущественно водная поверхность;
ГЛОНАСС 10 – почва с шероховатым рельефом и умеренным уклоном

The nature of spatiotemporal dependence of IDs is caused by significant difference of reflection coefficients and the terrain of the surficial reflecting water and soil layer.

The registration session of a surface of a fresh lake in the vicinity of Krasnoyarsk was held. The dipolar antenna focused vertically was located at the distance of 7 meters from the border of the water surface. The elevation of the antenna phase center was 4.4 m from water level. The coordinates of the receiving antenna were 56°03'49.9" N, 92°43'46.0" E, the absolute altitude was 170 m. The registration was carried out by MRK-32 receiver. The session duration was 3 h. 13 min. The registration scene of IDs and the polar diagram of satellites trajectories of sequential scanning of water and soil surface are presented in fig. 6, 7.

The nature of spatiotemporal dependence of IDs is caused by significant difference of reflection coefficients and the terrain of the surficial reflecting water and soil layer. Unlike the registration session on Lake Shira, the waterside of the fresh lake had flatter terrain and a layer of grassland and shrub vegetation.

There was held a registration session of an ice surface on the fresh lake in the vicinity of Krasnoyarsk with ice 4 cm thick. The registration scene and the polar diagram of angular coordinates of navigation satellites with the trajectories of effective scanning are presented in fig. 8.

The dipolar antenna focused vertically was located at the distance of 9 meters from the border of the water surface. The elevation of the antenna phase center was 4.4 m from water level. The coordinates of the receiving antenna were 56°03'50.0" N, 92°43'45.9" E, the absolute altitude was 170 m. The registration was carried out by MRK-32 receiver. The session duration was 2 h. 55 min.

Real part of complex dielectric capacity of fresh water at frequencies of 1–2 GHz and temperatures near zero is about 80, the one of ice is about 3. The presence of an ice layer essentially reduces the reflection coefficient of navigation satellites radio signals from the border of air-ice and additionally results in the interferential effect of a multilayer structure of the borders of air-ice and ice-water [12]. The IDs, created by GLONASS navigation satellites 18, 24 and GPS navigation satellite 21 are presented in fig. 9.

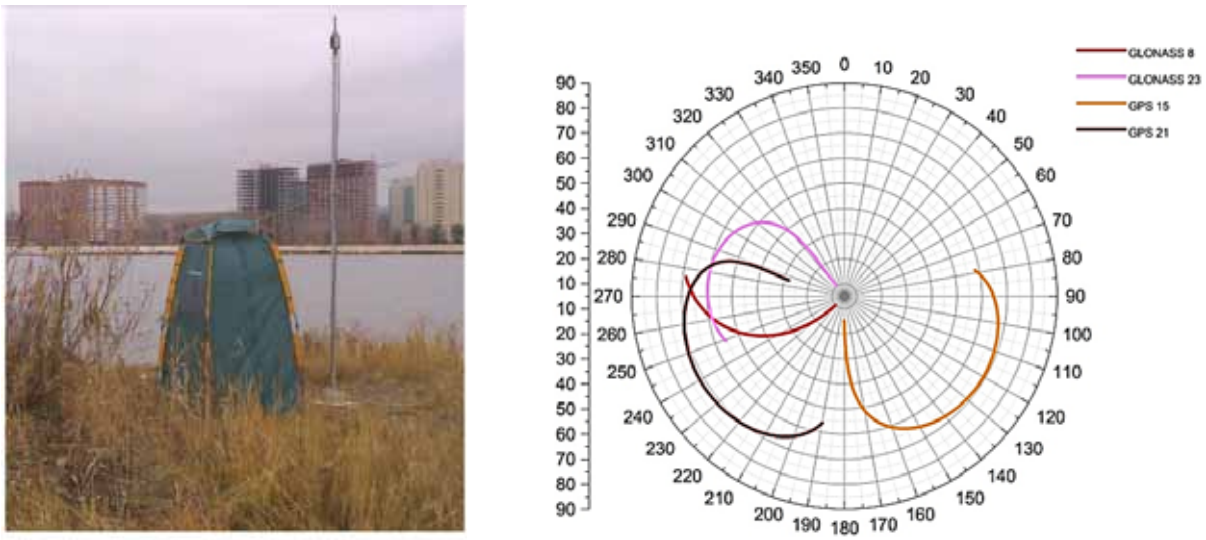

a *b*

Fig. 6. Sequential scanning of water and soil surfaces:
a – is the registration scene of IDs on the shore of a freshwater lake in the vicinity of Krasnoyarsk;
b – is a polar diagram of the angular coordinates of GLONASS satellites of the test platform on the shore of a freshwater lake in the vicinity of Krasnoyarsk

Рис. 6. Последовательное сканирование водной и почвенной поверхностей:
а – сцена регистрации ИД на берегу пресного озера в окрестности г. Красноярска; *б* – полярная диаграмма угловых координат спутников ГЛОНАСС тестовой площадки на берегу пресного озера в окрестности г. Красноярска

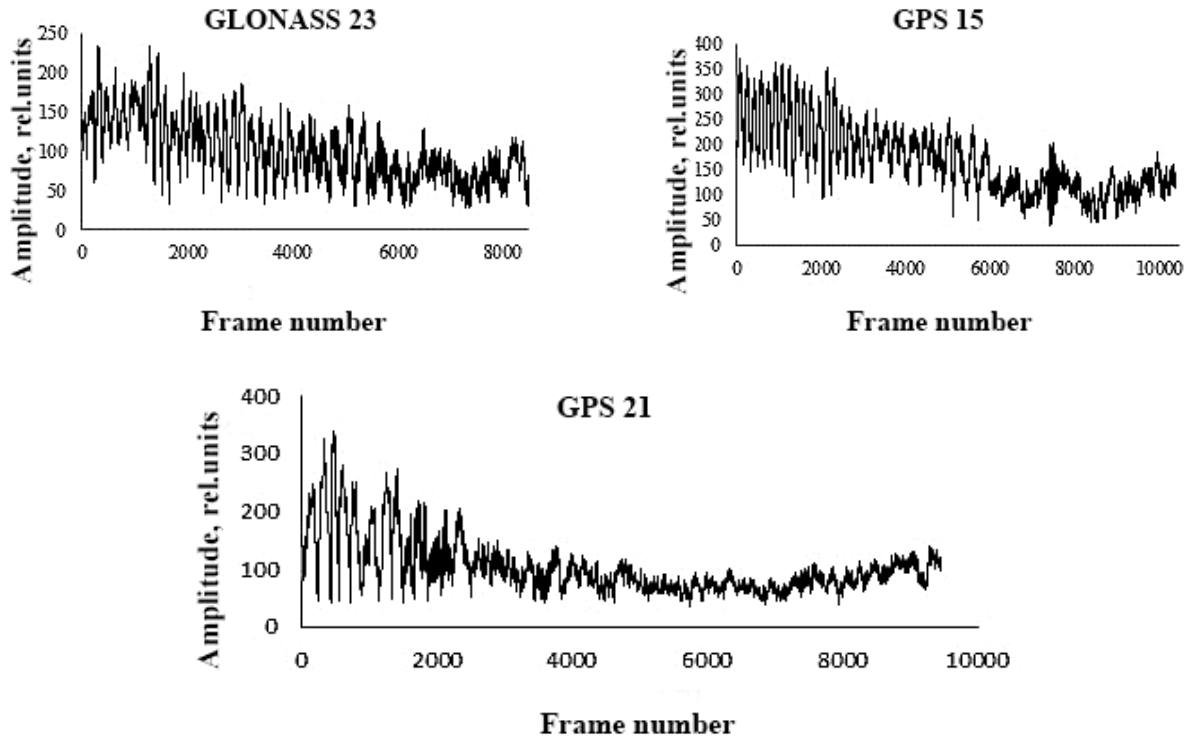

Fig.7. IDs of the test platform:
GLONASS 23 – shore site with natural soil; GPS 15 – mainly water surface; GPS 21 – shore and water surface

Рис. 7. ИД тестовой площадки:
ГЛОНАСС 23 – участок берега с естественной почвой; GPS 15 – преимущественно водная поверхность; GPS 21 – берег и водная поверхность

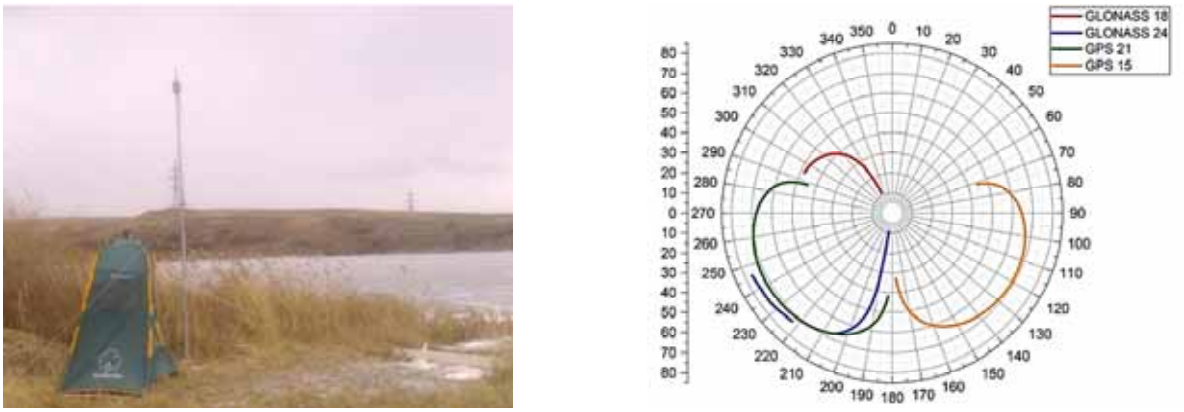

a *b*

Fig. 8. Sequential scanning of ice and soil surfaces:
a – is a registration scene of the IDs on the shore of the freshwater lake with ice cover; *b* – is a polar diagram of the angular coordinates of GLONASS and GPS satellites of the test platform on the shore of freshwater lake with ice cover

Рис. 8. Последовательное сканирование ледовой и почвенной поверхностей:
а – сцена регистрации ИД на берегу пресного озера с ледовым покрытием; *б* – полярная диаграмма угловых координат спутников ГЛОНАСС и GPS тестовой площадки на берегу пресного озера с ледовым покрытием

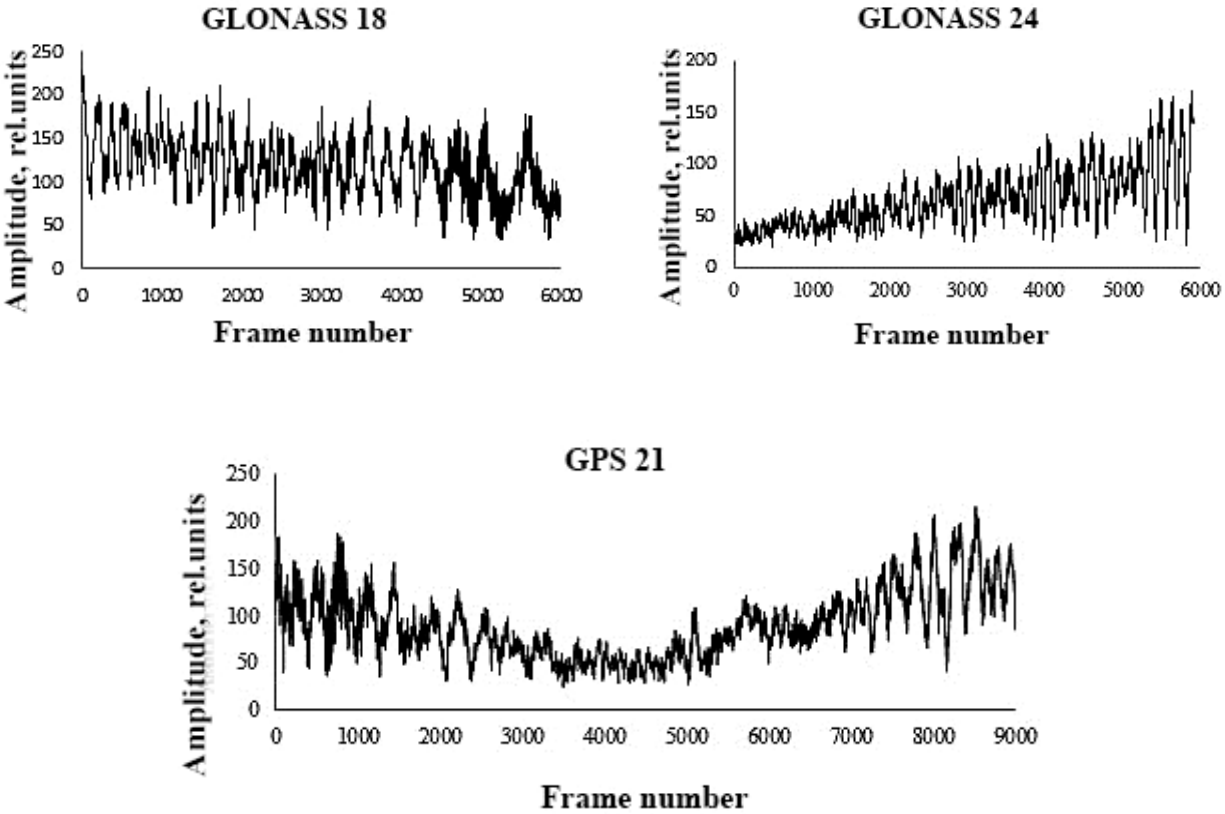

Fig. 9. IDs of the test platform:
GLONASS 18 – the shore site covered with snow; GLONASS 24 – mainly ice;
GPS 21 – the site of ice and shore covered with snow

Рис. 9. ИД тестовой площадки:
ГЛОНАСС 18 – участок берега, покрытый снегом; ГЛОНАСС 24 – преимущественно лёд;
GPS 21 – участок льда и берега, покрытого снегом

Interferential effects of a multilayer structure of water-ice are shown the most contrasting in the experimental data given above. The boundary lines of water-ice and ice-air are geometrically almost ideal, dielectric capacity of both environments are known. Direct measurements of thickness of an ice cover are available. There is a real perspective for development of an operational method and tool for remote measurement of thickness of an ice cover and its uniformity during the period from a freeze-up till spring destruction.

Radioscopy of the forest. There are many factors influencing radiowave propagation in a forest cover, they are caused by structural features of a forest crop and separate trees, a variety and seasonal changes of their electrophysical characteristics depending on the frequency range of radio waves [13–18]. The main reasons of characteristics changes of an electromagnetic field of GNSS signals in a reception point are:

1. Processes of attenuation due to losses of energy in stems, branches, needles and leaves;

2. Processes of diffraction on structure elements of trees that results in fluctuations of a radio signal amplitude and phase, change of its spectrum during wind loads on trees;

3. The resultant electromagnetic field in a reception point that represents an interferential field which constituents are:

– field components disseminated after diffraction;

– arising additional (for example, orthogonal) components of an electromagnetic field resulting in cross-polarization of the received signal;

– field reflection from the geological substrate of the forest resulting in additional fluctuations of a radio signal;

– change of forest density with seasonal changes resulting in change of a specific attenuation coefficient;

– change of forest humidity with the change of weather conditions;

– change of position of tree elements depending on a wind load resulting in field fluctuations;

Forests in terms of distribution and reflection of radio waves are heterogeneous environments which have electrodynamic parameters depending on the factors given above.

Currently, there is no uniform classification of forests. Different countries of the world classify forests by different characteristics.

There are some variants of the forests classification by geographic location (southeast, northwest forests), climate (tropical, subtropical, continental), type of prevailing vegetation (coniferous, broad-leaved, mixed), land configuration. Other forest classifications use the combination of morphological and seasonal characteristics (e.g. the evergreen coniferous or broad-leaved deciduous forests).

Depending on growth conditions (in open terrain or in forests), trees have the following features:

– trees, growing in open terrain, have branches practically all over the trunk, forming their crowns extended along the whole trunk height, with a different-scale set of structural elements: trunks, branches, needles, leaves;

– trees growing in forests, as a rule, have vertical direct trunks, their crowns have fewer branches which are placed closer to the top, in comparison with trees growing in open terrain [13].

Electrophysical characteristics of forests have a significant variable parameter – humidity. The amount of water in the wood of a growing tree varies from 30 to 100 % and is the indicator of a tree physiological state. A significant amount of atmospheric moisture in the forest area is held by tree crowns.

The general dielectric model of forests of different types and ages is a heterogeneous layered environment. The layer of trunks and the layer of crowns contain various elements: trunks, branches, needles, leaves. The layer of trunks as a set of vertically oriented trunks has a vertical extent equal approximately to the average height of a tree of the selected platform of a forest crop. The crown layer extent is determined from the tree top to the lower layer of alive branches. As a rule, both layers intercross, forming a structurally mixed environment.

The particularity of GNSS signals is a limited frequency range which wave lengths of radiation are comparable to the characteristic sizes of trunks and parts of branches, but much more than the sizes of needles and leaves. The two-layer dielectric model of the forest area allows calculating an effective dielectric capacity (EDC) separately for the layer of crowns and the layer of trunks. Wood substance of trunks and branches has anisotropic dielectric capacity [19]. Considering the anisotropy of the dielectric capacity of wood substance gives opportunity to structure a forest canopy on statistically isotropic layer of crowns and an anisotropic layer of trunks.

Spatiotemporal coordinates of navigation satellites position in combination with coordinates of location of the antenna and the border of the forest area allow determining precisely the trajectory of the signal trace through a forest canopy and the movements of the scattering volume of a forest canopy. This circumstance makes it possible to determine the coefficient of a linear attenuation with a coordinate referencing and to recover EDC connected with the biomass and humidity of a forest crop.

The antenna location was chosen near the forest border with a field of grassland vegetation with coordinates 55°59'27.7" N, 92°45'42.6" E. The standard antenna of the MRK-32 equipment was used. The elevation of the antenna over the soil level was 2.8 m. The axis of the antenna directional pattern was set up vertically. The antenna was located at the distance of ~ 1 m from forest crop border. The duration of continuous registration was 3 hours.

The scene and the scheme of measurements are presented in fig. 10.

The site of pine plantings of the forest belt is located near the Institute of physics, Siberian Branch of the Russian Academy of Science. The age of plantings is about 60 years old. Its category is a dense forest. The average values of tree parameters are: height of trees is 22 m, extent of crowns is 6 m, diameter is 0.26 m, distance between trees is 3.5 m. The trees are planted in lines, distance between lines is 3–4 m, the trees are not arranged inside a line, distances variance is from 1 to 10 m. Vertical extent of crowns inside the forest area is within 25 % of a tree height. There is no shrub layer. The direction azimuth of lines and borders of the forest belt is 47º.

The spatiotemporal dependences of the amplitude of the GNSS signals on time are given in fig. 11. The signal which passed through a forest canopy (wood) is drawn in red colour, the signal which passed through an empty space is drawn in black colour.

The change of signal amplitude differs considerably on signal traces through a forest and an empty space. The characteristic "grass" of the amplitude in an empty space is connected with the generator and receiver noise as well as with fluctuations of dielectric capacity of atmosphere and ionosphere.

When entering a forest canopy the signal attenuates on large-scale heterogeneity (tree trunks, large volumes of snow on branches, difference of their distribution in space) and is partially absorbed by small-scale elements of trees (thin branches, needles, leaves).

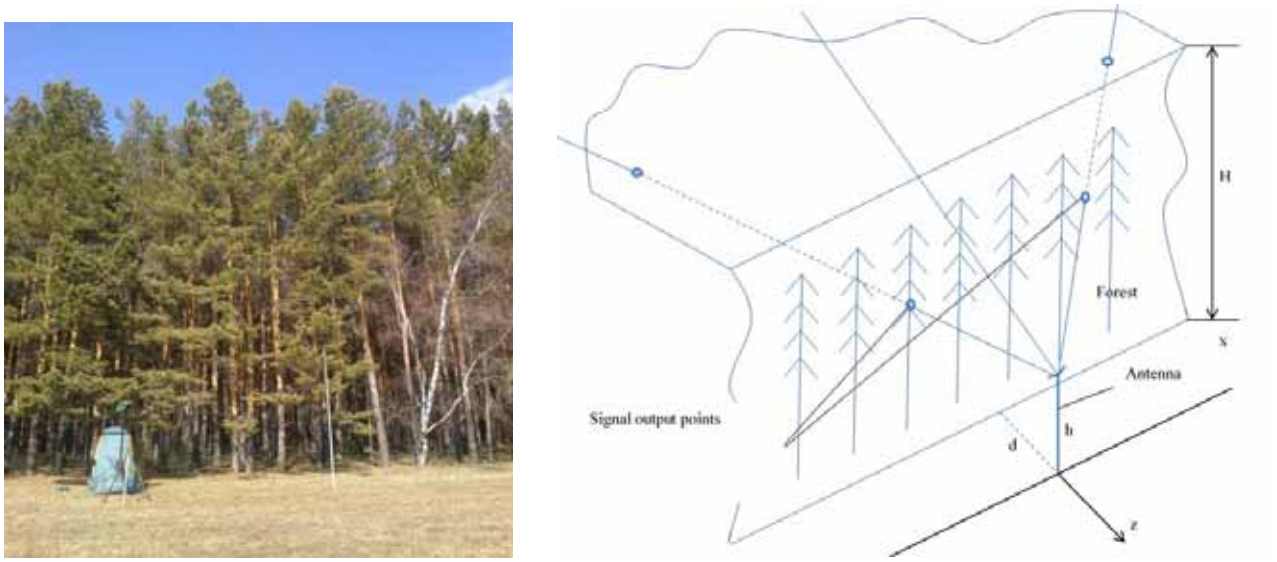

a *b*

Fig. 10. Scene and scheme of measurements:
a – is a scene of radioscopy of the forest; *b* – is a scheme of radioscopy of the forest with the antenna location near the forest crop border

Рис. 10. Сцена и схема измерений:
а – сцена радиопросвечивания леса; *б* – схема радиопросвечивания леса с расположением антенны у границы древостоя

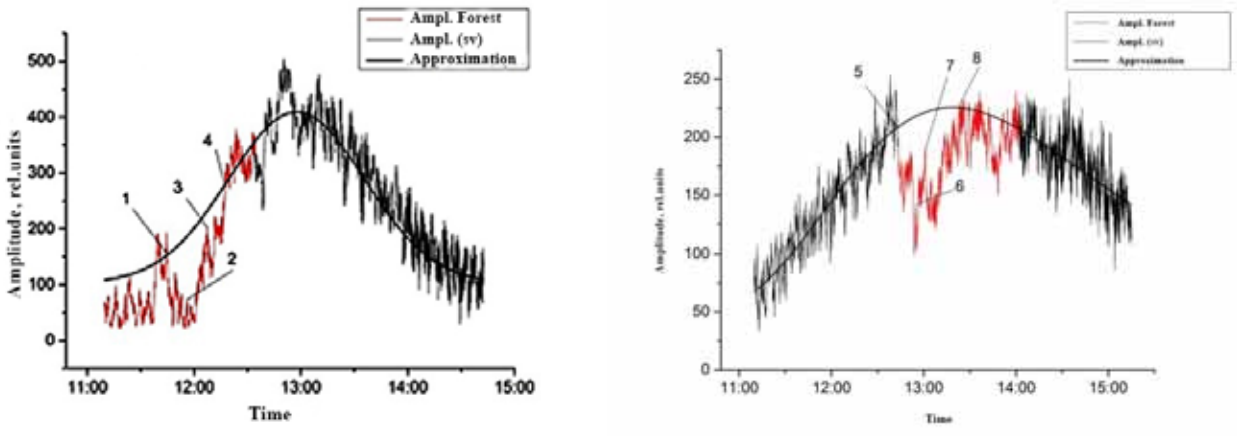

Fig. 11. The dependence of the amplitude of the GNSS signals on time.
1–8 are points of calculation of the coefficient of linear attenuation (table)

Рис. 11. Зависимости амплитуды сигналов ГНСС от времени.
1–8 точки расчета коэффициента погонного ослабления (см. таблицу)

Coefficient of linear attenuation in a forest crop

Point number	1	2	3	4	5	6	7	8
Azimuth (α), degrees	307.98	302.74	293.1	278.74	230.55	237.80	243.76	313.97
Angle of altitude (φ), degrees	59.06	64.69	69.78	73.24	66.69	72.75	76.11	84.75
L, m	19.47	17.64	15.73	13.44	20.54	11.13	12.58	13.83
– γ, dB/m	0.007	0.533	0.085	0.008	0.006	0.391	0.122	0.004

Spatiotemporal coordinates of navigation satellites position in combination with coordinates of location of the antenna and the border of the forest area allow determining precisely the trajectory of the signal trace through a forest canopy and the movements of the scattering volume of a forest canopy. This circumstance makes it possible to receive electrophysical characteristics of the forest and to recover humidity and biomass of a forest canopy with a coordinate referencing. Length of the trace (L) which the signal passed in the forest is calculated by the formula:

$$L = \frac{(H-h)\cos(\alpha) - d\,\mathrm{tg}(\varphi)}{\cos(\alpha)\sin(\varphi)}, \qquad (2)$$

where H is the average height of trees; h is the elevation of the antenna location; d is the distance from the antenna to the forest edge; α is a satellite azimuth; φ is a satellite elevation angle.

We approximate the signal which passed through an empty space taking into account the shape of the total curve received earlier for each satellite in the database of forward signals characteristics of the GLONASS and GPS groupings [8; 9]. Further, taking into account the position of the amplitude maximum at the elevation angle maximum value, we extrapolate the function for amplitude dependence of a forward signal from time by the time of a signal transmission through the forest. We determine signal amplitudes and corresponding to them traces lengths in the forest, we calculate coefficient values of linear attenuation γ for the selected points (frames) in fig. 11:

$$\gamma = -\frac{10Ln\frac{P}{P_0}}{L}, \qquad (3)$$

where P is the amplitude of a signal which passed through the forest; P_0 is the signal amplitude of an empty space. The results of calculation of linear attenuation coefficient for points 1–8 are given in table.

Variations of attenuation coefficients values are connected with spatial heterogeneity of distribution of trees elements throughout the forest canopy. It is possible to form a speckle pattern of a radio field of GNSS coherent signals scattered by the forest.

Conclusion. There were carried out test measurements of interferential diagrams from heterogeneous soil surfaces (salt marshes, asphalt), water surfaces of saline and freshwater bodies in summer period as well as at temperatures of an autumn freeze-up, including an ice covering of small thickness (4 cm).

The method of determination of local coefficient of linear attenuation of navigation satellites signals in a forest canopy was developed and approved along with the method of radioscopy of a forest area. The calibration variant was used according to a continuous consecutive writing of forward and analytical signals. Measurements of the linear attenuation coefficients of navigation satellites signals were made in the pinetum forest crop.

The received results are the basis for development of methods and technologies of continuous monitoring of earth covers characteristics and condition with the help of navigation satellites signals to solve a wide range of applied tasks.

References

1. Martin-Neira M. A Passive Reflectometry and Interferometry System (PARIS): Application to ocean altimetry. *ESA Journal*. 1993, Vol. 17, P. 331–355.

2. Kashkin V. B., Kokorin V. I., Mironov V. L. et al. [Experimental determination of electrophysical parameters of forest cover by using signals from GLONASS and GPS global navigation systems]. *Radiotekhnika i elektronika.* 2006, Vol. 51, No. 7, P. 825–830 (In Russ.).

3. Jin S., Cardellach E., Xie F. GNSS Remote Sensing. New York, London, Springer Dordrecht Heidelberg, 2014, 286 p.

4. Darayev A. M., Baykenova G. M., Nabiyeva A. A. [Research and comparison of technologies of satellite radio navigational systems on the basis of GPS and GLONASS]. *Vestnik KazNITU*. 2016, No. 1, P. 251–256 (In Russ.).

5. Martin-Neira M. GNSS-R future evolution. Abstract. Proc. IGARSS, 2015, Milan, Italy, Jul. 26–31, FR 1, G2.1.

6. Makarov D. S., Kharlamov D. V., Sorokin A. V. [The use of navigation satellites signals in monitoring earth covers]. *Reshetnevskie chteniya: materialy XXII Mezhdunar. nauch.-prakt. konf. (12–16 noyabrya 2018 g. Krasnoyarsk) : v 2 ch.* [Reshetnev Readings: Materials of XXII Intern. scientific. conf. : in 2 parts]. SibSAU. Krasnoyarsk, 2018. Part 1. P. 371–373 (In Russ.).

7. Makarov D. S., Tonkih V. S., Kharlamov D. V. et al. [Amplitude variations of forward signals of navigation satellites in monitoring of the earth surface]. *Materialy XII Mezhdunar. nauch.-prakt. konf. "Aktualnie problem aviacii i kosmonavtiki"* [Materials of XII Intern. Scientific. Conf "Current issues of aviation and cosmonautics"]. SibSAU. Krasnoyarsk, 2016, Vol. 1, P. 297–299 (In Russ.).

8. Fomin S. V., Sorokin A. V., Kharlamov D. V. [The database of spatio-temporal variations of forward signals amplitude of GLONASS and GPS near the Earth's surface]. *Reshetnevskie chteniya: Materialy XX Yubiley-*

noy Mezhdunar. Nauch.-prakt. Konf. [Reshetnev Readings : Materials of the XX Anniversary Intern. scientific-practical conf.]. SibSAU. Krasnoyarsk, 2016, Vol. 1, P. 381–385 (In Russ.).

9. Fomin S. V., Sorokin A. V., Kharlamov D. V. [Calibration of GLONASS and GPS signals in monitoring of the earth covers with the use of the database of forward signals characteristics near the Earth's surface]. *Regional'nye problemy distantsionnogo zondirovaniya Zemli. Materialy IV Mezhdunar. Nauch. Konf.i* [Regional problems of remote sensing of the Earth. Materials of the IV International Scientific Conference]. Krasnoyarsk, Siberian Federal University, 2017, P. 175–177 (In Russ.).

10. Mironov V. L., Mikhaylov M. I., Sorokin A. V. et al. [Diagnostics of soil humidity with the use of polarizing reflectograms of GLONASS and GPS signals]. *Vestnik SibGAU*. 2013, Vol. 51, No. 5, P. 107–109 (In Russ.).

11. Mironov V. L., Mikhaylov M. I., Muzalevsky K. V. et al. [Measurement of soil humidity in agricultural fields using GLONASS and GPS signals]. *Sovremennye problemy distantsionnogo zondirovaniya Zemli iz kosmosa*. 2014, Vol. 11, No. 4, P. 230–243 (In Russ.).

12. Mikhaylov M. I., Sorokin A. V., Mironov V. L. [The use of GLONASS and GPS signals to measure the thickness of an ice cover of freshwater bodies]. *Izvestiya Vuzov. Physics*. 2015, Vol. 58, No. 10/3, P. 70–72 (In Russ.).

13. Karev G. P. [Structural models of forest ecosystems]. *Sibirskiy Ekologicheskiy zhurnal*. 1999, No. 4, P. 381–396 (In Russ.).

14. Popov V. I. *Rasprostranenie radiovoln v lesakh* [Radio wave propagation in forests]. Moscow, Hotline – Telecom Publ., 2015, 392 p.

15. Yakubov V. P., Lysenko N. A. [Ultra wide-band sounding, Klayber growth model and the fractal dimension of a forest canopy]. *Izvestiya Vuzov. Physics*. 2012, Vol. 55, No. 8/2. P. 259–261 (In Russ.).

16. Sorokin A. V., Podoprigora V. G., Makarov D. S. [Scattering of navigation satellites signals on spatial inhomogeneities of the forest]. *Reshetnevskie chteniya : materialy XXI Mezhdunar. Nauch. Konf.* [Reshetnev readings: materials of the XXI International scientific conference]. Krasnoyarsk, Reshetnev SibGU, 2017, P. 416–417 (In Russ.).

17. Sorokin A. V., Podoprigora V. G., Ponomarev E. I. [The influence of gradient of electric-physical characteristics of the forest crop in the state of the radio signal of microwave band]. *Regional'nye problemy distantsionnogo zondirovaniya Zemli: Materialy V Mezhdunar. Nauch. Konf.* [Regional problems of remote sensing of the Earth: Materials of the V International Scientific Conference]. Krasnoyarsk, Siberian Federal University, 2018, P. 316–319 (In Russ.).

18. Podoprigora V. G., Sorokin A. V [Statistics of electrophysical parameters of the forest cover interacting with satellite signals of L-range]. *Regional'nye problemy distantsionnogo zondirovaniya Zemli : Materialy V Mezhdunar. Nauch. Konf.* [Regional problems f remote sensing of the Earth: Materials of the V International Scientific Conference]. Krasnoyarsk, Siberian Federal University, 2018, P. 163–165 (In Russ.).

19. Torgovnikov G. I. Dielectric Properties of Wood and Wood Based Materials. Berlin, Springer – Verlag, 1993, 194 p.

Библиографические ссылки

1. Martin-Neira M. A Passive Reflectometry and Interferometry System (PARIS): Application to ocean altimetry // ESA Journal. 1993. Vol. 17. P. 331–355.

2. Экспериментальное определение электрофизических параметров лесного покрова с использованием сигналов глобальных навигационных систем ГЛОНАСС и GPS / В. Б. Кашкин, В. И. Кокорин, В. Л. Миронов [и др.] // Радиотехника и электроника. 2006. Т. 51, № 7. С. 825–830.

3. Jin S., Cardellach E., Xie F. GNSS Remote Sensing. New York, London.: Springer Dordrecht Heidelberg. 2014. 286 p.

4. Дараев А. М., Байкенова Г. М., Набиева А. А. Исследование и сравнение технологий спутниковых радионавигационных систем на основе GPS и ГЛОНАСС // Вестник КазНИТУ. 2016. № 1. С. 251–256.

5. Martin-Neira M. GNSS-R future evolution. Abstract. Proc. IGARSS. Milan, Italy, Jul. 26–31, 2015. FR 1.G2.1.

6. Макаров Д. С., Харламов Д. В., Сорокин А. В. Использование сигналов навигационных спутников в мониторинге земных покровов // Решетневские чтения : материалы XXII Междунар. науч.-практ. конф. (12–16 ноября 2018, г. Красноярск) : в 2 ч. Ч. 1. С. 371–373.

7. Амплитудные вариации прямых сигналов навигационных спутников в мониторинге земной поверхности / Д. С. Макаров, В. С. Тонких, Д. В. Харламов [и др.] // Материалы XII Междунар. науч.-практ. конф., посвященной дню космонавтики. 2016. Т. 1. С. 297–299.

8. Фомин С. В., Сорокин А. В., Харламов Д. В. База данных пространственно-временных вариаций амплитуды прямых сигналов ГЛОНАСС и GPS вблизи поверхности Земли // Решетневские чтения : материалы XX Юбилейной Междунар. науч. конф. (9–12 ноября 2016, г. Красноярск). 2016. Ч. 1. С. 381–385.

9. Фомин С. В., Сорокин А. В., Харламов Д. В. Калибровка сигналов ГЛОНАСС и GPS в мониторинге земных покровов с использованием базы данных характеристик прямых сигналов вблизи поверхности Земли // Региональные проблемы дистанционного зондирования Земли : материалы IV Междунар. науч. конф. (12–15 сентября 2017, г. Красноярск) / Сиб. федер. ун-т ; науч. ред. Е. А. Ваганов ; отв. ред. Г. М. Цибульский. Красноярск, 2017. С. 175–177.

10. Диагностика влажности почвы с использованием поляризационных рефлектограмм сигналов ГЛОНАСС и GPS / В. Л. Миронов, М. И. Михайлов, А. В. Сорокин [и др.] // Вестник СибГАУ. 2013. Т. 51, № 5. С. 107–109.

11. Измерение влажности почвы сельскохозяйственных полей с использованием сигналов ГЛОНАСС и GPS / В. Л. Миронов, М. И. Михайлов, К. В. Музалевский [и др.] // Современные проблемы дистанци-

онного зондирования Земли из космоса. 2014. Т. 11, № 4. С. 230–243.

12. Михайлов М. И., Сорокин А. В., Миронов В. Л. Использование сигналов ГЛОНАСС и GPS для измерения толщины ледового покрова пресноводных водоемов // Известия вузов. Физика. 2015. Т. 58, № 10/3. С. 70–72 .

13. Карев Г. П. Структурные модели лесных экосистем // Сибирский экологический журнал. 1999. № 4. С. 381–396.

14. Попов В. И. Распространение радиоволн в лесах. М. : Горячая линия – Телеком, 2015. 392 с.

15. Якубов В. П., Лысенко Н. А. Сверхширокополосное зондирование, модель роста Клайбера и фрактальная размерность лесного полога // Известия вузов. Физика. 2012. Т. 55, № 8/2. С. 259–261.

16. Сорокин А. В., Подопригора В. Г., Макаров Д. С. Рассеяние сигналов навигационных спутников на пространственных неоднородностях леса // Решетневские чтения : материалы XXI Междунар. науч. конф. (08–11 ноября 2017, г. Красноярск) : в 2 ч. / СибГУ им. М. Ф. Решентнева. Красноярск, 2017. Ч. 1. С. 416–417.

17. Сорокин А. В., Подопригора В. Г., Пономарев Е. И. Влияние градиентов электрофизических характеристик древостоя на состояние радиосигнала СВЧ-диапазона // Региональные проблемы дистанционного зондирования : материалы V Междунар. науч. конф. (11–14 сентября 2018, г. Красноярск) / Сиб. федер. ун-т ; науч. ред. Е. А. Ваганов ; отв. ред. Г. М. Цибульский. Красноярск, 2018. С. 316–319.

18. Подопригора В. Г., Сорокин А. В. Статистика электрофизических параметров лесного покрова, взаимодействующего со спутниковыми сигналами L-диапазона // Региональные проблемы дистанционного зондирования : материалы V Междунар. науч. конф. (11–14 сентября 2018, г. Красноярск) / Сиб. федер. ун-т ; науч. ред. Е. А. Ваганов ; отв. ред. Г. М. Цибульский. Красноярск, 2018. С. 163–165.

19. Torgovnikov G. I. Dielectric Properties of Wood and Wood Based Materials. Berlin, Springer – Verlag. 1993. 194 p.

Makarov Daniil Sergeyevich – graduate student, junior research associate; laboratory of space systems and technologies; Federal Research Center “Krasnoyarsk Scientific Center of the SB RAS”. E-mail: mcdan3991@yandex.ru.

Kharlamov Dmitry Valentinovich – graduate student, junior research associate; laboratory of space systems and technologies; Federal Research Center “Krasnoyarsk Scientific Center of the SB RAS”. E-mail: dimafeadz@gmail.com.

Sorokin Anatoly Vasilyevich – Ph. D., associate professor, a professor, Reshetnev Siberian State University of Science and Technologies; research scientist, laboratory of space systems and technologies; Federal Research Center “Krasnoyarsk Scientific Center of the SB RAS”. E-mail: sorav@iph.krasn.ru.

Макаров Даниил Сергеевич – аспирант, младший научный сотрудник; лаборатория космических систем и технологий, Федеральный исследовательский центр «Красноярский научный центр СО РАН». E-mail: mcdan3991@yandex.ru.

Харламов Дмитрий Валентинович – аспирант, младший научный сотрудник; лаборатория космических систем и технологий, Федеральный исследовательский центр «Красноярский научный центр СО РАН». E-mail: dimafeadz@gmail.com.

Сорокин Анатолий Васильевич – кандидат физико-математических наук, доцент, профессор, Сибирский государственный университет науки и технологий имени академика М. Ф. Решетнева; научный сотрудник, лаборатория космических систем и технологий, Федеральный исследовательский центр «Красноярский научный центр СО РАН». E-mail: sorav@iph.krasn.ru.

UDC 004.056.55
Doi: 10.31772/2587-6066-2019-20-1-20-27

For citation: Merinov A. S., Nesterov K. A., Zhdanov O. N. [Improvement of the construction technique of substitution blocks for symmetric encryption algorithms]. *Siberian Journal of Science and Technology.* 2019, Vol. 20, No. 1, P. 20–27. Doi: 10.31772/2587-6066-2019-20-1-20-27

Для цитирования: Меринов А. С., Нестеров К. А., Жданов О. Н. Совершенствование методики конструирования блоков замен для алгоритмов симметричного шифрования // Сибирский журнал науки и технологий. 2019. Т. 20, № 1. С. 20–27. Doi: 10.31772/2587-6066-2019-20-1-20-27

IMPROVEMENT OF THE CONSTRUCTION TECHNIQUE OF SUBSTITUTION BLOCKS FOR SYMMETRIC ENCRYPTION ALGORITHMS

A. S. Merinov, K. A. Nesterov, O. N. Zhdanov*

Reshetnev Siberian State University of Science and Technology
31, Krasnoyarsky Rabochy Av., Krasnoyarsk, 660037, Russian Federation
*E-mail: onzhdanov@mail.ru

As it is known, block symmetric encryption algorithms are widely used to ensure information confidentiality. The resistance of encryption algorithms to the most common types of cryptanalysis is determined the quality of the blocks of substitutions.

In the present work, the development of a methodology for constructing substitution blocks is being continued.

In the first approach, Boolean functions with given cryptographic properties are used as component functions of substitution blocks. Previously, one of the authors proposed a reasonable methodology for the phased selection of Boolean functions for construction block.

In this paper, in addition to such cryptographic properties of Boolean functions, such as: balance, possessing a strict avalanche effect, possessing correlation immunity, for the first time the nonlinearity distances of the first and second orders of Boolean functions are considered simultaneously.

A study of the full set of Boolean functions of four variables was conducted. The result of it is the optimal set of Boolean functions for building substitution blocks when encrypted with the GOST 28147-89 algorithm.

In the second approach, the substitution block are determined by an irreducible polynomial over the Galois field, such a scheme, used in the Rijndael encryption algorithm, is considered to be strong.

The growth of calculating power of the computer necessitates an increase of the cryptographic strength of encryption algorithms.

The authors have proposed substitution blocks for each round of the Rijndael scheme, based on different irreducible polynomials. A study of compositions representing a different combination of specially selected irreducible polynomials for ten rounds was carried out and the optimal set of polynomials with the best values of the encryption quality indicators by the Rijndael scheme was obtained.

Keywords: replacement blocks, GOST, Rijndael, boolean function, block encryption algorithms, cryptographic stability.

СОВЕРШЕНСТВОВАНИЕ МЕТОДИКИ КОНСТРУИРОВАНИЯ БЛОКОВ ЗАМЕН ДЛЯ АЛГОРИТМОВ СИММЕТРИЧНОГО ШИФРОВАНИЯ

А. С. Меринов, К. А. Нестеров, О. Н. Жданов*

Сибирский государственный университет науки и технологий имени академика М. Ф. Решетнева
Российская Федерация, 660037, г. Красноярск, просп. им. газ. «Красноярский рабочий», 31
*E-mail: onzhdanov@mail.ru

Как известно, для обеспечения конфиденциальности информации широко применяются блочные симметричные алгоритмы шифрования. Стойкость алгоритмов шифрования к наиболее распространенным видам криптоанализа во многом определяется качеством блока замен.

В настоящей работе продолжается разработка методики построения блоков замен.

При первом подходе в качестве компонентных функций блоков замен используются булевы функции, обладающие заданными криптографическими свойствами. Ранее одним из авторов была предложена обоснованная методика поэтапного выбора булевых функций для конструирования блоков. Однако эта методика учитывала только расстояние нелинейности первого порядка.

В данной работе, помимо таких криптографических свойств булевых функций, как сбалансированность, обладание строгим лавинным эффектом, обладание корреляционным иммунитетом, впервые одновременно рассматриваются расстояния нелинейности первого и второго порядков булевых функций.

Проведено исследование полного множества булевых функций от четырех переменных, результатом которого является оптимальный набор булевых функций для построения блоков замен при шифровании алгоритмом ГОСТ 28147–89.

При втором подходе блок замены определяется неприводимым полиномом над полем Галуа. Такая схема применена в считающемся стойким алгоритме шифрования Rijndael.

Рост вычислительной мощности ЭВМ обуславливает необходимость увеличения криптостойкости алгоритмов шифрования.

Авторами предложены блоки замен для каждого раунда схемы Rijndael, основанные на различных неприводимых полиномах. Проведено исследование композиций, представляющих собой различное сочетание специально подобранных неприводимых полиномов в десяти раундах, что позволило выбрать оптимальное множество многочленов с наилучшими значениями показателей качества шифрования по схеме Rijndael.

Ключевые слова: блоки замен, ГОСТ, Rijndael, булевы функции, алгоритмы блочного шифрования, криптографическая стойкость.

Introduction. As it is known, block symmetric encryption algorithms are widely used to ensure confidentiality. The growth of computer processing power and the development of cryptanalysis methods require increasing the cryptographic stability of existing algorithms and the development of new ones. Researchers and practitioners are conducting work in this direction. The stability of the encryption algorithm to the most common types of cryptanalysis is determined by the quality of the replacement block, the substitution block. At present, it is already generally accepted that the quality of replacement units is characterized by the values of nonlinearity and avalanche effect [1; 2].

There are two main approaches to the construction of replacement tables.

Thus, in [3], a reasonable method was proposed for the step-by-step selection of Boolean functions that are components of the replacement block, which takes into account not only the nonlinearity of each of the functions making up the block, but also the nonlinearity of all possible nontrivial linear combinations. It is also noted that it is possible to simultaneously solve the problem of increasing stability, both to linear and differential cryptanalysis methods, if both nonlinearity and dynamic distance are used as selection criteria [4–6]. The methodology of step-by-step selection was programmatically implemented in relation to the algorithm of GOST 28147–89, currently considered to be very stable, in [1].

The most typical example of the second approach is also the Rijndael algorithm [7], which is considered to be stable, in which the replacement block is completely determined by an irreducible polynomial over the Galois field. In Rijndael the construction of Nyberg is used [8], which is a reflection in the form of multiplicatively inverse elements of the Galois field $GF(2^k)$:

$$y = x^{-1} \bmod d[f(z), p], \quad y, x \in GF(2^k), \qquad (1)$$

in combination with affine transformation:

$$b = A \cdot y + a, \quad a, b \in GF(2^k), \qquad (2)$$

where $f(z) = z^8 + z^4 + z^2 + z + 1$ – irreducible over the field $GF(2^8)$ polynomial; A – non-degenerate affine transformation matrix; a – shift vector; $p = 2$ – characteristic of the extended Galois field, $0^{-1} \equiv 0$ – by definition; a, b, x, y – elements of the extended Galois field $GF(2^k)$, which are considered as decimal numbers, or binary vectors, or polynomials of degree $k-1$.

Among the quality indicators of S-units, the following are most often distinguished [2]:

– maximum of the modules of the matrix elements of the correlation coefficients of the input and output bits;

– the number of zeros in the matrix of correlation coefficients;

– non-linearity, understood as the distance to the set of affine functions;

– algebraic degree of nonlinearity.

It is noted that the S-blocks of the Nyberg construction have many practically valuable cryptographic properties, such as high nonlinearity distance, homogeneous minimization of correlation coefficients, and relative simplicity of technical implementation both using the tabular method and using Galois field operations.

In the present work, research is continued in these two directions.

The study of the set of Boolean functions of four variables. The study of the full set of Boolean functions of four variables was carried out. In addition to cryptographic properties of Boolean functions, such as: balance, possessing a strict avalanche effect, possessing correlation immunity, for the first time the nonlinearity distances of the first and second orders of Boolean functions are simultaneously considered.

Nonlinearity of r- order $nl_r(f)$ of Boolean function f over F_2^n is called $\min_{\deg(l) \le r} d(f, l)$. Nonlinearity $nl_1(f)$ of Boolean function f is called the distance between f and a set of affine functions. Nonlinearity $nl_2(f)$ of Boolean function f is called the distance between f and a set of quadratic functions.

For example, a Boolean function of four variables with the following truth table:

$f = \{000101001001101\}$, its nonlinearity of the first order is 3 and the nonlinearity of the second order is 1.

The result of the study of the nonlinearity of the first and second orders Boolean functions of four variables is presented in tab. 1.

Table 1

Nonlinearity of the first and second orders of Boolean functions

Nonlinearity distance		Class scopes
1 order	2 order	
0	0	22
1	1	0
2	2	0
3	1	0
4	0	200
4	2	0
5	1	0
6	0	0

So, there are a total of 22 linear first-order Boolean functions and 200 second-order linear Boolean functions with these characteristics. Boolean functions with a first order nonlinearity distance equal to 0 will not be considered further, since the replacement blocks obtained from them are unstable to linear cryptanalysis [9].

The remaining 200 Boolean functions are linear functions of the second order, they are not enough to study the nonlinearity of higher orders. Therefore, Boolean functions not linear of the first and second orders were found, and the maximum value of the correlation coefficient of the replacement block when using these functions at absolute value was minimal.

The correlation properties of the substitution units were analyzed; Boolean functions with the same nonlinearity properties of the first and second orders were used as component functions. The results of the study are shown in tab. 2, which reflects the maximum correlation coefficient of the replacement unit in absolute value when using certain Boolean functions and the number of such functions.

Boolean functions with a first order nonlinearity distance equal to 1, 3, 5, and 6 are not balanced Boolean functions because they cannot be used as component functions of the replacement blocks of the encryption algorithm. Bijective replacement units with a maximum correlation coefficient of 0.25 were worked out, using Boolean functions with the following properties:

– the first order nonlinearity distance is 4;
– the second order nonlinearity distance is 2;
– balance;
– have a strict avalanche effect.

Bijective replacement blocks with a maximum correlation coefficient of 0.25 were constructed, using Boolean functions with the following properties:

– the first-order nonlinearity distance is 2;
– the second-order nonlinearity distance is 2;
– balance.

Table 2

Class volumes

Nonlinearity distance		The maximum modulus of the correlation coefficient of a bijective replacement block	Class volumes
1 order	2 order		
0	0	0	22
1	1	Doesn’t exist	0
2	2	0.25	1408
3	1	Doesn’t exist	0
4	0	0	304
4	2	0.25	5280
5	1	Doesn’t exist	0
6	0	Doesn’t exist	0

These Boolean functions do not satisfy the strict avalanche criterion; therefore, replacement blocks obtained from such Boolean functions are less resistant to the differential cryptanalysis method.

We distinguish two sets of Boolean functions that are most suitable to construct blocks of replacement.

For testing, the AES encryption algorithm was chosen and the following tests were used: series distribution, autocorrelation function, D. Knuth's correlation test:

– the first order nonlinearity distance is 4;
– the second-order nonlinearity distance is 2;
– balance;
– have a strict avalanche effect.

The power of the recieved set is 5280. The functions of this set can be recommended for use as a component of replacement blocks for the algorithms of GOST 28147-89, AES and (with minor and obvious changes) of similar algorithms.

The set of boolean functions used to build the replacement block is shown below. The test results presented in fig. 1–3, indicate the quality of the constructed replacement unit.

$$F = [0,0,0,0,0,1,1,1,0,1,1,1,0,1,1,0];$$

$$F = [0,0,0,0,1,0,1,1,1,0,1,1,1,0,0,1];$$

$$F = [0,0,1,1,1,1,0,1,0,0,0,1,1,0,1,0];$$

$$F = [1,0,1,0,0,1,0,0,1,0,1,1,1,1,0,0].$$

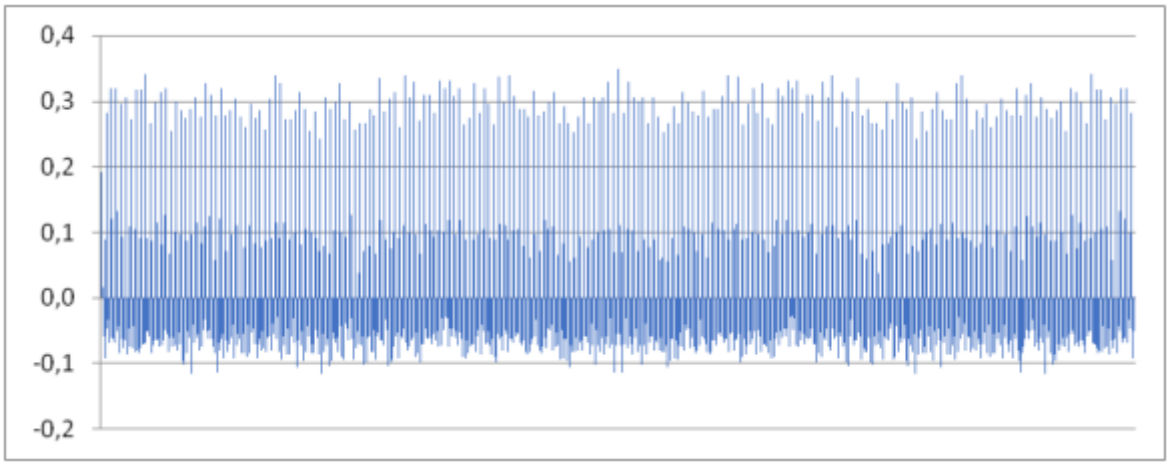

Fig. 1. Autocorrelation function

Рис. 1. Автокорреляционная функция

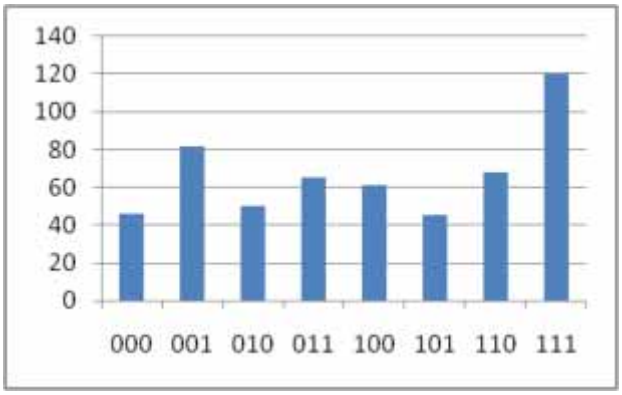

Fig. 2. Schedule distribution of series-triples

Рис. 2. График распределения серий троек

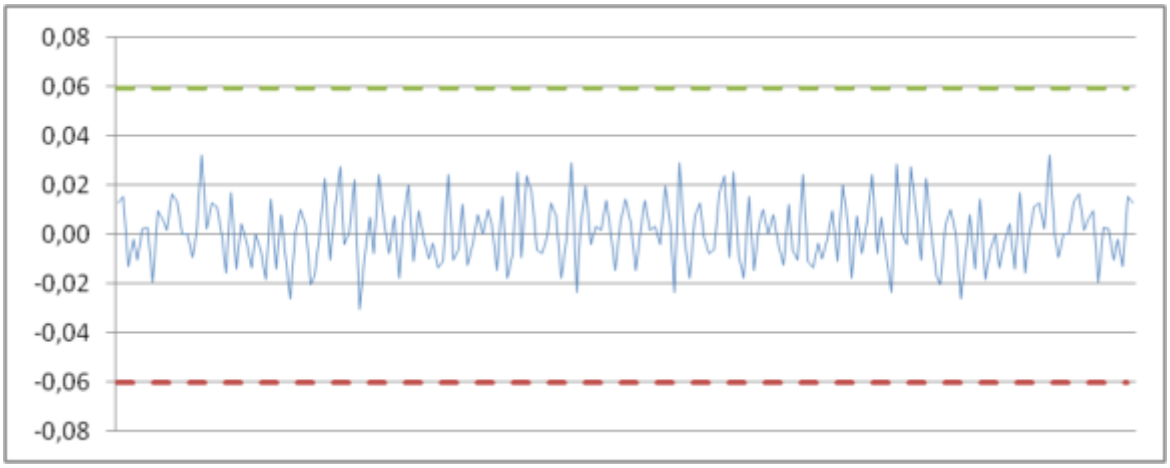

Fig. 3. The result of D. Knut's correlation test

Рис. 3. Результат проверки корреляции Д. Кнута

Selection of optimal irreducible polynomials for the implementation of the AES algorithm. One of the techniques for enhancing the durability of the AES algorithm is the construction of replacement blocks based not on one selected irreducible polynomial for all rounds, but on various irreducible polynomials chosen for each round. However, due to unacceptable computational complexity (10^{10} combinations), first it was decided to conduct a study of compositions, which are a different combination of five specially selected irreducible polynomials in ten rounds.

In works [10; 11], nonlinear transformations of the Nyberg construction were studied in detail on the basis of all isomorphic and automorphic representations of the fields. All irreducible polynomials over the fields are presented, and the values of the quality indicators determined by these S-blocks polynomials are calculated. The possibility of choosing one of the many irreducible polynomials is of practical importance.

After the publication of papers [5; 6; 10], it became possible to combine the advantages of the GOST and Rijndael approaches.

In article [11] the use of irreducible polynomial compositions is analyzed. The composition in this case is the alternation of two irreducible polynomials. Irreducible polynomials, with the most remarkable cryptographic characteristics, were taken from this article. Encryption was carried out using each of the polynomials on 20 texts (the same polynomial was used in each round).

As a result, cryptographic characteristics were obtained and a comparative analysis of indicators for each irreducible polynomial was carried out (tab. 3, 4). Polynomials are represented by their decimal equivalents, and filled cells show the most remarkable indicators for each irreducible polynomial.

As a result, irreducible polynomials were selected – 283, 319, 333, 355, 357, since they have minimum values of the maximum modulus of the correlation coefficients and the largest number of zero elements of the correlation matrix.

Then an encryption procedure was carried out with all possible combinations of selected irreducible polynomials and five open texts.

Using the same encryption quality criteria, the maximum of the modules of the matrix coefficients correlation elements and the number of zeros of the elements of the correlation matrix, correlation matrices were constructed and a comparative analysis of indicators for each composition was performed. The selection of the best compositions of irreducible polynomials, surpassing the rest of the compositions in cryptographic characteristics, was done.

Table 3

The maximum modulus of the correlation coefficients

№ text	Maximum of the modules of the correlation matrix elements									
	Irreducible polynomials									
	283	285	299	301	313	319	333	351	355	357
1	0.75	0.75	0.625	0.625	0.625	0.5	0.5	0.625	0.5	0.5
2	0.5	0.5	0.625	0.75	0.625	0.5	0.5	0.5	0.5	0.625
3	0.5	0.875	0.625	0.5	0.625	0.5	0.5	0.5	0.75	0.625
4	0.5	0.5	0.5	0.5	0.625	0.5	0.625	0.625	0.75	0.5
5	0.625	0.625	0.625	0.75	0.5	0.75	0.625	0.625	0.625	0.5
6	0.75	0.75	0.625	0.625	0.5	0.5	0.5	0.5	0.625	0.5
7	0.5	0.625	0.75	0.625	0.625	0.75	0.625	0.625	0.5	0.625
8	0.625	0.625	0.5	0.5	0.5	0.625	0.625	0.75	0.625	0.5
9	0.5	0.625	0.625	0.5	0.625	0.625	0.5	0.625	0.5	0.5
10	0.5	0.625	0.625	0.625	0.625	0.625	0.625	0.75	0.75	0.75
11	0.5	0.625	0.625	0.75	0.375	0.5	0.625	0.625	0.5	0.5
12	0.75	0.5	0.625	0.625	0.625	0.5	0.5	0.5	0.625	0.625
13	0.5	0.5	0.75	0.625	0.75	0.5	0.625	0.625	0.5	0.5
14	0.625	0.75	0.625	0.625	0.5	0.625	0.625	0.625	0.625	0.5
15	0.625	0.5	0.625	0.625	0.625	0.875	0.75	0.625	0.625	0.5
16	0.625	0.5	0.75	0.625	0.5	0.5	0.625	0.625	0.625	0.625
17	0.5	0.625	0.75	0.625	0.75	0.625	0.625	0.5	0.625	0.625
18	0.625	0.75	0.625	0.625	0.625	0.5	0.75	0.5	0.5	0.75
19	0.625	0.625	0.625	0.5	0.5	0.5	0.5	0.625	0.375	0.5
20	0.625	0.625	0.625	0.625	0.5	0.75	0.5	0.5	0.5	0.5

Table 4

The number of zeroes of the correlation matrix elements

№ text	The number of zeros of the correlation matrix									
	Irreducible polynomials									
	283	285	299	301	313	319	333	351	355	357
1	9	13	10	15	9	15	10	9	9	14
2	16	11	9	12	16	19	18	18	15	11
3	10	9	12	10	13	15	14	15	13	13
4	13	11	12	7	12	16	7	16	18	14
5	19	19	11	11	7	19	8	8	3	21
6	8	14	11	11	16	15	9	15	11	11
7	10	20	16	12	7	11	23	4	14	12
8	12	15	19	13	11	9	9	13	16	7
9	9	15	8	9	13	14	15	14	12	14
10	12	13	14	14	17	12	19	17	13	11
11	21	11	12	10	12	12	15	13	11	14
12	20	13	13	21	10	9	6	18	11	6
13	10	9	11	13	19	18	9	17	14	12
14	7	9	10	21	19	17	10	13	13	7
15	8	10	9	17	8	19	10	7	9	4
16	16	14	11	15	13	15	9	13	13	16
17	14	12	6	13	10	13	13	13	10	12
18	16	11	14	18	9	9	13	12	11	10
19	16	13	7	10	17	10	14	13	13	17
20	10	17	10	16	12	9	9	13	15	13

The composition here is a combination of five polynomials in ten rounds. For example, compositions 333, 283, 283, 319, 357, 283, 333, 355, 283, 333 (or 2001402302). Experiments have shown that the use of the listed irreducible polynomials in Rijndael encryption provides the best cryptographic strength indicators in comparison with others. Examples of the best and the worst compositions on two criteria are presented respectively in tab. 5, 6.

Table 5

Examples of the best compositions on the basis of two criteria

Maximum correlation coefficient	Number of zeroes	Composition
0.375	36	3104034331
0.375	34	3313210233
0.375	34	4142344410
0.375	34	4303234230
0.375	33	4202203343
0.375	33	4324342340
0.375	32	333434303
0.375	32	2422044342
0.375	32	4443342101
0.25	30	3241333141

Table 6

Examples of the worst compositions on the basis of two criteria

Maximum correlation coefficient	Number of zeroes	Composition
0.625	7	32000000003
0.75	9	32000000004
0.625	16	32000000140
0.875	11	32112010432
0.625	11	32112010433
0.75	12	32000000143
0.875	16	32000000222
0.625	13	32201110444
0.75	11	32201111000
0.875	14	32000001120

The data in the tab. 5 are not fully presented, since the output of all data would take several hundred pages, and their information content would tend to zero. The program, which is engaged in the calculation of the above data, can be found by clicking the following link [12].

The compositions presented in tab. 5, have high rates of cryptographic characteristics. The results of the study allow choosing the optimal set of polynomials with the best cryptographic properties, the combination of which

gives a high rating of the quality of encryption according to the AES scheme, which increases the cryptographic strength of the AES algorithm.

The developed method allows selecting encryption options in such a way that it can compete not only with the standard AES encryption algorithm, but also with other modern block encryption algorithms.

Conclusion. The results of the study of two approaches showed a good quality of substitution units construction, which ensures the best cryptographic performance indicators, both for the Rijndael algorithm and for GOST. On the basis of the obtained results, it is necessary to further explore possible options of increasing the strength of block encryption algorithms. It is interesting to compare the obtained results with their ternary counterparts, see [13].

Acknowledgment. The authors express their gratitude to Sokolov Artem Viktorovich.

Благодарности. Авторы выражают благодарность Соколову Артему Викторовичу.

References

1. Zhdanov O. N. *Metodica vibora kluchevoi informacii dla algoritmov blochnoigo shifrovania* [The method of selecting key information for the block cipher algorithm]. Moscow, INFRA-M Publ., 2013, 97 p.

2. Sokolov A. V. New methods for synthesizing nonlinear transformations of modern ciphers. Germany, Lap Lambert Academic Publishing, 2015, 100 p.

3. Mister S., Adams C. Practical S-box design. Workshop in selected areas of cryptography. SAC'96, 1996, P. 61–76.

4. Medvedeva T. E. [Evaluation of the cryptographic stability of the replacement tables of the algorithm State Standard 28147-89]. *Reshetnevskie chteniya.* 2012, Vol. 2, No.15, P. 66–667 (In Russ.).

5. Chalkin T. A., Zolotuchin V. U. [Development of a methodology for selecting parameters for the algorithm for constructing replacement nodes of the block cipher GOST 28147-89]. *Prikladnaya diskretnaya matematika. Prilozhenie.* 2010, No. 3, P. 20–21 (In Russ.)

6. FIPS 197. Advanced encryption standard. Available at: http://csrc.nist.gov/publications (accessed 10.10.2018).

7. Nyberg K. Differentially uniform mappings for cryptography. Advances in cryptology. Proc. of EUROCRYPT'93, Lecture Notes in Compuer Springer Verlag. Berlin, Heidelberg, New York, 1994, P. 55–65.

8. Mazurkov M. I., Sokolov A. V. [Nonlinear transformations on the basis of complete classes of isomorphic and automorphic representations of the field GF(256)]. *Izvestiya vuzov.* Vol. 56, No. 11 (In Russ.). Doi: https://doi.org/10.20535/S0021347013110022.

9. Agafanov I. V. *Kriptograficheskie svoystva nelineynykh bulevykh funktsiy* [Cryptographic properties of nonlinear boolean functions]. St. Petersburg, DHA&CAGD Publ., 2007, P. 1–24.

10. Mazurkov M. I., Sokolov A. V. [Cryptographic properties of the nonlinear transformation of the cipher Rijndael on the basis of complete classes of irreducible polynomials]. *Trudy Odesskogo politekhnicheskogo universiteta*. 2012. No. 2(39), P. 183–18.

11. Dmitriev M. A. [Possible options for increasing the cryptographic strength of encryption algorithms based on the Nyberg design]. *Siberian Journal of Science and Technology.* 2017, Vol. 18, No. 3, P. 505–503 (In Russ.).

12. Merinov A. S. The program that performs the encryption procedure by the method of selecting the optimal parameters for the implementation of the AES algorithm. Available at: https://yadi.sk/d/PrPh5I1E3WfwBz (accessed 9.10.2018).

13. Zhdanov O. N., Sokolov A. V. [Extending Nyberg construction on Galois fields of odd characteristic]. *Izvestiya vuzov. Radioelektronika.* 2017, Vol. 60, No. 12, P. 696–702 (In Russ.).

14. *GOST 28147–89. Sistemy obrabotki informatsii. Zashchita kriptograficheskaya. Algoritm kriptograficheskogo preobrazovaniya* [State Standard 28147–89. Information processing system. Cryptographic protection. Algorithm of cryptographic transformation]. Moscow, Standartinform Publ., 1996. 28 c.

15. Report on the Development of the Advanced Encryption Standard (AES) Available at: https://nvlpubs.nist.gov/nistpubs/jres/106/3/j63nec.pdf (accessed 11.10.2018).

Библиографические ссылки

1. Жданов О. Н. Методика выбора ключевой информации для алгоритма блочного шифрования. М. : Инфра-М, 2013. 97 с.

2. Соколов А. В. Новые методы синтеза нелинейных преобразований современных шифров. Германия. Саарбрюккен : Lambert Academic Publishing, 2015. 172 с.

3. Mister S., Adams C. Practical S-box design. Workshop in selected areas of cryptography. SAC'96. P. 61–76.

4. Медведева Т. Е. Оценка криптостойкости таблиц замен алгоритма ГОСТ 28147–89 // Решетневские чтения. 2012. Т. 2, № 15. С. 66–667.

5. Чалкин Т. А. Золотухин В. Ю. Разработка методики оценки зависимости криптостойкости алгоритма ГОСТ 28147–89 от выбранной ключевой информации // Прикладная дискретная математика. Приложение. 2010. № 3. С. 20–21.

6. FIPS 197. Advanced encryption standard [Электронный ресурс]. URL: http://csrc.nist.gov/ publications (дата обращения: 10.10.2018).

7. Nyberg K. Differentially uniform mappings for cryptography // Proc. of EUROCRYPT'93, Lecture Notes in Compuer Springer Verlag. Berlin, Heidelberg, New York, 1994. P. 55–65.

8. Мазурков М. И., Соколов А. В. Нелинейные преобразования на основе полных классов изоморфных и автоморфных представлений поля GF(256) // Известия вузов. Т. 56, № 11. Doi: https://doi.org/10.20535/S0021347013110022.

9. Агафонова И. В. Криптографические свойства нелинейных булевых функций. СПб. : DHA & CAGD, 2007. С. 1–24.

10. Мазурков М. И. Криптографические свойства нелинейного преобразования шифра Rijndael на базе полных классов неприводимых полиномов // Труды Одесского политехнического университета. 2012. Вып. 2(39). С. 183–18.

11. Дмитриев М. А. Возможные варианты повышения криптостойкости алгоритмов шифрования на основе конструкции Ниберг // Сибирский журнал науки и технологий. 2017. Т. 18, № 3. С. 505–509.

12. Merinov A. S. The program that performs the encryption procedure by the method of selecting the optimal parameters for the implementation of the AES algorithm [Электронный ресурс]. URL: https://yadi.sk/d/PrPh5I1E3WfwBz (дата обращения: 9.10.2018).

13. Жданов О. Н., Соколов А. В. О распространении конструкции Ниберг на поля Галуа нечетной характеристики // Известия вузов. Радиоэлектроника. 2017. Т. 60, № 12. С. 696–702.

14. ГОСТ 28147–89. Системы обработки информации. Защита криптографическая. Алгоритм криптографического преобразования. М. : Стандартинформ, 1996. 28 с.

15. Report on the Development of the Advanced Encryption Standard (AES) [Электронный ресурс] URL: https://nvlpubs.nist.gov/nistpubs/jres/106/3/j63nec.pdf (дата обращения: 11.10.2018).

Merinov Alexander Stanislavovich – Master student of the Department of Information Technology Security; Reshetnev Siberian State University of Science and Technology. E-mail: onzhdanov@mail.ru.

Nesterov Kirill Alexandrovich – Master student of the Department of Information Technology Security; Reshetnev Siberian State University of Science and Technology. E-mail: onzhdanov@mail.ru.

Zhdanov Oleg Nikolayevich – Cand. Sc., Associate Professor of the Department of Information Technology Security; Reshetnev Siberian State University of Science and Technology. E-mail: onzhdanov@mail.ru.

Меринов Александр Станиславович – магистрант; кафедра безопасности информационных технологий, Сибирский государственный университет науки и технологий имени академика М. Ф. Решетнева. E-mail: onzhdanov@mail.ru.

Нестеров Кирилл Александрович – магистрант; кафедра безопасности информационных технологий, Сибирский государственный университет науки и технологий имени академика М. Ф. Решетнева. E-mail: onzhdanov@mail.ru.

Жданов Олег Николаевич – кандидат физико-математических наук, доцент; кафедра безопасности информационных технологий, Сибирский государственный университет науки и технологий имени академика М. Ф. Решетнева. E-mail: onzhdanov@mail.ru.

UDC 519.23+519.245
Doi: 10.31772/2587-6066-2019-20-1-28-34

For citation: Ushanov S. V., Ogurtsov D. A. [Estimation of the Frocini criteria and omega square criteria statistics by the statistical tests method for a mixture of normal distributions]. *Siberian Journal of Science and Technology.* 2019, Vol. 20, No. 1, P. 28–34. Doi: 10.31772/2587-6066-2019-20-1-28-34

Для цитирования: Ушанов С. В., Огурцов Д. А. Оценка методом статистических испытаний статистики критериев Фроцини и омега-квадрат для смеси нормальных распределений // Сибирский журнал науки и технологий. 2019. Т. 20, № 1. С. 28–34. Doi: 10.31772/2587-6066-2019-20-1-28-34

ESTIMATION OF THE FROCINI CRITERIA AND OMEGA SQUARE CRITERIA STATISTICS BY THE STATISTICAL TESTS METHOD FOR A MIXTURE OF NORMAL DISTRIBUTIONS

S. V. Ushanov*, D. A. Ogurtsov

Reshetnev Siberian State University of Science and Technology
31, Krasnoyarsky Rabochy Av., Krasnoyarsk, 660037, Russian Federation
*E-mail: ushanov_sv@mail.ru

A lot of sets of subjects and objects in biology, industry, management can be divided into a number of classes, each of which corresponds to a certain distribution component. When analyzing a mixture of distributions, it is necessary to estimate its parameters (task 1) and to assess the correspondence of empirical and theoretical distribution functions (task 2).

To solve the first problem, numerical algorithms that implement the method of moments and the maximum likelihood method are used. In this paper, the problem of estimating the distribution parameters is solved by minimizing the goodness measure by the Quasi-Newton method.

The second problem is solved by comparing the empirical and theoretical distribution functions by one or several statistical goodness measures. Statistics of the distribution of these measures depends on the sample size, the method of forming data and estimating distribution parameters. The paper examines the goodness measure between Frocini and omega-square (Kramer – Mises – Smirnov). The evaluation of the statistics of the goodness measure was carried out by the simulation method based on the results of 50000 statistical tests. In each of the tests, the distribution parameters were estimated by minimizing the calculated value of the corresponding goodness measure. The results of simulation modeling allow estimating the statistics of the parameters of a mixture of distributions.

The results of solving the considered problems for a mixture of two normal distributions of size 240 are presented.

Keywords: Frocini statistics, omega-square statistics, statistical tests, mixture of distributions.

ОЦЕНКА МЕТОДОМ СТАТИСТИЧЕСКИХ ИСПЫТАНИЙ СТАТИСТИКИ КРИТЕРИЕВ ФРОЦИНИ И ОМЕГА-КВАДРАТ ДЛЯ СМЕСИ НОРМАЛЬНЫХ РАСПРЕДЕЛЕНИЙ

С. В. Ушанов*, Д. А. Огурцов

Сибирский государственный университет науки и технологий имени академика М. Ф. Решетнева
Российская Федерация, 660037, г. Красноярск, просп. им. газ. «Красноярский рабочий», 31
*E-mail: ushanov_sv@mail.ru

Многие совокупности субъектов и объектов в биологии, промышленности, управлении можно условно разделить на ряд классов, каждому из которых соответствует определенная компонента смеси распределения. При анализе смеси распределений необходима оценка ее параметров (задача 1) и оценка соответствия эмпирической и теоретической функций распределения (задача 2).

Для решения первой задачи обычно применяют численные алгоритмы, реализующие метод моментов и метод максимального правдоподобия. В работе задача оценки параметров распределения решается минимизацией критерия согласия квазиньютоновским методом.

Вторая задача решается сравнением эмпирической и теоретической функций распределения одним или несколькими статистическими критериями согласия. Статистика распределения этих критериев зависит от объема выборки, способа формирования данных и оценки параметров распределения. В работе рассматриваются критерии согласия Фроцини и омега-квадрат (Крамера – Мизеса – Смирнова). Оценка статистики

критериев согласия проводилась методом имитационного моделирования по результатам 50000 статистических испытаний. В каждом из испытаний параметры распределения оценивались минимизацией расчетного значения соответствующего критерия согласия. Результаты имитационного моделирования позволяют оценить статистику параметров смеси распределений.

Представлены результаты решения рассмотренных задач для смеси двух нормальных распределений объемом 240.

Ключевые слова: статистика Фроцини, статистика омега-квадрат, статистические испытания, смесь распределений.

Introduction. One of the tasks of the initial processing of experimental observations is the choice of the distribution law, which adequately describes the random variable for the observed sample. A great number of sets of subjects and objects in biology, industry, management can be divided into a number of classes, each of which corresponds to a specific component of the distribution mix. In biological populations, it is possible to distinguish objects with average values of indicators, objects – indicators which are higher than average ("leaders") and objects – indicators that are lower than average ("outsiders") [1]. The dynamics of mass transfer processes of chemical technology depends on the size distribution of the raw materials, which is also determined by a mixture of distributions [2–4].

When analyzing a mixture of distributions, it is necessary to estimate its parameters (task 1) and to evaluate the compliance of empirical and theoretical distribution functions (task 2).

To solve the first problem, usually numerical algorithms are used that implement the method of moments [5] and the maximum likelihood method [6–8]. The peculiarity of this problem solution by the maximum likelihood method for a mixture of distributions is the presence of several local extrema. In this paper, the problem of estimating the distribution parameters is solved by minimizing the agreement criterion by Quasi-Newton methods in MathCad [9] and MATLAB [10] environments.

The second problem is solved by comparing the empirical and theoretical distribution functions by one or several statistical criteria of agreement [5; 11]. Statistics of the distribution of these criteria depends on the sample size, the method of forming data and estimating distribution parameters [12]. The paper examines the criteria of consent Frocini [13; 14]

$$\mathrm{Fr}(Xv, a) = \frac{1}{\sqrt{n}} \cdot \sum_{i=1}^{n} \left| F(Xv_i, a) - \frac{i - 0.5}{n} \right|,$$

and omega square (Kramer – Mises – Smirnov) [15; 16]

$$\mathrm{KMC}(Xv, a) = \frac{1}{12n} + \sum_{i=1}^{n} \left(F(Xv_i, a) - \frac{i - 0.5}{n} \right)^2,$$

where Xv – variational series of random variable X; n – sample size; i – number of the element of the variation series; a – distribution parameters; $F(Xv_i, a)$ – the value of the integral distribution function for the element of a variational series Xv_i.

The probability density function for a mixture of distributions consisting of K components has the form:

$$f(x, a, \mu) = \sum_{j=1}^{k} \mu_j \cdot f_j(x, a_j), \ \sum_{j=1}^{k} \mu_j = 1,$$

where x – random value; a, μ– distribution parameters; μ_j – the proportion of the j-th component in the mixture.

For a mixture of normal distributions, the probability density of the j-th component is determined by the expression

$$f_j(x, a_j) = \frac{1}{a_{j,0} \cdot \sqrt{2\pi}} \cdot \exp\left(-\frac{1}{2} \left(\frac{x - a_{j,0}}{a_{j,1}} \right)^2 \right),$$

where $a_{j,0}$, $a_{j,1}$ – estimates of expected value and standard deviation.

The computer approach developed in the works of B. Yu. Lemeshko makes it possible to evaluate the statistics of the compliance criteria when testing various complex hypotheses [10; 16].

When conducting statistical tests, it is necessary to take into account the repetition period of the generated pseudo-random numbers. In the MathCad system, this period for a generator of normally distributed random variables is $784.4 \cdot 10^6$ [17]. For sample size n = 1000, this allows to conduct $7 \cdot 10^5$ statistical tests. At the level of significance $\alpha \in [0.001; 0.999]$, the maximum error in estimating the statistics of the criteria under consideration does not exceed 0.0005 [14].

Results of computational experiments. The paper discusses the application of the Frocini criteria [18] and omega-square in estimating the distribution parameters for the analyzed sample by minimizing the calculated value of the corresponding criterion. In each computational experiment for evaluating the statistics of the compliance criteria, 50000 statistical tests were conducted.

In fig. 1 the experimental errors in determining the hydrodynamic quality of the whip beams with a limited buoyancy margin are shown [19] (sample size n = 240), in fig. 2 distribution functions that approximate the empirical data with a mixture of two normal distributions are presented; in tab. 1, estimates of distribution parameters obtained by minimizing the Frocini criterion and omega-square are presented.

The maximum deviation between the integral functions of the mixture of distributions, the parameters of which are obtained by minimizing the Frocini criteria and the omega-square is 0.001 for x = –0.13, and between the probability density functions is 0.0078 for x = 0.10.

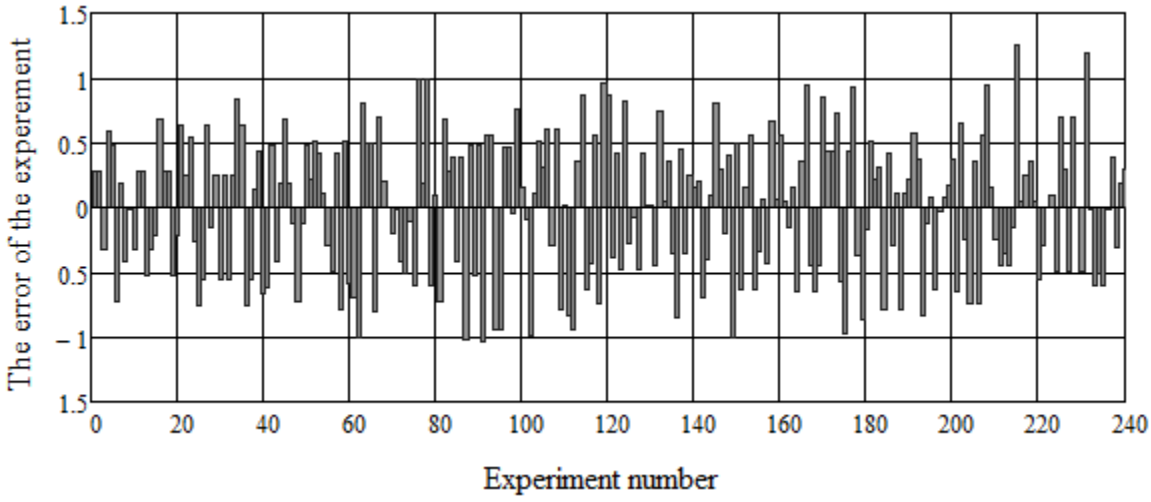

Fig. 1. Experimental errors in determining the hydrodynamic quality of whip beams with a limited buoyancy margin [19]

Рис. 1. Ошибки экспериментов при определении гидродинамического качества хлыстовых пучков с ограниченным запасом плавучести [19]

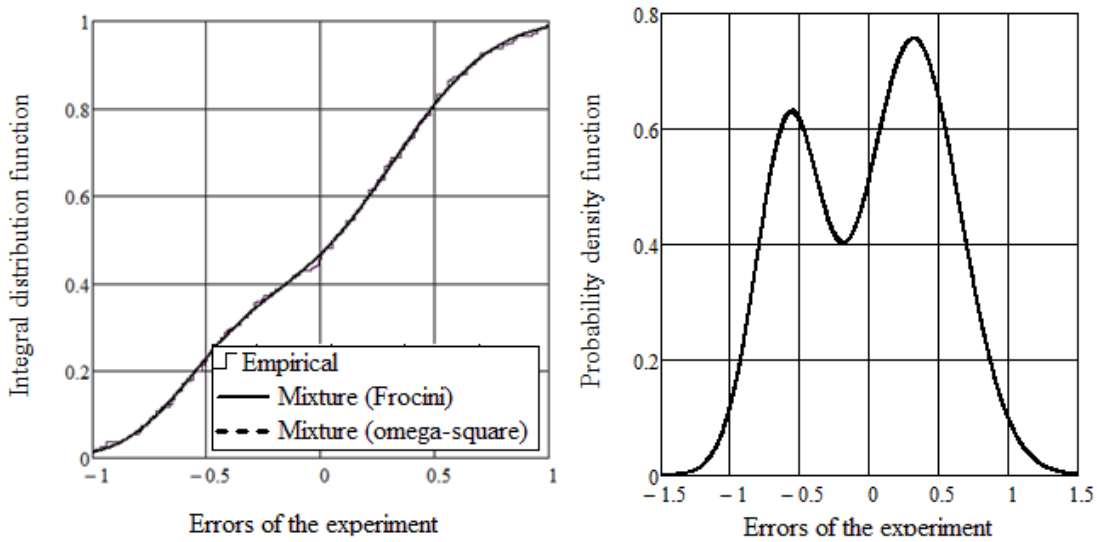

Fig. 2. Empirical and theoretical function of normal distributions mixture

Рис. 2. Эмпирическая и теоретическая функции смеси нормальных распределений

Table 1

The optimal values of the parameters of the mixture of distributions and their estimates obtained by statistical testing (M = 5000, n = 240) by minimizing the Frocini criterion and omega-square

Parameter		Optimal value	Expected value	Median	Borders of 95 % Confidence Interval	
					lower	upper
$a_{1.0}$	*	–0.574	–0.569	–0.575	–0.672	–0.437
	**	–0.576	–0.574	–0.580	–0.671	–0.450
$a_{1.1}{}^2$	*	0.0566	0.0588	0.0556	0.0279	0.112
	**	0.0549	0.0545	0.0510	0.0249	0.105
$a_{2.0}$	*	0.322	0.318	0.320	0.198	0.438
	**	0.318	0.317	0.318	0.199	0.434
$a_{2.1}{}^2$	*	0.104	0.119	0.116	0.067	0.191
	**	0.103	0.118	0.116	0.068	0.188
μ_1	*	0.361	0.367	0.366	0.243	0.514
	**	0.357	0.353	0.349	0.231	0.483

*Calculations by Frocini criterion; **calculations based on the omega-square test.

Table 2

Calculated and critical values of the Frocini and omega-square criteria for a mixture of 2 normal distributions with a sample size of n = 240

Goodness measure		Calculated values	Critical value at significance level α					
			0.05	0.10	0.15	0.20	0.25	0.30
Frocini	*	0.0776	0.146	0.136	0.130	0.125	0.121	0.118
	**	0.0785						
Omega-square	*	0.0104	0.0348	0.0301	0.0277	0.0257	0.0241	0.0229
	**	0.0102						

Distribution parameters obtained by minimizing the criteria: * Frocini; **omega-square.

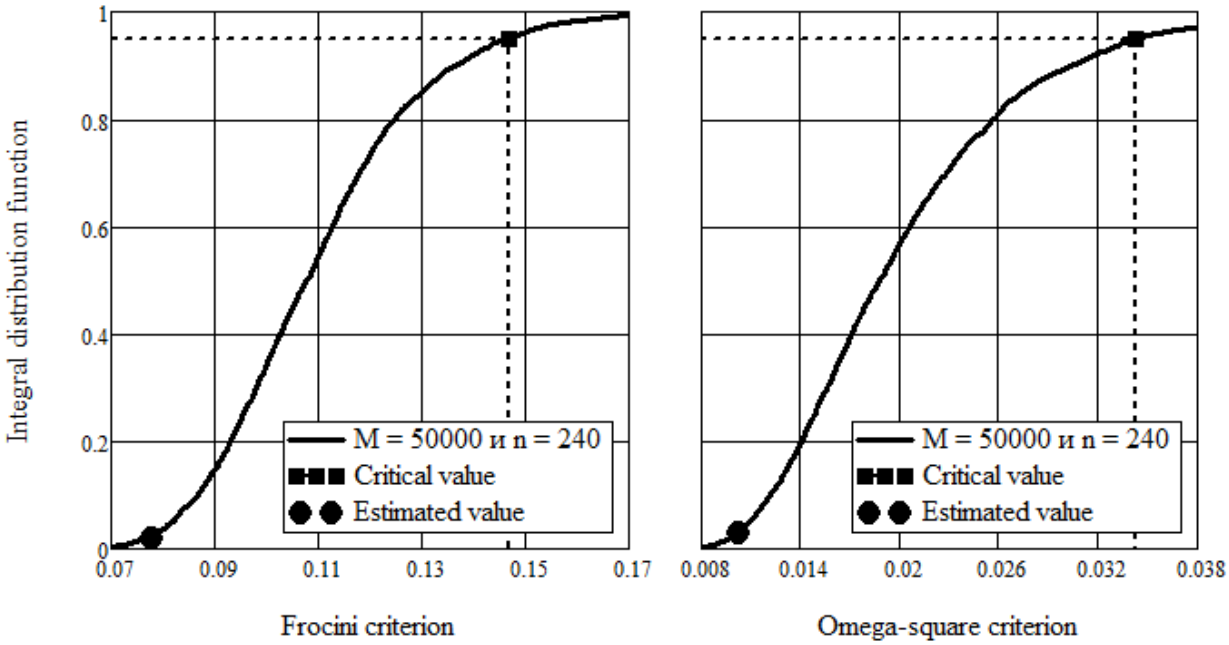

Fig. 3. The results of testing the hypothesis of compliance with the empirical distribution function and the mixture function of two normal distributions by Frocini and omega-square criteria

Рис. 3. Результаты проверки гипотезы соответствия эмпирической функции распределения и функции смеси двух нормальных распределений по критериям Фроцини и омега-квадрат

The calculated and critical values of the Frocini and omega-square criteria for a mixture of 2 normal distributions with a sample size of n = 240 are presented in tab. 2.

The visualization of the results of testing the hypothesis of compliance with the empirical distribution function with the mixture function of two normal distributions according to the Frocini and omega-square criteria is presented in fig. 3.

The simulation modeling results allow to evaluate the statistics of the parameters of the distributions mixture. In fig. 4–6 the results of the evaluation of the distribution of the parameters of the first and second components of the mixture, obtained from the results of statistical tests for the Frocini and omega-square agreement criteria, are presented.

Conclusion. The results of computational experiments allow to conclude about the effectiveness of obtaining estimates of distributions mixture parameters, minimizing the calculated values of the goodness measures. The use of different goodness measures allows improving the quality of the found estimates. The differences in the estimates of the parameters of the mixture of two normal distributions, obtained by minimizing the Frocini and omega-square criteria for experimental samples, did not exceed 1 %.

Evaluation of the distribution parameters in combination with the simulation method for evaluating the statistics of the goodness measure allows to test the complex hypothesis of consistency between the empirical and theoretical distribution functions. A related result of this task is an assessment of the statistics of the distribution parameters and confidence intervals of their change.

The choice of the minimum number of components of a distributions mixture is determined by the condition of accepting the hypothesis of compliance with the empirical and theoretical distribution functions.

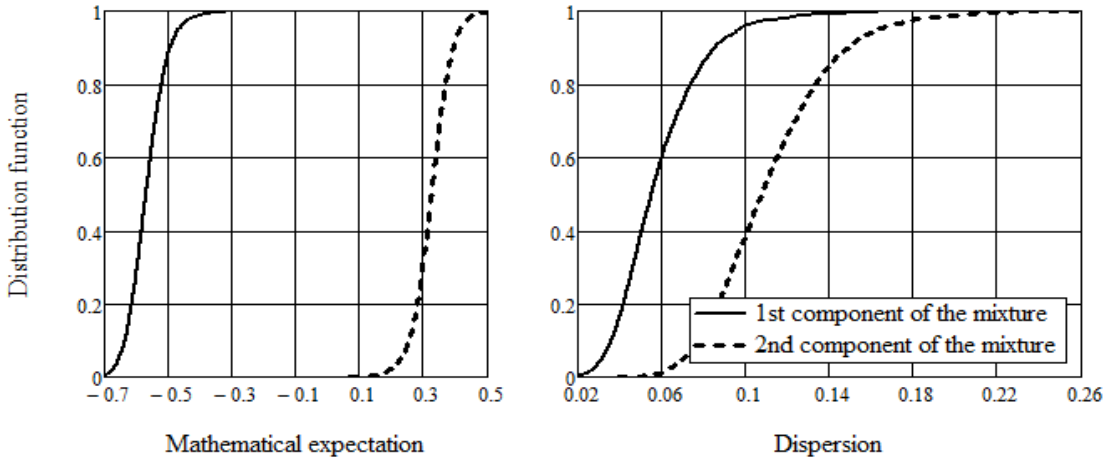

Fig. 4. Estimates of the distribution functions of expected values and dispersions of the mixture components

Рис. 4. Оценки функций распределения математических ожиданий и дисперсий компонентов смеси

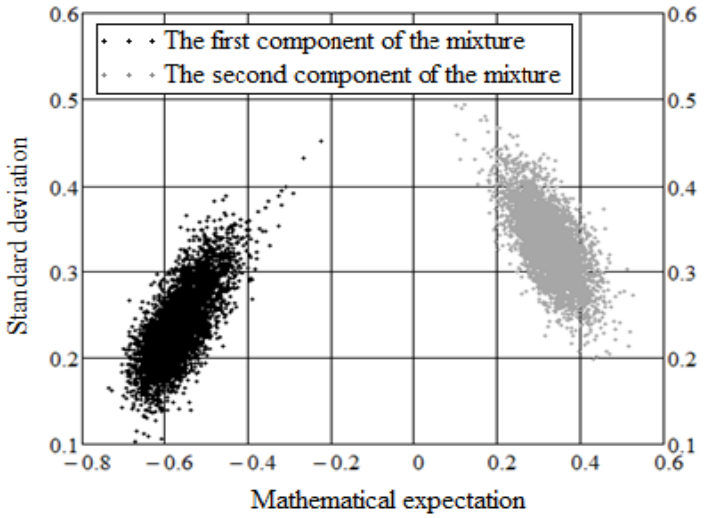

Fig. 5. Estimates of the distribution of the parameters of the first
and second components of the mixture

Рис. 5. Оценки распределения параметров первой и второй компоненты смеси

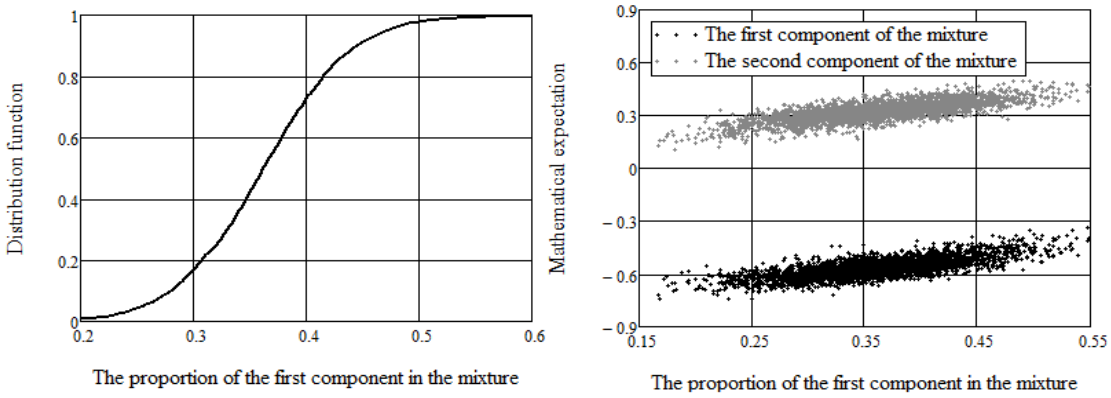

Fig. 6. Estimates of the distribution of the mathematical expectation of the first and the second components
and the proportion of the first component in the mixture

Рис. 6. Оценки распределения математических ожиданий первой и второй компоненты
и доли первой компоненты смеси

References

1. Pavlov I. N., Ushanov S. V. [Study of the distribution of trees by diameter analysis methods for mixtures of distributions]. *Vestnik SibGTU*. 2005, No. 1, P. 38–46 (In Russ.).

2. Ushanova V. M. *Kompleksnaia pererabotka drevesnoi zeleni i kory pikhty sibirskoi s polucheniem produktov, obladaiuhshikh biologicheskoi aktivnost'iu. Dokt. Dis.* [Complex processing of wood greens and Siberian fir bark to give products having biological activity. Doct. Dis.]. Krasnoiarsk, 2012, 34 p.

3. Ushanova V. M., Ushanov S. V. [Study of the process of extraction of fir bark by Siberian liquefied carbon dioxide]. *Vestnik Krasgau*. 2009, No. 12 (39), P. 39–44 (In Russ.).

4. Ushanova V. M., Ushanov S. V. *Ekstragirovaniye drevesnoy zeleni i kory pikhty sibirskoy szhizhennym dioksidom ugleroda i vodno-spirtovymi rastvorami* [Extraction of wood greens and Siberian fir bark with liquefied carbon dioxide and water-alcohol solutions]. Krasnoyarsk, 2009, 191 p.

5. Kobzar A. I. *Prikladnaya matematicheskaya statistika. Dlya inzhenerov i nauchnykh rabotnikov* [Applied mathematical statistics. For engineers and scientists]. Moscow, Fizmatlit Publ., 2006, 816 p.

6. Vetrov P. P., Kropotov D. A., Osokin A. A. [The automatic determination of the number of components in the mixture of normal distributions]. *Zhurnal vychislitel'noy matematiki i matematicheskoy fiziki*. 2010, Vol. 50, No. 4, P. 770–783 (In Russ.).

7. Korolev V. Yu. *EM-algoritm, yego modifikatsii i ikh primeneniye k zadache razdeleniya smesey veroyatnostnykh raspredeleniy. Teoreticheskiy obzor* [EM-algorithm, its modifications and their application to the problem of separation of probability distributions. Theoretical review]. Moscow, IPI RAN Publ., 2007, 102 p.

8. Celeux G., Chauveau D., Diebolt J. On Stochastic Versions of the EM algorithm: An Experimental study in the Mixture Case. *Journal of Statis. Comput. Simul.* 1996, Vol. 55, P. 287–314.

9. Ohorsin B. A. *Prikladnaya matematika v sisteme MathCad* [Applied Mathematics in the MathCad system]. Moscow, Lan' Publ., 2008, 352 p.

10. Goldstein A. M. *Optimizatsiya v srede MatLAB* [Optimization in MatLAB]. Perm, 2015, 192 p.

11. Lemeshko B. Yu, Lemeshko S. B., Postovalov S. N., Chimitov E. V. *Statisticheskiy analiz dannykh, modelirovaniye, issledovaniye veroyatnostnykh zakonomernostey. Komp'yuternyy podkhod* [Statistical data analysis, modeling, probabilistic regularities research. Computer approach]. Novosibirsk, NGTU Publ., 2011, 888 p.

12. Orlov A. I. [Non-parametric criteria for the agreement of Kolmogorov, Smirnov, omega-square and errors in their application]. *Nauchnyy zhurnal KubGAU*. 2014, No. 97 (03), P. 1–29 (In Russ.).

13. Frozini B. V. A survey of a class of goodness-of-fit statistics. *Metron*. 1978, Vol. 36, No. 1–2, P. 3–49.

14.Ogurtsov D. A., Ushanov S. V. [Evaluation of statistics of the criterion of the normality of the Frozini distribution by the method of statistical tests]. *Aktual'nyye problemy aviatsii i kosmonavtiki*. 2017, Vol. 2, No. 3, P. 290–292 (In Russ.).

15. Martynov G. V. *Kriterii omega-kvadrat* [Criteria omega square]. Moscow, Nauka Publ., 1978, 78 p.

16. Ogurtsov D. A., Ushanov S. V. [Evaluation of statistics on the normality of the distribution of the omega-square method of statistical tests]. *Aktual'nyye problemy aviatsii i kosmonavtiki*. 2017, Vol. 2, No. 3, P. 293–295 (In Russ.).

17. Lemeshko B. Yu. *Neparametricheskiye kriterii soglasiya. Rukovodstvo po primeneniyu* [Non-parametric compliance criteria. Application Guide]. Moscow, INFRA-M Publ., 2014, 163 p.

18. Ushanov S. V., Ogurtsov D. A. [Estimation of statistics of the criterion for the normality of the Frozini distribution using the statistical test method in MATHCAD]. *Reshetnevskiye chteniya.* 2018, Vol. 2. No. 22, P. 171–173 (In Russ.).

19. Zhuk A. Yu. [Hydrodynamic qualities of whip beams made of wood with a limited margin of buoyancy]. *Sistemy. Metody. Tekhnologii.* 2014, No. 4 (24), P. 160–165 (In Russ.).

Библиографические ссылки

1. Павлов И. Н., Ушанов С. В. Исследование распределения деревьев сосны по диаметру методами анализа смесей распределений // Вестник СибГТУ. 2005. № 1. С. 38–46.

2. Ушанова В. М. Комплексная переработка древесной зелени и коры пихты сибирской с получением продуктов, обладающих биологической активностью : автореф. дисс. … докт. тех. наук. Красноярск : СибГТУ, 2012. 34 с.

3. Ушанова В. М., Ушанов С. В. Исследование процесса экстрагирования коры пихты сибирской сжиженным диоксидом углерода // Вестник КрасГАУ. 2009. № 12 (39). С. 39–44.

4. Ушанова В. М., Ушанов С. В. Экстрагирование древесной зелени и коры пихты сибирской сжиженным диоксидом углерода и водно-спиртовыми растворами. Красноярск, 2009. 191 с.

5. Кобзарь А. И. Прикладная математическая статистика. Для инженеров и научных работников. М. : Физматлит, 2006. 816 с.

6. Ветров Д. П., Кропотов Д. А., Осокин А. А. Автоматическое определение количества компонент в EM-алгоритме восстановления смеси нормальных распределений // Журнал вычислительной математики и математической физики. 2010. Т. 50, № 4. С. 770–783.

7. Королёв В. Ю. EM-алгоритм, его модификации и их применение к задаче разделения смесей вероятностных распределений. Теоретический обзор. М. : ИПИРАН, 2007. 102 с.

8. Celeux G., Chauveau D., Diebolt J. On Stochastic Versions of the EM algorithm // An Experimental study in the Mixture Case, Journal of Statis. Comput. Simul. 1996, Vol. 55, P. 287–314.

9. Охорзин В. А. Прикладная математика в системе MathCad. М. : Лань, 2008. 352 с.

10. Гольдштейн А. М. Оптимизация в среде MatLAB. Пермь, 2015. 192 с.

11. Статистический анализ данных, моделирование, исследование вероятностных закономерностей. Компьютерный подход : монография / Б. Ю. Лемешко, С. Б. Лемешко, С. Н. Постовалов [и др.]. Новосибирск : Изд-воНГТУ, 2011. 888 с.

12. Орлов А. И. Непараметрические критерии согласия Колмогорова, Смирнова, омега-квадрат и ошибки при их применении // Научный журнал КубГАУ. 2014. № 97 (03). С. 1–29.

13. Frozini B. V. A survey of a class of goodness-of-fit statistics, Metron. 1978. Vol. 36, № 1–2. P. 3–49.

14. Огурцов Д. А., Ушанов С. В. Оценка статистики критерия нормальности распределения Фроцини методом статистических испытаний // Актуальные проблемы авиации и космонавтики. 2017. Т. 2, № 3. С. 290–292.

15. Мартынов Г. В. Критерии омега-квадрат. М. : Наука, 1978. 78 с.

16. Огурцов Д. А., Ушанов С. В. Оценка статистики критерия нормальности распределения омега-квадрат методом статистических испытаний // Актуальные проблемы авиации и космонавтики. 2017. Т. 2, № 3. С. 293–295.

17. Лемешко Б. Ю. Непараметрические критерии согласия. Руководство по применению. М. : Инфра-М, 2014. 163 с.

18. Ушанов С. В., Огурцов Д. А. Оценка статистики критерия нормальности распределения Фроцини методом статистических испытаний в MATHCAD // Решетневские чтения. 2018. Т. 2, № 22. С. 171–173.

19. Жук А. Ю. Гидродинамические качества хлыстовых пучков из древесины с ограниченным запасом плавучести // Системы. Методы. Технологии. 2014. № 4 (24). С. 160–165.

Ushanov Sergey Viktorovich – Cand. Sc., Associate Professor, Head of the Department of Higher Mathematics and Computer Science; Reshetnev Siberian State University of Science and Technology. E-mail: ushanov_sv@mail.ru.

Ogurtsov Dmitrii Aleksandrovich – student of group 23-7 of the Institute of Informatics and Telecommunications; Reshetnev Siberian State University of Science and Technology. E-mail:dim_ogu@mail.ru.

Ушанов Сергей Викторович – кандидат технических наук, доцент, заведующий кафедрой высшей математики и информатики; Сибирский государственный университет науки и технологий имени академика М. Ф. Решетнева. E-mail:ushanov_sv@mail.ru.

Огурцов Дмитрий Александрович – студент группы 23-7; Инстут информатики и телекоммуникаций; Сибирский государственный университет науки и технологий имени академика М. Ф. Решетнева. E-mail:dim_ogu@mail.ru.

UDC 004.054
Doi: 10.31772/2587-6066-2019-20-1-35-39

For citation: Yakimov I. A., Kuznetsov A. S., Skripachev A. M. [Optimizing the readability of tests generated by symbolic execution]. *Siberian Journal of Science and Technology.* 2019, Vol. 20, No. 1, P. 35–39. Doi: 10.31772/2587-6066-2019-20-1-35-39

Для цитирования: Якимов И. А., Кузнецов А. С., Скрипачев А. М. Оптимизация читаемости порождаемых при символьных вычислениях тестов // Сибирский журнал науки и технологий. 2019. Т. 20, № 1. С. 35–39. Doi: 10.31772/2587-6066-2019-20-1-35-39

OPTIMIZING THE READABILITY OF TESTS GENERATED BY SYMBOLIC EXECUTION

I. A. Yakimov*, A. S. Kuznetsov, A. M. Skripachev

Siberian Federal University
79/10, Svobodnyy Av., Krasnoyarsk, 660041, Russian Federation
*E-mail: ivan.yakimov.research@yandex.ru

Taking up about half of the development time, testing remains the most common method of software quality control and its disadvantage can lead to financial losses. With a systematic approach, the test suite is considered to be complete if it provides a certain amount of code coverage. At the moment there are a large number of systematic test generators aimed at finding standard errors. Such tools generate a huge number of difficult-to-read tests that require human verification which is very expensive. The method presented in this paper allows improving the readability of tests that are automatically generated using symbolic execution, providing a qualitative reduction in the cost of verification. Experimental studies of the test generator, including this method as the final phase of the work, were conducted on 12 string functions from the Linux repository. The assessment of the readability of the lines contained in the optimized tests is comparable to the case of using words of a natural language, which has a positive effect on the process of verification of test results by humans.

Keywords: dynamic symbolic execution, natural language model, the problem of tests verification by humans.

ОПТИМИЗАЦИЯ ЧИТАЕМОСТИ ПОРОЖДАЕМЫХ ПРИ СИМВОЛЬНЫХ ВЫЧИСЛЕНИЯХ ТЕСТОВ

И. А. Якимов*, А. С. Кузнецов, А. М. Скрипачев

Сибирский федеральный университет
Российская Федерация, 660041, г. Красноярск, просп. Свободный, 79/10
*E-mail: ivan.yakimov.research@yandex.ru

Занимая около половины времени разработки, тестирование остается наиболее распространенным методом контроля качества программного обеспечения (ПО). Его недостаток может приводить к финансовым потерям. При систематическом подходе тестовый набор считается полным, если он обеспечивает определенное покрытие кода. На данный момент существует большое количество систематических генераторов тестов, направленных на поиск стандартных ошибок. Подобные инструменты порождают огромное количество трудночитаемых тестов, обладающих высокой ценой проверки человеком. Представленный в данной работе метод позволяет улучшить читаемость тестов, автоматически сгенерированных при помощи символьных вычислений, и обеспечивает качественное снижение данной цены. Экспериментальные исследования генератора тестов, включающего данный метод в качестве заключительной фазы работы, были проведены на 12-строковых функциях из репозитория Linux. Оценка степени читаемости строк, содержащихся в оптимизированных тестах, сопоставима со случаем использования слов натурального языка, что положительно сказывается на процессе верификации результатов тестирования человеком.

Ключевые слова: динамические символьные вычисления, модель естественного языка, проблема проверки тестов человеком.

Introduction. On the one hand**,** modern software systems tend to be highly complicated and expensive in development. On the other hand, software development itself is a time-consuming and error-prone process. It is very important to find serious errors before they cause any damage. Thus, in order to help developers in finding errors some bug searching methods have been developed. Software testing is one of the most popular bug searching methods. However, it is a time-consuming task that takes about a half of the development time. In order to reduce

the time expenditures associated with testing several test automation techniques have been proposed.

One of the most popular approaches to the test automation is a code-based test generation [1; 2]. Some systematic code-based test generation techniques have been developed for the last few decades. Two of them are: Search-Based Software Testing (SBST) and Dynamic Symbolic Execution (DSE). Any systematic test generation method relies on some sort of a code coverage metric. Only test data with appropriate code coverage is considered to be adequate. In order to provide required code coverage a coverage criterion needs to be defined. The popular coverage criteria are: instruction-coverage and branch-coverage. Both DSE and SBST are aimed to provide systematic code coverage for a target program.

In order to generate test cases with SBST-based tool the goal of testing needs to be defined in terms of fitness (objective) function [3]. It is convenient to use a branch coverage criterion as a goal of testing when using SBST. SBST-based tools launch target programs on some random input data. The program alternates the input data in an iterative way optimizing the value of the fitness function. Only when the fitness function is optimized the goal of testing is achieved. Final input data represents the desired test case.

DSE-based [4–6] tools maintain symbolic state in addition to the concrete (usual) state of the target program. During the execution of a target program it collects constraints on the program variables. This constraint system is called a path constraint or a PC. A PC represents an equivalence class of input data that leads the target program through the corresponding path. The execution of the target program forks on each decision point (for example conditional operator if-else) providing branch coverage. When the execution of the target program is completed, appropriate test input data can be obtained by solving the PC.

In general, code-based test generators tend to produce lots of almost unreadable test data. It is hard to verify such unreadable test data manually. This problem is called the Human Oracle Cost Problem [7]. Afshan et al. [8] proposed a method of improving readability of test cases produced by SBST-based tools. They used a character-level bigram model of a natural language to drive the search process toward more readable results. In order to do this, they added readability estimation of the target test data into the fitness function.

A character-level bigram model of a natural language is defined in terms of ordered pairs of characters, i. e. bigrams. Let (c_i, c_{i-1}) be a bigram, then $P(c_i \mid c_{i-1})$ is a probability of co-occurrence of c_i and c_{i-1}, in the language corpus, where the language corpus is a large collection of written texts. Let also $P\left(c_1^n\right)$ be a probability of belonging the whole string c_1^n of length n to the language corpus. The bigram model estimates probability $P\left(c_1^n\right)$ as shown in the equation below:

$$\hat{P}\left(c_1^n\right) \approx \prod_{i=1}^{n} P\left(c_i \mid c_{i-1}\right)$$

In order to compare strings of different length $\hat{P}$ has to be normalized always. Readability estimation N is defined as a normalized value of $\hat{P}$ as shown in equation below:

$$N\left(c_1^n\right) = \hat{P}\left(c_1^n\right)^{1/n}.$$

This work proposes a new method for improving readability of test data generated by DSE-based tools. In contrast to the work of Afshan et al. [8] we do not rely on any kind of fitness function. The improvement process is performed by changing a PC after the execution of the target progrem. To the best of our knowledge this is the first readability optimization method in context of the DSE.

Methods. The workflow of the proposed system includes two main stages. At the first stage, the system produces a path constraint PC, which is an abstract representation of a program state. At the second stage, the system optimizes readability of the PC constraining it with the help of a character-level bigram model. As mentioned above, every PC represents an equivalence class of some test inputs and is associated with a single program path. Some of those inputs might be more "readable" than the others. Informally speaking, the goal of the algorithm is to find "the most readable" input within the set of all possible inputs corresponding to the given PC.

Example. Let us first provide an example of the readability optimization process. Let us say we have a strlen as a target function. It takes a null-terminated string S = {'a1', a2, a3, '\0'} as an input, where eash a_i is a symbolic value and '\0' is a "concrete" terminator. The initial state of the program is represented in figure, *a*. The optimizer concretizes S transforming it into the string "yes\0". Firstly, the algorithm tries to make each a_i printable as shown in figure, *b*. Secondly, it attempts to make all of the *a-s* alphabetic as shown in figure, *c*. Finally, it attempts to rearrange a_s in an appropriate order using the bigram model. Results are shown in figure, *d.*

Memory graph. The optimizer operates on a memory graph M [9] which is an internal representation of the test data. Each node of M belongs to one of the following types: scalar (concrete or symbolic) value (*a*); concrete pointer to another node (*b*); array of nodes of a concrete length (*c*). Actually, every string S within M is represented as an array of scalar nodes.

Formal definition. A pseudocode of the algorithm is represented in Algorithm 1. The goal of the optimizer is to maximize the value of readability estimation S (N) for every string S within M. Thus, the optimizer considers only strings within M. It never violates the current PC and never changes concrete values that PC contains. The optimizer is only allowed to put constraints on symbolic values when it is safe. At the first step, it tries to make each symbolic value within S to be "alphabetic" or at least "printable". After that, it uses a bigram model in order to make the whole string being more like a "real word". During this process, every single string S within M is transformed in the following way.

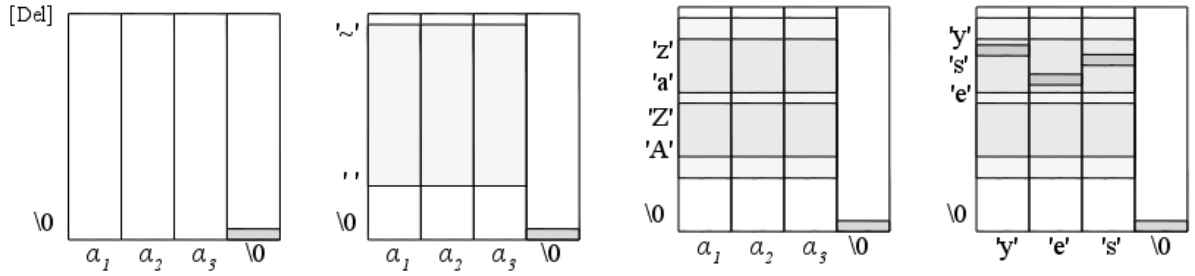

a *b* *c* *d*

An example of a readability optimization algorithm work

Пример работы алгоритма по оптимизации читаемости

1. **Narrowing.** At this stage the optimizer tries to increase the readability of every symbolic character a_i within S:

– Firstly, it tries to make each a_i printable constraining it with (' ' $\le a_i \le$ '~');

– If it is successful, it then tries to make it alphabetical applying additional constraint ('A' $\le a_i \le$ 'Z' $\vee$ 'a' $\le \le a_i \le$ 'z').

2. **Concretization.** At the beginning, the optimizer focuses on the first value a_1 of the current string S. If it is possible, it tries to "assign" a random alphabetic value to the a_1 constraining it with (a_1 = *some random alphabetic character*). At the next step, the optimizer traverses through all the bigrams (a_i, a_{i+1}), where $i = 1 \ldots n - 1$, within string S. Let (a_i , a_{i+1}) be the current bigram, then:

– Firstly, the optimizer takes a concrete value of a_i. Note that if a_i is symbolic the optimizer calls the SMT-solver for its value.

– Secondly, if a_{i+1} is a symbolic value the optimizer tries to obtain the "most probable" value *val* of a_{i+1} in terms of the bigram model. If it is successful, it than attempts to apply the (a_{i+1} = *val*) constraint to a_{i+1}.

Algorithm 1 Improving readability

```
1: procedure Narrowing (Memory graph M)
2:   for all s ∈ M do
3:     if s is a string of length n then
4:       for all i ∈ {1, 2,..., n} do
5:         printable → Probe ((' ' ≤ a_i ≤ '~'))
6:         if printable = true then
7:           Probe ((('A' ≤ a_i ≤ 'Z') ∨ ('a' ≤ a_i ≤ 'z')))
8:         end if
9:       end for
10:    end if
11:  end for
12: end procedure
13: procedure Concretization (Memory graph M)
14:  for all s ∈ M do
15:    if s is a string of length n then
16:      if a_1 is symbolic then
17:        alpha ← random alphabetic character
18:        Probe ((a_1 = alpha))
19:      end if
20:      for all i ∈ {1, 2,..., n − 1} do
21:        fst ← Value (a_i)
22:        if fst is alphabetic ∧ a_{i+1} is symbolic then
23:          snd ← Next (fst)
24:          Probe (( a_{i+1} = snd))
25:        end if
26:      end for
27:    end if
28:  end for
29: end procedure
30: function Value (Scalar node a of memory graph M)
31:   if a contains concrete value then
32:     return value of a
33:   else if a contains symbolic value then
34:     Ask external SMT-solver for value of a
35:     return value returned by SMT-solver
36:   end if
37: end function
38: function Probe (Constraint e)
39:   Push a new scope into internal stack of SMT-solver
40:   PC' ← PC ∧ e
41:   if PC' is satisfiable then
42:     PC ← PC'
43:     return true
44:   else
45:     Pop the scope from internal stack of SMT-solver
46:     return false
47:   end if
48: end function
49: function Next (ASCII symbol a)
50:   b ← most probable symbol in bigram (a, b)
51:   return b
52: end function
```

Conservativeness of the algorithm. Each optimized test case leads a target program through the same path as a corresponding non-optimized version. Before applying new constraints to the current PC, the optimizer tries applying it in a fresh new scope of an external SMT-solver. If it fails, the optimizer safely pops the scope out of the stack rolling the PC back to its previous version. Only in case when the new constraint does not violate the current PC, the optimizer is allowed to apply it.

Results. In order to test the proposed system we have implemented a tool on top of the LLVM compiler infrastructure [10] and CVC4 [11] SMT-solver. We have also used a bigram model based on very large language corpora [12]. Note that before starting to work with the system a user should write a simple driver in the C-language.

Experimental results

Function	Input	Coverage	None	Basic	Bigram
strlen	[6]	5:100%	–	0.08	0.10
strnlen	[6]5	6:100%	–	0.08	0.10
strcmp	[6][6]	15:100%	–	0.04	0.05
strncmp	[6][6]5	16:100%	–	0.04	0.05
sysfs_streq	[6][6]	39:100%	–	0.05	0.07
strcpy	[6][6]	35:100%	–	0.08	0.10
strncpy	[6][6]5	36:100%	–	0.08	0.10
strcat	[10][5]	40:100%	–	0.07	0.08
strncat	[10][5]4	41:100%	–	0.07	0.08
strstr	[6][3]	19:90%	–	0.12	0.14
strnstr	[6][3]2	4:80%	–	0.09	0.10
strpbrk	[6][6]	10:80%	–	0.03	0.03

The system has been tested on 12 string-processing functions from the Linux [13] repository. Each function takes integer values and strings as an input. Experimental results are represented in table. The Input column displays an encoded format of the input data. Here notation "[n]" = $\{a_1, a_2,...,a_{n-1},'\backslash 0'\}$ represents a null-terminated string of symbolic values a_i; k represents some concrete integer. For example, strnlen "[6] 5" means that strnlen takes a single symbolic string of size 6 and an integer literal "5". The only exception is strpbrk function that takes concrete string "aeouy" as its second argument. Code coverage estimated with gcov tool is displayed in column *Coverage* in format x:y %, where x is a number of generated test cases and y is a percentage of covered instructions. Columns *None*, *Basic* and *Bigram* display average values of readability estimation N for test data generated during different experiments.

Experimental results. The results of test generation without optimization are displayed in column *None*. As the non-optimized data includes no alphabetic characters, the readability estimation is not defined in this case. The *Basic* method involves only the first, *Narrowing* phase of the optimization process. In this case, readability estimation $N \approx 0.07$ in average with standard deviation $\sigma = 0.03$. On the other hand, the *Bigram* method involves both, *Narrowing* and *Concretization* phases of the optimization. In case of *Bigram* $N \approx 0.08$ in average and $\sigma = 0.03$. Thus, the *Bigram* method shows the best results in this experimental study.

Discussion. Let us discuss the experimental results in more details on the example of the strcpy function. Strcpy function takes two string arguments - buffer A and source B. It copies data from B to A modifying A. It then returns the pointer to the modified version of A represented as A'. Thus, the format of each generated test case is (A, B) => A'. In order to give meaning to the discussion, let us suppose that the generated test cases have to be verified by a human.

Each non-optimized output contains no printable characters. Thus, we represent generated data as arrays of 8-bit integers. In this case, the real data generated with the help of CVC4 looks like: {1, 1, 1, 1, 1, 0}, {1, 1, 1, 0, 0, 0} => {1, 1, 1, 0, 0, 0}. Making sense of this data might be confusing to anyone trying to evaluate the quality of the implementation of the strcpy function. On the other hand, the so-colled Bigram method produces well-readable and less-confusing data: ("kesth", "pre") => "pre".

Configuring the optimizer. The optimizer can be configured in many ways. If the first symbol of the string is not constrained, then external SMT-solver tends to return similar results for all strings. As a consequence, without randomization of the first symbol the results look like "athes", "ath" => "ath" etc. Moreover, as the Bigram method uses the most probable values of the second characters of each bigram sometimes it tends to produce cycles like "athesthes...." etc. In order to avoid such cycles, we use the same selection algorithm as the "roulette wheel" method [14].

In addition to the bigram-based improving readability optimization we have implemented a simple "optimizer" for numeric values. In fact, numeric values generated by SMT-solvers tend to vary in a very wide range. For example, let us suppose we are testing some implementation of the quicksort algorithm. One of the generated test cases might look like: {22773760, 22773760, −2147483648, 2147483584} 4 => {−2147483648, 22773760, 22773760, 2147483584}. It is highly confusing to anyone who is trying to make a meaningful interpretation of such an unreadable test data. The optimizer incrementally tries to constraint each integer symbolic value within a memory graph M using Probe method from Algorithm 1. Let a_i be a symbolic integer contained by M. At first, the optimizer tries to apply the constraint ($-10 \le a_i \le 10$) to each a_i. If it is not successful it then tries to apply ($-100 \le a_i \le 100$) etc. The optimized version of the test case mentioned before looks like: {2, 2, −3, 5} 4 => {−3, 2, 2, 5}.

Reliability. In fact, the readability estimation of strings of different length varies in a wide range. The value of "pure" readability estimation $\hat{P}(S)$ tends to zero for very long strings. As a result, it is not reliable to compare the readability estimation of strings of different length. This negative effect is eliminated by normalization. We should further note that the goal of our research does not include the examination of the bigram model itself. However, in order to verify the readability estimation method used in the experimental study we tested it in isolation. We have tested this method using a list of Top-100 English words. The resulting readability estimation is 0, 10 which is compatible with the experimental results. Finally, the reliability of the experimental results achieved by any

code-based test generator depends on the provided code coverage. In the given experiments the instruction coverage is 95% in average and it is 100 % for 9 functions. In case of functions with non-100 % coverage the NULL-returning branch is not covered. We can confidently say that the obtained results are reliable enough.

Conclusions. This work introduces a new method of readability optimization in context of Dynamic Symbolic Execution based on a natural language model. This method has been successfully examined against 12 string-processing functions from the Linux repository. The experimental results show that this algorithm significantly improves the readability of automatically-generated test data. The readability of the optimized test cases is compatible to the readability of human-written texts. Developers who manually verify generated test data would take advantage of using this method.

References

1. Anand S., Burke E. K., Tsong Yueh Chen et al. An Orchestrated Survey of Methodologies for Automated Software Test Case Generation. *Journal of Systems and Software*. 2013, Vol. 86, No. 8, P. 1978–2001. Doi: 10.1016/j.jss.2013.02.061.

2. Cadar C., Godefroid P., Khurshid S. et al. Symbolic Execution for Software Testing in Practice: Preliminary Assessment. *Proceedings of the 33rd International Conference on Software Engineering (ICSE '11)*. ACM, New York, 2011, P. 1066–1071. Doi: 10.1145/1985793.1985995.

3. Tracey N., Clark J., Mander K. et al. An automated framework for structural test-data generation. *Proceedings of the 13th IEEE International Conference on Automated Software Engineering*. 1998, P. 285–288. Doi: 10.1109/ASE.1998.732680.

4. Cadar C., Ganesh V., Pawlowski P. M. et al. EXE: Automatically Generating Inputs of Death. *Proceedings of the 13th ACM Conference on Computer and Communications Security (CCS '06)*. ACM, New York, 2006, P. 322–335. Doi: 10.1145/1180405.1180445.

5. Godefroid P., Klarlund N., Sen K. DART: Directed Automated Random Testing. *Proceedings of the 2005 ACM SIGPLAN conference on Programming language design and implementation*. 2015, P. 213–223. Doi: 10.1145/1064978.1065036.

6. King J. C. Symbolic Execution and Program Testing. *Communications of the ACM*. 1976, Vol. 19, No. 7, P. 385–394. Doi: 10.1145/360248.360252.

7. Barr E. T., Harman M., McMinn P. et al. The Oracle Problem in Software Testing: A Survey. *IEEE Transactions on Software Engineering*. 2015, Vol. 41, No. 5, P. 507–525. Doi: 10.1109/TSE.2014.2372785.

8. Afshan S., McMinn P., Stevenson M. Evolving Readable String Test Inputs Using a Natural Language Model to Reduce Human Oracle Cost. *IEEE the 6th International Conference on Software Testing, Verification and Validation*. 2013, P. 352–361. Doi: 10.1109/ICST.2013.11.

9. Sen K., Marinov D., Agha G. CUTE: A Concolic Unit Testing Engine for C. *Proceedings of the 10th European software engineering conference held jointly with 13th ACM SIGSOFT international symposium on Foundations of software engineering (ESEC/FSE-13)*. 2005, P. 263–272. Doi: 10.1145/1095430.1081750.

10. Lattner C., Adve V. LLVM: A Compilation Framework for Lifelong Program Analysis & Transformation. *Proceedings of the International Symposium on Code Generation and Optimization: Feedback-directed and Runtime Optimization (CGO '04)*. IEEE Computer Society, Washington, 2004, P. 75.

11. Barrett C., Conway C. L., Deters M. et al. CVC4. *Proceedings of the 23rd International Conference on Computer Aided Verification (CAV'11)*. Springer-Verlag, Berlin, Heidelberg, 2011, P. 171–177.

12. Jones M. N., Mewhort D. J. K. Case-sensitive letter and bigram frequency counts from large-scale English corpora. *Behavior Research Methods, Instruments and Computers*. 2004, Vol. 36, No. 3, P. 388–996.

13. Linus Torvalds et al. Linux kernel source tree. Available at: https://github.com/torvalds/linux (accessed: 20.11.2018).

14. Lipowski A., Lipowska D. Roulette-wheel selection via stochastic acceptance. *Physica A: Statistical Mechanics and its Applications*. 2012, Vol. 391, No. 6, P. 2193–2196. Doi: 10.1016/j.physa.2011.12.004.

Yakimov Ivan Aleksandrovich – Senior lecturer; Institute of space and informational technologies, Siberian Federal University. E-mail: ivan.yakimov.research@yandex.ru.

Kuznetsov Aleksandr Sergeevich – Cand. Sc., Assistant professor; Institute of space and informational technologies, Siberian Federal University. E-mail: ASKuznetsov@sfu-kras.ru

Skripachev Anton Mikhailovich – Master's degree student; Institute of space and informational technologies, Siberian Federal University. E-mail: skram@list.ru.

Якимов Иван Александрович – старший преподаватель; Институт космических и информационных технологий, Сибирский федеральный университет. E-mail: ivan.yakimov.research@yandex.ru.

Кузнецов Александр Сергеевич – кандидат технических наук, доцент; Институт космических и информационных технологий, Сибирский федеральный университет. E-mail: ASKuznetsov@sfu-kras.ru.

Скрипачев Антон Михайлович – магистрант; Институт космических и информационных технологий, Сибирский федеральный университет. E-mail: skram@list.ru.

Раздел
Part
2

АВИАЦИОННАЯ И РАКЕТНО-КОСМИЧЕСКАЯ ТЕХНИКА

AVIATION AND SPACECRAFT ENGINEERING

UDC 629.8
Doi: 10.31772/2587-6066-2019-20-1-42-53

For citation: Birukov V. I., Nazarov V. P., Kurguzov A. V. [Estimation of the efficiency of spacecraft transportation with minimal radiation degradation of solar cells]. *Siberian Journal of Science and Technology.* 2019, Vol. 20, No. 1, P. 42–53. Doi: 10.31772/2587-6066-2019-20-1-42-53

Для цитирования: Бирюков В. И., Назаров В. П., Кургузов А. В. Оценка эффективности транспортировки космических аппаратов с минимальной радиационной деградацией солнечных фотоэлементов // Сибирский журнал науки и технологий. 2019. Т. 20, № 1. С. 42–53. Doi: 10.31772/2587-6066-2019-20-1-42-53

ESTIMATION OF THE EFFICIENCY OF SPACECRAFT TRANSPORTATION WITH MINIMAL RADIATION DEGRADATION OF SOLAR CELLS

V. I. Birukov[1], V. P. Nazarov[*2], A. V. Kurguzov[1]

[1]Moscow Aviation Institute (National Research University)
4, Volokolamskoe highway, A-80, GSP-3, 125993, Moscow, Russian Federation
[2] Reshetnev Siberian State University of Science and Technology
31, Krasnoyarsky Rabochy Av., Krasnoyarsk, 660037, Russian Federation
*E-mail: nazarov@sibsau.ru

Transport operations that ensure the change of the orbit of a spacecraft or its transfer to the departure trajectory are an integral part of almost all space missions. Increasing requirements for the efficiency of transporting spacecraft form the need to search for possible ways to increase this efficiency and assess the characteristics associated with the proposed methods.

Current boosters and interorbital tugs, as a rule, use a chemically powered cruise engine, although solutions with the use of an electric jet engine are becoming more common. Due to the high rate of the outflow of working fluid which is much higher than that of combustion products in a chemical engine, the efficiency of use of the substance mass by an electric jet engine significantly exceeds this indicator for a chemical engine. However, the low thrust provided by the electric jet engine leads to high duration of the transport operation and, as a result, to considerable time of exposure to the outer space factors, in particular, radiation. Therefore, the use of the electric jet engine only does not always meet the requirements for the mission.

One of the promising ways to increase the efficiency of transport operations is the combination of the traditional chemical and electric jet engines in the propulsion system. Various aspects of the use of such an integrated propulsion system (IPS) consisting of a solar electric jet system and "Fregat" booster were considered, for example, in the framework of "Dvina TM" research project.

Unlike a chemical engine, in which energy is released from chemical bonds, the energy for accelerating the working fluid by an electric jet engine is supplied from outside. Solar batteries are the most widespread energy source in near-earth orbits, where the amount of solar radiation is sufficient to meet the energy needs of a spacecraft. Solar batteries are sensitive to radiation, damage accumulates in their internal structure and their characteristics degrade. Therefore, there is a need to account for the radiation dose accumulated during the execution of the transport operation and to evaluate the reduction in the efficiency of solar batteries. Uneven irradiation intensity in the radiation belts formed by the Earth's magnetic field (Van Allen belts) can be taken into account if the assessment of the radiation intensity at the trajectory points of the maneuver is made using the Earth radiation belt model.

The paper proposes a method that allows taking into account the effect of ionizing radiation on the degradation of solar batteries when performing a transport operation using an integrated propulsion system based on a liquid-propellant rocket engine and an electric jet engine, taking into account the chosen trajectory and the model of the Earth's radiation belt.

Keywords: integrated propulsion system, electric jet engine, Van-Allen radiation belt, solar battery, degradation.

ОЦЕНКА ЭФФЕКТИВНОСТИ ТРАНСПОРТИРОВКИ КОСМИЧЕСКИХ АППАРАТОВ С МИНИМАЛЬНОЙ РАДИАЦИОННОЙ ДЕГРАДАЦИЕЙ СОЛНЕЧНЫХ ФОТОЭЛЕМЕНТОВ

В. И. Бирюков[1], В. П. Назаров[*2], А. В. Кургузов[1]

[1]Московский авиационный институт (национальный исследовательский университет)
Российская Федерация, 125993, г. Москва, А-80, ГСП-3, Волоколамское шоссе, 4
[2]Сибирский государственный университет науки и технологий имени академика М. Ф. Решетнева
Российская Федерация, 660037, просп. им. газ. «Красноярский рабочий», 31
[*]E-mail: nazarov@sibsau.ru

Неотъемлемой составляющей практически всех космических миссий являются транспортные операции, обеспечивающие изменение орбиты космического аппарата или перевод его на отлетную траекторию. Повышающиеся требования к эффективности транспортировки космических аппаратов формируют потребность в поиске возможных способов ее увеличения и оценке характеристик, сопутствующих предлагаемым способам.

Применяемые в настоящее время разгонные блоки и межорбитальные буксиры, как правило, используют маршевый двигатель на химическом топливе, хотя все чаще встречаются решения с применением электроракетного двигателя. Благодаря высокой скорости истечения рабочего тела, значительно превышающей скорость истечения продуктов горения в химическом двигателе, эффективность использования массы вещества электроракетным двигателем значительно превышает этот показатель для химического двигателя. Однако малая тяга, обеспечиваемая электроракетным двигателем, приводит к высокой длительности транспортной операции и, как следствие, к значительному времени воздействия факторов космического пространства, в частности, радиационного излучения, поэтому применение только электроракетного двигателя не всегда удовлетворяет требованиям к миссии.

Одним из перспективных направлений повышения эффективности транспортных операций является комбинирование в составе двигательной установки традиционного химического и электроракетного двигателей. Различные аспекты применения подобной комбинированной двигательной установки, состоящей из солнечной электроракетной установки и разгонного блока «Фрегат», рассматривались, например, в рамках НИР «Двина ТМ».

В отличие от химического двигателя, в котором энергия высвобождается из химических связей, энергия для ускорения рабочего тела электроракетным двигателем подводится извне. Наибольшее распространение в качестве источника энергии на околоземных орбитах, где величина солнечного излучения достаточна для удовлетворения потребностей космического аппарата в энергии, получили солнечные батареи. Солнечные батареи чувствительны к радиации, в их внутренней структуре накапливаются повреждения и их характеристики деградируют, поэтому существует потребность в учете накопленной за время выполнения транспортной операции радиационной дозы и оценке снижения эффективности солнечных элементов. Неравномерная интенсивность облучения в сформированных магнитным полем Земли радиационных поясах (пояса Ван Аллена) может быть учтена, если проводить оценку интенсивности радиации в точках траектории выполнения маневра с использованием модели радиационных поясов Земли.

В работе предлагается метод, позволяющий учесть воздействие ионизирующего излучения на деградацию солнечных батарей при выполнении транспортной операции с использованием комбинированной двигательной установки на основе ЖРД и ЭРДУ с учетом выбранной траектории и модели радиационного пояса Земли.

Ключевые слова: комбинированная двигательная установка, электроракетный двигатель, радиационный пояс Земли, солнечная батарея, деградация.

Introduction. Transport operations that ensure the change of the orbit of a spacecraft or its transfer to the departure trajectory are an integral part of almost all space missions. Increasing requirements for the efficiency of transporting spacecraft form the need to search for possible ways to increase this efficiency and assess the characteristics associated with the proposed methods. Current boosters and interorbital tugs, as a rule, use a chemically powered cruise engine, although solutions with the use of an electric jet engine are becoming more common [1]. Due to the high rate of the outflow of working fluid which is much higher than that of combustion products in a chemical engine, the efficiency of use of the substance mass by an electric jet engine significantly exceeds this indicator for a chemical engine [2]. However, the low thrust provided by the electric jet engine leads to high duration of the transport operation and, as a result, to considerable time of exposure to the outer space factors, in particular, radiation [3–5]. Therefore, the use of the electric jet engine only does not always meet the requirements for the mission.

One of the promising ways to increase the efficiency of transport operations aimed at changing the orbit of a spacecraft or transferring it to departure trajectories is the use of an electric jet engine as a part of a booster with a traditional chemical propulsion system [6]. It is assumed that this combination of engines of different types allows using a particular engine in different phases of the transport operation, increasing its overall efficiency. Various aspects of the use of such an integrated propulsion system consisting of a solar electric jet system and “Fregat” booster was considered in the framework of “Dvina TM” research project [7].

Unlike a chemical engine, in which energy is released from chemical bonds, the energy for accelerating the working fluid by an electric jet engine is supplied from outside. Solar batteries (SBs) based on semiconductor photocells are the most widespread energy source in near-earth orbits, where the amount of solar radiation is sufficient to meet the energy needs of a spacecraft. SBs are subject to degradation under the influence of high-energy charged particles [8–10]. Uneven irradiation intensity in radiation belts formed by the Earth’s magnetic field (Van Allen belts) [11; 12] suggests that accounting for the intensity of radiation exposure should be carried out along the trajectory of the maneuver and taking into account the model of the Earth’s radiation belts.

To assess the impact of heavy ions (HIs) on the degree of degradation of the SBs, design programs have been established in Russia and abroad. For example, in Russia, the Research Institute of Applied Mechanics and Electrodynamics (RIAME) of Moscow Aviation Institute (MAI) created BUKSIR program [13], which allows estimating by calculation the degree of degradation of any of the

30 types of solar batteries depending on the spacecraft flight altitude, orbit inclination and time spent in this orbit.

European Space Agency (ESA) has developed SPENVIS (Space Environment Information System) program [14], which allows estimating radiation doses accumulated by spacecraft and their elements during the flight, depending on the specified orbits and time spent on them. The program also made it possible to predict a decrease in the efficiency of SBs during their active existence depending on the types of SB cells, types and thickness of protective coatings, and to take into account the obtained data when designing both the spacecraft themselves and their electric power supply (EPS) systems and developing ballistic maneuvers extending the active lifetime (ALT) of spacecraft (SC).

Existing software for evaluating the effects of radiation on spacecraft, such as SHIELDOS, SPENVIS, STK SEET, allows calculating the integral dose accumulated by the SB, assessing the degradation of photocells depending on their type and thickness of the protective coating. However, this software does not satisfy the needs of studying the characteristics of degradation of solar cells when performing active maneuvers using high and low thrust engines according to a specific cyclogram, which occurs when performing a transport operation using an integrated propulsion system. Therefore, basic methods and algorithms published in the public domain were used to conduct the study and a method that allows solving the problem in the desired formulation was proposed on their basis.

Considerable flight duration on low thrust engines requires substantial computational powers to perform numerical integration of differential equations used for the mathematical description of various phases of the general maneuver. The need for practical implementation of the numerical experiment required the simplification of the models in use, the optimization of the algorithms and computational methods in use, as well as the application of computers with high computational capabilities.

Motion Model. The transport operation of the coplanar transition between circular orbits (from low to high) was investigated. In general, the problem of estimating the effect of the composition of an integrated propulsion system on the integral dose of radiation when orbiting a spacecraft was considered by the authors earlier in [15]. In addition to the methodological interest in terms of developing a method for assessing the degradation of solar panels and the effect of the composition of the integrated propulsion system on it, such an operation may be of practical interest, since there are promising projects for placing into geosynchronous orbits for which the transport operation has a high similarity with the idealized one [16].

The flight maneuver between coplanar circular orbits (from a smaller to a bigger one) consists of 2 phases (fig. 1):

1. Gomanovsky flight using high-thrust engines;

2. Retrieval of the spacecraft to the target high-elliptical orbit along a spiral trajectory by low-thrust engines.

The optimality of a two-pulse flight along a semi-elliptical trajectory in the chemical phase is shown in [17]. The flight between circular coplanar orbits with the help of a low-thrust engine is considered in [18].

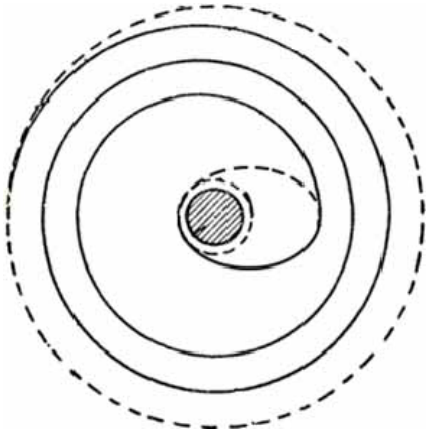

Fig. 1. Flight trajectory of artificial earth satellite (AES) from low earth orbit (LEO) to geostationary earth orbit (GSO) using integrated propulsion system (IPS)

Рис. 1. Траектория перелета искусственного спутника Земли (ИСЗ) с низкой околоземной орбиты (НОО) на геостационарную околоземную орбиту (ГСО) с использованием комбинированной двигательной установки (КДУ)

Knowing the initial mass of the SC, the parameters of the used propulsion engines (PE) that are parts of the IPS (thrust, specific impulse), the parameters of the initial and final orbits, one can enter a parameter $k \in (0 \div 1)$ that determines the position of the intermediate circular orbit to which the SC is placed using the high-thrust engine along Gomanovsky transition orbit.

$$R_2 = R_1 + k(R_3 - R_1), \quad (1)$$

where R_1 is the radius of the LEO, R_3 is the radius of the GSO.

The parameter k uniquely specifies the radius of the intermediate orbit R_2. A cyclogram of engine operation can be constructed on the basis of analytical dependencies.

The first phase of the maneuver is performed according to Gomanovsky two-pulse flight. On the basis of ballistic calculations, for a given ratio of orbits $\bar{r} = \frac{r_2}{r_1}$ the necessary increments for the first and second pulses are the following:

$$\Delta V_1 = V_1\left(\sqrt{\frac{2\bar{r}}{\bar{r}+1}} - 1\right), \quad (2)$$

$$\Delta V_2 = V_1 \frac{1}{\sqrt{\bar{r}}}\left(1 - \sqrt{\frac{2}{\bar{r}+1}}\right), \quad (3)$$

where V_1 is the velocity of the SC in the initial circular orbit:

$$V_1 = \sqrt{\frac{\mu_E}{r_1}}, \quad (4)$$

where μ_E is the gravitational parameter of the Earth.

The required expenses of the working fluid will be:

$$\Delta m = M\left(1 - \exp\left(-\frac{\Delta V}{I_{SP}}\right)\right), \quad (5)$$

where M is the mass of the apparatus before issuing the corresponding impulse; I_{SP} is the specific impulse realized by the CE (chemical engine).

Pulse durations will be:

$$\Delta t = I_{SP}\frac{\Delta m}{R}, \quad (6)$$

where R is the thrust of CE.

Moments of impulses:

$$t_0 = 0, \quad (7)$$

$$t_1 = \pi\sqrt{\frac{a^3}{\mu_E}}, \quad (8)$$

where a is the semi-major axis of the transition ellipse.

As a result of the first phase, the SC is transferred to a circular orbit with the radius r_2. The second phase of the transport operation begins with the firing of an electric jet engine and a long transition along a spiral trajectory. Engine thrust during the entire time the maneuver is executed coincides with the velocity vector. The calculations are done according to the formulas proposed in [5]

$$\Delta t = \frac{M}{\dot{m}}\left(1 - \exp\left(\frac{\sqrt{\mu_E}}{I_{SP}}\left(\frac{1}{\sqrt{r_3}} - \frac{1}{\sqrt{r_2}}\right)\right)\right), \quad (9)$$

gives an approximation sufficient for the problems to be solved.

The result of the second phase of the transport operation is the transition to the target circular orbit.

Radiation field model. Depending on the SC parameters, the initial and final orbits and the parameter k, the SC will move along different trajectories passing through areas of space with different levels of ionizing radiation from outer space (IROS).

Ionizing radiation includes the following types of radiation [9; 19–23]:

– radiation from the natural radiation belts of the Earth (NRBE) (protons, electrons, α-particles, nuclei);

– solar cosmic rays (SCR) (protons, electrons, α-particles);

– solar wind (protons, electrons, α-particles);

– galactic cosmic rays (GCR) (protons, electrons, α-particles, nuclei);

– particles in the external magnetosphere (protons, electrons, α particles), albedo particles (protons, neutrons), UDS-radiation from unclosed drift shells (protons, electrons), particles precipitating during magnetic disturbances (protons, electrons) and others.

Galactic cosmic radiation is characterized by small fluxes (up to 5 particles × cm^{-2} × s^{-1}) and high particle energies (up to 10^{20} eV).

The primary cosmic rays of galactic origin can be attributed to sources of NRBE particles (high-energy protons resulting from the decay of albedo neutrons formed by GCR particles interacting with atmospheric nuclei).

SCRs are formed during chromospheric solar flares. Large fluxes of high-energy SCR particles can pose a radiation hazard to semiconductor radio-electronic products (REP), which are a part of the SC instrument cluster. The total dose of radiation received by a spacecraft throughout the maneuver can be obtained by integration of individual doses obtained while the spacecraft is at a particular point in space, the level of IR (ionizing radiation) in which is known.

A dipole is adopted as a model of the Earth's magnetic field, whose axis is shifted relative to the geographic axis by 11.4 degrees [20; 24–26]. It is known that the intensity of charged particles fluxes has a high spatial gradient. A change in distance by 3 % creates a change in the flux intensity by 10 times at small heights in the inner zone. Therefore, it is not possible to use the dipole model in Cartesian or polar coordinates to determine the intensity of charged particles fluxes. One must use a coordinate system suitable for this task.

The most commonly used coordinate system is that of McIlwain [27–29], in which the fluxes of charged particles with equal intensity are placed on surfaces that can be described in *L-B* coordinates. A spatial distribution of intensities which formed the basis of the AP8 and AE8 models for protons and electrons, respectively [30] was obtained on the basis of experimental data collected during launches of the satellite for studying the Earth's magnetosphere.

Since solar cells cannot be protected by a layer of considerable thickness, it is necessary to use the values of both protons and electrons of the entire energy spectrum for the purpose of studying the effect of HIs on their degradation. Fluence is conveniently accumulated in the energy zones described in documents AP8 and AE8. Integral fluence accumulated during the entire transport operation can be obtained by integrating with preservation of the division of the influencing flows into energy zones (separately for protons and electrons):

$$D(E) = \int_T P(\vec{r}, E)dt, \quad (10)$$

where D is the accumulated fluence for HIs with energy in the range of E zone; $P(\vec{r}, E)$ is the intensity of radiation at the point of space $\vec{r} = [x\,y\,z]^T$ for HI with energy in E zone.

The model of solar cells degradation. Solar cells are the most common source of energy for SC. Solar cells based on monocrystalline silicon are the most common ones, their production technology is well developed, and the efficiency of modern elements is high. Elements based on gallium arsenide are less common; they have a number of advantages and greater efficiency, but their production is relatively poorly developed, and the cost is noticeably higher than that of silicon ones.

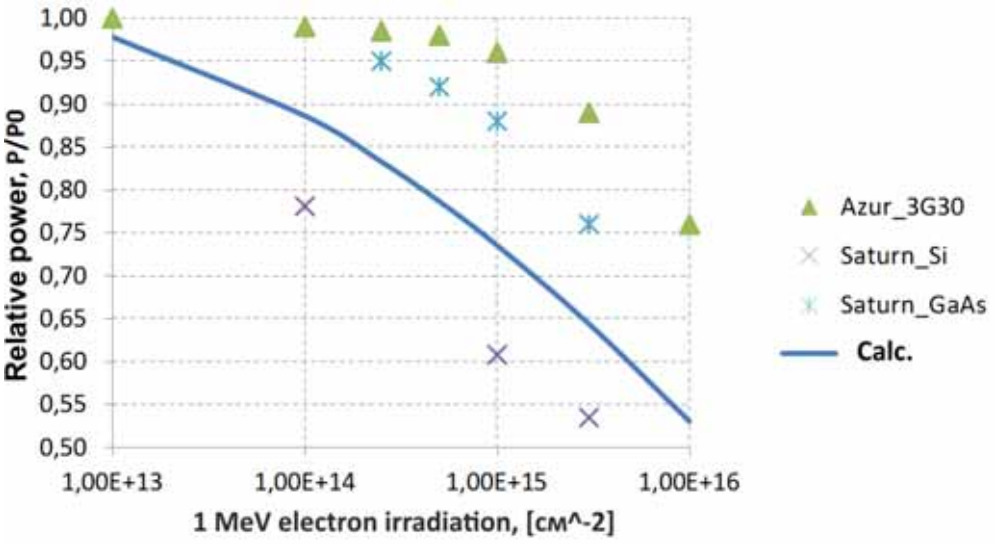

Fig. 2. Degradation of solar cells power depending on the integral fluence of 1 MeV monoenergetic electrons

Рис. 2. Деградация мощности солнечных фотоэлементов в зависимости от интегрального флюенса моноэнергетических электронов 1 МэВ

Solar cells operating in space conditions undergo the effect of gradual degradation of their characteristics under the influence of defects accumulation due to the influence of HIs [31]. Several mechanisms of the influence of HIs on the solar cells structure are known and theoretically described [9].

There are a number of techniques [8; 32; 33] for estimation of the degradation of solar cells characteristics under the influence of radiation exposure. JPL method was used for the purpose of the conducted research. According to this method the effect of mono-energetic electron flux with energy of 1 MeV on solar cells without protective coating is experimentally evaluated. Measurements are carried out on installations with an appropriate energy source and a measurement system that records changes in the characteristics of solar cells. The dependence of the characteristics (short circuit current, no-load voltage, maximum power) on the total effect of the radiation flux is constructed on the basis of the experimental data obtained. On the basis of theoretical models of degradation and their subsequent verification by experiments, it is generally accepted that the effects of other HIs can be reduced to the effects of electrons with the energy of 1 MeV. Thus, it becomes possible to determine the net effect from different types of HIs (electrons and protons) of a wide energy spectrum taking into account various protective coatings.

The formula proposed in [13] which describes the decrease in power from the integral fluence

$$\frac{N}{N_0} = 1 + 0.0241 \cdot \log\left(\frac{D_\Sigma}{10^{12}}\right) - 0.0466 \cdot \left[\log\left(\frac{D_\Sigma}{10^{12}}\right)\right]^{1.8}, \quad (11)$$

agrees well with the experimental data on solar cells provided by manufacturers [34–36] (fig. 2).

Integral fluences accumulated during the transport operation in various energy spectra can be converted into an equivalent monoenergetic fluence of electrons with energy of 1 MeV for a given type of protective coating according to the formula (12) published in [8]:

$$\Phi_{1MeVelectron} = \int \frac{d\Phi_E(E_E)}{dE_E} \cdot RDC(E_E, t)\, dE_E + C_{PE} \int \frac{d\Phi_P(E_P)}{dE_P} \cdot RDC(E_P, t)\, dE_P, \quad (12)$$

where $\frac{d\Phi_E(E_E)}{dE_E}$, $\frac{d\Phi_P(E_P)}{dE_P}$ is fluence density of electrons and protons on the energy spectrum, $RDC(E_E, t)$, $RDC(E_P, t)$ is the function of equivalent damage from the action of HIs with energy E with a protective coating of thickness t, C_{PE} is the experimental coefficient of conversion of proton fluence into electron fluence.

Algorithm and simulation. The data obtained during the ballistic planning of a transport operation form a sequence diagram of a transport operation. This approach allows solving the following tasks:

– to check the correctness of the ballistic planning;

– to get the fluence values at the point of space where the SC is currently located and to determine the integral dose of exposure.

The dynamics of SC flight is simulated in the geocentric inertial coordinate system. To reduce computational complexity, it is considered that the starting point of the maneuver coincides with the axis of the inertial GCS (geocentric coordinate system). The axis of the magnetic dipole rotates with the rotation of the Earth. To calculate the level of IR (ionizing radiation) at the current point in space, the coordinates of the inertial GCS are converted into dipole coordinates, after which the IR values are calculated in accordance with AP8 model.

A mathematical model was constructed to study the effect of phase distribution for IPS engines on the integral dose obtained by the SC during the time of the maneuver. The model solves the following main tasks:

– flight planning;

– iterative modeling;

– estimation of the radiation intensity of electrons and protons of different energy spectrum.

The algorithm of numerical calculations corresponding to the proposed model is shown in fig. 3 and consists of a series of sequential operations:

1. The SC parameters and the IPS engines parameters are set.

2. The initial and final orbits, the distribution of the trajectory maneuver between phases 1 and 2 are set.

3. The initial state vector (position, speed, acceleration) is set.

4. The scheduler performs calculations according to the specified parameters and draws a sequence diagram for starting the engines.

5. The solver performs the sequence diagram step by step, determining the coordinates of the SC at the next step, calculates and sums up the value of the particle flux at a given point in space.

6. The output unit forms a flight trajectory and an output data set corresponding to a given input data set.

Simulation results. Final characteristics and flight trajectories were obtained for different phase relations. An example of the resulting trajectory is shown in fig. 4.

The effect of the parameter k determining the ratio of the fraction of the total maneuver per part of the transport operation performed by the booster to the integral dose of radiation obtained by the SC during the execution of the maneuver was studied during the simulation. The parameter k varied in the range of 0÷1 with a step of 0.1.

The following parameters and initial conditions were adopted for the research:

– the transport operation consists in the transition between circular coplanar orbits. The initial orbit (LEO) is 200 km high in the equatorial plane, the final orbit (GSO) is 35786 km high;

– the initial mass of the entire system is 3000 kg;

– CE: thrust is 20000 N, specific impulse is 330 s;

– EJE: thrust is 0,2N, specific impulse is 2000 s.

The analytical formulas used for planning the cyclogram of a transport operation are verified by the method of numerical integration using a physico-mathematical model. Deviations of the radius of the final orbit from the specified one obtained by numerical integration based on an analytically planned cyclogram are reflected in fig. 5

The flow of HIs is calculated by energy zones for each point of the trajectory. Fig. 6 shows the calculated equivalent fluence of a monoenergy flux of electrons with the energy of 1 MeV.

Calculations of residual efficiency carried out by formula (11) for different k (fig. 7) show that transport operations with $k < 0.3$ have a significant effect on the degradation.

Due to the variable integration step, the number of calculated points of the trajectory for the most complicated case did not exceed 800 thousand (fig. 8).

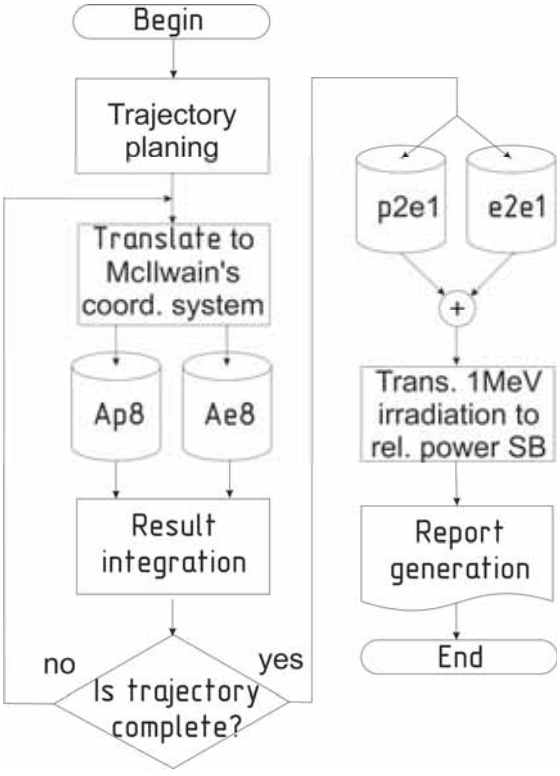

Fig. 3. Simulation flowchart

Рис. 3. Блок-схема алгоритма моделирования

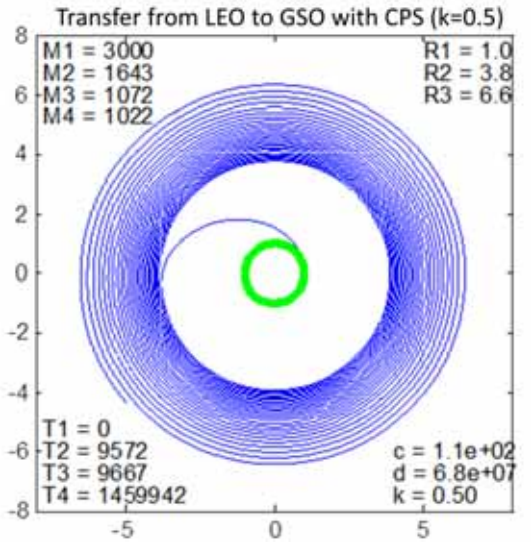

Fig. 4. Trajectory example

Рис. 4. Пример траектории

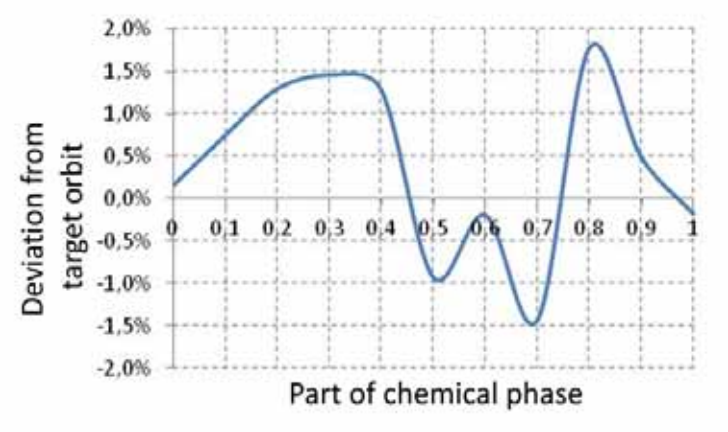

Fig. 5. Deviations of the radius of the final orbit from the specified one

Рис. 5. Отклонения радиуса конечной орбиты от заданного

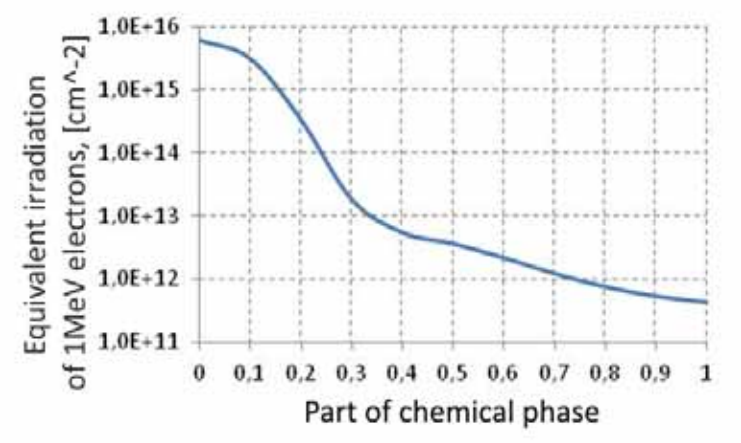

Fig. 6. Fluence of an equivalent flux of 1MeV monoenergetic electrons

Рис. 6. Флюенс эквивалентного потока моноэнергетических электронов 1МэВ

In previous calculations performed with a fixed integration step the number of calculation points exceeded 10 million, which made the calculation of the equivalent fluence impracticable within a reasonable time frame.

The specified accuracy of integration was selected taking into account the balance between the required computational power and the deviations of the calculations over the entire range of the coefficient k. The computational complexity illustrated by the time of calculation depending on the parameter k (fig. 9) is significant even at the current level of computational tools and required special measures to obtain results in a finite time.

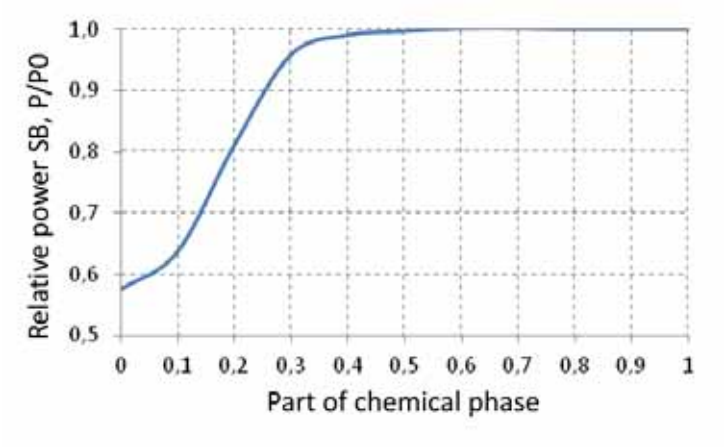

Fig. 7. Residual efficiency of SBs

Рис. 7. Остаточный КПД СБ

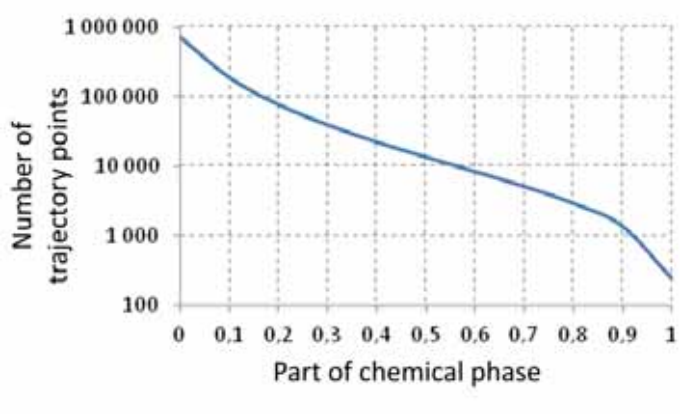

Fig. 8. The number of points of the trajectory

Рис. 8. Количество точек траектории

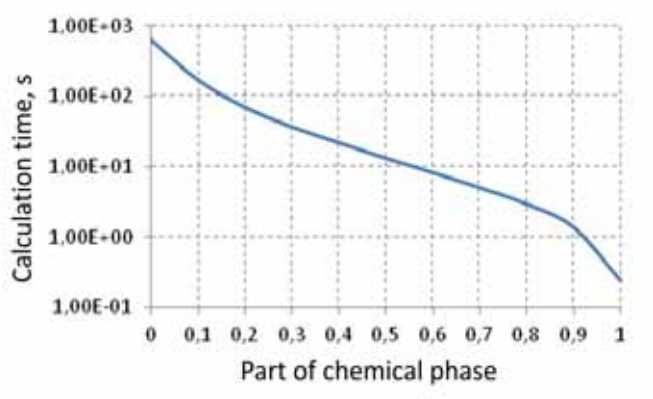

Fig. 9. Required calculation time depending on the parameter k

Рис. 9. Требуемое время расчета в зависимости от параметра k

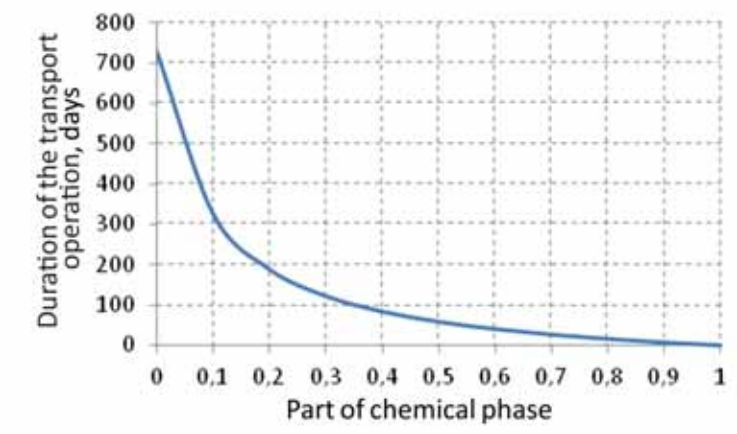

Fig. 10. Duration of the transport operation

Рис. 10. Длительность транспортной операции

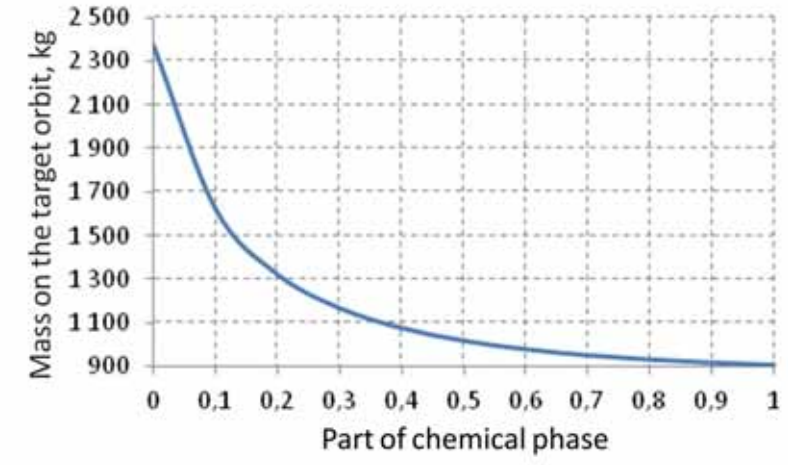

Fig. 11. Mass on the final orbit

Рис. 11. Масса на конечной орбите

The duration of the transport operation depending on the parameter k is displayed in fig. 10.

The mass dependence in the final orbit is shown in fig. 11. It can be seen that the use of EJE in the booster allows placing a large mass into the final orbit.

Conclusion. The influence of the choice of the ratio between the parts of the performed maneuver between different types of engines of the integrated propulsion system of the booster is considered. A method is proposed by which the influence of ionizing radiation in near-Earth space on the degradation of the characteristics of a SC solar battery has been evaluated. It is shown that the use of a low thrust engine throughout the transport operation leads to a significant amount of accumulated radiation dose and, as a result, to decrease in the efficiency of the solar battery. Reducing the efficiency requires increasing the area of the SB and, accordingly, increasing its mass. The use of IPS consisting of high and low thrust engines allows not only flexibly controlling the flight time, varying the ratio between the phases of the transport operation performed by various types of engines, but also reducing the degradation of SB from the effects of ionizing radiation, providing a short time of SC presence in the Earth radiation belt zones due to the implementation of this phase using IPS. The developed methodology and the results obtained are an integral part of the work on a reasonable choice of the composition of the integrated propulsion system based on “Fregat” booster with an additional EJE.

References

1. [Express-AM6, the replenishment of the orbital grouping of Russia]. *Sibirskiy Sputnik.* 2014, Vol. 369, No. 15, P. 1–3 (In Russ.).

2. Gilzin K. A. *Elektricheskie mezhplanetnye korabli* [Electric Interplanetary Ships]. Moscow, Nauka Publ., 1970, 267 p.

3. *The Radiation Design Handbook.* European Space Agency. ESTEC, Noordwijk, the Nederland, 1993, 444 p.

4. Birukov V. I., Birukova M. V. [Algorithm for predicting the radiation impact on the microsatellite equipment]. *Vestnik Moskovskogo aviatsionnogo instituta.* 2013, Vol. 20, No. 3, P. 40–49 (In Russ.).

5. Getselev I. V., Zubarev A. I., Pudovkin O. L. [Radiation situation on board spacecraft]. *Strategic Missile Forces, TsIPK.* 2001, No. 77, 316 p.

6. Belik A. A., Egorov Yu. G., Kulkov V. M. et al. [Analysis of the design and ballistic characteristics of a combined circuit for launching a spacecraft into a geostationary orbit using medium-class launch vehicles]. *Aerokosmicheskaya Tekhnika i Tekhnologiya*. 2011, Vol. 81, No. 4, P. 17–21 (In Russ.).

7. Technical task for an integral part of the development work "Creating a unified transport module based on a solar electric propulsion system for launch vehicles of medium and heavy classes". "*Development of a flight demonstrator of a unified transport module based on a solar electric propulsion system*". Code: OCD "Dvina-TM". 2017. 18 p.

8. Messenger S. R. *Space Solar Cell radiation damage modeling*. US Naval Research Laboratory, Washington D. C. 2016. 48 p.

9. Tapero K. I., Ulimov V. N., Chelnov A. M. *Radiatsionnye Effekty v Kremnievykh Integral'nykh Skhemakh Kosmicheskogo Primeneniya* [Radiation effects in silicon integrated circuits for space applications]. Moscow, BINOM, Laboratoriya znaniy Publ., 2012, 226 p.

10. Fahrenbruch A. L., Bube R. H. *Solnechnye Elementy: Teoriya i Eksperiment* [Solar Elements: Theory and Experiment]. Moscow, Energoautomizdat Publ., 1987, 247 p.

11. Van Allen J. A., Ludwig G. H., Ray E. C., McIlwain C. E. Observation of High Intensity Radiation by Satellites 1958 Alpha and Gamma. *Jet Propulsion.* 1958, No. 28, P. 588–592.

12. Murzin S. V. *Vvedenie v fiziku kosmicheskikh luchey* [Introduction to the physics of cosmic rays]. Moscow, Atomizdat Publ., 1979, 197 p.

13. Vasiliev Yu. B. [Radiation degradation of solar cells working in space]. *Aerokosmicheskaya Tekhnika i Tekhnologiya*. 2007, Vol. 43, No. 7, P. 116 (In Russ.).

14. SPENVIS – Space ENVironment Information System, ESA. Available at: https://www.spenvis.oma.be/ (accessed: 09.07.2016).

15. *Razrabotka evropeyskoy global'noy navigatsionnoy sputnikovoy sistemy Galileo* [The development of the European global navigation satellite system Galileo]. TsNIIMASH Newsletter, 2 p.

16. Birukov V. I., Nazarov V. P., Kurguzov A. V. [Influence of the energy characteristics of a combined propulsion system on the integral dose of radiation when a spacecraft is placed in a geostationary orbit]. *Siberian Journal of Science and Technology.* 2018, Vol. 19, No. 1, P. 50–58 (In Russ.).

17. Okhotsimsky D. E., Sikharulidze Yu. G. *Osnovy mekhaniki kosmicheskogo poleta* [Basics of Space Flight Mechanics]. Moscow, Nauka Publ., 1990, 321 p.

18. Grishin S. D., Leskov L. V. *Elektricheskie raketnye dvigateli* [Electric Spacecraft Rocket Engines]. Moscow, Mashinostroenie Publ., 1989, 317 p.

19. *GOST 25645.211–85. Bezopasnost' radiatsionnaya ekipazha kosmicheskogo apparata v kosmicheskom polete. Kharakteristiki yadernogo vzaimodeystviya protonov* [State Standard 25645.211–85. Safety of the radiation crew of the spacecraft in space flight. Characteristics of the nuclear interaction of protons]. Moscow, Standartinform Publ., 1986. 14 p.

20. Galper A. M. Earth's Radiation Belt. *Soros Educational Journal*. 1999, No. 6, P. 75–81.

21. Kozlov A. A., Chumakov I. R. [Algorithm for evaluating the structural protection of spacecraft]. *Radiatsionnaya stoykost' elektronnykh system. "Stoykost'-2004". Nauchno-tekhnicheskiy sbornik.* 2004, Iss. 7, P. 21–22 (In Russ.).

22. Space Model, t. 2. The impact of the space environment on the materials and equipment of space vehicles. Moscow, *MSU SINP*, 2007, P. 317.

23. *GOST RV 20.57.308–98. Radiatsionnaya stoykost'. Metody rascheta* [State Standart RV 20.57.308–98. Radiation resistance. Methods of calculation]. Moscow, 1995. 55 p.

24. Barth J. Applying modeling space radiation environments. 1997 IEEE Nuclear and Space Radiation Effects. Short Course. Applying Computer Simulation Tools to Radiation Effects Problems. *Snowmass Conference Center*. Snowmass Village, Colorado. 21 July 1997, P. 354–367.

25. Runcorn S. K. The Magnetism of the Earth's Body. Handbuch der Physik XLVII "Geophysik I", Springer, 1956, P. 498–533.

26. Voronov S. A., Gal'per A. M., Kirillov-Ugrymov V. G., Koldashev S. V., Popov A. V. [The charge composition of a stream of high-energy electrons and positrons of the Earth's radiation belt]. *Pis'ma v ZhETF*. 1986, Vol. 43, Iss. 5, P. 240–241 (In Russ.).

27. McIlwain C. E. Coordinates for Mapping the Distribution of Magnetically Trapped Particles. *Jour. Geophysical Res*. 1961, Vol. 66, P. 3681–3691.

28. Fox N., Burch J. L. The Van allen probes mission. Springer, 2013. 579 p.

29. McIlwain K. E. Coordinates for mapping the distribution of particles trapped by the geomagnetic field. *Operation Starfish. Collection of articles.* Ed. I. A. Zhulina. Moscow, Atomizdat Publ., 1964, 216 p.

30. NASA SP-3024 Models of the trapped radiation environment. Vol. I: Inner Zone, National AERONAUTICS AND SPACE ADMINISTRATION, Washington D. C., 1966, P. 178.

31. Visentine J., Kinard W., Pinkerton R. MIR Solar Array Experiment. *36th AIAA Aerospace Sciences Meeting and Exhibit*. Jan. 11–14 1999, Reno, NV. P. 194–218.

32. Tada H. Y., Carter J. R., Anspaugh B. E., Downing R. G. *Solar cell Radiation Handbook*. JPL Publication 82–69, 1982. 216 p.

33. OST 134-1034-2003. Methods for testing and assessing the durability of on-board radio electronic equipment for space vehicles to the effects of electronic and proton emissions of electronic and proton emissions of space through dose effects.

34. *Solnechnye batarei, PAO "Saturn"* [Solar batteries, JSC "Saturn"] (In Russ.). Available

at: http://saturn-kuban.ru/produktsiya/solnechnye-batarei/ (accessed: 21.09.2016).

35. *Fotoelektricheskie preobrazovateli, PAO "Saturn"* [Photoelectric converter, JSC "Saturn"] (In Russ.). Available at: http://saturn-kuban.ru/produktsiya/ solnechnye-atarei/fotoelektricheskie-preobrazovateli/ (accessed: 17.11.2017).

36. Guter W. Space solar cells – 3G30 and next generation radiation product. Available at: https://www.e3s-conferences.org/articles/e3sconf/pdf/ 2017/ 04/e3sconf_espc2017_03005.pdf (accessed 03.05.2017).

Библиографические ссылки

1. «Экспресс-АМ6» пополнение орбитальной группировки России // Сибирский спутник. 2014. № 15 (369). 8 с.

2. Гильзин К. А. Электрические межпланетные корабли. 2-е изд. перераб. и дополн. М. : Наука, 1970. 267 с.

3. The Radiation Design Handbook. European Space Agency. ESTEC, Noordwijk, the Nederland, 1993. 444 p.

4. Бирюков В. И., Бирюкова М. В. Алгоритм прогнозирования радиационного воздействия на аппаратуру микроспутника // Вестник Московского авиационного института. 2013. Т. 20, № 3. С. 40–49.

5. Гецелев И. В., Зубарев А. И., Пудовкин О. Л. Радиационная обстановка на борту космических аппаратов // РВСН. 2001. № 77. 316 с.

6. Анализ проектно-баллистических характеристик комбинированной схемы выведения космического аппарата на геостационарную орбиту с использованием ракет-носителей среднего класса / А. А. Белик, Ю. Г. Егоров, В. М. Кульков [и др.]. // Авиационно-космическая техника и технология. 2011. № 4 (81). С. 17–21.

7. Техническое задание на составную часть опытно-конструкторской работы «Создание унифицированного транспортного модуля на основе солнечной электроракетной двигательной установки для ракетносителей среднего и тяжелого классов». «Разработка летного демонстратора унифицированного транспортного модуля на основе солнечной электроракетной двигательной установки». Шифр: ОКР «Двина-ТМ». 2017. 18 с.

8. Messenger S. R. *Space Solar Cell radiation damage modeling*. US Naval Research Laboratory, Washington D. C. 2016. 48 p.

9. Таперо К. И., Улимов В. Н., Членов А. М. Радиационные эффекты в кремниевых интегральных схемах космического применения. М. : БИНОМ. Лаборатория знаний, 2012. 226 с.

10. Фаренбрух А. Л., Бьюб Р. Х. Солнечные элементы: теория и эксперимент / под ред. М. М. Колтуна. М. : Энергоатомиздат, 1987. 247 с.

11. Van Allen J. A., Ludwig G. H., Ray E. C., McIlwain, C. E. Observation of High Intensity Radiation by Satellites 1958 Alpha and Gamma // Jet Propulsion. 1958. № 28. P. 588–592.

12. Мурзин С. В. Введение в физику космических лучей. М. : Атомиздат, 1979. 197 с.

13. Васильев Ю. Б. Радиационная деградация солнечных батарей при работе в космосе // Авиационно-космическая техника и технология. 2007. № 7 (43). 116 с.

14. SPENVIS – SPace ENVironment Information System, ESA [Электронный ресурс]. URL: https://www.spenvis.oma.be/ (дата обращения: 20.11.2018).

15. Развитие европейской глобальной навигационной спутниковой системы Галилео // ЦНИИМАШ, Информационный бюллетень. 2 с.

16. Бирюков В. И., Назаров В. П., Кургузов А. В. Влияние энергетических характеристик комбинированной двигательной установки на интегральную дозу радиации при выводе космического аппарата на геостационарную орбиту // Сибирский журнал науки и технологий. 2018. Т. 19, № 1. С. 50–58.

17. Охоцимский Д. Е., Сихарулидзе Ю. Г. Основы механики космического полета. М. : Наука, 1990. 321 с.

18. Гришин С. Д., Лесков Л. В. Электрические ракетные двигатели космических аппаратов. М. : Машиностроение, 1989. 317 с.

19. ГОСТ 25645.211–85. Безопасность радиационная экипажа космического аппарата в космическом полете. Характеристики ядерного взаимодействия протонов. М. : Стандартинформ, 1986. 14 р.

20. Гальпер, А. М. Радиационный пояс Земли // Соросовский образовательный журнал, 1999. № 6. С. 75–81.

21. Козлов А. А., Чумаков А. И. Алгоритм оценки конструкционной защиты космических аппаратов // Радиационная стойкость электронных систем «Стойкость-2004» : науч.-техн. сб. 2004. Вып. 7. С. 21–22.

22. Воздействие космической среды на материалы и оборудование космических аппаратов // Модель космоса. 2007. Т. 2. 308 с.

23. ГОСТ РВ 20.57.308–98. Радиационная стойкость. Методы расчета. М., 1995. 55 с.

24. Barth J. Applying modeling space radiation environments // 1997 IEEE Nuclear and Space Radiation Effects. Short Course. Applying Computer Simulation Tools to Radiation Effects Problems. Snowmass Conference Center. Snowmass Village, Colorado. 21 July 1997. P. 354–867.

25. Runcorn S. K. The Magnetism of the Earth's Body. Handbuch der Physik XLVII "Geophysik I", Springer, 1956, P. 498–533.

26. Зарядовый состав потока высокоэнергичных электронов и позитронов радиационного пояса Земли / С. А. Воронов, А. М. Гальпер, В. Г. Кирилловв-Угрюмов [и др.] // Письма в ЖЭТФ. 1986. Т. 43, № 5. С. 240–241.

27. McIlwain C. E. Coordinates for Mapping the Distribution of Magnetically Trapped Particles // Jour. Geophysical Res. 1961. № 66. P. 3681–3691.

28. Fox N., Burch J. L. The Van allen probes mission. Springer, 2013. 579 p.

29. Мак Илуэйн К. Е. Координаты для отображения распределения частиц, захваченным геомагнит-

ными полем // Операция Морская звезда : сб. статей / под ред. И. А. Жулина. М. : Атомиздат, 1964. 261 с.

30. NASA SP-3024 Models of the trapped radiation environment. Vol. I: Inner Zone, National AERONAUTICS AND SPACE ADMINISTRATION, Washington D. C., 1966, P. 178.

31. Visentine J., Kinard W., Pinkerton R. MIR Solar Array Experiment. *36th AIAA Aerospace Sciences Meeting and Exhibit*. Jan. 11–14 1999, Reno, NV. P. 194–218.

32. Tada H. Y., Carter J. R., Anspaugh B. E., Downing R. G. *Solar cell Radiation Handbook*. JPL Publication 82–69, 1982. 216 p.

33. ОСТ 134-1034–2003. Методы испытаний и оценки стойкости бортовой радиоэлектронной аппаратуры космических аппаратов к воздействию электронных и протонных излучений космического пространства по дозовым эффектам.

34. Солнечные батареи. ОАО «Сатурн» [Электронный ресурс]. URL: http://saturn-kuban.ru/produktsiya/solnechnye-batarei/ (дата обращения: 21.09.2016).

35. Фотоэлектрические преобразователи. ОАО «Сатурн» [Электронный ресурс]. URL: http://saturn-kuban.ru/produktsiya/solnechnye-batarei/fotoelektricheskie-preobrazovateli/ (дата обращения: 17.11.2017).

36. Guter W. Space solar cells – 3G30 and next generation radiation hard product [Электронный ресурс]. URL: https://www.e3s-conferences.org/articles/e3sconf/pdf/2017/ 04/ e3sconf_espc2017_03005.pdf (дата обращения: 03.05.2017).

Biruykov Vasiliy Ivanovich – professor, Dr. Sc., Moscow Aviation Institute (National Research University). E-mail: aviatex@mail.ru.

Nazarov Vladimir Pavlovich – Cand. Sc., professor, head of Department of Aircraft Engines, Reshetnev Siberian State University of Science and Technology. E-mail: nazarov@sibsau.ru.

Kurguzov Alexey Vyacheslavovich – Postgraduate Student; Moscow Aviation Institute (National Research University). E-mail: mandigit@yandex.ru.

Бирюков Василий Иванович – доктор технических наук, профессор; Московский авиационный институт (национальный исследовательский университет). E-mail: aviatex@mail.ru.

Назаров Владимир Павлович – кандидат технических наук, профессор, заведующий кафедрой двигателей летательных аппаратов; Сибирский государственный университет науки и технологий имени академика М. Ф. Решетнева. E-mail: nazarov@sibsau.ru.

Кургузов Алексей Вячеславович – аспирант, Московский авиационный институт (национальный исследовательский университет). E-mail:mandigit@yandex.ru.

UDC 629.786.2.015.4
Doi: 10.31772/2587-6066-2019-20-1-54-61

For citation: Bondarenko A. Yu., Mitin A. Yu., Tolchenov V. A., Eykhorn A. N., Yuranev O. A. [An approach to ground testing of rockets and space vehicles on transient processes by copra-spring stand]. *Siberian Journal of Science and Technology.* 2019, Vol. 20, No. 1, P. 54–61. Doi: 10.31772/2587-6066-2019-20-1-54-61

Для цитирования: Бондаренко А. Ю., Митин А. Ю., Толченов В. А., Эйхорн А. Н., Юранев О. А. О способе проведения наземной отработки изделий ракетно-космической техники на переходные процессы с использованием копрово-пружинного стенда // Сибирский журнал науки и технологий. 2019. Т. 20, № 1. С. 54–61. Doi: 10.31772/2587-6066-2019-20-1-54-61

AN APPROACH TO GROUND TESTING OF ROCKETS AND SPACE VEHICLES ON TRANSIENT PROCESSES BY COPRA-SPRING STAND

A. Yu. Bondarenko, A. Yu. Mitin, V. A. Tolchenov, A. N. Eykhorn*, O. A. Yuranev

Central Scientific-Research Institute of Mechanical Engineering
4, Pionerskaya St., Korolev, 141070, Russian Federation
*E-mail: EykhornAN@tsniimash.ru

The authors propose an approach to research tests of copra-spring stand, designed for testing rockets and spacecraft on inertial forces of a pulse character. The authors present the design of the stand, consisting of two main parts: mobile and stationary.

The authors present a method for calculating the magnitude of the load factors and the oscillation frequency of the test object, and calculate the parameters for adjusting the spring stiffness. They describe the possibility of carrying out dynamic tests for imitating transient loads that hermetic structures such as modules of habitable orbital stations, loaded by internal pneumatic pressure, withstand during their lifecycle.

The authors present the results of research tests when the stand without any additional weight was falling from the height of 20, 35 and 50 mm. They determine the levels of axial and transverse accelerations on the envelope of the stand and the lower ring. A comparison of the original and filtered signal from the load factor sensors obtained in each test case was made. The authors present the results of calculating accelerations of the moving part of the stand using the video processing of the experiment. To determine the position of the stand envelope they developed special software. The essence of the software was to determine the coordinate of the border of the color change from the frame height from a light color to a darker one using averaging in rows. The authors show that the results of a comparison of manual frame-by-frame measurement and data obtained by the software method indicate a sufficient convergence of the results using a drop from the height of 20 mm experiment. The comparison of axial loads obtained by various methods is given, when the moving part of the stand is thrown from the height of 20, 35 and 50 mm, respectively. The zero time points for the video and accelerometers were determined so that the first maximum is reached simultaneously.

According to the results of research tests, the authors describe the development and validation of the finite element model of the stand. The calculations were carried out in a nonlinear formulation, which makes it possible to correctly take into account the loading of the stand at all stages, using the method of direct solution of the equations of motion. The authors show the results if calculating the time dependences of displacements and load factors at the sensor installation places and a comparison with the experimental results, which shows a good convergence.

Keywords: copra-spring stand, ground tests, transient processes.

О СПОСОБЕ ПРОВЕДЕНИЯ НАЗЕМНОЙ ОТРАБОТКИ ИЗДЕЛИЙ РАКЕТНО-КОСМИЧЕСКОЙ ТЕХНИКИ НА ПЕРЕХОДНЫЕ ПРОЦЕССЫ С ИСПОЛЬЗОВАНИЕМ КОПРОВО-ПРУЖИННОГО СТЕНДА

А. Ю. Бондаренко, А. Ю. Митин, В. А. Толченов, А. Н. Эйхорн*, О. А. Юранев

Центральный научно-исследовательский институт машиностроения
Российская Федерация, 141070, Московская обл., г. Королев, ул. Пионерская, 4
*E-mail: EykhornAN@tsniimash.ru

Описывается подход к проведению исследовательских испытаний копрово-пружинного стенда, служащего для воспроизведения инерционных нагрузок импульсного характера. Описывается конструкция стенда, состоящего из двух основных частей: подвижной и неподвижной.

Приводится метод расчета величины перегрузки и частоты колебаний объекта испытаний, а также производится расчет параметров регулировки жесткости пружин. Описывается возможность проведения

динамических испытаний для воспроизведения нагружения герметичных конструкций типа модулей обитаемых орбитальных станций при переходных процессах с учетом внутреннего пневматического давления.

Описывается процесс проведения исследовательских испытаний стенда. Высота сброса равнялась 20, 35 и 50 мм. Определены уровни осевых и поперечных перегрузок на обечайке стенда и нижнем кольце. Приводится сравнение исходного и фильтрованного сигнала с датчиков перегрузок, полученных при каждом случае испытаний. Для определения положения обечайки стенда разработано специальное программное обеспечение, суть которого заключалась в определении координаты границы перехода цвета по высоте кадра из светлого цвета в более тёмный с использованием осреднения в строках. Сравнение ручного покадрового замера и данных, полученных программным методом, для одного из экспериментов показывает их хорошее согласование. Это указывает на хорошее качество определения перегрузок обечайки стенда. Приведено сравнение перегрузок, полученных различными способами, при сбросе подвижной части стенда с различных высот. Нулевые моменты времени для видео и акселерометров были определены так, чтобы достигалось совпадение по первому максимуму.

По результатам исследовательских испытаний была разработана и валидирована конечно-элементная модель стенда. Расчеты проводились в нелинейной постановке, позволяющей корректно учесть нагружение стенда на всех этапах, с использованием метода прямого интегрирования уравнений движения. Определены временные зависимости перемещений и перегрузок в местах установки датчиков, а также проведено сравнение с результатами эксперимента.

Ключевые слова: копрово-пружинный стенд, испытания, переходные процессы.

Introduction. As experience confirms the most intensive dynamic loads of launch vehicle and space vehicle structures occur in a low frequency range i.e. up to 100 Hz and are realized in transient processes. Processes of this kind appear when rising and dropping propulsion system thrust; when starting the launch vehicle and dividing its stages; under the influence of wind gusts as well as in various abnormal situations [1; 2].

The replacement of a non-stationary process with an equivalent harmonic loading using a vibration stand [3–5] is a generally accepted method of such ground based experimental testing of dynamic effects. However, with such testing it is possible to obtain significant differences in the maximum levels of overloads and the number of loading cycles with the peak level is ten times higher than the real one [6; 7]. This is especially important in case when it is necessary to conduct dynamic tests of rocket and space technology products that have already been in flight operation.

Therefore, an alternative approach to the rocket and space technology ground testing (its structures, instrumentation and mounting equipment) is proposed, the essence of which is the direct reproduction of transient processes.

A copra-spring stand (fig. 1) installed in the testing room of TsNIIMash temperature and static strength department may be used for this purpose [8–10].

Stand description. Structurally, the stand consists of two parts: mobile and stationary which move in the vertical direction relative to one another. As it is shown in fig. 1 the mobile part includes a stand envelope, vibration isolators and a lower ring. The stationary part includes a strong ring, guide supports, a top ring and special latches. The stationary part is fixed to the floor. A test object is attached to the mobile part, whereat it together with the test object is raised on a pointed height and dropped down. On coming in contact the lower ring is attached to the stationary part into a whole by the special latches. The loading occurs in the process of braking on the base with the compression springs.

Testing on the copra-spring stand can logically be divided into three parts:

1. Raising the stand to the required height and hanging by level with the help of turnbuckles. Before the next step the stand should be at rest.
2. Opening the latches and the stand is in a freefall until it touches the lower ring with the stationary part.
3. Locking the lower ring of the mobile part with the special latches and measuring the load factor on the mobile part.

The load factors and the oscillation frequency of the test object are defined by the number of springs used, their total stiffness and drop height. The calculation of the experiment parameters may be approximately performed by means of energy conservation law, body motion during free fall and the theory of mass oscillation on the constant stiffness spring [11].

Nevertheless, this approach does not take into account the mutual movement of the stand moving parts due to prestressing of elastic connectors between them. This process may be modeled using the finite-element method. The test simulation was performed with the use of MSC Nastran software and includes two calculations:

1. At the first stage constant inertial load displacement of model nodes is calculated. A vector of initial displacement of the system which is held with the latch before the drop is a result of this calculation.
2. The results of the first calculation are used as the initial conditions for the second one to simulate the stand motion in the field of gravitation and its oscillation on the compression springs after the impact with the base.

The stand allows the loading of such objects as ICC modules, advanced long-term orbital stations, advanced launch vehicle elements, reusable space and aerospace systems, advanced manned and transport vehicles weighing up to 20 t.

There is no analog for the copra-spring stand with such characteristics [12]. There are just stands which reproduce dynamic loads for the test objects of lower masses [13]. Another distinctive feature is creating loads of hermetic structures such as modules of habitant orbital stations with internal pneumatic pressure. It is possible due to placement of the stand into a pneumatic hydro box RM-2 (fig. 2).

A test object is loaded into the box through the upper end opening which may, if necessary, be closed with the armored cover plate if required. The energy intensity of the breaking test object may come up to $30 \cdot 10^6$ atm-l under hydraulic and $10 \cdot 10^6$ atm-l under pneumatic loading.

For loading with internal overpressure when performing the tests an independent pneumatic system is mounted onto the copra-spring stand (fig 3).

The pressure source (fig. 3, pos. *1*) is selected on the basis of volume and required value of the test object prescribed pressure. The balloon reducer (fig. 3, pos. *2*) lowers the pressure providing the necessary pressure in the test object. The safety valve (fig. 3, pos. *3*) releases the pressure when the required value is exceeded. For complete pressure relief from the test object (fig. 3, pos. *5*) a relief valve is provided. The internal pressure is monitored according to the pressure sensor readings (fig. 3, pos. *4*).

Research tests operation. Research tests were carried out on the described above stand. They included a drop of the mobile part on the stationary one without the test object. The drop heights were 20, 35 and 50 mm (three drops from each height). Herewith, the levels of axial and transverse overloads on the envelope of the stand and the lower ring were determined. During the tests a minimum set of springs (4 pcs) was used; the expected frequency of the stand longitudinal oscillations was ~3 Hz.

The primary transducers location is shown in fig. 4. The magnitude of the overloads was determined by the accelerometers readings and the dump height was estimated by the readings of the displacement sensors.

When testing the axial load on the upper ring was measured by the parameters of B1, B4, B10 and B13. In fig. 5 raw results by the parameters of B4, B13 obtained by the drop from the height of 20 mm are shown.

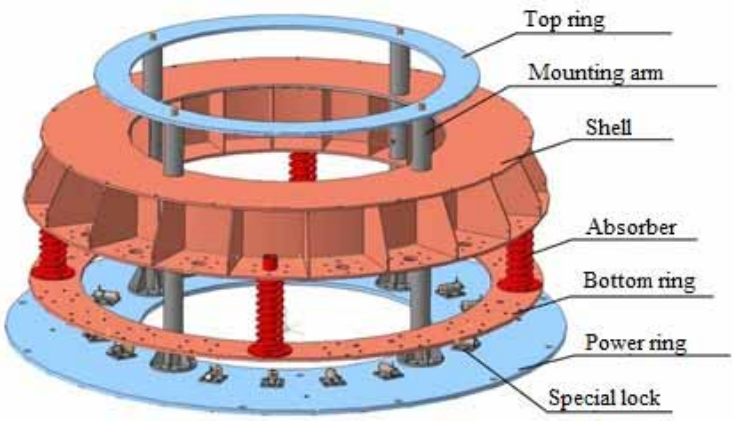

Fig. 1. General view of the main elements of the copra-spring stand

Рис. 1. Общий вид основных исполнительных элементов копрово-пружинного стенда

Fig. 2. General view of the pneumatic hydro box RM-2

Рис. 2. Общий вид пневмогидробокса РМ-2

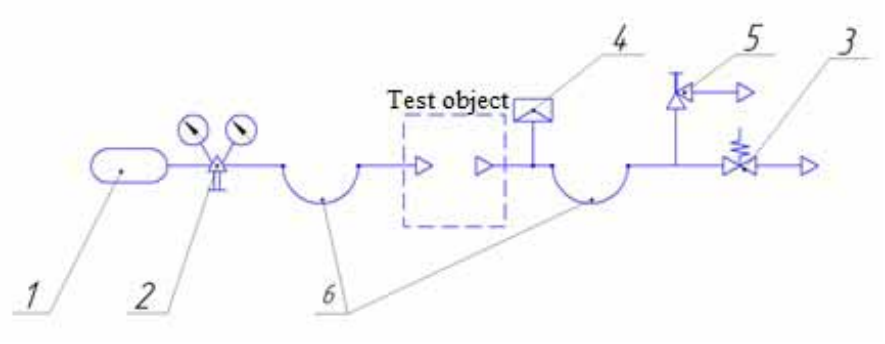

Fig. 3. Internal pressure loading system:
1 – pressure source (balloon etc.); *2* – balloon reducer; *3* – manual adjustable safety valve; *4* – pressure meter; *5* – adjustable manual faucet; *6* – flexible sleeves

Рис. 3. Система нагружения внутренним давлением:
1 – источник давления (баллон, рампа, моноблок и т. п.); *2* – редуктор баллонный; *3* – клапан предохранительный регулируемый ручной; *4* – датчик давления; *5* – вентиль ручной регулируемый; *6* – гибкие рукава

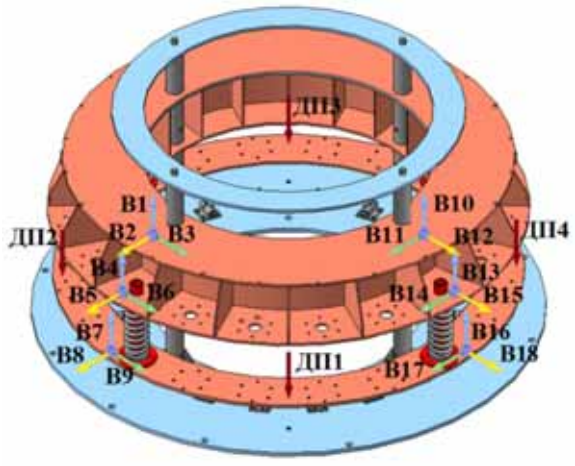

Fig. 4. Layout of primary transducers:
ДП1…ДП4 – Motion sensors; B1…B18 – accelerometers

Рис. 4. Схема размещения первичных преобразователей:
ДП1…ДП4 – датчики перемещения; B1…B18 – акселерометры

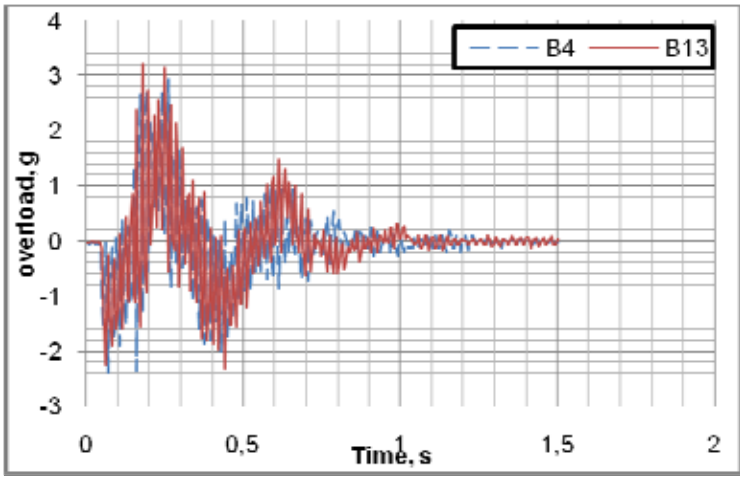

Fig. 5. Raw results from the sensors B4, B13. Drop from the height of 20 mm

Рис. 5. Необработанные результаты с датчиков B4, B13. Сброс с высоты 20 мм

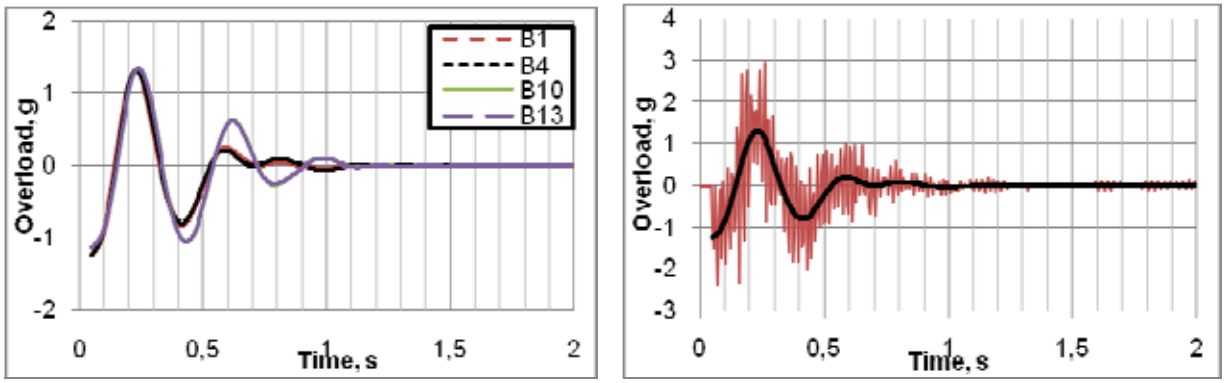

Fig. 6. Comparison of low-frequency components of basic overloads for various parameters (*left*). Comparison of the original and filtered process (*right*). Drop from the height of 20 mm

Рис. 6. Сравнение НЧ-составляющих записей осевых перегрузок по различным параметрам (*слева*) и сравнение исходного и фильтрованного процесса (*справа*) при сбросе с 20 мм

The high-frequency component of the overload data records is related to the self-oscillation excitation of the stand parts. At this stage the stand vibrations at the main longitudinal frequency arouse great interest. Therefore, the data on overloads were filtered out with a low-pass filter without a phase change using the Matlab software. Within the low-frequency range of axial overloads the parameters located in the same vertical plane do not differ (fig. 6, *left*), that is why non-coplanar sensors B4 and B13 were chosen for further study. The differences of these sensors readings are due to the presence of an additional component from the transverse oscillations of the stand envelope at frequencies close to the fundamental frequency of the longitudinal vibrations.

In fig. 6 (*right*) the comparison of raw and filtered signals for the sensor B4 when dropped from the height of 20 mm is shown. A similar pattern may be observed in other tests.

Along with the readings of the overloads sensors, when analyzing the results, an assessment was made of overloads levels based on the video of the stand envelope displacement with a frame rate of 120 fps.

To determine the position of the stand envelope special software was developed. The essence of the software was to determine the coordinate of the color transition boundary by the height of the frame from light to darker colour using averaging in rows. To break video record into the frames and cut pieces from frames the open program “ffmpeg” was used. For verification of the developed software manual frame-by-frame measurement of the stand envelope coordinates from time to time was made for one of the experiments.

It turned out that the developed method allows to determine the displacement of the stand mobile part with good accuracy. Thus, the obtained video data may be used for interpretation as well. The further video recordings were processed with the use of the open library PIL (Python Imaging Library). The obtained records of displacement were smoothed out with a low-frequency filter without the phase displacement in order to eliminate interference of records errors and cutting inaccuracies. Axial overloads were calculated by double differentiation of displacement records over time.

A comparison of overloads obtained in various methods when the stand mobile part was dropped from the height of 35 mm is shown in fig. 7. Zero points in time were defined so that the acceleration peaks coincided.

The comparison of overload levels in parameter B4 for a series of three drops from the height of 35 mm is shown in fig. 8. As the figure shows these overload levels are in good agreement.

According to the research tests, the finite element model of the stand was developed and validated under MCS Nastran [14; 15] (fig. 9).

The copra-spring stand structure is a three-dimensional mechanical system of complex design-layout scheme whose parts possess essentially different bending and dissipative characteristics. The finite element method was used for calculation. This calculation was carried out in a nonlinear formulation which made it possible to correctly take into account the stand loading at all the stages using the direct integration method of the equations of motion.

In order to simulate the inelastic nature of the mobile and stationary parts collision at the contact position, an additional force is applied to the central assembly on the stand lower part. The magnitude of the force is chosen in such a way as to avoid reverse movement of the mobile part.

The calculation was carried out using the direct integration method of the equations of motion. The damping parameters were set in such a way that the calculated values of the accelerations corresponded best to the measured ones. As a result, the time dependences of displacements and overloads at the sensor installation sites were determined, and a comparison was made with the experimental results.

In fig. 10 a comparison of experimental (recorded and obtained by video processing) and calculated overloads at the sensor B4 installation site is shown. All the data is given after the low-frequency filtration.

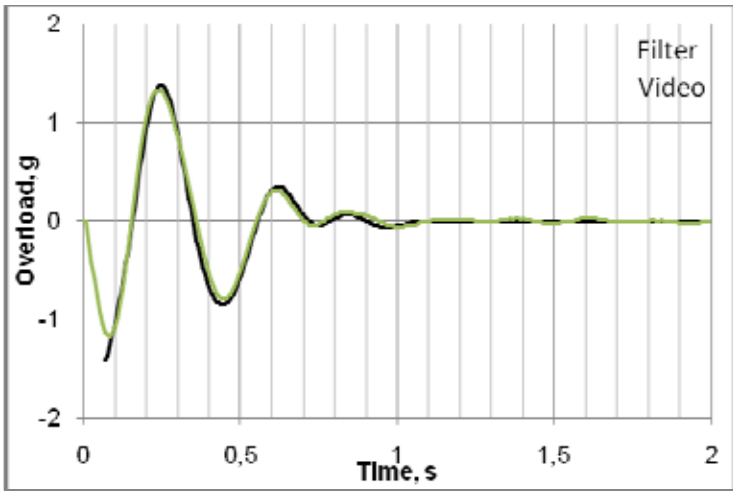

Fig. 7. Comparison of data with accelerometer and video.
Drop from the height of 35 mm

Рис. 7. Сравнение данных с акселерометра и видео
при сбросе с высоты 35 мм

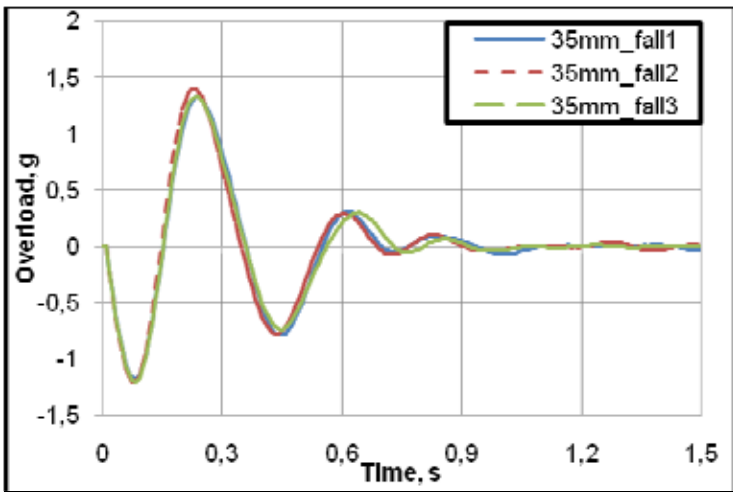

Fig. 8. Overload comparison. Drop from the height of 35 mm

Рис. 8. Сравнение перегрузок при сбросах с высоты 35 мм

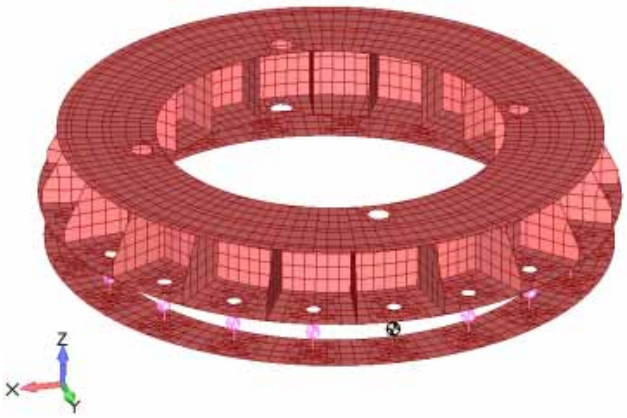

Fig. 9. Finite element model of the movable part of the copra-spring stand

Рис. 9. Конечноэлементная модель подвижной части
копрово-пружинного стенда

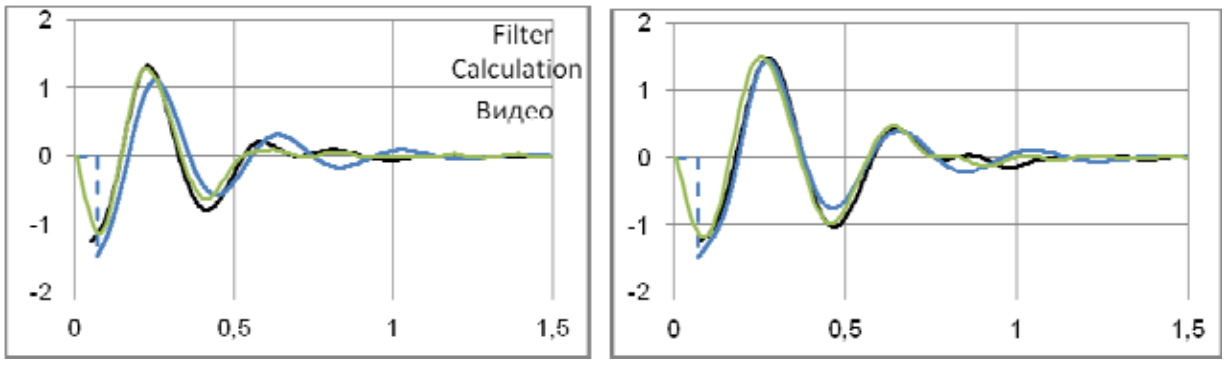

Fig. 10. Comparison of calculated and experimental overloads. Drop from the height of 20 mm (*left*) and drop form the height 50 mm (*right*). High-frequency components in dependencies are deleted

Рис. 10. Сравнение расчетных и экспериментальных перегрузок при сбросе ОИ с высоты 20 мм (*слева*) и 50 мм (*справа*). ВЧ-составляющие в зависимостях убраны

As the fig. 10 shows it was possible to achieve good agreement between the calculated and experimental data at the fundamental frequency of the stand longitudinal vibrations (~3 Hz for the used set of springs).

The high-frequency component in the overloads records (see fig. 5) is due to the bending vibrations of the stand envelope at the frequency of ~ 55 Hz (53.6 Hz and 55.2 Hz in the calculation model). Such a coincidence of the calculated and experimental tones additionally indicates the correctness of the developed model. It should be noted that this frequency may vary significantly depending on the test object and equipment used.

Conclusion. Thus, according to the results of the conducted research tests, it was possible to achieve a good agreement between the calculated and experimental data on overloads at the main frequency of the stand longitudinal vibrations. The developed model may be used to determine the test conditions and loads evaluation of the test object. Before testing, it is recommended to conduct a series of drops without the test object for additional validation of the stand finite element model.

References

1. Soyuz User's Manual, Iss. 2, Revision 0. March 2012, Arianespace.

2. Proton Launch System Mission Planner's Guide, LKEB-9812-1990, Iss. 1, Revision 7, 2009.

3. Karmishin A. V., Likhoded A. I., Panichkin N. G. *Osnovy otrabotki prochnosti raketno-kosmicheskikh konstruktsiy* [The principles of stress support of space-rocket designs]. Moscow, Mashinostroenie Publ., 2007, 470 p.

4. Belyayev I. T., Zernov I. A. *Tekhnologiya sborki i ispytaniy kosmicheskikh apparatov* [Assembly and tests of space vehicles]. Moscow, Mashinostroenie Publ., 1990, 352 p.

5. Anisimov A. V., Asatur'yan V. S., Balakirev Yu. G. et al. *Metodologicheskiye osnovy nauchnykh issledovaniy pri obosnovanii napravleniy kosmicheskoy deyatel'nosti, oblika perspektivnykh kosmicheskikh kompleksov i sistem ikh nauchno-tekhnicheskogo soprovozhdeniya. T. 5. Metodologiya issledovaniy prochnosti i dinamiki raketnositeley i kosmicheskikh apparatov* [The basics of methodology of scientific research on substantiation of fields of space research, appearance of perspective spacecraft and systems of their scientific and technological support. Vol. 5. Methdodlogy of research of strength and dynamics of space rockets and spacecraft]. Moscow, Dashkov i K° Publ., 2016, 376 p.

6. Lipnitskiy Yu. M., Likhoded A. I., Sidorov V. V. [A comparative analysis of the loading spectra of structures with vibration excitation and acoustic pressure pulsations]. *Kosmonavtika i raketostroyeniye*. 2007, No. 2(47), P. 84–93 (In Russ.).

7. Bondarenko A. Yu., Sidorov V. V. [An approach to ground simulation of space vehicle loading, caused by transient processes]. *Kosmonavtika i raketostroyeniye*. 2016, No. 3(88), P. 77–82 (In Russ.).

8. Kolozeznyy A. E. [Tasks of strength tests centers in the field of finite-element modelling. Part 1]. *Kosmonavtika i raketostroyeniye*. 2014, No. 4(77), P. 164–170 (In Russ.).

9. Aleksandrov S. S., Bondarenko A. Yu., Eykhorn A. N. et al. [Copra-spring stand for loading of spaceraft inertial forces of a pulse character]. *Kosmonavtika i raketostroyeniye*. 2017, No. 4(97), P. 65–70 (In Russ.).

10. A. Yu. Bondarenko, A. Yu. Mitin, V. A. Tolchenov et al. [An approach to ground testing of rockets and space vehicles on transient processes by copra--spring stand]. *Materialy XXII Mezhdunar. nauch. konf. "Reshetnevskie chteniya"* [Materials XXII Intern. Scientific. Conf "Reshetnev reading"]. Krasnoyarsk, 2018, P. 326–328 (In Russ.).

11. Babakov I. M. *Teoriya kolebaniy* [The theory of oscillations]. Moscow, Nauka Publ., 1968, 560 p.

12. Evropeytsev A. A., Mazhirin V. F., Podzorov V. N. et al. *Ispytanie konstruktsiy ili sooruzheniy na vibratsiyu, na udarnye nagruzki* [Tests of structures and spacecraft on vibration and shock loads]. Patent RF, G01M7/00, 2005.

13. Karmishin A. V., Skurlatov E. D., Startsev V. G. et al. *Nestatsionarnaya aerouprugost' tonkostennykh konstruktsiy* [Nonlinear aeroelasticity of thin-walled structures]. Moscow, Mashinostroenie Publ., 1982, 240 p.

14. Zenkevich O., Morgan K. *Konechnyye elementy i approksimatsiya* [Finite element and approximation]. Moscow, Mir Publ., 1986, 320 p.

15. MD NASTRAN. Dynamic Analysis User's Guide. MSC. Software Corporation, 2010. 556 p.

Библиографические ссылки

1. Soyuz User's Manual, Iss. 2, Revision 0. March 2012, Arianespace.

2. Proton Launch System Mission Planner's Guide, LKEB-9812-1990, Iss. 1, Revision 7, 2009.

3. Основы отработки прочности ракетно-космических конструкций / А. В. Кармишин, А. И. Лиходед, Н. Г. Паничкин [и др.]. М. : Машиностроение, 2007. 471 с.

4. Беляев И. Т., Зернов И. А. Технология сборки и испытаний космических аппаратов. М. : Машиностроение, 1990. 352 с.

5. Методологические основы научных исследований при обосновании направлений космической деятельности, облика перспективных космических комплексов и систем их научно-технического сопровождения. Т. 5. Методология исследований прочности и динамики ракет-носителей и космических аппаратов / А. В. Анисимов, В. С. Асатурьян, Ю. Г. Балакирев [и др.]. М. : Дашков и К, 2016. 376 с.

6. Липницкий Ю. М., Лиходед А. И., Сидоров В. В. Сравнительный анализ спектров нагружения элементов конструкций при их вибрационном возбуждении и пульсациях акустического давления // Космонавтика и ракетостроение. 2007. № 2. С. 84–93.

7. Бондаренко А. Ю., Сидоров В. В. Методический подход к наземной отработке конструкций ракетно-космической техники при нагрузках, возникающих в результате переходных процессов // Космонавтика и ракетостроение. 2016. № 3(88). С. 77–82.

8. Колозезный А. Э. Задачи прочностных испытательных центров в эпоху численного моделирования. Ч. 1 // Космонавтика и ракетостроение. 2014. № 4(77). С. 164–170.

9. Копрово-пружинный стенд для нагружения космических аппаратов инерционными силами импульсного характера / С. С. Александров, А. Ю. Бондаренко, А. Н. Эйхорн [и др.] // Космонавтика и ракетостроение. 2017. № 4(97). С. 65–70.

10. Подход к наземным испытаниям ракет и космических аппаратов на переходных процессах на стенде Копра-рессора // Решетневские чтения (12–16 нояб. 2018, г. Красноярск) / под общ. ред. Ю. Ю. Логинова ; СибГУ им. М. Ф. Решетнева. 2018. С. 326–328.

11. Бабаков И. М. Теория колебаний. М. : Наука, 1968. С. 560.

12. Патент G01M7/00. Испытание конструкций или сооружений на вибрацию, на ударные нагрузки / Европейцев А. А., Мажирин В. Ф., Подзоров В. Н. [и др.]. Опубл. 10.04.2005.

13. Нестационарная аэроупругость тонкостенных конструкций / А. В. Кармишин, Э. Д. Скурлатов, В. Г. Старцев [и др.]. М. : Машиностроение, 1982. 240 с.

14. Зенкевич О., Морган К. Конечные элементы и аппроксимация : пер. с англ. М. : Мир, 1986. 320 с.

15. MD NASTRAN. Dynamic Analysis User's Guide. MSC. Software Corporation, 2010. 556 p.

Bondarenko Andrei Yurevich – Junior Researcher; Federal State Unitary Enterprise "Central Scientific-Research Institute of Mechanical Engineering". E-mail: EykhornAN@tsniimash.ru.

Mitin Andrei Yurevich – Junior Researcher; Federal State Unitary Enterprise "Central Scientific-Research Institute of Mechanical Engineering". E-mail: MitinAY@tsniimash.ru.

Tolchenov Vladimi Alexeyevich – Engineer; Federal State Unitary Enterprise "Central Scientific-Research Institute of Mechanical Engineering". E-mail: EykhornAN@tsniimash.ru.

Eykhorn Alexander Nikolaevich – the head of the stand – the head of the group; Federal State Unitary Enterprise "Central Scientific-Research Institute of Mechanical Engineering". E-mail: EykhornAN@tsniimash.ru.

Yuranev Oleg Aleksandrovich – head of the laboratory; Federal State Unitary Enterprise "Central Scientific-Research Institute of Mechanical Engineering". E-mail: JuranevOA@tsniimash.ru.

Бондаренко Андрей Юрьевич – младший научный сотрудник; федеральное государственное унитарное предприятие «Центральный научно-исследовательский институт машиностроения». E-mail: EykhornAN@tsniimash.ru.

Митин Андрей Юрьевич – младший научный сотрудник; федеральное государственное унитарное предприятие «Центральный научно-исследовательский институт машиностроения». E-mail: MitinAY@tsniimash.ru.

Толчёнов Владимир Алексеевич – инженер; федеральное государственное унитарное предприятие «Центральный научно-исследовательский институт машиностроения». E-mail: EykhornAN@tsniimash.ru.

Эйхорн Александр Николаевич – начальник стенда – руководитель группы; федеральное государственное унитарное предприятие «Центральный научно-исследовательский институт машиностроения». E-mail: EykhornAN@tsniimash.ru.

Юранев Олег Александрович – начальник лаборатории; федеральное государственное унитарное предприятие «Центральный научно-исследовательский институт машиностроения». E-mail: JuranevOA@tsniimash.ru.

UDC 629.7.042.2.001.24:622.998
Doi: 10.31772/2587-6066-2019-20-1-62-67

For citation: Gusev S. A., Nikolaev V. N. [Parametric identification of the heat condition of radio electronic equipmentin airplane compartment]. *Siberian Journal of Science and Technology.* 2019, Vol. 20, No. 1, P. 62–67. Doi: 10.31772/2587-6066-2019-20-1-62-67

Для цитирования: Гусев С. А., Николаев В. Н. Параметрическая идентификация теплового состояния радиоэлектронного оборудования в приборном отсеке самолёта // Сибирский журнал науки и технологий. 2019. Т. 20, № 1. С. 62–67. Doi: 10.31772/2587-6066-2019-20-1-62-67

PARAMETRIC IDENTIFICATION OF THE HEAT CONDITION OF RADIO ELECTRONIC EQUIPMENTIN AIRPLANE COMPARTMENT

S. A. Gusev [1,2], V. N. Nikolaev [3*]

[1] Institute of Computational Mathematics and Mathematical Geophysics SB RAS
6, Academika Lavrent'eva Av., Novosibirsk, 630090, Russian Federation
[2] Novosibirsk State Technical University
20, K. Marksa Av., Novosibirsk, 630073, Russian Federation
[3] Siberian Aeronautical Research Institute Named After S. A. Chaplygin
21, Polzunova St., Novosibirsk, 630051, Russian Federation
* E-mail: sag@osmf.sscc.ru

A mathematical model of the aircraft avionics thermal state describing the heat exchange of the onboard equipment housing with a honeycomb structure made of a carbon fiber composite, the process of heat transfer of the onboard equipment elements and the air is developed. The considered heat transfer process in a heterogeneous medium is described by the boundary value problem for the heat equation with boundary conditions of the third kind. To solve the direct problem of the onboard equipment housing with a honeycomb structure thermal state, the Monte- Carlo method on the basis of the probabilistic representation of the solution in the form of an expectation of the functional of the diffusion process is used. The inverse problem of the honeycomb structure heat exchange is solved by minimizing the function of the squared residuals weighted sum using an iterative stochastic quasigradient algorithm. The developed mathematical model of the onboard equipment in the unpressurized compartment thermal state is used for optimizing the temperature and airflow of the thermal control system of the blown onboard equipment in the unpressurized compartment of the aircraft.

Keywords: mathematical model, thermal state, honeycomb structure, parabolic boundary value problem.

ПАРАМЕТРИЧЕСКАЯ ИДЕНТИФИКАЦИЯ ТЕПЛОВОГО СОСТОЯНИЯ РАДИОЭЛЕКТРОННОГО ОБОРУДОВАНИЯ В ПРИБОРНОМ ОТСЕКЕ САМОЛЁТА

С. А. Гусев[1,2], В. Н. Николаев[3*]

[1]Институт вычислительной математики и математической геофизики СО РАН
Российская Федерация, 630090, г. Новосибирск, просп. академика Лаврентьева, 6
[2]Новосибирский государственный технический университет
Российская Федерация, 630073, г. Новосибирск, просп. Карла Маркса, 20
[3]Сибирский научно-исследовательский институт авиации имени С. А. Чаплыгина
Российская Федерация, 630051, г. Новосибирск, ул. Ползунова, 21
*E-mail: sag@osmf.sscc.ru

Разработана математическая модель теплового состояния бортового радиоэлектронного оборудования летательного аппарата, описывающая теплообмен корпуса бортового оборудования с сотовой конструкцией из углепластикового композита, процесс теплопередачи элементов бортового оборудования и воздушной среды. Рассматриваемый процесс переноса тепла в неоднородной среде описывается краевой задачей для уравнения теплопроводности с граничными условиями третьего рода. Для решения прямой задачи теплового состояния сотовой конструкции корпуса бортового оборудования использован метод Монте-Карло на основе вероятностного представления решения в виде математического ожидания функционала от диффузионного процесса. Обратная задачи теплообмена сотовой конструкции решена путем минимизации функции взвешенной суммы квадратов невязок с помощью итерационного стохастического квазиградиентного алгоритма. Разработанная математическая модель теплового состояния бортового оборудования в негерметизирован-

ном отсеке была применена для оптимизации температуры и расхода воздуха системы обеспечения теплового режима продуваемого бортового оборудования в негерметизированном отсеке летательного аппарата.

Ключевые слова: математическая модель, тепловое состояние, сотовая конструкция, гетерогенные структуры, параболическая краевая задача.

Introduction. To design the aircraft avionics with a given reliability is necessary to determine the required thermal characteristics of the insulated body of avionics and thermal control system. To do this, the study of the thermal state of avionics in the aircraft compartment, using a mathematical model of their thermal state is conducted. The model should take into account the unsteady heat transfer of the insulated housing, the transfer of heat energy from one part of the equipment to another by the air flow, the convective heat transfer of the equipment elements.

The mathematical model will be a system of partial differential equations and ordinary differential equations, the number of which can reach tens or hundreds for real equipment. Therefore, it is necessary to develop effective methods for solving direct and inverse problems in the study of heat transfer of elements of onboard equipment and estimation of the error of parametric identification.

A physical model of the thermal state of onboard equipment in the compartment of the aircraft. The thermal condition of the onboard equipment in the aircraft compartment is formed by external and internal factors. External factors include heat exchange between the outer surface of the avionics and the air environment, radiation heat exchange of the outer surface of avionics and other surfaces in the compartment. Inside the onboard equipment, thermal energy is released by the elements of the onboard equipment and is withdrawn or supplied by the heat supply system [1].

Mathematical model of the thermal state of onboard equipment in the aircraft compartment. The body of the onboard equipment in the aircraft compartment is a structure that includes a heat-protective honeycomb panel made of carbon fiber composite filled with air. The process of heat transfer in honeycomb panels is described by the boundary value problem for the heat equation with discontinuous coefficients. To solve this boundary value problem, the Monte-Carlo method based on stochastic differential equations is used in combination with the method of wandering in moving spheres [2]. In general, the heat transfer process in the carbon fiber panel is described by the equations [1; 3]:

$$C_{cv}(x)\,T_{cv,t} = (\lambda_{cv}(x)\,T_{cv,x})_x, \quad 0 < x < l,\ 0 < t \le t_k; \qquad (1)$$

$$\lambda_{cv}(x)\,F_{cv}\,T_{cv,x} = \alpha_{cv,out}(t)\,F_{cv}\,(T_{cv}(t,x) - T_{air,out}(t)) + Q_{cv,out}, \quad x = 0; \qquad (2)$$

$$\lambda_{cv}(x)\,F_{cv}\,T_{cv,x} = \alpha_{cv,in}(t)\,F_{cv}\,(T_{air,in}(t) - T_{cv}(t,x)) + Q_{cv,in}, \quad x = l; \qquad (3)$$

$$T_{cv}(0,x) = T_0(x), \quad 0 < x < l, \qquad (4)$$

where

$$C_{cv}(x) = \begin{cases} C_{compo}, & x \in compo; \\ C_{air}, & x \in air, \end{cases}$$

$$\lambda_{cv}(x) = \begin{cases} \lambda_{compo}, & x \in compo; \\ \lambda_{air}, & x \in air, \end{cases}$$

It means, that the coefficients C_{cv}, λ_{cv} depend on which layer the heat transfer is considered.

In equations (1)–(4) the following notations are used: $T_{cv}(t,x)$ – the temperature of the honeycomb panel; $T_{cv,t}$ – the first derivative T_{cv} of t; $T_{cv,x}$ – the first derivative T_{cv} of x; $T_{cv,x,x}$ – the second derivative T_{cv} of x; $C_{cv}(x)$ – volumetric heat capacity of the case honeycomb panel, determined by the heat capacity of the composite C_{compo} and air capacity C_{air}; $\lambda_{cv}(l)$ – the thermal conductivity of the honeycomb panel, determined by the thermal conductivity of the composite λ_{compo} and air thermal conductivity λ_{air}; $\alpha_{cv,out}$ – heat transfer coefficient of the outer surface of the equipment housing; $\alpha_{cv,in}$ – heat transfer coefficient of the inner surface of the equipment housing; F_{cv} – the area of the equipment body for external and internal heat exchange; $Q_{cv,out}$ – heat energy of external sources; $T_{air,out}$ – the air temperature in the compartment; t – time; $T_{air,in}$ – air temperature in onboard equipment or its part; l – the thickness of the honeycomb panel.

The process of heat transfer of the elements of the onboard equipment is presented in the form of an ordinary differential equation describing the convective-radiation heat transfer with the surrounding structures:

$$T_{m,t} = \alpha_{air,m}(t)\,F_{air,m}/C_m(T_{air}(t) - T_m) + \sum_m g_{j,m}/C_m\,T_j^4(t)/T_{ms}^4 - c_0\varepsilon_m\,F_m/C_m T_m^4 + Q_m/C_m, \qquad (5)$$

where T_m – the temperature of *m*-element of onboard equipment; $T_{m,t}$ – the first derivative T_m of t; $\alpha_{air,m}$ – heat transfer coefficient of *m*-element of onboard equipment; $F_{air,m}$ – the area of *m*-element of onboard equipment in convective heat exchange; C_m – heat capacity of *m*-element of onboard equipment; $g_{j,m}$ – radiation heat transfer coefficient of the system "*j*-element – *m*-element of onboard equipment"; ε_m – emission black ratio of *m*-element; Q_m – heat dissipation or heat absorption energy of *m*-element by onboard equipment from the air conditioning system and converted from electrical energy.

The equation of air heat exchange in the unpressurized blown onboard equipment is presented in the form of an

ordinary differential equation describing the convective heat transfer of the inner surface of the housing of the on-board equipment, the elements of the on-board equipment and the enthalpy transfer from one part of the on-board equipment to another:

$$T_{air,k,t} = \alpha_{cv,in}(t) F_{cv} / C_{air,k} [T_{cv}(t,x) - T_{air,k} + \\ + \sum_j \alpha_{air,j} F_{air,j} / C_{air,k} (T_j - T_{air,k}) + \\ + c_p J_{air,k} F_k / C_{air,k} (T_{air,k-1} - T_{air,k}); \quad x = l, \qquad (6)$$

where $T_{air,k-1}, T_{air,k}$ – air flow temperatures respectively in $(k-1)$ and k parts of onboard equipment; $J_{air,k}$ – the mass rate of the air flow in k part of onboard equipment; F_k – the total area of the air channels in k part of onboard equipment; c_p – specific heat capacity of air; $C_{air,k}$ – heat capacity of air in k part of onboard equipment.

Summation in equation (6) is carried out according to the *j*-element included in the *k*-part of the on-board equipment.

Heat capacity of air $C_{air,k}$ is calculated by the equation:

$$C_{air,k} = c_p \rho_{air,k} (W_{air,ent} F_{air,ent} \Delta t + V_{air,k}), \qquad (7)$$

where $\rho_{air,k}$ – air density in *k*-part of onboard equipment; $W_{air,ent}$ – air velocity at the inlet to the on-board equipment; $F_{air,ent}$ – the area of air channels at the inlet to the first part of the on-board equipment; Δt – time discretization interval in solving a system of differential equations; $V_{air,k}$ – air volume in *k*-part of the on-board equipment.

Heat transfer coefficients of surfaces $\alpha_{cv,out}$, $\alpha_{cv,in}$, $\alpha_{air,m}$ in equations (2)–(6) will be calculated using the methods described in [3; 4].

The coefficients of radiation heat transfer in equation (5) are determined by the Monte-Carlo method [5].

Application of the Monte Carlo method to solve the direct problem of the thermal state of the honeycomb structure of the housing of onboard equipment. In the case where the honeycomb panel (figure) the housing of the onboard equipment is considered as a homogeneous medium with averaged coefficients of volumetric heat capacity and thermal conductivity, heat transfer through the housing of the onboard equipment is described by equations (1)–(4). However, the averaged thermophysical properties of inhomogeneous medium can vary with a change in the direction of heat flow [6]. For this reason, we also consider the determination of the thermal state of a honeycomb panel as a solution to a three-dimensional boundary value problem for the thermal conductivity equation with a discontinuous thermal diffusivity. Due to the peculiarities of the method used, it is assumed that the thermal diffusivity coefficients of the composite and the air are constant.

There is a description of the boundary value problem below. The area in which the boundary value problem under consideration is defined is a rectangular parallelepiped $G = (-l_1, l_1) \cdot (-l_2, l_2) \cdot (0, l_3)$. Where *G* is the union of two disjoint subsets: $G = G_1 \cup G_2$, where G_1 – is a subset, corresponding to the frame and plates limiting the panel, G_2 is the union of subsets, corresponding to the cells with air. The considered heat transfer process takes place on the time interval [0,T] and is described by the following boundary value problem for the heat equation:

$$\frac{\partial T_{cv}}{\partial t} = \sum_{i=1}^{3} \frac{\partial}{\partial x_i} \left(a(x) \frac{\partial T_{cv}}{\partial x_i} \right), \qquad (8)$$

where

$$a(x) = \begin{cases} a_{compo}, x \in G_1 \\ a_{cair}, x \in G_2 \end{cases};$$

$$\left. \frac{\partial T_{cv}}{\partial x_1} \right|_{x_1 = -l_1} = 0, \quad \left. \frac{\partial T_{cv}}{\partial x_1} \right|_{x_1 = l_1} = 0; \qquad (9)$$

$$\left. \frac{\partial T_{cv}}{\partial x_2} \right|_{x_2 = -l_2} = 0, \quad \left. \frac{\partial T_{cv}}{\partial x_2} \right|_{x_2 = l_2} = 0; \qquad (10)$$

$$-\lambda_{cv} \left. \frac{\partial T_{cv}}{\partial x_3} \right|_{x_3 = l} = \alpha_{cv,out}(t) (T_{cv} - T_{air,out}(t)); \qquad (11)$$

$$\lambda_{cv} \left. \frac{\partial T_{cv}}{\partial x_3} \right|_{x_3 = l} = \alpha_{cv,in}(t) (T_{cv} - T_{air,in}(t)). \qquad (12)$$

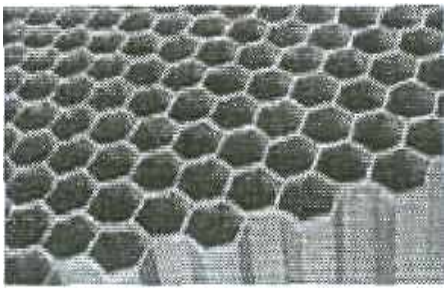

Honeycomb housing design of onboard equipment

Сотовая конструкция корпуса
бортового оборудования

In (8)–(12) equations the following designations are used: a_{compo}, a_{air} – thermal diffusivity coefficients of the composite and air, respectively; $\alpha_{cv,out}$, $\alpha_{cv,in}$ – heat transfer coefficients of the panel surface and the air environment outside and inside the onboard equipment, respectively; $T_{air,out}$, $T_{air,in}$ – air temperature at the outer side of the panel and the inner, respectively.

In [7] the existence of generalized solutions of boundary value problems with discontinuous coefficients is proved. Moreover, these solutions can be approximated by solutions of boundary value problems, in which the coefficients are the approximations of the initial discontinuous coefficients. For example, it is possible to obtain an approximate solution of the original problem by solving the problem with smoothed coefficients based on integral averaging [8]. In this paper we propose to determine the approximate solution of the problem as a problem with smoothed coefficients by the Monte-Carlo method based on the probability of representation of the solution in the form of a mathematical expectation of the functional of the diffusion process. Initially, in work [9] the estimates of the mathematical expectation of this functional were determined on the basis of the numerical solution of stochastic differential equations by the Euler method. The disadvantage of this method is its great complexity. A significant acceleration of the calculation was obtained using the combined method proposed in [2], in which the calculation of the trajectories of the diffusion process in air – filled cells (G2) was carried out by the method of wandering through moving spheres, and along the frame, bounding the plates (G1) and in their close area – by the Euler method. Note that the use of the combined method is possible only in the case of constant thermal properties of the substances that make up the honeycomb panel. A detailed description of the combined method is given in work [2].

Algorithm of parametric identification of mathematical model of thermal condition of onboard equipment. To determine the vector of the coefficients θ of the model of the thermal state of the honeycomb panel, the minimum of the function $\Phi(\theta)$ of the weighted sum of squares of residuals [10] using an iterative minimization algorithm with the derived functions $\Phi(\theta)$ should be defined. For this purpose, it is suggested to use a variant of the stochastic quasigradient algorithm with variable metric [8], in which approximations to the minimum point are constructed according to the rule:

$$\theta^{k+1} = \theta^k - \rho_k \mathrm{H}^k \nabla^k \Phi, \quad k = 0, 1, \ldots, \qquad (13)$$

where H^k – a random square matrix of size $l \times l$; $\nabla^k \Phi$ – gradient of the objective function at a point θ^k; ρ_k – step parameter.

Matrix sequence H^k is calculated by the scheme:

$$\mathrm{H}^0 = I, \mathrm{H}^{k+1} + (I - \mu_k \nabla^{k+1}\Phi \cdot (\Delta^{k+1}\theta)^T)\mathrm{H}^k, \quad \Delta^{k+1}\theta = \theta^{k+1} - \theta^k. \qquad (14)$$

Parameter μ_k is chosen from the equality $\mu_k = \mu / (\left|\nabla^{k+1}\Phi\right| \cdot \left|\Delta^{k+1}\theta\right|$, where μ – is such a constant, that $0 < \mu < 1$.

At each step of the algorithm, the step parameter is automatically adjusted ρ_k. If $\Phi(\theta^{k+1}) > \Phi(\theta^k)$, so $\rho_{k+1} = \rho_k / \gamma$, where $\gamma > 1$ – is a fixed parameter. If $\Phi(\theta^{k+1}) < \Phi(\theta^k)$, so the following sequence of actions is performed: $\rho_{k,i} = \rho_k{}^i \gamma$, $\theta^{k+1,i} = \theta^k - \rho_{k,i} \mathrm{H}^k \nabla^k \Phi$, and the calculation $\Phi(\theta^{k+1,i})$, $i = 0, 1, \ldots$.

These actions are performed until the value of the function Φ decreases and the conditions are met: $\rho_{\min} \le \rho_{k,i} \le \rho_{\max}$ ($\rho_{\min}, \rho_{\max}$ – minimum, maximum step length, respectively) and $i < i_{\max}$ ($i_{\max}$ – the specified maximum number of iterations to increase the step). The values θ^{k+1}, ρ_{k+1} are assumed to be equal to the values $\theta^{k+1,i}$, $\rho_{k,i}$ that are equal to the minimum of the obtained values $\Phi(\theta)$.

Parametric identification of a mathematical model of the thermal state of the other elements of onboard equipment proposed to carry out the composition method of the steepest descent method, Newton method and quasi-Newton method of Broyden – Fletcher – Goldfarb – Shanno [11].

When solving a rigid system of ordinary differential equations, it is proposed to use the implicit Rosenbrock method of the second order [12].

Estimation of the parameters of the mathematical model of the avionics compartment of the aircraft. Verification of the proposed theoretical method was performed for onboard equipment in the aircraft compartment, which is a block of onboard equipment in the body with a honeycomb design. The unit is blown with air from the thermal control system. The air cools or heats the elements of the onboard equipment located in the compartment. The elements of the block are separated by air layers. At the same time, the thickness of the honeycomb structure, temperature and air consumption of the system for ensuring the thermal regime of the onboard equipment unit were optimized.

The main criterion for optimizing the thickness of the honeycomb structure, temperature and air flow of the thermal control system is the air temperature in the equipment unit within the limits of 283.15–293.15 K.

The air temperature in the compartment is adjustable from 253.15 K to 328.15 K [13; 14]. At the same time, the values of the airflow in the thermal control system must be within the range of 1.5–2.0 kg/s.

The coefficient of thermal conductivity of the honeycomb structure of the block body is $\lambda_{cv} = 8 \cdot 10^{-2}$ W/(m·K).

The thickness of the honeycomb structure l_{cv} of the block body took $2 \cdot 10^{-2}$–$5 \cdot 10^{-2}$ m.

The vector of coefficients of the model

$$\Theta = [\, l_{\mathrm{cv}} \quad T_{stm} \quad G_{stm} \,]^T \qquad (15)$$

includes the thickness of the honeycomb structure l_{cv} in m, the necessary characteristics of the system to ensure the thermal control (the values of air temperature T_{stm} in K and air flow consumption G_{stm} in kg/s).

Estimates of the coefficients of the model $\hat{\bar{\Theta}}$ thickness of the honeycomb structure, for temperature and airflow consumption, respectively, are equal:

$$\hat{\bar{\Theta}} = [0.003 \quad 287.4 \quad 1.9]^T .$$

Joint confidence intervals $\Delta\Theta^*$ of uncertainty of coefficient estimates (15) $\hat{\bar{\Theta}}$ with confidence probability $\beta = 0.99$ are, respectively, equal to

$$\Delta\Theta^* = [0.0004 \quad 5.0 \quad 0.08]^T .$$

Joint confidence intervals $\Delta\Theta^*$ of each of the sought coefficients are obtained by the method given in [15].

Conclusion. A theoretical method for determining the parameters of the housing of avionics with honeycomb structures and the system of providing the thermal control of avionics on the basis of the developed mathematical model of the thermal state of avionics of the aircraft is proposed.

The determination of the thermal state of the honeycomb structure is carried out by a combined method, in which the calculation of the trajectories of the diffusion process in the cells filled with air is based on the method of wandering through the moving spheres, and along the frame, limiting plates and in their close area – by the Euler method.

A stochastic quasigradient algorithm with a variable metric is used for parametric identification of the mathematical model of the thermal state of the honeycomb structure of the housing of the onboard equipment.

The proposed method makes it possible to optimize the thermal parameters of the housing of the onboard equipment and the system of ensuring the thermal control in the design of onboard equipment.

Acknowledgments. The work of Gusev S. A. was supported by the RFBR grant No. 17-01-00698 A.

Благодарности. Работа Гусева С. А. поддержана грантом РФФИ № 17-01-00698 А.

References

1. Voronin G. I. *Air-conditioning systems onboard the aircrafts*. Moscow, Mashinostroenie Publ., 1973, 443 p.

2. Gusev S. A., Nikolayev V. N. Using a Monte Carlo Method for Estimation of the Thermal Process in the Honeycomb Panel. *Siberian Journal of Science and Technology*. 2017, Vol. 18, No. 4, P. 719–726 (In Russ.).

3. Dul'nev G. N., Tarnovskii N. N. *Thermal conditions of electronics*. Leningrad, Energiya Publ., 1971, 248 p.

4. Dul'nev G. N., Pol'shchikov B. V., Potyagailo A. Yu. Algorithms for hierarchical modeling of heat transfer processes in complex electronic systems. Radioelektronika. *Electronics*. 1979, No. 11, P. 49–54 (In Russ.).

5. Nikolaev V. N., Gusev S. A., Makhotkin O. A. Mathematical model of the convective radiant heat exchange of the venting heat-insulated unpressurized bay of the aircraft. *A series of the aircraft strength*. 1996, No. 1, P. 98–108 (In Russ.).

6. Misnar A. The thermal conductivity of solids, liquids, gases and their compositions. Moscow, Mir Publ., 1968, 460 p.

7. Ladyzhenskaya O. A., Solonnikov V. A., Ural't-seva N. N. *Linear and quasilinear equations of parabolic type*. Moskow, Nauka Publ., 1967, 736 p.

8. Sobolev S. L. *Applications of functional analysis in mathematical physics*. Moscow, Nauka Publ., 1988, 336 p.

9. Gusev S. A. Application of SDEs to Estimating Solutions to Heat Conduction Equations with Discontinuous Coefficients. *Numerical Analysis and Applications*. 2015, Vol. 8, No. 2, P. 122–134.

10. Himmelblau D. *Process analysis by statistical methods*. New York, Wiley, 1970, 463 p.

11. Gill P., Murray E. Quasi-Newton methods for unconstrained optimization. *Journal of the Institute of Mathematics and its Applications*. 1971, Vol. 9, No. 1, P. 91–108.

12. Artem'ev S. S., Demidov G. V., Novikov E. A. *Minimization of ravine functions by numerical method for the stiff sets of equations solving*. Preprint no. 74. Data center of Siberian Department of the Academy of Sciences of the USSR. Novosibirsk, 1980, 13 p.

13. Nikolayev V. N. Theoretical and Experimental Investigation of the Photographic Reconnaissance Plane Instrument bay Thermal State. *Journal of Siberian Federal University. Engineering & Technologies*. 2011, Vol. 3, No. 4, P. 337–347.

14. GOST RV 20.39.304-98. Complex system of General technical requirements. Equipment, instruments, devices and equipment for military purposes. Requirements for resistance to external factors. Moscow, Gosstandart of Russia Publ., 1998, 55 p.

15. Nikolaev V. N., Gusev S. A. Mathematical simulation of the unmanned aerial vehicle unpressurized compartment thermal state. *Herald Novosibirsk State Technical University.* 2018, No. 2 (71), P. 23–38 (In Russ.).

Библиографические ссылки

1. Воронин Г. И. Системы кондиционирования на летательных аппаратах. М. : Машиностроение, 1973. 443 с.

2. Гусев С. А., Николаев В. Н. Численно-статистический метод для решения задач теплообмена в теплозащитных конструкциях сотового типа // Сибирский журнал науки и технологий. 2017. Т. 18, № 4. С. 719–726.

3. Дульнев Г. Н., Тарновский Н. Н. Тепловые режимы электронной аппаратуры. Л. : Энергия, 1971. 248 с.

4. Дульнев Г. Н., Польщиков Б. В., Потягайло А. Ю. Алгоритмы иерархического моделирования процессов теплообмена в сложных радиоэлектронных комплексах // Радиоэлектроника. 1979. № 11. С. 49–54.

5. Николаев В. Н., Гусев С. А., Махоткин О. А. Математическая модель конвективно-лучистого теплообмена продуваемого теплоизолированного негерметичного отсека летательного аппарата. Прочность летательных аппаратов. Расчет на прочность элементов авиационных конструкций // Науч.-техн. сб. 1996. Вып. 1. С. 98–108.

6. Миснар А. Теплопроводность твердых тел, жидкостей, газов и их композиций. М. : Мир, 1968. 460 с.

7. Ладыженская О. А., Солонников В. А., Уральцева Н. Н. Линейные и квазилинейные уравнения параболического типа. М. : Наука, 1967. 736 с.

8. Соболев С. Л. Некоторые применения функционального анализа в математической физике. М. : Наука, 1988. 336 с.

9. Gusev S. A. Application of SDEs to Estimating Solutions to Heat Conduction Equations with Discontinuous Coefficients // Numerical Analysis and Applications. 2015. Vol. 8, No. 2. P. 122–134.

10. Химмельблау Д. Анализ процессов статистическими методами : пер. с англ. М. : Мир, 1973. 957 с.

11. Gill P., Murray E. Quasi-Newton methods for unconstrained optimization // Journal of the institute of mathematics and its applications. 1971. Vol. 9, No. 1. P. 91–108.

12. Артемьев С. С., Демидов Г. В., Новиков Е. А. Минимизация овражных функций численным методом для решения жестких систем уравнений. Новосибирск, 1980. 13 с. (Препринт / ВЦ СО АН СССР; № 74).

13. Николаев В. Н. Экспериментально-теоретические исследования теплового состояния приборного отсека фоторазведчика // Journal of Siberian Federal University. Engineering & Technologies. 2011. Vol. 3, No. 4. P. 337–347.

14. ГОСТ РВ 20.39.304–98. Комплексная система общих технических требований. Аппаратура, приборы, устройства и оборудование военного назначения. Требования стойкости к внешним воздействующим факторам. М. : Госстандарт России, 1998. 55 с.

15. Николаев В. Н., Гусев С. А. Математическое моделирование теплового состояния негерметизированного отсека беспилотного летательного аппарата // Научный вестник Новосибирского государственного технического университета. 2018. № 2 (71). С. 23–38.

Gusev Sergey Anatolyevich – Dr.Sc., Senior Researcher, Institute of Computational Mathematics and Mathematical Geophysics SB RAS; Professor, Novosibirsk State Technical University. E-mail: sag@osmf.sscc.ru.

Nikolaev Vladimir Nikolaevich – Dr. Sc., Head of Department, Siberian Aeronautical Research Institute Named After S. A. Chaplygin. E-mail: sibnia@sibnia.ru.

Гусев Сергей Анатольевич – доктор физико-математических наук, старший научный сотрудник, Институт вычислительной математики и математической геофизики СО РАН; профессор, Новосибирский государственный технический университет. E-mail: sag@osmf.sscc.ru.

Николаев Владимир Николаевич – доктор технических наук, начальник отдела, Сибирский научно-исследовательский институт авиации имени С. А. Чаплыгина. E-mail: sibnia@sibnia.ru.

UDC 629.78:531.395
Doi: 10.31772/2587-6066-2019-20-1-68-73

For citation: Zhang Zikun, Zimin V. N., Krylov A. V., Churilin S. A. [The definite questions of simulation of transformable space structures dynamics]. *Siberian Journal of Science and Technology.* 2019, Vol. 20, No. 1, P. 68–73. Doi: 10.31772/2587-6066-2019-20-1-68-73

Для цитирования: Джан Ц., Зимин В. Н., Крылов А. В., Чурилин С. А. Некоторые аспекты моделирования динамики трансформируемых космических конструкций // Сибирский журнал науки и технологий. 2019. Т. 20, № 1. С. 68–73. Doi: 10.31772/2587-6066-2019-20-1-68-73

THE DEFINITE QUESTIONS OF SIMULATION OF TRANSFORMABLE SPACE STRUCTURES DYNAMICS

Zikun Zhang, V. N. Zimin*, A. V. Krylov, S. A. Churilin

Bauman Moscow State Technical University
5, 2-nd Baumanskaya St., building 1, Moscow, 105005, Russian Federation
*E-mail: zimin@bmstu.ru

This paper describes large transformable space structures with various configuration in the folded transport position and in the open working one. As an example, simulation of transformable space structures dynamics is shown for the antenna circuit foldable load-bearing frame with diameter of 5 m. For investigation of the foldable frame deployment dynamics, a design scheme presented by a system of rigid bodies connected with each other by hinges is accepted as it is simple, but at the same time it considers features of the structure well enough. For performing stress analysis of the foldable frame elements during deployment, the frame shape at the certain time point of deployment, when relative velocities of adjacent elements are ultimate, is chosen. As a results of calculation using MSC.Adams software, positions, velocities and accelerations of the centres of mass of the foldable frame elements as well as the angular velocities and accelerations of the elements for each time step of the deployment are obtained. To perform stress analysis of the foldable load-bearing frame, finite element model of the frame is developed using MSC.Patran/Nastran software. As a results of investigation of stressed and deformed states of antenna circuit foldable frame elements both without taking into account damping and with consideration of damping, stresses arising in the foldable frame elements at the certain time points during deployment are found.

Keywords: transformable structures, deployable structures, dynamics, modeling, simulation, movement, configuration, model.

НЕКОТОРЫЕ АСПЕКТЫ МОДЕЛИРОВАНИЯ ДИНАМИКИ ТРАНСФОРМИРУЕМЫХ КОСМИЧЕСКИХ КОНСТРУКЦИЙ

Ц. Джан, В. Н. Зимин*, А. В. Крылов, С. А. Чурилин

Московский государственный технический университет имени Н. Э. Баумана
Российская Федерация, 105005, Москва, 2-я Бауманская ул., 5, стр. 1
*E-mail: zimin@bmstu.ru

Рассматриваются крупногабаритные трансформируемые космические конструкции, имеющие разные конфигурации в транспортном состоянии и рабочем положении. Моделирование динамики трансформируемых космических конструкций рассмотрено на примере складного несущего силового каркаса антенного контура диаметром 5 м. Для анализа динамики раскрытия принимается простая, достаточно хорошо учитывающая особенности конструкции расчетная схема в виде системы абсолютно твердых тел, связанных между собой шарнирными соединениями. В качестве расчетной схемы для определения напряженно-деформированного состояния элементов каркаса при раскрытии принимается его форма в определенный момент времени, когда относительные скорости соседних элементов максимальны. В результате расчета в программном комплексе MSC.Adams получены координаты, скорости и ускорения центров масс элементов каркаса, а также их угловые скорости и ускорения. Для определения напряженно-деформированного состояния каркаса в программном комплексе MSC.Patran/Nastran построена его конечно-элементная модель. В результате расчета напряженно-деформированного состояния элементов каркаса без учета и с учетом демпфирования получены значения возникающих в них напряжений в определенные моменты времени.

Ключевые слова: трансформируемые конструкции, динамика, моделирование, движение, конфигурация, модель.

Introduction. The intensive development of space technology poses the task of creating of fundamentally new large space structures [1; 2]. A necessary stage of their development is a preliminary investigation of the characteristics of both free and controlled such structures' motion by means of mathematical modeling of their dynamics.

Mathematical modeling of dynamics of such structures is a subject of wide research. The main methods of analysis of the mechanical behavior of large space structures are described in [3]. Transformable large space structures have different configurations in the transport state and in the operating position in orbit. As a rule, deployment of the developed transformable structures, is unique process for each considered system, however, in some cases it is possible to find a common way of modeling the dynamics of their deployment. A model that is simple but well enough considering the special features of structures consisting of tens, hundreds and even thousands elements interconnected by hinges is accepted as a design scheme [4–9]. System of differential equations of transformable structure elements motion is usually known as a model of dynamics of such structure, and a numerical solution of these equations is usually understood as the mathematical modeling of structure dynamics.

Calculation model for the analysis of the deployment of the circuit antenna frame. Among the large space structures, a special place is occupied by the multi-link transformable circuit antennas, the load-bearing frame of which provides the minimal dimensions of the structure in the folded transport position and required rigidity of the structure in the unfolded working one (fig. 1). The frame consists of one-type elements connected by elastic hinges. The elements can be made of both metals and composite materials (fig. 2). The hinges contain one-sided stops to provide of deployment of the reflector into the opened working position, making desired shape of the reflecting surface its maintenance during operating life. Deployment of considered structures occurs automatically due to potential energy accumulated in the elastic elements of the hinges when the reflector had been being folded into the transport state. Computer modeling of steps of the multi-link load-bearing frame deployment gives us an opportunity to consider various schemes of this process and evaluate correctness of the technical solutions incorporated in the structure's scheme at the project level.

Modeling of deployment of the load-bearing frame with a diameter of 5 m using MSC.Adams and MSC. Patran/Nastran software is under consideration [10].

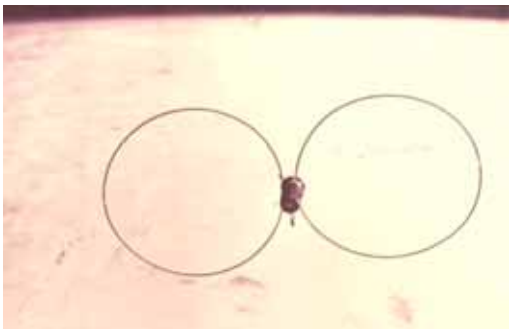

Fig. 1**.** The spacecraft with circular transformable antennas with diameters of 20 m

Рис. 1. Космический корабль с трансформируемыми кольцевыми антеннами диаметром 20 м

a *b*

Fig. 2. The elements of transformable space structures:
a – shaped rectangular panels; *b* – thin-walled quill rods of unidirectional carbon fiber reinforced polymer with longitudinal fibers orientation

Рис. 2. Элементы трансформируемых космических конструкций:
а – прямоугольные профилированные панели; *б* – тонкостенные трубчатые стержни из однонаправленного углепластика с продольным расположением волокон

The folding load-bearing frame consists of two packets of shaped rectangular panels $550 \times 230 \times 6$ mm (13 panels per package) one side of which is pivotally connected with the spacecraft, and another side the same way is connected with short closing panel.

As a design scheme for studying of dynamics of the antenna folding frame deployment using MSC.Adams, a system of rigid bodies interconnected by hinges is accepted. At a certain relative position of the adjacent panels during the deployment, restrictions limiting mutual angular displacement of panels are applied to provide holding of the antenna frame in the operating unfolded position. The panels of the foldable antenna frame are connected with each other by external and internal hinges modeled by means of "axial joint" elements (Revolute Joint in terms of Adams software). Torsion springs in the hinges are modeled by means of elastic and dissipative elements with linear dependencies of the moments from the opening angles and the relative angular velocities of the panels (Torsion Spring in terms of Adams software), the stiffness coefficient, viscous resistance coefficient and preliminary angles of twist of the springs for which are given. The external and internal hinges have different preliminary angles of twist, which have been chosen the way to provide a circle shape of the folding load-bearing frame in the operating unfolded position.

The panels are modeled by rigid rectangular parallelepipeds with dimensions of $550 \times 230 \times 6$ mm. The density of the equivalent material of the panels in Adams is chosen so that the mass of the simulated non-profiled panels is equal to the mass of the real profiled panels. The moments of inertia of the panels in Adams are taken equal to the moments of inertia of the real profiled panels.

Free ends of the panels placing in the base of the left and right packets are considered to be hinged.

The power characteristic of each of the elastic and dissipative elements modeling the torsion spring in the hinges [11–13] is determined by the following ratio

$$M_i(\varphi_i, \dot{\varphi}_i) = c_i(\varphi_{tw_i} - \varphi_i) - \mu_i \dot{\varphi}_i,$$

where c_i is the stiffness coefficient of the i-th spring; μ_i is the coefficient of viscous resistance of the i-th spring; φ_i is the current opening angle of adjacent panels; φ_{tw_i} is the preliminary angle of twist of the i-th spring.

At a certain relative position of the adjacent panels when they are opening, and the opening angle φ_i reaches a certain value φ_{stop_i} corresponding to operating position of panels, restrictions limiting the mutual angular displacement of the panels are applied to panels by the certain making of their hinges. Physically the restrictions are made as various stops, which are modeled by massless elastic and damping elements with nonlinear dependency of the moment from the opening angle and can be written as

$$M_{\text{stop}_i}(\varphi_i, \dot{\varphi}_i) = \begin{cases} 0, & \text{if } \varphi_i < \varphi_{\text{stop}_i} \\ -c_{\text{stop}_i}(\varphi_i - \varphi_{\text{stop}_i}) - \mu_{\text{stop}_i}\dot{\varphi}_i, & \text{if } \varphi_i \geq \varphi_{\text{stop}_i} \end{cases},$$

where c_{stop_i} is the stiffness coefficient of the i-th elastic element; μ_{stop_i} is the coefficient of viscous resistance of the i-th damping element; φ_{stop_i} is value of the opening angle of adjacent panels, when the placing on the stop is getting; $\dot{\varphi}_i$ is the relative angular velocity of the adjacent panels.

When moving, adjacent panels can rotate towards each other and touch each other. The model contains stops preventing a contact between the panels. They are presented by massless elastic elements with nonlinear dependency of the moment from the opening angle

$$M_{\text{cont}_i}(\varphi_i) = \begin{cases} 0, & \text{if } \varphi_i > \varphi_{\text{cont}_i}, \\ -c_{\text{cont}_i}(\varphi_i - \varphi_{\text{cont}_i}), & \text{if } \varphi_i \leq \varphi_{\text{cont}_i}, \end{cases}$$

where c_{cont_i} is the stiffness coefficient of the i-th elastic element; φ_{cont_i} is value of the i-th opening angle, when the adjacent elements are in contact.

As a result of calculations, dependencies of coordinates, speeds and accelerations of centres of mass of the load-bearing frame panels from time, as well as dependencies their angular speeds and accelerations from time were received.

Analysis of stressed state of the frame elements. The stressed state of the elements of the load-bearing frame during its deployment is determined by the impact loads arising when the adjacent frame panels are placing on the stops. The impact loads are obtained from the analysis of the frame deployment dynamics using the MSC. Adams software.

Simulation shows that the panels of the load-bearing frame are placed on the stops at the different time points. At each time point, various groups of panels in different places of the frame reach their stops. Several time points are chosen when relative velocities of the adjacent panels from the certain group are ultimate.

To investigate the stressed state of the load-bearing frame panels during deployment, in MSC. Patran/Nastran software the frame shape at the selected moments is adopted as a design scheme. At each considered moment it is supposed that panels are placed on their stops and the structure behaves as an elastic rod with specified characteristics. This approach gives the safety margin, since the mobility of frame panels relative to each other leads to reduction of real stresses due to the loss of kinetic energy in the joints.

Knowing value of the angular velocity of the hinged first panel of one of the packets and knowing values of the angular velocities of the other panels of the packet, the velocity field at the certain points of each panel of the packet is determined by the formula $\boldsymbol{v}_n = \boldsymbol{v}_p + \boldsymbol{\omega} \times \boldsymbol{r}$, where $\boldsymbol{v}_p$ is the speed of the poles, for which each joint on the antenna frame from the attachment base point to the short closing panel is consistently accepted; $\boldsymbol{\omega}$ is the angular velocity vector of the corresponding panel; $\boldsymbol{r} = \boldsymbol{r}_n - \boldsymbol{r}_p$, $\boldsymbol{r}_p$ is the radius vector of the pole, $\boldsymbol{r}_n$ is the radius vector of the point, where the velocity is determined. The radius vectors are specified in the inertial frames of reference whose origins are located at the places of hinge fastening for each frame packet on a rigid base. Velocities of the opposite packets panels are taken equal in magnitude and opposite in direction. Thus, the opening of the frame occurs symmetrically.

The angular velocities of the panels as well as the velocities of their centres of mass (hereinafter used to test calculation of velocities of the selected model points) obtained for each time step of the deployment calculation are exported from Adams to a certain file as a table. To find velocities of the model selected points from the dependency given above for each selected moment of time a C++ program was written.

To perform stress analysis of the frame panels, finite element model of the frame was built using MSC.Patran/Nastran software. Analysis of the stressed and deformed state of antenna frame was carried out by means of Direct Transient Response analysis (SOL 109, study of transient process) both without taking into account damping and with consideration of damping.

Each panel is divided into ten "beam" finite elements. In total, the model consists of 270 such elements. All finite elements including elements at the panel boundaries are rigidly connected to each other. The panels placed at the base of the left and right packet are considered to be clamped by their free ends.

As a dynamic model of the folding frame the finite element model is accepted

$$M\ddot{\boldsymbol{u}} + D\dot{\boldsymbol{u}} + K\boldsymbol{u} = \boldsymbol{P},$$

where M, D, K are mass, damping and stiffness matrices respectively, $\boldsymbol{P}$ is the external loads vector, $\boldsymbol{u}$ is the vector of nodal displacements, $\dot{\boldsymbol{u}}$ is the vector of nodal velocities. In our case $\boldsymbol{P} = 0$.

Calculated values of velocities in the selected points of the frame model are taken as initial conditions for calculation of the transient process using MSC. Nastran software, that is, when $t = 0$: $\boldsymbol{u}(0) = \boldsymbol{u}_0$, $\dot{\boldsymbol{u}}(0) = \dot{\boldsymbol{u}}_0$, where $\boldsymbol{u}_0$, $\dot{\boldsymbol{u}}_0$ are vectors of the initial nodal displacements and velocities.

In accordance with the recommendations presented in the MSC. Nastran user manuals, transient response analysis time integration step should be selected taking the conditions as at least ten steps per response period time for the maximal frequency of interest. Then, if we take into account first ten frequencies of natural oscillations of the antenna frame in the plane of deployment, in our case the time integration step will be equal to

$$\Delta t = \frac{T_{10}}{10} = \frac{1}{10 \cdot f_{10}} = \frac{1}{10 \cdot 9\,\text{Hz}} \approx 0,01\,\text{sec}.$$

At the same time, it is recommended to take the time integration step finding within $\Delta t = 10^{-4}...10^{-3}$ sec. interval, so to obtain more accurate stress values, the time integration step during the calculations was taken equal to $\Delta t = 10^{-3}$ sec.

Structural damping in Direct Transient Response analysis is taken into account by usage of the equivalent viscous damping. For the sinusoidal displacement response with constant amplitude, the structural damping force is constant and the viscous damping force is proportional to the frequency. For such a response, the two damping forces are equal at some frequency. Having done calculations without damping it was clear that the frequency of the structure oscillations under the impact had closed value to the second natural oscillations frequency in the plane of the opening of the frame. So the second natural oscillations frequency was chosen as a frequency of equivalence of structural damping and viscous one.

As a results of investigation of stressed and deformed states of antenna circuit foldable frame elements both without taking into account damping and with consideration of damping, stresses arising in the foldable frame elements at the certain time points during deployment are found.

Fig. 3 shows the stressed state of the antenna frame at the time point of $t = 5.925$ sec., when small stresses occur, looking all considered cases. The values of the stresses occurring in the panels are shown the same.

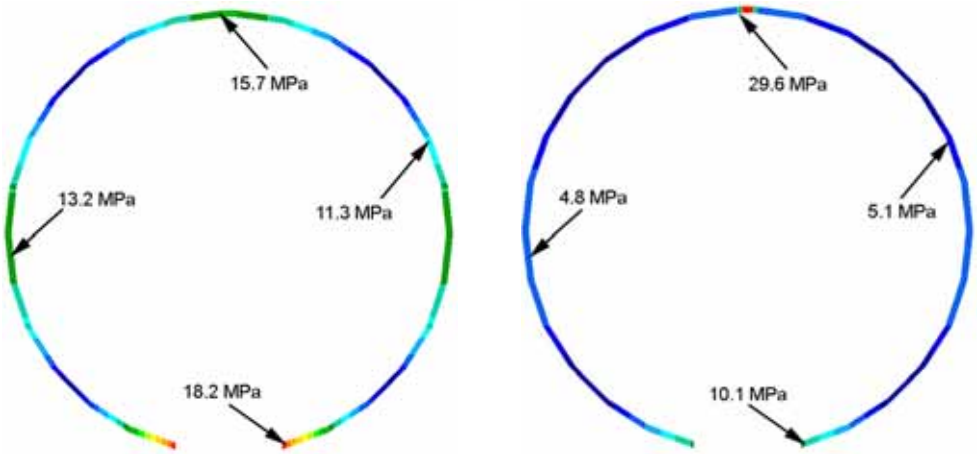

a *b*

Fig. 3. Stressed state of the antenna frame at time point of $t = 5.925$ sec.:
a – without consideration of damping; *b* – with consideration of damping

Рис. 3. Напряжения в момент времени $t = 5{,}925$ с.:
а – без демпфирования; *б* – с демпфированием

Conclusion. It is possible to reduce or even exclude impact loads during the process of uncontrolled deployment by reducing the initial potential energy of the springs, i.e. by changing the elastic characteristics of the spring elements included in the structure. At the same time, the angular velocities at the time of placing of adjacent structural elements on the stops will accordingly decrease. This will lead to decreasing of the velocities determining the magnitude of the impact impulse acting on the considered elastic transformable structure. However, this way is not always possible, since besides the smooth and reliable deployment of the transformable structures, it is necessary to guarantee their following operation in orbit. Therefore, in order to provide a controlled transformation of the system from the transport folded position to the operating opened one, it is necessary either to develop the structure with an additional cable synchronization system, or to replace the springs by operating drives. This will significantly complicate the structure and increase its mass. It is possible to create large transformable space structures in orbit, using for their deployment actuators made of materials with a shape memory effect [14; 15].

There are several types of actuators based on materials with shape memory effect. One of them can be called a one-dimensional direct-acting actuator, the another one – an actuator with aftereffect, which uses a spring or differential drive making an active retarding force and damping for creating force of actuator itself.

References

1. Lopatin A. V., Rutkovskaya M. A. [The review of designs of modern transformed space antennas. Part 1]. *Vestnik SibGAU.* 2007, No. 2(15), P. 51–57 (In Russ.).

2. Lopatin A. V., Rutkovskaya M. A. [The review of designs of modern transformed space antennas. Part 2]. *Vestnik SibGAU.* 2007, No. 3(16), P. 78–81 (In Russ.).

3. Banichuk N. V., Karpov I. I., Klimov D. M. et al. *Mekhanica bol'shikh kosmicheskikh konstruktsiy* [Mechanics of large space structures]. Moscow, Faktorial Publ., 1997, 302 p.

4. Wittenburg J. *Dinamika system tviordykh tel* [Dynamics of multibody systems]. Moscow, Mir Publ., 1980, 292 p.

5. Boykov V. G. [Simulation of the mechanical systems dynamics using EULER software]. *SAPR i Graphika.* 1998, No. 1, P. 38–48 (In Russ.).

6. Boykov V. G. [Software complex for the automated dynamic analysis of multicomponent mechanical systems EULER]. *SAPR i Graphika.* 2000, No. 9, P. 17–20 (In Russ.).

7. Bakulin D. V., Borzikh S. V., Ososov N. S., Shchiblev Yu. N. [Modeling dynamics of opening large-sized solar batteries]. *Izvestiya RAN. Matematicheskoe modelirovanie.* 2004, Vol. 16, No. 6, P. 88–92 (In Russ.).

8. Borzikh S. V., Ilyasova I. R. [Simulation and experimental development of deployment of large-sized multi-link solar batteries of spacecrafts]. *Engineering Journal: Science and Innovation*. 2012, No. 8 (8), P. 60–68 (In Russ.).

9. Kuznetsova A. O. [Research of the dynamics of the motion of uncovered mechanical systems with elastic ties]. *Vestnik SibGAU.* 2005, No. 3, P. 135–138 (In Russ.).

10. Schesniak S., Romanov A., Khitrov I. et al. [Designing and calculation of large-sized deployable structures using MSC. Software simulation software technology]. *CADmaster.* 2009, No. 2–3 (47–48), P. 28–38 (In Russ.).

11. Krylov A. V., Churilin S. A. [Simulation of Deployment of Multi-Link Closed Space Structures]. *Engineering Journal: Science and Innovation.* 2012, No. 8 (8), P. 80–91 (In Russ.).

12. Krylov A. V., Churilin S. A. [Methods of deployable multilink structures elements stressed state investigation]. *Russian physics journal.* 2013, Vol. 56, No. 7–3, P. 170–172 (In Russ.).

13. Zimin V. N., Krylov A. V., Meshkovskiy V. Ye. et al. [Features of the Calculation Deployment Large Transformable Structures of Different Configurations]. *Science and Education of the Bauman MSTU. Electronic Journal.* 2014, No. 10, P. 179–191 (In Russ.). Doi: 10.7463/1014.0728802.

14. Molodtsov G. A., Bitkin B. E., Simonov V. F. et al. *Formostabil'nyye i intellektual'nyye konstruktsii iz kompozitsionnykh materialov* [Form-stable and intelligent structures made of composite materials]. Moscow, Mashinostroyenie Publ., 2000, 352 p.

15. Liand C., Rogers C. A. Design of shape memory alloy actuators. *Journal of intelligent material systems and structures*. 1997, Vol. 8, P. 303–313.

Библиографические ссылки

1. Лопатин А. В., Рутковская М. А. Обзор конструкций современных трансформируемых космических антенн. Ч. 1 // Вестник СибГАУ. 2007. № 2(15). С. 51–57.

2. Лопатин А. В., Рутковская М. А. Обзор конструкций современных трансформируемых космических антенн. Ч. 2 // Вестник СибГАУ. 2007. № 3(16). С. 78–81.

3. Механика больших космических конструкций / Н. В. Баничук, И. И. Карпов, Д. М. Климов [и др.]. М. : Факториал, 1997. 302 с.

4. Виттенбург Й. Динамика систем твердых тел. М. : Мир, 1980. 292 с.

5. Бойков В. Г. Моделирование динамики механических систем в программном комплексе EULER // САПР и графика. 1998. № 1. С. 38–48.

6. Бойков В. Г. Программный комплекс автоматизированного динамического анализа многокомпонентных механических систем EULER // САПР и графика. 2000. № 9. С. 17–20.

7. Бакулин Д. В., Борзых С. В., Ососов Н. С., Щиблев Ю. Н. Моделирование процесса раскрытия крупногабаритных солнечных батарей // Известия РАН. Математическое моделирование. 2004. № 6. С. 88–92.

8. Борзых С. В., Ильясова И. Р. Моделирование и экспериментальная отработка процесса раскрытия крупногабаритных многозвенных солнечных батарей космических аппаратов // Инженерный журнал: наука и инновации. 2012. № 8. С. 60–68.

9. Кузнецова А. О. Исследование динамики движения раскрывающихся механических систем

с упругими связями // Вестник СибГАУ. 2005. № 3. С. 135–138.

10. Проектирование и расчет крупногабаритных раскрывающихся конструкций с помощью программных комплексов MSC.Software / С. С. Щесняк, А. В. Романов, И. В. Хитров [и др.] // CAD master. 2009. № 2–3 (47–48). С. 28–38.

11. Крылов А. В., Чурилин С. А. Моделирование развертывания многозвенных замкнутых космических конструкций // Инженерный журнал: наука и инновации. 2012. № 8 (8). С. 80–91.

12. Крылов А. В., Чурилин С. А. Методика определения напряженно-деформированного состояния элементов трансформируемых многозвенных конструкций // Известия вузов. Физика. 2013. Т. 56, № 7/3. С. 170–172.

13. Особенности расчета раскрытия крупногабаритных трансформируемых конструкций различных конфигураций / В. Н. Зимин, А. В. Крылов, В. Е. Мешковский [и др.] // Наука и образование. 2014. № 10. С. 179–191. Doi: 10.7463/1014.0728802.

14. Формостабильные и интеллектуальные конструкции из композиционных материалов / Г. А. Молодцов, Б. Е. Биткин, В. Ф. Симонов [и др.]. М. : Машиностроение, 2000. 352 с.

15. Liand C., Rogers C. A. Design of shape memory alloy actuators // Journal of intelligent material systems and structures. 1997. Vol. 8. P. 303–313.

Zhang Zikun – postgraduate student; Bauman Moscow State Technical University. E-mail: 89738415@qq.com.

Zimin Vladimir Nikolaevich – first pro-rector, scientific work pro-rector, Dr. Sc., professor; Bauman Moscow State Technical University. E-mail: zimin@bmstu.ru

Krylov Aleksey Vladimirovich – Ph. D., associate professor; deputy head of the Spacecrafts and Carrier Rockets Department; Bauman Moscow State Technical University. E-mail: kav1982@bmstu.ru

Churilin Sergey Aleksandrovich – principal engineer; Bauman Moscow State Technical University. E-mail: churilin@bmstu.ru

Джан Цыкунь – аспирант; Московский государственный технический университет имени Н. Э. Баумана. E-mail: 89738415@qq.com.

Зимин Владимир Николаевич – доктор технический наук, профессор, первый проректор – проректор по научной работе; Московский государственный технический университет имени Н.Э. Баумана. E-mail: zimin@bmstu.ru.

Крылов Алексей Владимирович – кандидат технических наук, доцент, заместитель заведующего кафедрой космических аппаратов и ракет-носителей; Московский государственный технический университет имени Н. Э. Баумана. E-mail: kav1982@bmstu.ru

Чурилин Сергей Александрович – ведущий инженер; Московский государственный технический университет имени Н. Э. Баумана. E-mail: churilin@bmstu.ru.

UDC 621.316.71
Doi: 10.31772/2587-6066-2019-20-1-74-86

For citation: Shkolnyi V. N., Semenov V. D., Kabirov V. A., Sukhorukov M. P., Torgaeva D. S. [The method of synthesis of the digital controller for a solar energy conversion channel of the solar battery in the power supply system of a spacecraft]. *Siberian Journal of Science and Technology.* 2019, Vol. 20, No. 1, P. 74–86. Doi: 10.31772/2587-6066-2019-20-1-74-86

Для цитирования: Школьный В. Н., Семенов В. Д., Кабиров В. А., Сухоруков М. П., Торгаева Д. С. Методика синтеза цифрового регулятора для канала преобразования энергии солнечной батареи в системе электропитания космического аппарата // Сибирский журнал науки и технологий. 2019. Т. 20, № 1. С. 74–86. Doi: 10.31772/2587-6066-2019-20-1-74-86

THE METHOD OF SYNTHESIS OF THE DIGITAL CONTROLLER FOR A SOLAR ENERGY CONVERSION CHANNEL OF THE SOLAR BATTERY IN THE POWER SUPPLY SYSTEM OF A SPACECRAFT

V. N. Shkolnyi[1], V. D. Semenov[2], V. A. Kabirov[2], M. P. Sukhorukov[2]*, D. S. Torgaeva[2]

[1]JSC "Academician M. F. Reshetnev "Information Satellite Systems"
52, Lenin St., Zheleznogorsk, Krasnoyarsk region, 662972, Russian Federation
[2]Tomsk State University of Control Systems and Radioelectronics, Research Institute of Space Technologies
40, Lenina Av., Tomsk, 634050 Russian Federation
*E-mail: max_sukhorukov@mail.ru

A method of synthesizing a digital controller for a solar energy conversion channel in a power supply system of a spacecraft is presented. The method is based on the initial functional diagram of the pulse converter and the method of switching discontinuous functions. In accordance with the technique, which is formally presented in the form of eight consecutively executed items, a block diagram of the shunt converter has been developed in the basis of switching functions, which is taken as an example for testing the technique. The shunt converter is one of the three energy conversion channels in modern power supply systems of a spacecraft. The block diagram showed that all nonlinearity of the system can be reduced to nonlinearities of two multiplication links and nonlinearity of a pulse-width modulator. The possibility and acceptability of joint linearization of each of the specified nonlinear multipliers with a pulse-width modulator at the selected operating point is shown. A linearized block diagram of the control object was obtained, after which the transformation and simplification of the block diagram to a convenient form for calculation was carried out. Using the transfer functions of the linearized block diagram, the logarithmic frequency characteristics were calculated analytically and the results of their comparison with the frequency characteristics obtained experimentally on a simulation model, which confirmed their identity in the working frequency domain, were presented. At the same time, the specified simulation model of a shunt pulse converter, built in the Simulink package of the Matlab design environment, took into account all the mentioned nonlinearities of the real converter. According to the obtained logarithmic characteristics, a classical synthesis of the analogue prototype correcting section was produced. The transition from the analog correcting section of the prototype to the implementation of the digital correcting section is shown. Simulation modeling of a closed-loop power supply system with a synthesized analog controller, in its mode of operation from a solar battery, confirmed the correctness of the methodology and the achievement of the goals. The results of the work are intended to create a new onboard energy conversion equipment for power supply systems of high-potential spacecrafts. The scope of application of the project results is space instrumentation.

*Keywords**:** synthesis of digital controller, technical optimum, simulation modeling, shunt converter, power supply system, spacecraft.*

МЕТОДИКА СИНТЕЗА ЦИФРОВОГО РЕГУЛЯТОРА ДЛЯ КАНАЛА ПРЕОБРАЗОВАНИЯ ЭНЕРГИИ СОЛНЕЧНОЙ БАТАРЕИ В СИСТЕМЕ ЭЛЕКТРОПИТАНИЯ КОСМИЧЕСКОГО АППАРАТА

В. Н. Школьный[1], В. Д. Семенов[2], В. А. Кабиров[2], М. П. Сухоруков[2] *, Д. С. Торгаева[2]

[1]АО «Информационные спутниковые системы» имени академика М. Ф. Решетнёва»
Российская Федерация, 662972, г. Железногорск Красноярского края, ул. Ленина, 52
[2]Томский государственный университет систем управления и радиоэлектроники,
НИИ космических технологий
Российская Федерация, 634050, г. Томск, просп. Ленина, 40
*E-mail: max_sukhorukov@mail.ru

Представлена методика синтеза цифрового регулятора для канала преобразования энергии солнечной батареи в системе электропитания космического аппарата, основанная на исходной функциональной схеме импульсного преобразователя и методе коммутационных разрывных функций. В соответствии с методикой, формально представленной в виде восьми последовательно выполняемых пунктов, в базисе коммутационных функций разработана структурная схема шунтового преобразователя, который взят в качестве примера для проверки методики. Шунтовой преобразователь является одним из трех каналов преобразования энергии в современных системах электропитания космических аппаратов. Структурная схема показала, что все нелинейности системы можно свести к нелинейностям двух звеньев умножения и нелинейности широтно-импульсного модулятора. Показана возможность и допустимость совместной линеаризации каждого из указанных нелинейных звеньев умножителей с широтно-импульсным модулятором в выбранной рабочей точке. Получена линеаризованная структурная схема объекта управления, после чего проведено преобразование и упрощение структурной схемы к удобному для расчета виду. По передаточным функциям линеаризованной структурной схемы аналитически рассчитаны логарифмические частотные характеристики и приведены результаты их сравнения с частотными характеристиками, снятыми экспериментально на имитационной модели, которые подтвердили их идентичность в рабочей частотной области. При этом указанная имитационная модель шунтового импульсного преобразователя, построенная в пакете Simulink среды проектирования Matlab, учитывала все упомянутые нелинейности реального преобразователя. По полученным логарифмическим характеристикам произведен классический синтез аналогового корректирующего звена прототипа. Показан переход от аналогового корректирующего звена прототипа к реализации цифрового корректирующего звена. Имитационное моделирование замкнутой системы электропитания с синтезированным аналоговым регулятором в режиме ее работы от солнечной батареи подтвердило правильность методики и достижение поставленных целей. Результаты работы предназначены для создания новой бортовой энергопреобразующей аппаратуры систем электропитания перспективных космических аппаратов. Областью применения результатов проекта является космическое приборостроение.

Ключевые слова: синтез цифрового регулятора, технический оптимум, имитационное моделирование, шунтовой преобразователь, система электропитания, космический аппарат.

Introduction. One of the most important onboard systems of automatic spacecraft (SC) is the power supply system (PSS), which is a combination of primary and secondary current sources, energy conversion equipment and output voltage stabilization with the necessary control and automation [1; 2].

When developing a PSS of a SC, it is necessary to take into account many disturbing influences that affect the quality of the output voltage, the static and dynamic characteristics of the PSS adversely. Such impacts include changes in load resistance and power supply sources, degradation of primary energy sources, etc., which, in turn, leads to the need in building an automatic control system that ensures stable PSS operation with a given accuracy over the entire range of changes in these disturbances.

At present, control systems (CS) on an analog element base [3–7], which are often called analog control systems for short, are widely used in the PSS of a SC. When solving problems of improving the reliability of the PSS and at the same time improving its overall mass and functional characteristics, it becomes obvious that analog control systems fit the physical limit of the possibility of improving their functional parameters and overall mass characteristics [8].

The next stage in the development of the PSS of a SC is the transition to control systems built on a digital element base, also called digital control systems (DCS). Digital control systems, compared to analogue CSs, can provide [9] higher reliability, reduced weight and dimensions of the power supply system (including the cable network), and electronic anticountermeasures of transmission of the control signal.

In addition, digital control will allow to expand the functionality of the CS, simplify the creation of their modifications and embeddability of various devices in the structure. Digital control systems for their intended purpose allow to exchange data with the on-board control complex over a high-speed data interface, and this function is already widely used. However, the systems of direct digital control of energy-converting equipment, including pulse converters of electrical energy parameters, despite these obvious advantages, are practically not used at the moment, and analog control systems are widely used. This situation in the field of direct digital control systems application is connected with the fact that digital systems contain analog-digital converters, digital blocks for implementing signal modulators and digital communication interfaces for closing negative feedback circuits. As it is well known digital nodes and blocks cause delays in signals that are similar in nature to breaks of transport delays, which complicates the synthesis of correcting sections greatly.

Purpose. The purpose of this work is to develop a method of synthesis of the digital controller for a solar energy conversion channel of a solar battery in a power supply system of a spacecraft.

Method of synthesis of the digital controller.

The method of synthesis of the digital controller will be considered in the following sequence:

1. Develop a mathematical model of a pulse converter (control object) in the form of a block diagram con-

structed in the basis of discontinuous switching functions according to a given functional diagram.

2. Select nonlinear links and linearize them at a given operating point on the block diagram obtained in the basis of discontinuous switching functions, presenting each nonlinear link by a combination of linearized links, in order to obtain a linearized block diagram of the control object.

3. Determine the necessary transfer functions of the system, including the linearized transfer function of the open-ended control object based on the obtained linearized block diagram.

4. Compare the frequency characteristics of the linearized open unadjusted control object, obtained from its linearized transmission links, with the experimental "low-signal" frequency characteristics of the open unadjusted control object, taken on its simulation model built in the Simulink package of the Matlab design environment; if the compared frequency characteristics coincide with a given quantitative accuracy, the linearized model can be considered adequate.

5. Build a family of frequency characteristics of an open unadjusted control object using its linearized transfer functions at the "extreme" operating points of the system, meaning the "extreme" working points of the steady state point of the controlled object at the minimum and maximum values of all disturbing factors.

6. Synthesize the necessary type of analog correction link and its parameters assuming that the linearized model adequately describes the open control object and using the classical methods of synthesizing linear control systems for this reason.

7. Build a simulation model (for example, in the Simulink package of the Matlab design environment) of a closed-loop control system with the parameters of the corrective element obtained in step 6, and check the static and dynamic characteristics of the synthesized analogue controller.

8. Make a z-transformation of the transfer function of the discrete circuit and synthesize a digital correction link using the known transfer function of the analog correction link and a bilinear transition. If necessary, check the dynamic characteristics of the automatic control system (ACS) with a digital correction link on the simulation model in the Matlab environment, taking into account the delay.

The control object for the direct digital control system is the voltage stabilization module (VSM) of the energy-conversion complex, which includes three types of energy conversion channels:

– "SlB conversion channel" intended to convert the energy of on-board solar batteries into a constant stabilized output bus voltage to which the load is connected;

– "memory conversion channel" intended for charging onboard batteries with a stabilized current, the value of which can be changed by an external signal;

– "StB conversion channel" intended to convert the energy of the on-board storage batteries into a constant stabilized voltage of the output bus to which the load is connected;

Each of the energy conversion channels is a power pulse converter of electrical energy with or without feedback, providing a given law of operation. It can be made on the basis of parallel connection of several pulse converters. The number of channels, the number of parallel-connected converters in the channel and the order of their inclusion is determined by the load power, the number of solar and rechargeable batteries, and the accepted operation algorithm.

Let us consider the PSS of a SC when operating a SlB conversion channel, made on the basis of a shunt converter (fig. 1), on the topology of a boost converter ($L1$, $VT1$, $VD1$, $C3$) with negative feedback implemented by a digital control system (DCS). Since the solar battery operates on the current branch of its current-voltage characteristic, it was represented in this diagram as a current source I_{SlB}. The feedback signal U_f from the voltage sensor VS, connected to the output of the SlB channel, is converted by the ADC into digital for, subtracted from the signal of the setting voltage u and then through the correcting element CS, the digital pulse-width modulator PWM and driver D are fed to the power switch $VT1$ of the shunt converter.

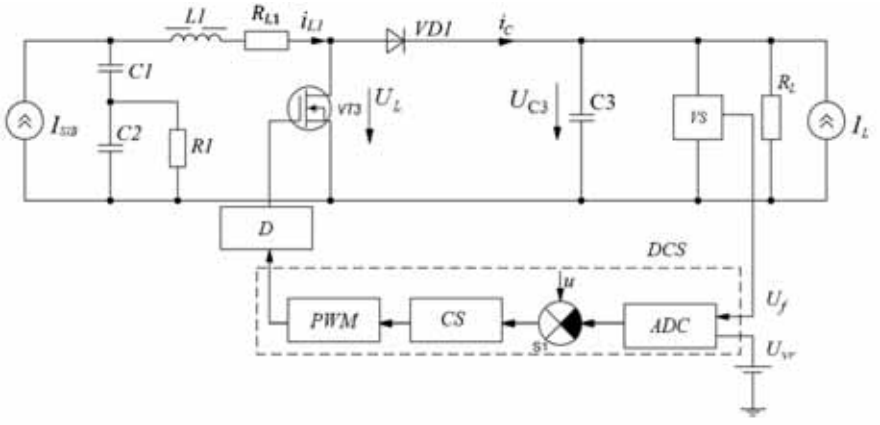

Fig. 1. Functional diagram of the shunt converter with a digital control system

Рис. 1. Функциональная схема шунтового преобразователя
с цифровой системой управления

The scheme uses a pulse-width modulator of the first kind (PWM1) with a delay of one sweep signal. It is PWM1 that is implemented in digital control systems based on microcontrollers. The current source I_L is designed to simulate the disturbing effect of the load current on the stabilization system. The input filter, assembled on elements $C1$, $C2$, $R1$, is intended [10] for smoothing the voltage ripples on the solar battery (current source I_{SlB}). The output filter $C3$ is designed to smooth the ripple on the load, indicated by the equivalent resistance R_L.

To implement the proposed method for the synthesis of a corrective element, in accordance with step 1, it is necessary to present a mathematical model of a shunt energy converter in the form of a structural diagram built in the basis of discontinuous switching functions. The digital control system, at this stage of the study, is considered ideal, assuming that the ADC performs the conversion instantaneously with infinitely high frequency, and the adder S1 and the corrective section of the short circuit are equivalent under these assumptions to the ideal analog link. Such a structural scheme, built according to the method described in [11], is presented in fig. 2. This block diagram is obtained by representing the inductances L and the capacities C of the shunt converter by ideal integrators with the corresponding coefficients $1/L$ and $1/C$. The resistors in the power circuit of the shunt converter are replaced by instantaneous links with transfer coefficients R, if it is a current-to-voltage link, or $1/R$, if it is a voltage-to-current link. The summation of voltages and currents in the respective voltage circuits and current nodes reflect the adders *S1 – S6* of the block diagram. The key part of the shunt converter, consisting of the power transistor *VT1* and diode *VD1*, is represented by two unidirectional controlled transmission links made in the form of multipliers marked with *X*. And one of the links $X1$ plays the role of the current transfer link i_{L1} of the input choke $L1$ to the output capacitor $C3$, and the second $X2$ takes the role of the transmission link of the output voltage U_{C3} in the input circuit of the choke $L1$. Both links of the multipliers $X1$ and $X2$ are controlled by a common signal $(1–F_K(t))$, which is fed to their control inputs. As it was mentioned above, an ideal digital control system is analog and consists of an instantaneous voltage sensor with a transfer coefficient *Cs*; source of voltage $u(t)$; adder $S7$; analog model of the correcting section (AMCS), with an unknown transfer function and analog model of a pulse-width modulator (AM PWM), which in its turn converts a continuous signal $x(t)$ acting on the output of the AMCS in a pulse signal $F_K(t)$, which is a switching function of the shunt converter, and accepts values “0” or “1”. The analog models of the corrective link of the AMCS and the pulse-width modulator AM PWM will be understood as some decisive blocks of an analog computer that implement the corresponding signal conversion functions. This condition will allow us to present block diagrams in the form of temporary functions.

The block diagram of fig. 2 which is built in the basis of switching discontinuous functions, clearly shows all the internal feedbacks of the shunt converter and the role that these connections play in the system, and also allows one to select non-linear transmission links.

In this diagram, the nonlinear signal transmission links are the pulse-width modulator PWM (its analog model) and the multipliers $X1$, $X2$, which are described by the relations

$$\begin{aligned} i_C(t) &= \left[1 - F_K(t)\right] \cdot i_{L1}(t), \\ u_L(t) &= \left[1 - F_K(t)\right] \cdot u_{C3}(t), \end{aligned} \tag{1}$$

where $i_C(t)$, $u_L(t)$ – are output signals of multipliers $X1$, $X2$; $i_{L1}(t)$, $u_{C3}(t)$ – are input signals of the multipliers (state variables of the described dynamic system), which are fed to the "power" input of the corresponding multiplier; $[1–F_K(t)]$ is a control signal that is generated by a PWM block and is fed to the control inputs of both multipliers.

Assuming that the continuous part of the SlB transform channel (control object) has the properties of a low-pass filter, which is naturally always performed with high quality requirements for the output voltage, the impulse switching function $[1–F_{\text{K}}(t)]$ can be reduced to a continuous function. Indeed, in the steady state operation of the system, a continuous signal $x(t)$ at the input of AM PWM can be represented as the sum of the constant component of the signal X_0, which characterizes the operating point of the steady state mode, and the small deviation dx of this signal from X_0. In this case, the output of AM PWM sets the switching function F_{K0}, the relative duration of which will correspond to the signal X_0, if the signal $x(t)$ is normalized and its maximum value is equal to one. Thus, under the condition of signal normalization $x(t)$, expressions (1), describing the operation of multipliers, can be rewritten in the form (2), where the time dependence of the values used is not indicated to simplify the expression.

$$\begin{aligned} i_C &= (1 - x) \cdot i_{L1}, \\ u_L &= (1 - x) \cdot i_{C3}. \end{aligned} \tag{2}$$

Since now expressions (2) describe the product of continuous functions, they can be linearized by the formula for finding the differential of the product, which allows us to obtain

$$\begin{aligned} di_C &= \left(1 - X_0\right) \cdot di_{L1} - I_{L10} \cdot dx, \\ du_L &= \left(1 - X_0\right) \cdot du_{C3} - U_{C30} \cdot dx, \end{aligned} \tag{3}$$

where di_C, di_{L1}, du_L, du_{C3}, dx – are small deviations of the corresponding signals from their steady-state values I_{C0}, I_{L0}, U_{L0}, U_{C30}, X_0. According to expressions (3), each of the multipliers and analog models of PWM, which are nonlinear links, are replaced by two linear instantaneous links [12] with transfer coefficients $(1–X_0)$, I_{L10} and $(1–X_0)$, U_{C30}, respectively, as well as adders (subtractors) $S8$ and $S9$, as shown in fig. 3. Since the rest sections of the block diagram in fig. 2 are linear, then the whole system becomes linearized. However, it should be remembered that in a linearized system, the variables are small deviations of signals from their steady-state value, therefore these signals are marked with a “tilde” icon.

Further simplification of the linearized block diagram and its reduction to the form shown in fig. 4 is a cumbersome task rather than a complex one.

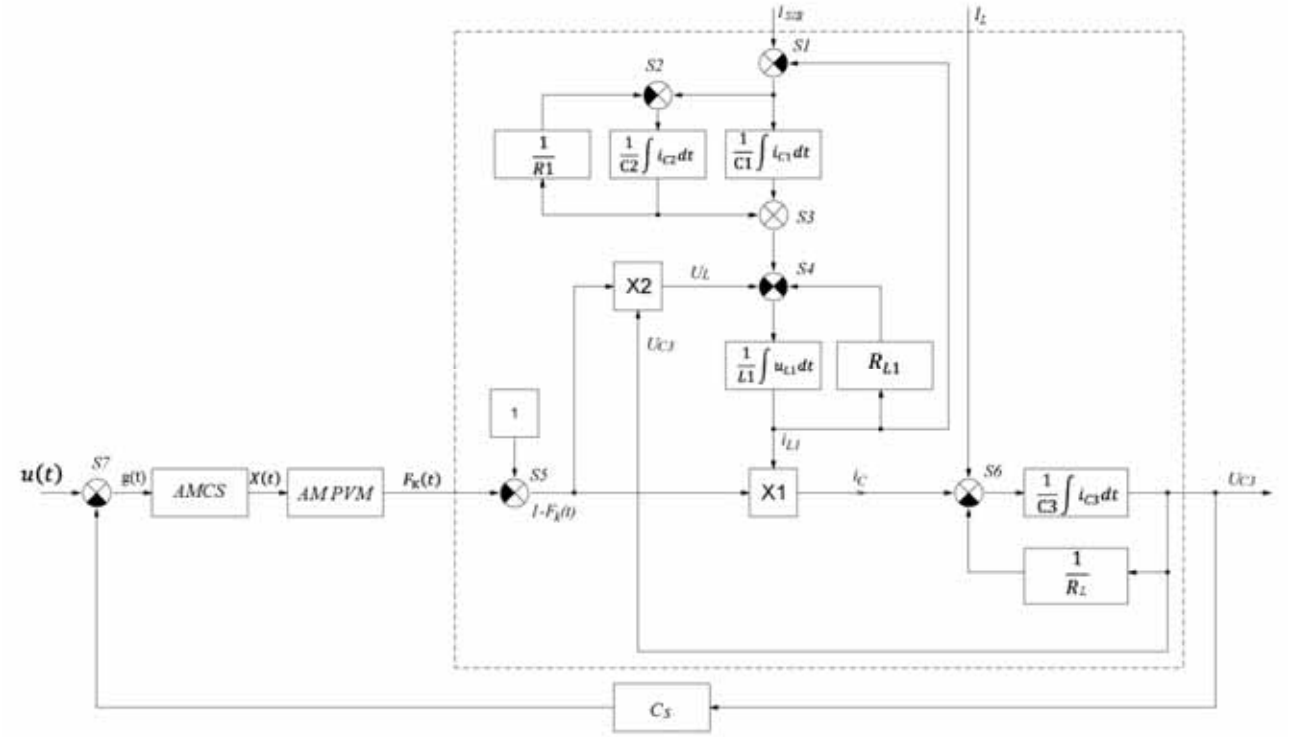

Fig. 2. Block diagram of the shunt converter with input filter and control system

Рис. 2. Структурная схема шунтового преобразователя с входным фильтром и системой управления

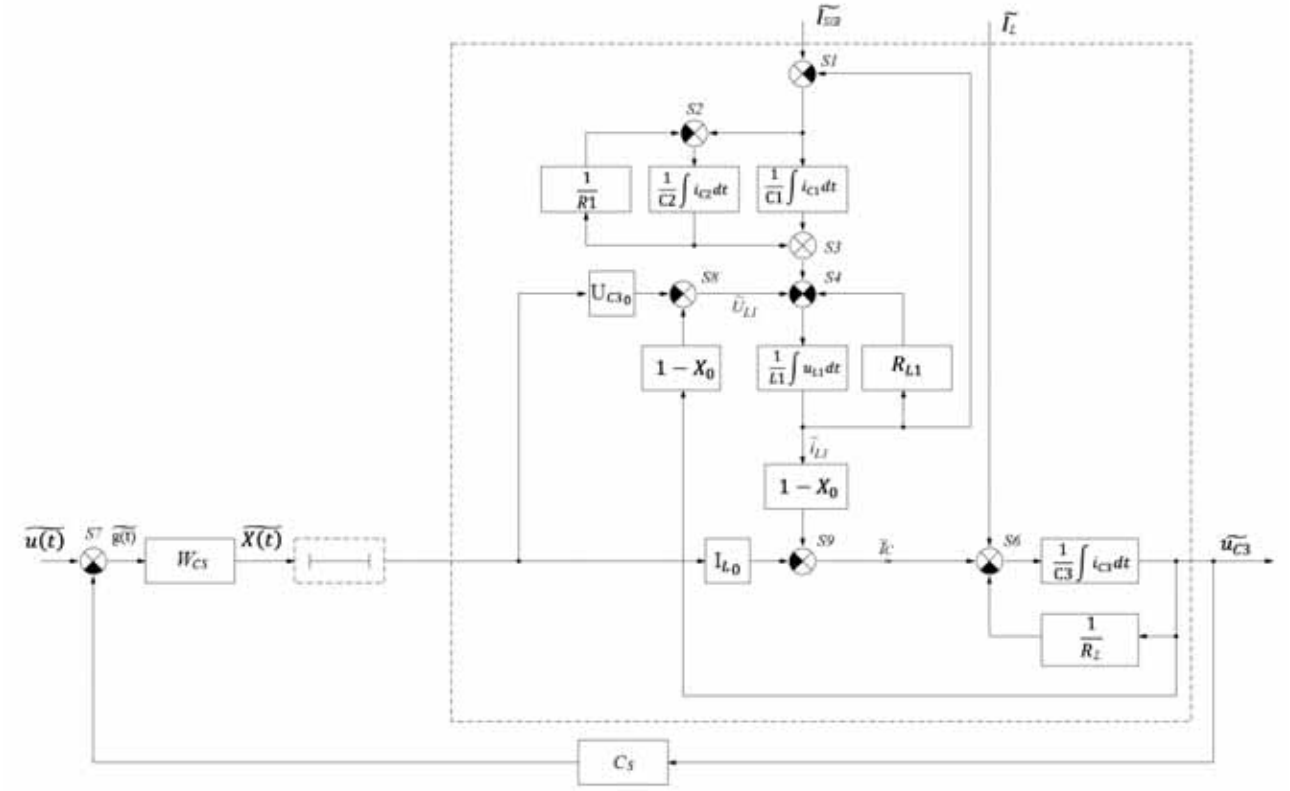

Fig. 3. Linearized block diagram of the shunt converter with input filter and control system

Рис. 3. Линеаризованная структурная схема шунтового преобразователя
с входным фильтром и системой управления

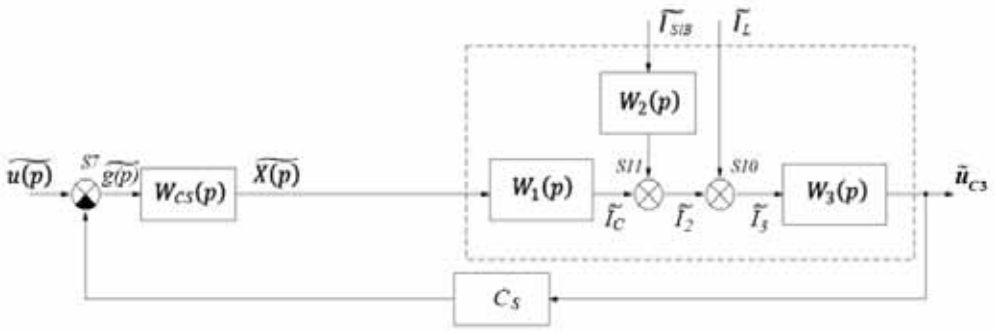

Fig. 4. Simplified linearized mathematical model of the shunt converter with input filter and control system

Рис. 4. Упрощенная линеаризованная математическая модель шунтового преобразователя с входным фильтром и системой управления

Formulas 4–6 allow us to determine the transfer functions of the links $W_1(p) - W_3(p)$ shown in fig. 4

$$W_1(p) = \frac{\tilde{I}_C(p)}{\tilde{X}(p)} = \left[\frac{U_{C3_0} \cdot \frac{1}{R_{L1}} \cdot \frac{1}{\left(\frac{L1}{R_{L1}} p + 1\right)} \cdot (1 - X_0)}{\frac{1}{R_{L1}} \cdot \frac{1}{\left(\frac{L1}{R_{L1}} p + 1\right)} \cdot \left(\frac{1}{C1p} + \frac{R1}{R1C2p + 1}\right) + 1} - I_{L_0} \right]; \quad (4)$$

$$W_2(p) = \frac{\tilde{I}_2(p)}{\tilde{I}_{SIB}(p)} = \frac{\frac{1}{R_{L1}} \cdot \frac{1}{\left(\frac{L1}{R_{L1}} p + 1\right)} \cdot \left(\frac{1}{C1p} + \frac{R1}{R1C2p + 1}\right) \cdot (1 - X_0)}{\frac{1}{R_{L1}} \cdot \frac{1}{\left(\frac{L1}{R_{L1}} p + 1\right)} \cdot \left(\frac{1}{C1p} + \frac{R1}{R1C2p + 1}\right) + 1}; \quad (5)$$

$$W_3(p) = \frac{\tilde{U}_{C3}(p)}{\tilde{I}_3(p)} = \frac{\frac{R_L}{R_L C3p + 1} \left[\frac{1}{R_{L1}} \cdot \frac{1}{\left(\frac{L1}{R_{L1}} p + 1\right)} \cdot \left(\frac{1}{C1p} + \frac{R1}{R1C2p + 1}\right) + 1 \right]}{\frac{R_L}{R_L C3p + 1} \cdot \frac{1}{R_{L1}} \cdot \frac{1}{\left(\frac{L1}{R_{L1}} p + 1\right)} \cdot (1 - X_0)^2 + \frac{1}{R_{L1}} \cdot \frac{1}{\left[\frac{L1}{R_{L1}} p + 1\right]} \cdot \left(\frac{1}{C1p} + \frac{R1}{R1C2p + 1}\right) + 1}. \quad (6)$$

Checking the adequacy of the obtained linearized structural diagram in fig. 3 and the simplified block diagram in fig. 4, which can also be called small-signal models of the system, is carried out according to the method given in [13]. This technique means to make a simulation model of a pulsed shunt converter with open-loop feedback in the software design environment Matlab.

Simulink; to take down logarithmic amplitude and phase-frequency characteristics on this model using the means provided by the software environment during the experiment; to compare the characteristics obtained experimentally on the model, with the characteristics calculated by the small-signal model (linearized block diagram) with a broken feedback loop. Feedback loop in fig. 3 is broken at the output of the analog model of the correcting section AMCS, and the delay link, shown conventionally by a dotted line, is not yet taken into account. This means that in the synthesis of the transfer function of the correcting element, the influence of the delay is neglected. The test signal is sent to the system input $x(t) = X_0 + (dx) \cdot \sin \omega t$, while X_0 determines the operating point of the steady state, the "small" amplitude dx of the sine determines the small deviation from the operating point, and the frequency ω changes in the desired range. The transfer function of an open object with respect to a control action, the adequacy of which is further proved, will have the form (7), with $\tilde{I}_L = 0$ и $\tilde{I}_{SIB} = 0$.

$$W_y(p) = \frac{\tilde{U}_{C3}(p)}{\tilde{X}(p)} = W_1(p) \cdot W_2(p). \quad (7)$$

The results of such a test are presented in fig. 5. Dependencies shown in fig. 5 confirm the adequacy of the linearized block diagram in fig. 3 and the simplified scheme in fig. 4 in the considered frequency range.

To determine the parameters of the correcting section, in accordance with paragraph 6 of the proposed methodology, it is necessary to build a family of Bode diagrams of an open loop uncorrected system at the "extreme" operating points. The definition of "extreme" operating points becomes clear if we pay attention to the fact that in expressions 4–6, the electrical parameters of the circuit characterizing its mode of operation are used as transfer coefficients of the links, for example, U_{C30}, X_0, I_{L0}, which, in turn, depend on current I_{SIB} and load resistance R_L. Fig. 6, *a* shows the families of characteristics when the current of the solar battery I_{SIB} is changed and the load

resistance R_L is in the range from their minimum value to the maximum, which explains the use of the term "extreme" operating points.

Based on this family of characteristics, obtained according to a linearized block diagram and presented in fig. 6, *a*, in accordance with paragraph 6 of the proposed methodology, the type of correcting section (7) and its coefficients were synthesized:

$$W_{CS}(p) = \frac{\tilde{X}(p)}{\tilde{g}(p)} = K_{kr}\frac{T_1 p + 1}{p(T_2 p + 1)}, \qquad (8)$$

where $K_{kr} = 2{,}4\cdot 10^4$ с$^{-1}$; $T_1 = 0{,}005$ с; $T_2 = 6{,}6\cdot 10^{-6}$.

The Bode diagrams of the corrected system, corresponding to the same "extreme" points of the variation range of the parameters, are presented in fig. 6, *b*, from which it is possible to determine the obtained stability reserves (16 dB, 35 degrees) with the worst combinations of the considered parameters.

To test the dynamic characteristics of the SlB channel, in the Simulink package of the Matlab design environment, its simulation model was built (fig. 7, *a*) with closed feedback and a synthesized analog correcting section (8). The model parameters are presented in table, the internal structure of the PWM1 unit is shown in fig. 7, *b*, and the scheme of the *T*1 trigger subsystem is shown in fig. 7, *c*. If it is necessary, the proposed simulation model can take into account and verify the effect of the delay section, which, according to the authors of [14], does not allow accurate calculation of the correcting section parameters and requires their experimental verification.

The results of the simulation modeling of the SC PSS during SlB channel operation with closed feedback and a synthesized corrective link are shown in fig. 8.

Analysis of the simulation modeling results shows that when the I_n load current varies in the range from 3 to 7 A, the steady-state voltage U_n on the power bus of the power supply load does not change, which indicates a zero static control error. From the given time diagrams it can be seen that with sharp changes in the load current I_n, the voltage spikes U_n do not go beyond the permissible range. The overshoot of voltage during load dropping is 0.8 %, the voltage fall during load rise is 0.94 %, the durations of transient processes during loading current dropping and rise are 3.3 ms and 4.3 ms respectively.

The obtained transfer functions and the achieved dynamic characteristics correspond to the analog correcting section. To determine the parameters of the transfer function of the corresponding discrete correcting section, it is necessary to implement the bilinear form of the transition from the Laplace transform to the *z*-transform, by replacing the Laplace operator p [15] in the transfer function $W_{cs}(p)$ (analogue function of the prototype):

$$W_{cs}(z) = W_{cs}(p)\big|_p, \text{ when } p = \frac{2(z-1)}{T(z+1)}, \qquad (9)$$

where T is the sampling period of the digital correcting section. After that, it is necessary to reduce the transfer function to the canonical form (10).

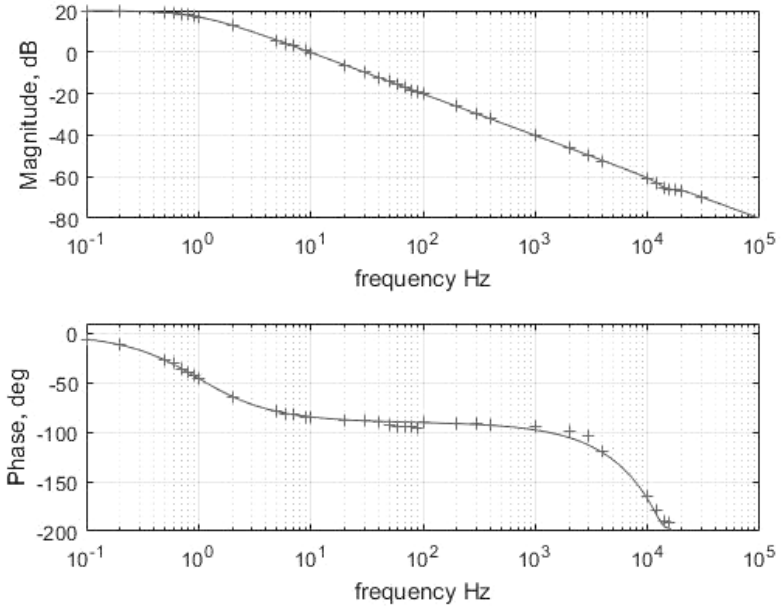

Fig. 5 Bode diagrams in the nominal mode of operation constructed on the small-signal model of the expression (7) (solid lines) and taken on the simulation model (marked with a "+" sign)

Рис. 5. ЛАЧХ и ЛФЧХ в номинальном режиме работы, построенные по малосигнальной модели выражение (7) (сплошные линии) и снятые на имитационной модели (помечены знаком «+»)

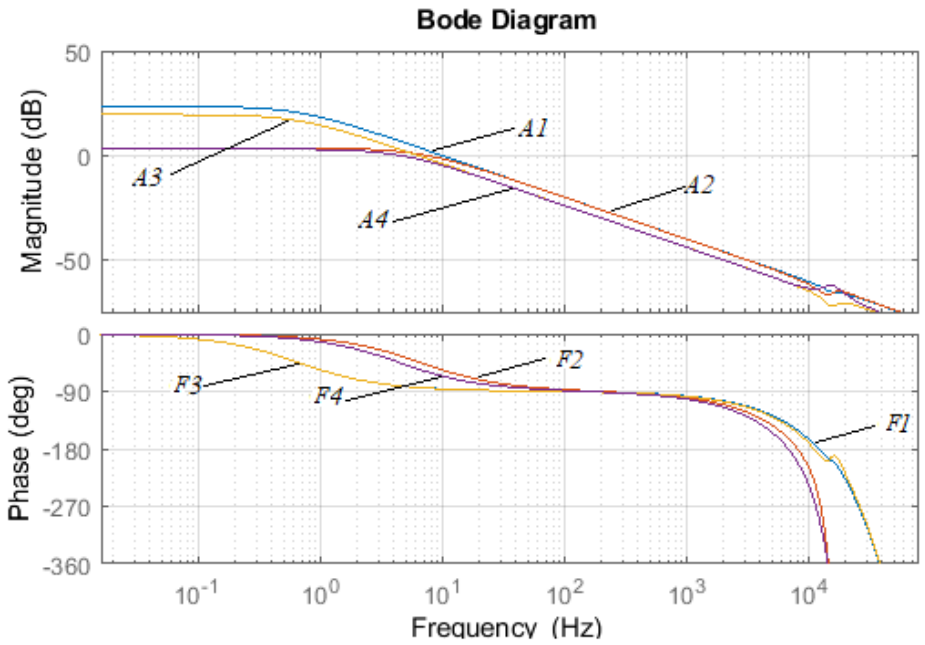

a

A1, F1: $X_0 = 0.9324$, $I_{SlB} = 7.4$A, $R_L = 200\Omega$
A2, F2: $X_0 = 0.3243$, $I_{SlB} = 7.4$A, $R_L = 20\Omega$
A3, F3: $X_0 = 0.8936$, $I_{SlB} = 4.7$A, $R_L = 200\Omega$
A4, F4: $X_0 = 0.2908$, $I_{SlB} = 4.7$A, $R_L = 30\Omega$

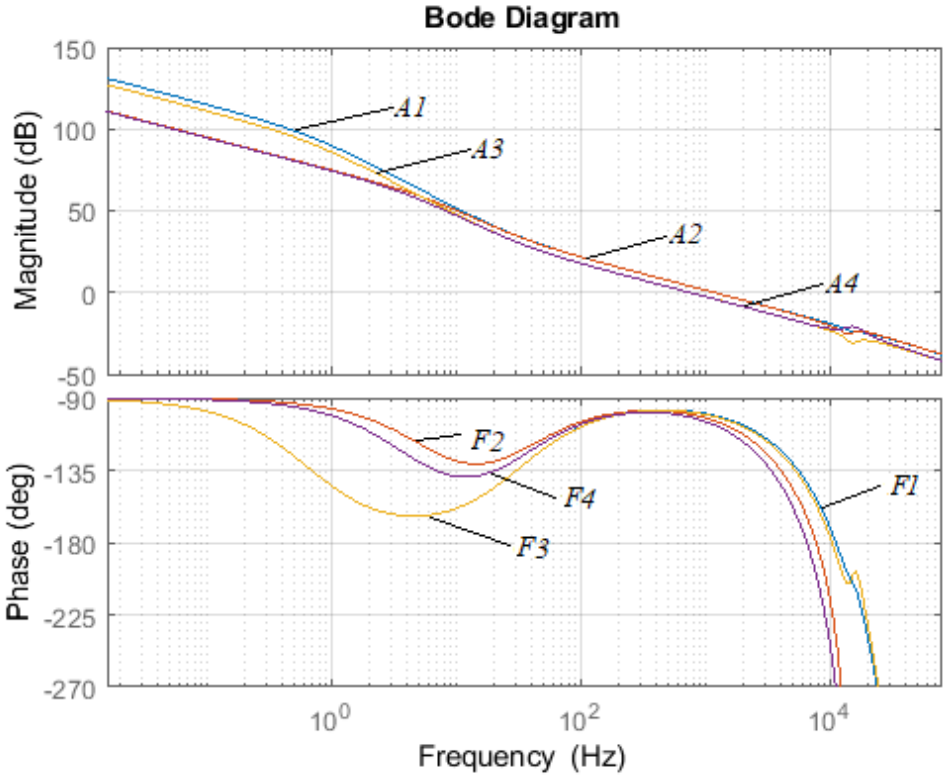

b

Fig. 6. Bode diagrams:
a – open-loop uncorrected system; *b* – open-loop corrected system

Рис. 6. Логарифмические частотные характеристики:
a – разомкнутой нескорректированной системы; *b* – разомкнутой скорректированной системы

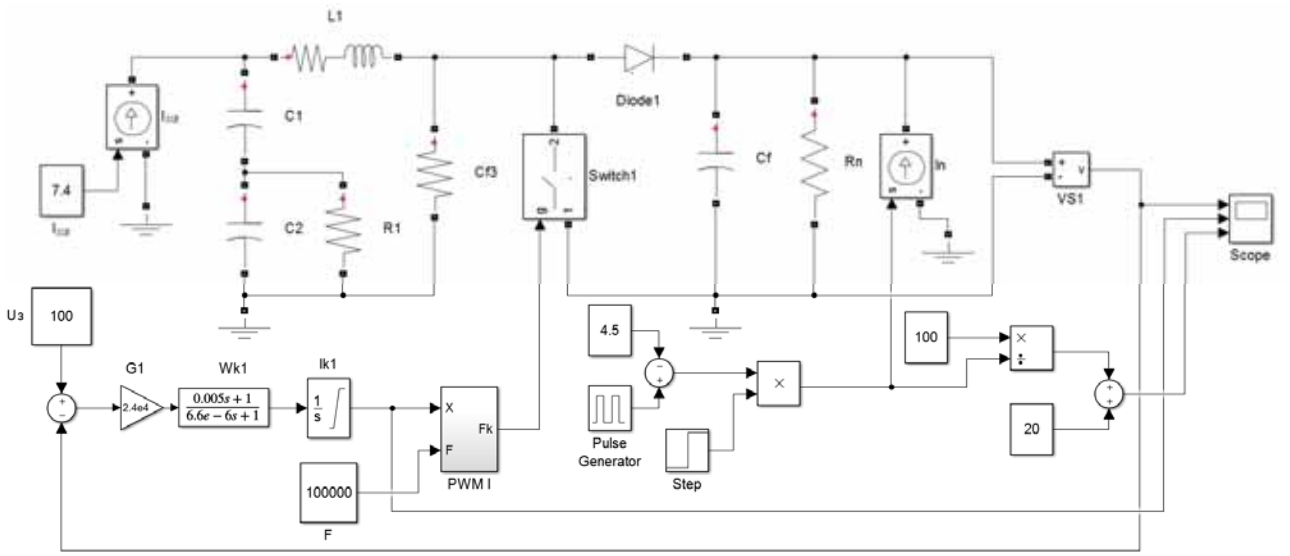

a

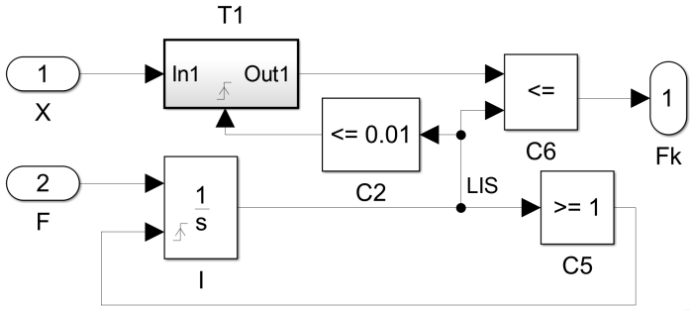

b

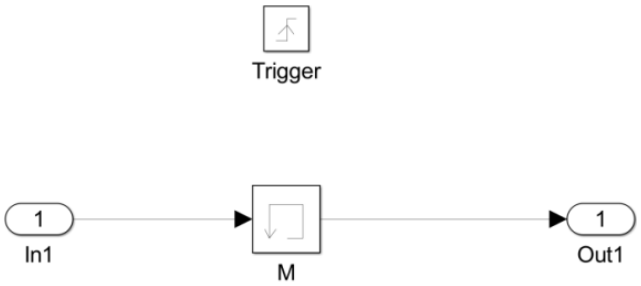

c

Fig. 7. Simulation model:
a – energy conversion channel SlB; *b* – subsystem model PWM1; *c* – subsystem model *T*1

Рис. 7. Имитационная модель:
a – канала преобразования энергии БС; *b* – модель подсистемы ШИМ I; *c* – модель подсистемы *T*1

The parameters of the simulation model elements of the shunt converter

Symbol	Value	Symbol	Value
*C*1	1 μF	R_L	Varies in range 13.5 ... 135 Ohm
*C*2	1 μF	I_{SlB}	7.4 A
*R*1	10 Ohm	I_L	Impulse: from 0 to 4 A.
*L*1	170 μF	*Diode1, Switch 1*	Ideal
R_{L1}	33 mOhm	*F*	100000Hrz
*C*3	1200 μF	*Uз*	Setpoint voltage: 1V

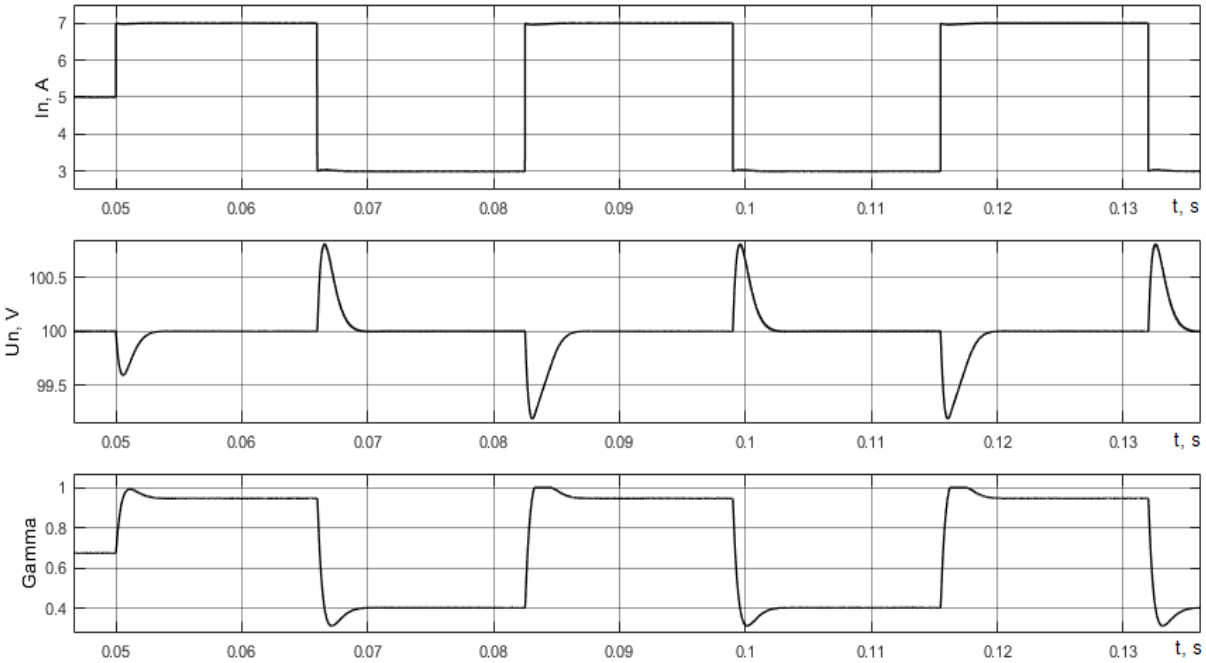

Fig. 8. Timing diagrams of the load current (I_n), on-load voltage (U_n), the control signal at the input of the PWM modulator of the SlB channel (Gamma)

Рис. 8. Временные диаграммы тока нагрузки (I_n), напряжения на нагрузке (U_n), сигнала управления на входе ШИМ-модулятора канала БС (Gamma)

For the transfer function of the correcting section with the parameters specified in (8), the coefficients of expression (10) have the following numerical values: b_0 = 51.7759; b_1 = 0.1034; b_2 = –51.6724; a_1 = 1.1380; a_2 = –0.1380; $T = 10^{-5}$ c.

$$W_{cs}(z) = \frac{\left(b_0 + b_1 z^{-1} + b_2 z^{-2}\right)}{\left(1 - a_1 z^{-1} - a_2 z^{-2}\right)}, \qquad (10)$$

Expression (10) makes it easy to go to the recurrence relation (11) and the difference equation (12)

$$\tilde{x}[i] = \sum_{j=0}^{m} b_j \cdot \tilde{g}[i-j] + \sum_{j=1}^{n} a_j \cdot \tilde{x}[i-j], \qquad (11)$$

where $j = 0,1...m$ – is the number of coefficients in the expression (10), i – is the current reading of the input $g(i)$ and output $x(i)$ signals of the correcting section

$$x(k) = b_0 \cdot g(k) + b_1 \cdot g(k-1) + b_2 \cdot g(k-2) - a_1 \times$$
$$\times x(k-1) - a_2 \cdot x(k-2). \qquad (12)$$

Differential equation (12) allows us to calculate the output signal of the digital correcting section from the readings of the input signal, thus realizing the digital implementation of the obtained analog correcting section, in accordance with paragraph 9 of the proposed method. The loading diagram of the synthesized correcting section, which is also a numerical simulation model of a digital controller, is shown in fig. 9. This scheme is constructed according to expression (12), and the z^{-1} link presented in the diagram is a delay link for one sampling rate period.

Fig. 10 shows the timing diagrams of the output voltage, obtained by abruptly changing the load current, with analog and digital correcting sections.

The diagrams shown in fig. 10 are obtained on a simulation model of a closed SAR (fig. 7) with an analog correcting section, the parameters of which are given on the model, and with a digital correcting section (10) under the same conditions as the SAR with an analog correcting section.

Comparison of timing diagrams in fig. 10 with timing diagrams in fig. 8 shows that they differ quantitatively by no more than 0.01–0.02 V, that is, they practically coincide.

Conclusion. The method of synthesizing a digital controller for a channel of converting the solar battery energy in a power supply system of a spacecraft based on a block diagram of a converter and on the method of switching discontinuous functions has been developed.

On the basis of the proposed methodology, the type and coefficients of the correcting section were selected, providing the necessary stability stocks.

The parameters of the correcting section are chosen so that the characteristics of the system are close to the settings of the technical optimum.

It was shown on the simulation model built in the Simulink package of the Matlab design environment that with the selected type of correcting section and the selected numerical values of its coefficients, the system ensures stable operation throughout the claimed range of disturbance changes. This suggests that, despite the presence of delays in the digital information processing channel and in the PWM channel, the proposed method allows us to synthesize a digital control system of a power supply device for a spacecraft that meets the specified requirements for accuracy and speed.

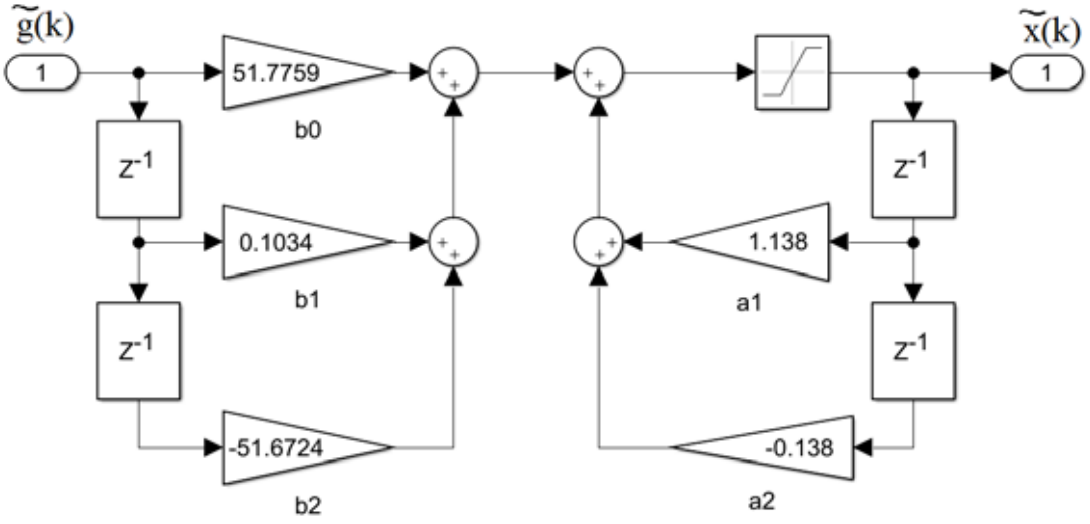

Fig. 9. Simulation model of the digital controller

Рис. 9. Имитационная модель цифрового регулятора

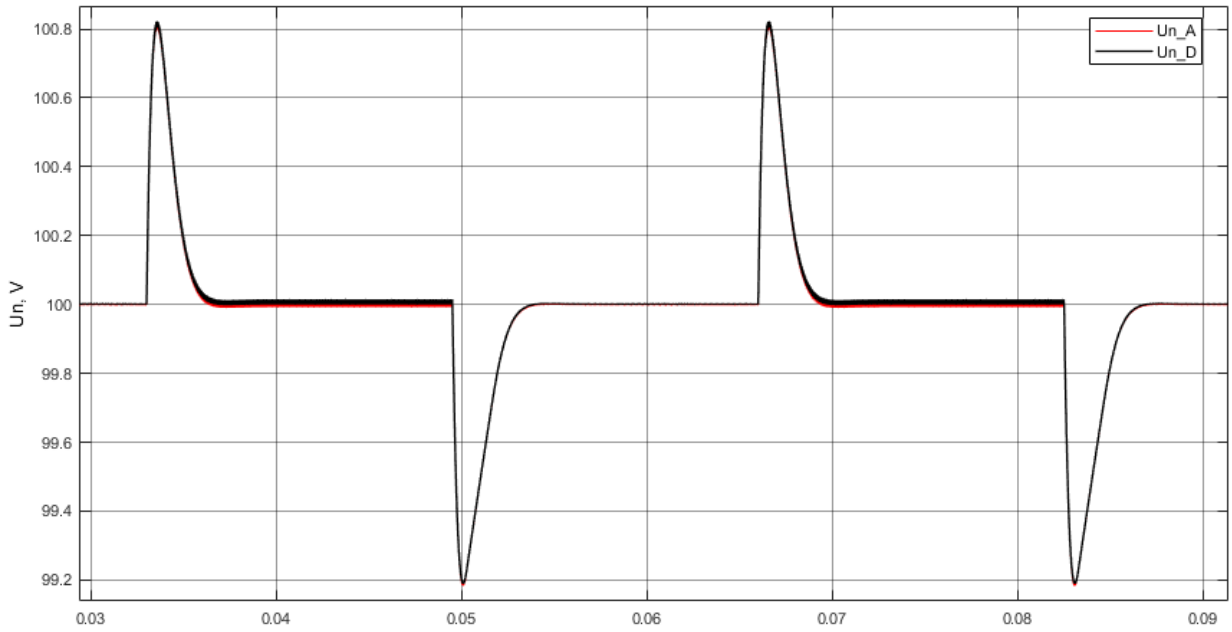

Fig. 10. Timing diagrams of the output voltage with an abrupt change in the load current, obtained in a system with analog and digital correcting sections

Рис. 10. Временные диаграммы выходного напряжения при скачкообразном изменении тока нагрузки, полученные в системе с аналоговым и цифровым корректирующими звеньями

Acknowledgements. The work was performed in the framework of implementation of the RF Government Decree from April 9, 2010 No. 218, and the contract between the JSC “ISS” and the Ministry of Education and Science of the Russian Federation from December 1, 2015 № 02.G25.31.018.

Благодарности. Работа выполнена в рамках реализации Постановления Правительства РФ от 09.04.2010 № 218 и договора между АО «ИСС» и Минобрнауки РФ от 01.12.2015 № 02.G25.31.018.

Reference

1. Shinyakov Yu. A. [Energy analysis of structural diagrams of power systems for automatic space vehicles]. *Izvestiya Tomskogo politekhnicheskogo universiteta.* 2006, Vol. 309, No. 8, P. 152–155 (In Russ).

2. Soustin B. P., Ivanchura V. I., Chernyshev A. I., Islyaev Sh. N. *Sistemy elektropitaniya kosmicheskikh apparatov* [Spacecraft power supply systems]. Novosibirsk, VO Nauka, Sibirskaya izdatel'skaya firma Publ., 1994, 318 p.

3. Greenwood C., Lenhart S., Inenaga B., Jennings C., Mendelsohn A., Staley M., Vaughan R. Super power subsystem development and application on the 1300 family of spacecraft. *20th AIAA International Communication Satellite Systems Conference and Exhibit.* May 12–15 2002.

4. Abbas A. In-Orbit Performance of Lockheed Martin's Electrical Power Subsystem for A2100 Communication Satellite, *AIAA*. 2000, 28 p.

5. Garrigos A., Carrasco J. A., Blanes J. M., Sanchis-Kilders E. A power conditioning unit for high power geo satellites based on the sequential switching shunt series regulator. *IEEE MELECON Electrotechnical Conference*. May 16–19 2006, P. 1186–1189.

6. Ich D. Ngo Evolution of Solar Array Shunt Regulators for Boeing Satellites. *7th International Energy Conversion Engineering Conference.* August 2–5 2009.

7. Soubrier L., Trehet E. High Power PCU for Alphabus: PSR100V. *Proceedings of the 9th European Space Power Conference.* France, 2011.

8. Nepomnyashchiy O. V., Krasnobaev Yu. V., Titovskiy S. N., Khabarov V. A. [Microelectronic control devices for power energy-transforming modules of power supply systems for prospective space vehicles]. *Zhurnal Sibirskogo federal'nogo universiteta. Seriya: Tekhnika i tekhnologii.* 2012, Vol. 5, No 2, P. 162–168 (In Russ.).

9. Nepomnyashchiy O. V., Veysov E. A., Krasnobaev Yu. V., Kapulin D. V. [Methods and algorithms for microprogram control of high-speed impulse voltage regulators for power supply of on-board equipment of perspective space vehicles]. *Vestnik SibGAU.* 2010, No. 4(25), P. 14–18 (In Russ.).

10. Kazantsev Yu. M., Gordeev K. G., Lekarev A. F., Cherdantsev S. P., Gavrilov A. M. [Current transformer of solar battery energy in the spacecraft power supply system]. *Izvestiya Tomskogo politekhnicheskogo universiteta.* 2011, Vol. 319, No 4, P. 148–153 (In Russ.).

11. Kobzev A. V., Semenov V. D., Fedinykh E. K. [Application of the commutation discontinuous functions method for constructing mathematical models of power converters]. *Doklady TUSURa.* 2011, No. 2(24), P. 58–63(In Russ.).

12. Kabirov V. A., Semenov V. D. [A small-signal converter model using the commutation discontinuous function method]. *Nauchnaya sessiya TUSUR-2017: materialy Mezhdunar. Nauch.-tekhn. Konf. studentov, posvyashchennoy 55-letiyu TUSURa. Tomsk, 10–12 maya 2017 g. V 8 ch.* [Scientific session of TUSUR-2017 : proceedings of international. science.-tech. Conf. students dedicated to the 55th anniversary of TUSUR. In 8 part]. Tomsk, V-Spektr Publ., 2017, Part. 2, 272 p. (In Russ.).

13. Kabirov V. A [Experimental study of the small-signal frequency characteristics of a shunt voltage converter]. *XIV Mezhdunar. Konf. studentov, aspirantov i molodykh uchenykh "Perspektiva razvitiya fundamental'nykh nauk"* [XIV international. Conf. students, postgraduates and young scientists "Prospect of development of fundamental Sciences"]. Tomsk, TPU Publ., 2017, Vol. 7, P. 54–56 (In Russ.).

14. Guretskiy Kh. *Analiz i sintez sistem upravleniya s zapazdyvaniem* [Analysis and synthesis of control systems with delay]. Per. s pol'skogo. Moscow, Mashinostroenie Publ., 1974, 210 p.

15. Bychkov Yu. A., Zolotnitskiy V. M., Chernyshev E. P., Belyanin A. N. *Osnovy teoreticheskoy elektrotekhniki* [Fundamentals of theoretical electrical engineering]. Sankt-Peterburg, Lan' Publ., 2009, 340 p.

Библиографические ссылки

1. Шиняков Ю. А. Энергетический анализ структурных схем систем электроснабжения автоматических космических аппаратов // Известия Томского политехнического университета. 2006. Т. 309, № 8. С. 152–155.

2. Системы электропитания космических аппаратов / Б. П. Соустин, В. И. Иванчура, А. И. Чернышев, Ш. Н. Исляев. Новосибирск : ВО «Наука» ; Сибирская издательская фирма, 1994. 318 с.

3. Super power subsystem development and application on the 1300 family of spacecraft / C. Greenwood, S. Lenhart, B. Inenaga [et al.] // 20th AIAA International Communication Satellite Systems Conference and Exhibit 12–15, May 2002.

4. Abbas A. In-Orbit Performance of Lockheed Martin's Electrical Power Subsystem for A2100 Communication Satellite // AIAA. 2000. 28 p.

5. A power conditioning unit for high power geo satellites based on the sequential switching shunt series regulator / A. Garrigos, J. A. Carrasco, J. M. Blanes, E. Sanchis-Kilders // IEEE MELECON Electrotechnical Conference. May 16–19, 2006. P. 1186–1189.

6. Ich D. Ngo Evolution of Solar Array Shunt Regulators for Boeing Satellites // 7th International Energy Conversion Engineering Conference. August 2–5, 2009.

7. Soubrier L., Trehet E. High Power PCU for Alphabus: PSR100V // Proceedings of the 9th European Space Power Conference. France, 2011.

8. Микроэлектронные устройства управления силовыми энергопреобразующими модулями систем электропитания перспективных космических аппаратов / О. В. Непомнящий, Ю. В. Краснобаев, С. Н. Титовский, В. А. Хабаров // Журнал Сибирского федерального университета. Серия: Техника и технологии. 2012. Т. 5, № 2. С. 162–168.

9. Методы и алгоритмы микропрограммного управления быстродействующими импульсными стабилизаторами напряжения для организации питания бортовой аппаратуры перспективных космических аппаратов / О. В. Непомнящий, Е. А. Вейсов, Ю. В. Краснобаев, Д. В. Капулин // Вестник СибГАУ. 2010. № 4(25). С. 14–18.

10. Токовый преобразователь энергии солнечной батареи в системе электропитания космических аппаратов / Ю. М. Казанцев, К. Г. Гордеев, А. Ф. Лекарев [и др.]. // Известия Томского политехнического университета. 2011. Т. 319, № 4. С. 148–153.

11. Кобзев А. В., Семенов В. Д., Федиых Е. К. Применение метода коммутационных разрывных функций для построения математических моделей силовых преобразователей // Доклады ТУСУРа. 2011. № 2(24). С. 58–63.

12. Кабиров В. А., Семенов В. Д. Малосигнальная модель ШИМ преобразователя при использовании метода коммутационных разрывных функций // Научная сессия ТУСУР-2017 : материалы Междунар. науч.-техн. конф. студентов, посвященной 55-летию ТУСУРа : в 8 ч. Томск, 10–12 мая 2017 г. Ч. 2. Томск : В-Спектр, 2017. 272 с.

13. Кабиров В. А. Экспериментальное исследование малосигнальных частотных характеристик шунтового преобразователя напряжения // Перспектива развития фундаментальных наук : XIV Междунар. конф. студентов, аспирантов и молодых ученых. Т. 7. Томск : Изд-во ТПУ, 2017. С. 54–56.

14. Гурецкий Х. Анализ и синтез систем управления с запаздыванием : пер. с польского. М. : Машиностроение, 1974. 210 с.

15. Основы теоретической электротехники / Ю. А. Бычков, В. М. Золотницкий, Э. П. Чернышев, А. Н. Белянин. СПб. : Лань, 2009. 340 с.

Shkolnyi Vadim Nikolaevich – Ch. designer of design and testing of REA; JSC “Information Satellite Systems” named after academician M. F. Reshetnev”. E-mail: shkolnyy@iss-reshetnev.ru.

Semenov Valery Dmitrievich – Cand. Sc., Professor of Industrial Electronics Department; Tomsk State University of Control Systems and Radioelectronics, Research Institute of Space Technologies. E-mail: svd@ie.tusur.ru.

Kabirov Vagiz Alexandrovich – Head of Microprocessor Devices and Systems Laboratory of Industrial Electronics Department; Tomsk State University of Control Systems and Radioelectronics, Research Institute of Space Technologies. E-mail: fva@vipelec.com.

Sukhorukov Maxim Petrovich – Head of Digital Control Systems Laboratory; Tomsk State University of Control Systems and Radioelectronics, Research Institute of Space Technologies. E-mail: max_sukhorukov@mail.ru.

Torgayeva Darya Sergeevna – Junior Researcher of Digital Control Systems Laboratory; Tomsk State University of Control Systems and Radioelectronics, Research Institute of Space Technologies. E-mail: belial1349@mail.ru.

Школьный Вадим Николаевич – главный конструктор проектирования и испытаний РЭА; АО «Информационные спутниковые системы» имени академика М. Ф. Решетнева». E-mail: shkolnyy@iss-reshetnev.ru.

Семенов Валерий Дмитриевич – кандидат технических наук, профессор кафедры промышленной электроники; Томский государственный университет систем управления и радиоэлектроники, НИИ космических технологий. E-mail: svd@ie.tusur.ru.

Кабиров Вагиз Александрович – заведующий лабораторией микропроцессорных устройств и систем кафедры промышленной электроники; Томский государственный университет систем управления и радиоэлектроники, НИИ космических технологий. E-mail: fva@vipelec.com.

Сухоруков Максим Петрович – заведующий лабораторией цифровых систем управления; Томский государственный университет систем управления и радиоэлектроники, НИИ космических технологий. E-mail: max_sukhorukov@mail.ru.

Торгаева Дарья Сергеевна – младший научный сотрудник лаборатории цифровых систем управления; Томский государственный университет систем управления и радиоэлектроники, НИИ космических технологий. E-mail: belial1349@mail.ru.

Раздел
Part
3

ТЕХНОЛОГИЧЕСКИЕ ПРОЦЕССЫ И МАТЕРИАЛЫ

TECHNOLOGICAL PROCESSES AND MATERIALS

UDC 669/713-048/25
Doi: 10.31772/2587-6066-2019-20-1-88-98

For citation: Ivanov Yu. F., Eresko S. P., Ahmadeev Yu. H., Lopatin I. V., Klopotov A. A. [Development of combined electron-ion-plasma method for formation of multiphase submicro-nanoscale alloys based on aluminum]. *Siberian Journal of Science and Technology*. 2019, Vol. 20, No. 1, P. 88–98. Doi: 10.31772/2587-6066-2019-20-1-88-98

Для цитирования: Иванов Ю. Ф., Ереско С. П., Ахмадеев Ю. Х., Лопатин И. В., Клопотов А. А. Разработка комбинированного электронно-ионно-плазменного метода формирования многофазных субмикро-наноразмерных сплавов на основе алюминия // Сибирский журнал науки и технологий. 2019. Т. 20, № 1. С. 88–98. Doi: 10.31772/2587-6066-2019-20-1-88-98

DEVELOPMENT OF COMBINED ELECTRON-ION-PLASMA METHOD FOR FORMATION OF MULTIPHASE SUBMICRO-NANOSCALE ALLOYS BASED ON ALUMINUM

Yu. F. Ivanov[1], S. P. Eresko[2], Yu. H. Ahmadeev[1], I. V. Lopatin[1], A. A. Klopotov[3,4*]

[1]Institute of High Current Electronics of the SB RAS
2/3, Akademicheskiy Av., Tomsk, 634055, Russian Federation
[2]Reshetnev Siberian State University of Science and Technology
31, Krasnoyarsky Rabochy Av., Krasnoyarsk, 660037, Russian Federation
[3]Tomsk State University of Architecture and Building
2, Solyanaya Sq., 6340032, Tomsk, Russian Federation
[4]National Research Tomsk State University
36, Lenin Av., Tomsk, 634050, Russian Federation
[*]E-mail: klopotovaa@tsuab.ru

Aluminum-based alloys are widely used in many branches of modern industry (aviation, mechanical engineering, shipbuilding, instrument-making, energy and medicine, etc.). The promising method for further expanding the scope of these alloys is surface treatment based on the use of concentrated energy fluxes (laser beams, plasma flows, powerful ion beams, continuous and pulsed electron beams). The purpose of this paper is to establish the possibilities of integrated electron-ion-plasma modification of the structure and properties of the surface layer of technically pure aluminum A7. The surface alloy was formed in a single vacuum cycle using the "KOMPLEX" facility (ISE SB RAS) by spraying a titanium film with a thickness of 0.5 μm and the subsequent irradiation with an intense pulsed electron beam in the aluminum melting mode. After 20 "spraying/irradiation" cycles, nitriding (540 °C, 8 h) of the formed surface alloy was performed in a low-pressure gas discharge plasma using the plasma generator "PINK". Surface alloy studies were carried out applying the modern materials science methods (scanning and transmission electron diffraction microscopy, X-ray phase analysis, determination of hardness and wear resistance). The choice of elements alloying the surface layer of aluminum was based on the analysis of binary state diagrams of Al-N, Al-Ti, Ti-N systems and the isotermal section of the ternary system Al-Ti-N. It has been shown that formation of an entire series of binary and ternary compounds, including MAX-phases of the composition Ti_2AlN and Ti_4AlN_3, is observed under equilibrium conditions in the Al-Ti-N system. The carried out research has allowed to state that an integrated method of electron-ion-plasma modification of technically pure A7 aluminum by nitriding (540 °C, 8 h) of the surface alloy formed by pulsed melting in vacuum of the Al-Ti system (20 "spraying/irradiation" cycles with an electron beam with parameters 10 J/cm^2; 50 μs; 10 pulses; the titanium film thickness in each cycle 0.5 μm) leads to formation of a multiphase multielement submicro-nanocrystalline surface layer up to 20 μm thick. It is shown that the mechanical (microhardness) and tribological (wear resistance and friction coefficient) properties of the formed surface layer exceed manifold the properties of the original commercially pure aluminum A7.

Keywords: aluminum, electron-ion-plasma processing, nitriding, structural researches, nanostructure, properties.

РАЗРАБОТКА КОМБИНИРОВАННОГО ЭЛЕКТРОННО-ИОННО-ПЛАЗМЕННОГО МЕТОДА ФОРМИРОВАНИЯ МНОГОФАЗНЫХ СУБМИКРОНАНОРАЗМЕРНЫХ СПЛАВОВ НА ОСНОВЕ АЛЮМИНИЯ

Ю. Ф. Иванов[1], С. П. Ереско[2], Ю. Х. Ахмадеев[1], И. В. Лопатин[1], А. А. Клопотов[3,4*]

[1]Институт сильноточной электроники СО РАН
Российская Федерация, 634055, г. Томск, просп. Академический, 2/3
[2]Сибирский государственный университет науки и технологий имени академика М. Ф. Решетнева
Российская Федерация, 660037, г. Красноярск, просп. им. газеты «Красноярский рабочий», 31
[3]Томский государственный архитектурно-строительный университет
Российская Федерация, 634003, г. Томск, пл. Соляная, 2
[4]Национальный исследовательский Томский государственный университет
Российская Федерация, 634055, Томск, ул. Ленина 36
[*]E-mail: klopotovaa@tsuab.ru

Сплавы на основе алюминия широко используются во многих отраслях современной промышленности (авиации, машиностроении, кораблестроении и приборостроении, энергетике, медицине и т. д.). Перспективными методами дальнейшего расширения сферы применения данных сплавов является поверхностная обработка, основанная на использовании концентрированных потоков энергии (лучи лазера, потоки плазмы, мощные ионные пучки, непрерывные и импульсные электронные пучки). Целью настоящей работы является установление возможностей комплексного электронно-ионно-плазменного модифицирования структуры и свойств поверхностного слоя технически чистого алюминия марки А7. Формирование поверхностного сплава осуществляли в едином вакуумном цикле на установке «КОМПЛЕКС» (ИСЭ СО РАН) путем напыления пленки титана толщиной 0,5 мкм и последующего облучения интенсивным импульсным электронным пучком в режиме плавления алюминия. После 20 циклов «напыления/облучения» проводили азотирование (540 ^oC, 8 ч) сформированного поверхностного сплава в плазме газового разряда низкого давления с использованием плазмогенератора «ПИНК». Исследования поверхностного сплава осуществляли методами современного материаловедения (сканирующая и просвечивающая электронная дифракционная микроскопия, рентгенофазовый анализ, определение твердости и износостойкости). Выбор легирующих поверхностный слой алюминия элементов был основан на анализе бинарных диаграмм состояний систем Al-N, Al-Ti, Ti-N и изотерического сечения тройной системы Al-Ti-N. Показано, что в равновесных условиях в системе Al-Ti-N наблюдается формирование целого ряды двойных и тройных соединений, в том числе и MAX-фаз состава Ti_2AlN и Ti_4AlN_3. В результате выполненных исследований установлено, что комплексный метод электронно-ионно-плазменного модифицирования технически чистого алюминия марки А7 путем азотирования (540 ^oC, 8 ч) поверхностного сплава, сформированного импульсным плавлением в вакууме системы Al-Ti (20 циклов «напыления/облучения» электронным пучком с параметрами 10 Дж/см^2; 50 мкс; 10 имп.; толщина пленки титана в каждом цикле 0,5 мкм), приводит к формированию многофазного многоэлементного субмикронанокристаллического поверхностного слоя толщиной до 20 мкм. Показано, что механические (микротвердость) и трибологические (износостойкость и коэффициент трения) свойства сформированного поверхностного слоя многократно превосходят свойства исходного технически чистого алюминия А7.

Ключевые слова: алюминий, азотирование, структурные исследования, электронно-ионно-плазменная обработка, наноструктура, свойства.

Introduction. Titanium and aluminum-based alloys are widely used in the aerospace industry, mechanical engineering and shipbuilding, medicine, etc. [1; 2]. In many cases extension of scope of these materials is based on the improvement of properties of a surface layer of a detail or product. It happens due to formation of wear resistant, hard and super hard coatings; creation of multi-element multiphase sub-micro nanocrystal surface layers; and integrated processing combining formation of multi-purpose coatings on preliminary modified surface of a detail [1–5]. Perspective methods of surface treatment are those based on the use of concentrated energy streams (laser beams, plasma streams, powerful ion beams, continuous and pulse electron beams) [5–12]. Employing this approach allows to drastically improve material properties connected with modifying surface layer condition (hardness, wear resistance, resistance to the influence of hostile environment, etc.) [5–13]. One of the perspective methods of metals and alloys surface treatment is the approach based on the integrated impact of plasma streams and intensive pulse electron beams on the material surface [5; 13].

The purpose of the present research is to find opportunities for integrated electronic ion-plasma modification of the structure and properties of commercially pure aluminum surface layer.

Material and method of research. Material of research – commercially pure aluminum A7 brand (0.15Si, 0.16Fe, 0.01Cu, 0.03Mn, 0.02Mg, 0.04Zn, 0.03Ga, 0.01Ti, balance Al, weight. %) [14]. Specimen dimensions 15×15×5 mm. The surface alloy was formed in a single vacuum cycle using the “KOMPLEX” facility

(ISE SB RAS) by spraying a titanium film with a thickness of 0.5 μm and the subsequent irradiation with an intense pulsed electron beam in the aluminum melting mode. After 20 "spraying/irradiation" cycles, nitriding (540 °C, 8 h) of the formed surface alloy was performed in a low-pressure gas discharge plasma using the plasma generator "PINK". Research into the element and phase structure, defective substructure condition was carried out applying the methods of scanning electron microscopy (Philips SEM-515 with microanalyzer EDAX ECON IV) and transmission diffraction electron microscopy (JEOL JEM-2100 F), X-ray diffraction analysis (X-ray diffractometer Shimadzu XRD 6000). Material properties were characterized by hardness (PMT 3, indentation load 0.2 H). Tribological studies (wear resistance and friction coefficient identification) were carried out on tribometer Pin on Disc and Oscillating TRIBOtester (TRIBOtechnic, France) under the following parameters: steal ball of 6 mm diameter, track radius – 2 mm, indentation load and track length vary depending on the ware resistance factor of the material under study.

Results and discussions. Fig. 1 shows binary state diagrams Al-N, Al-Ti, Ti-N and Isothermal section of the ternary system Al-Ti-N. Two of the three alloying elements of the ternary system Al-Ti-N are metals, while the third one nitrogen is a non-metal and belongs to VB group of the Periodic table. Nitrogen atoms possess five electrons on the outer *s*- and *p*-shells ($[He]2s^2 2p^3$). With such electronic structure nitrogen quite easily attaches three more electrons which is a characteristic of non-metal.

System Al-N. Nitrogen is almost insoluble in Al neither in liquid, nor in hard states [15]. In the Al-N system existence of only one connection in the field of the stoichiometric structure of AlN with hexagonal structure was found (Pearson's symbol *hP*4, pr. gr. $R6_3ts$, ZnS prototype) (fig. 1).

System Ti-N. Titan possess a characteristic of activel interaction with nitrogen. It finds reflection in formation of compounds in the Ti-N system in the form of solid solutions with variable structures and with wide areas of homogeneity: β–(Ti,N), α–(Ti,N), δ–TiN_X (*cF*8, NaCl) (fig. 1) [16]. In compounds δ–TiN_X atoms Ti form a metal face-centered cubic sublattice, where in octahedral interstices interstitial (nitrogen) or vacancies may be present. In not stoichiometric disordered compound δ–TiN_X change of structural vacancies concentration causes wide area of homogeneity. Under the temperature of ~ 1100 °C and content of N atoms ~33% from the phase δ–TiN_X nitride ε–Ti_2N (*tP*6, anti-TiO_2) with the narrow area of homogeneity is formed. Besides, in a number of studies existence of three intermediate phases was identified: ζ–Ti_4N_{3-X} (*hR*8) [17], η–Ti_3N_{2-X} (*hR*6, VTa_2C_2) [18; 19], Ti_4N_{3-x} (*hR*2, V_4C_3) [17; 18].

System Al-Ti-N. Inside isothermal triangle in the system Al–Ti–N existence of three nitride compounds of strong stoichiometric ratio was found (fig. 1): τ_1–Ti_3AlN (Pearson's symbol *cP*5, prototype $CaTiO_3$) [22; 23]; τ_2–Ti_2AlN (*hP*8, Cr_2AlC) [24]; τ_3–Ti_4AlN_3 (*hP*16, Ti_4AlN_3) [25]. Apart from that, in [26–28] metastable condition $Ti_{1-x}Al_xN$ (cF8, NaCl).

Out of the three compounds formed in the system Al-Ti-N, compound τ_1–Ti_3AlN proves the most stable [29] and belongs to the phase group H [30]. Literature shows that there are several ways of how compounds τ_1–Ti_2AlN can be prepared. Let us demonstrate the synthesis of particles with Ti_2AlN phase. First, under exothermic reaction of powders Al and Ti in nitrogen atmosphere [31]. Second, as a result of powders Al and TIN hot pressing and subsequent homogenization of samples under the temperature 850 °C within 200 hours [32]. Third, when sintering under above 1500 °C from powders AlN and Ti [33; 34]. Fourth, as a result of 24 hours roasting under between 1275 °C and 1600 °C and 1100 MPa of powder bland Al, Ti, TiN and AlN nitrides pressed under room temperature [35]. Fifth, when nitriding Al-Ti alloys as a result of roasting under 1000 °C [36]. Sixth, when heating a powder bland consisting of two parts Ti and one part of AlN under 1400 °C for 48 hours under the pressure of ≈ 40 MPa [24]. Seventh, powder bland AlN and Ti vacuum sintering under 10^{-3} Pa for 16 hours [37].

Recently great attention is drawn to perspective materials – polycrystalline nanolaminates. This class of materials represents machine processed ceramics which is stable at high temperatures [38–41]. In terms of structure nanolaminates, which are called still MAX phases, [42] represent threefold compounds with structure $M_{n+1}AX_n$ (M = transition metal, A = element of IIIA or IVA group of the Periodical table, X = C or N, *n* accepts integer values 1, 2, 3). MAX are phases representing laminated hexagonal structure with space group $P6_3/mmc$ with two formula units in a space unit (fig. 2). The unique distinctive feature of these materials is a laminated crystal lattice, a natural arrangement of layers of atoms M- and A-elements.

According to literature [42], more than 70 of the popular nanolaminates are titanium nitride-based. They are phases Ti_2AlN (211) and Ti_4AlN_3 (413), where element X is nitrogen.

In the light of the aforesaid it is possible to assume that application of the high-energy electronic ion-plasma integrated processing of aluminum surface in a uniform vacuum cycle combining formation of "film (titanium)/(aluminum) substrate" system, radiation with an intensive pulse electron beam of aluminum surface in the melting mode, and subsequent saturation of the alloyed layer with nitrogen atoms of low pressure gas category plasma can lead to specific structural and phase states which will cause formation of a multiphase surface with the increased physical and mechanical properties. The research of commercially pure aluminum modified layer phase structure was conducted applying the methods of X-ray diffraction analysis. It is revealed that the surface layer is multiphase material and contains α-Ti (5.2 mass. %), Al_3Ti (58.4 mass. %), AlN (24.2 mass. %) and Al (12.2 mass. %).

The undertaken research showed that the surface layer up to 20 microns thick has sub-microcrystalline, typical structure of which is provided in fig. 3.

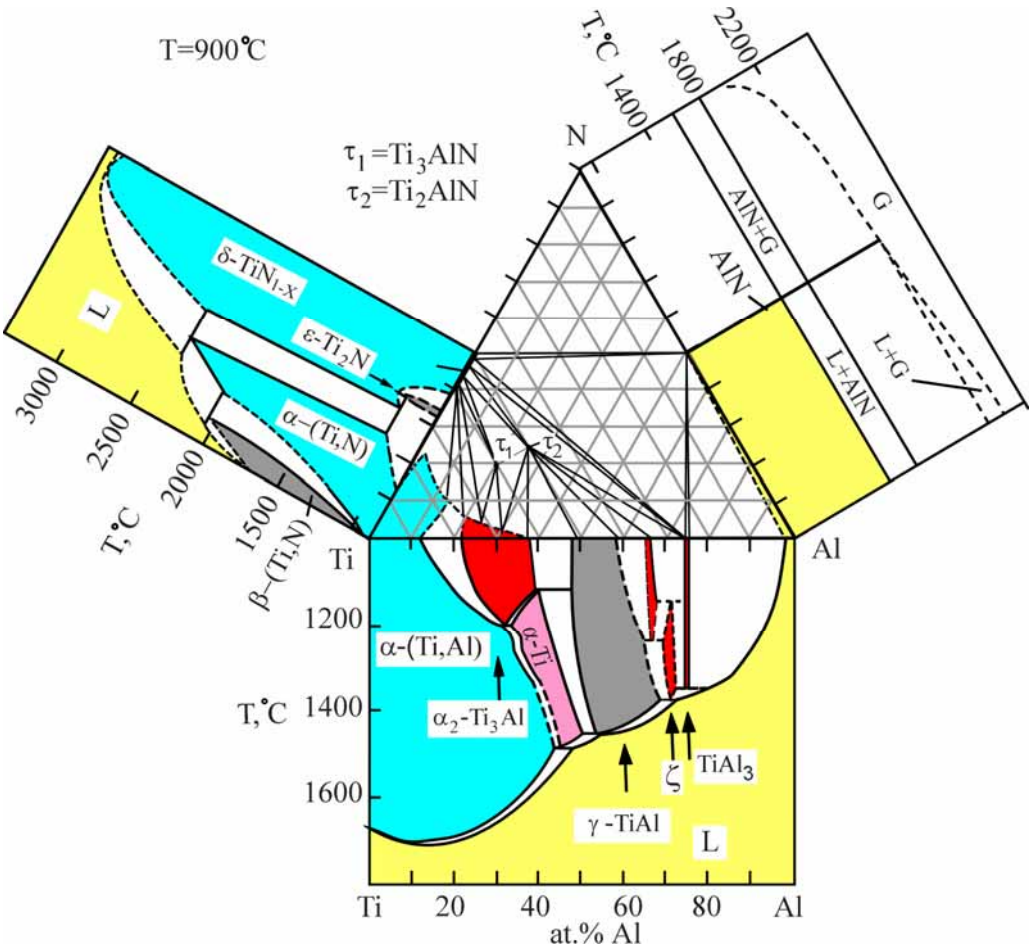

Fig. 1. Isothermal section at 900 °C of the Al-Ti-N ternary system [20; 21] and binary state diagrams of the Al-N [15], Al-Ti [15] and Ti-N systems [16]

Рис. 1. Изотермическое сечение при 900 °C тройной системы Al-Ti-N [20; 21] и бинарные диаграммы состояний систем Al-N [15], Al-Ti [15] и Ti-N [16]

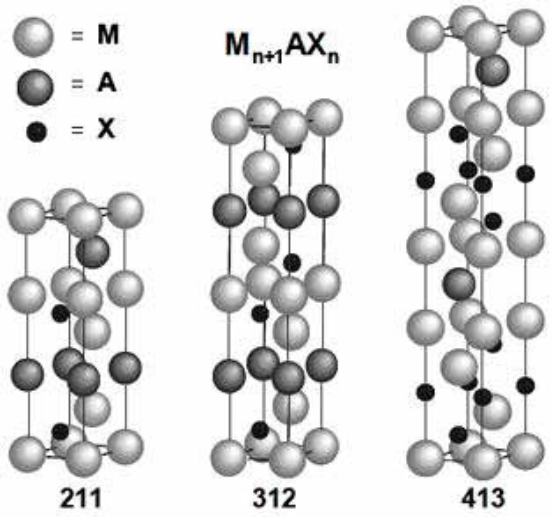

Fig. 2. Crystal structure of MAX-phases with transition metals (M) with layers of elements A (C or N) from groups IIIA and IVA [41]

Рис. 2. Кристаллическая структура MAX-фаз с переходными металлами (M) со слоями из элементов A (C или N) из групп IIIA и IVA [41]

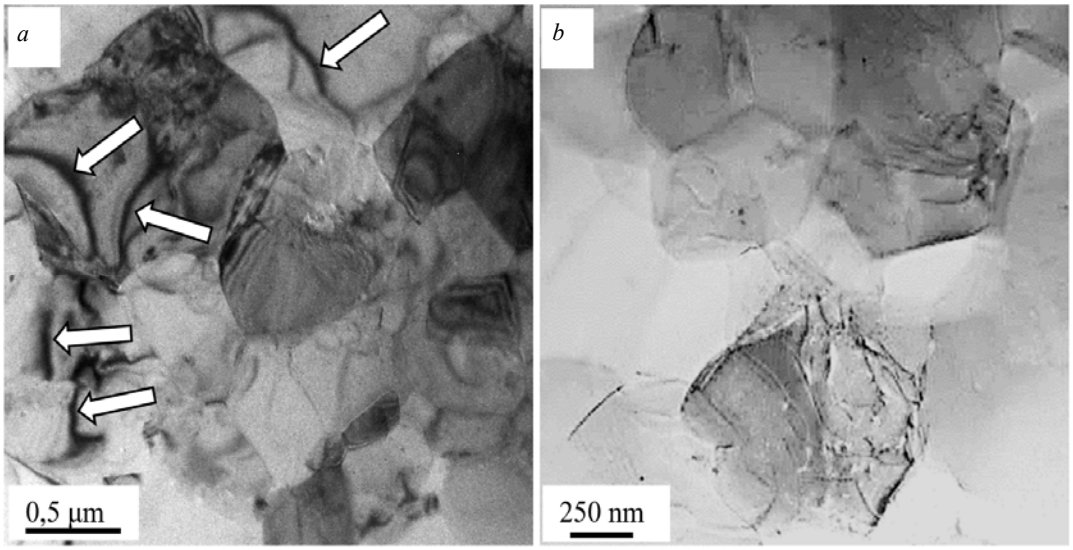

Fig. 3. Electron-microscopic image of the surface layer of commercially pure aluminum grade A7 modified by nitriding (540 °C, 8 h) of a surface alloy formed by pulsed melting in a vacuum of the Al-Ti system (20 sputtering/irradiation cycles) with an electron beam with parameters J/cm^2; 50 μs; 10 imp.; titanium film thickness in each cycle 0.5 μm):
a – arrows indicate bend contours of extinctions; *b* – dislocational substructure of material

Рис. 3. Электронно-микроскопическое изображение поверхностного слоя технически чистого алюминия марки А7, модифицированного путем азотирования (540 °С, 8 ч) поверхностного сплава, сформированного импульсным плавлением в вакууме системы Al-Ti (20 циклов «напыления/облучения» электронным пучком с параметрами 10 Дж/см^2; 50 мкс; 10 имп.; толщина пленки титана в каждом цикле 0,5 мкм):
a – стрелками указаны изгибные контуры экстинкции; *b* – дислокационная субструктура материала

Crystallite sizes change ranging from 0.2 microns up to 0.9 microns.

Crystallites have various forms changing from globular to facetted. In crystallites volumes a dislocation substructure in the form of chaotically distributed dislocations is observed (fig. 3, *b*). The scalar density of dislocations changes in limits $(0.8 \div 1.1)\times10^{10}$ cm^{-2}.

Electronic and microscopic image of crystallites is characterized by a large number of flexural extiction contours (fig. 3, contours are specified by arrows). Existence on electronic and microscopic images of such contours indicates curvature torsion of a crystal lattice of the studied foil that testifies, in turn, elastic tension of the studied material layer [43]. Generally, contours start from crystallite border lines. This fact proves that the crystallite border lines are the source of material elastic tension [44]. A number of studies [45–47] shows that the cross sizes of a flexural extinction contour are inversely proportional to tension amplitude of this particular foil section. Analyzing the electronic and microscopic image of the material structure shown in fig. 3, it can be noted that the cross sizes of flexural contours are minimum at crystallites border lines and are maximum in the center of the crystallite. Therefore, amplitude of curvature torsion of a crystal lattice of material is minimal in the center of crystallites while increases as approaching the border line of the section.

Applying the methods of the micro-diffraction analysis with the subsequent indicating of micro-diffraction patterns it was found that crystallites are formed by the phases α-Ti, Al_3Ti and Al that was also revealed by the methods of the X-ray phase analysis. In most cases grains of α-titanium and aluminum are located in chains parallel to the modifiable surface of a sample.

On borders of crystallites extended layers having nanocrystal structure with particles size of 10-20 nanometers are observed. A typical image of such structure is show in fig. 4. The microdiffraction patterns analysis received from similar foil sections shows that nanocrystals are aluminum nitrides. As a rule, such layers are formed along the titan aluminide Al_3Ti grain sections borders. Nanodimensional allocations of aluminum nitride particles are found in aluminum grains volume as well.

Electronic microscope JEOL JEM-2100 F allows studies applying the methods of electron microprobe analysis, distribution of chemical elements forming the material. Results of such research of the modified layer of commercially pure aluminum are given in fig. 5. Nitrogen atoms distribution in the structure of the studied material attracts a lot of attention. It is clear that in the aluminum layer (substrate), adjacent to the modified layer (the lower part of the picture in fig. 5) atoms of nitrogen are distributed unevenly, concentrating along borders of a cellular dislocation substructure. In aluminum grains volume located in the modified layer (specified by an arrow fig. 5), atoms of nitrogen form nanodimensional objects which are obviously aluminum nitride particles.

Properties of thealuminnum modified layer was characterized by the size of microhardness and wear resistance.

As a result of the research it was revealed that modifying of commercially pure aluminum of A7 brand by nitriding (540 °C, 8 h) of the surface alloy formed by pulse melting in the system vacuum.

Al-Ti (20 cycles “dusting/radiation” via the electron beam with the parameters of 10 J/cm^2; 50 microsec; 10 imp.; thickness of titan film in each cycle equals 0.5 microns) leads to formation of a surface layer which microfirmness by 9 times exceeds the hardness of the initial material, wear resistance is 400 times higher, friction coefficient is 3.5 times less than that of the initial material.

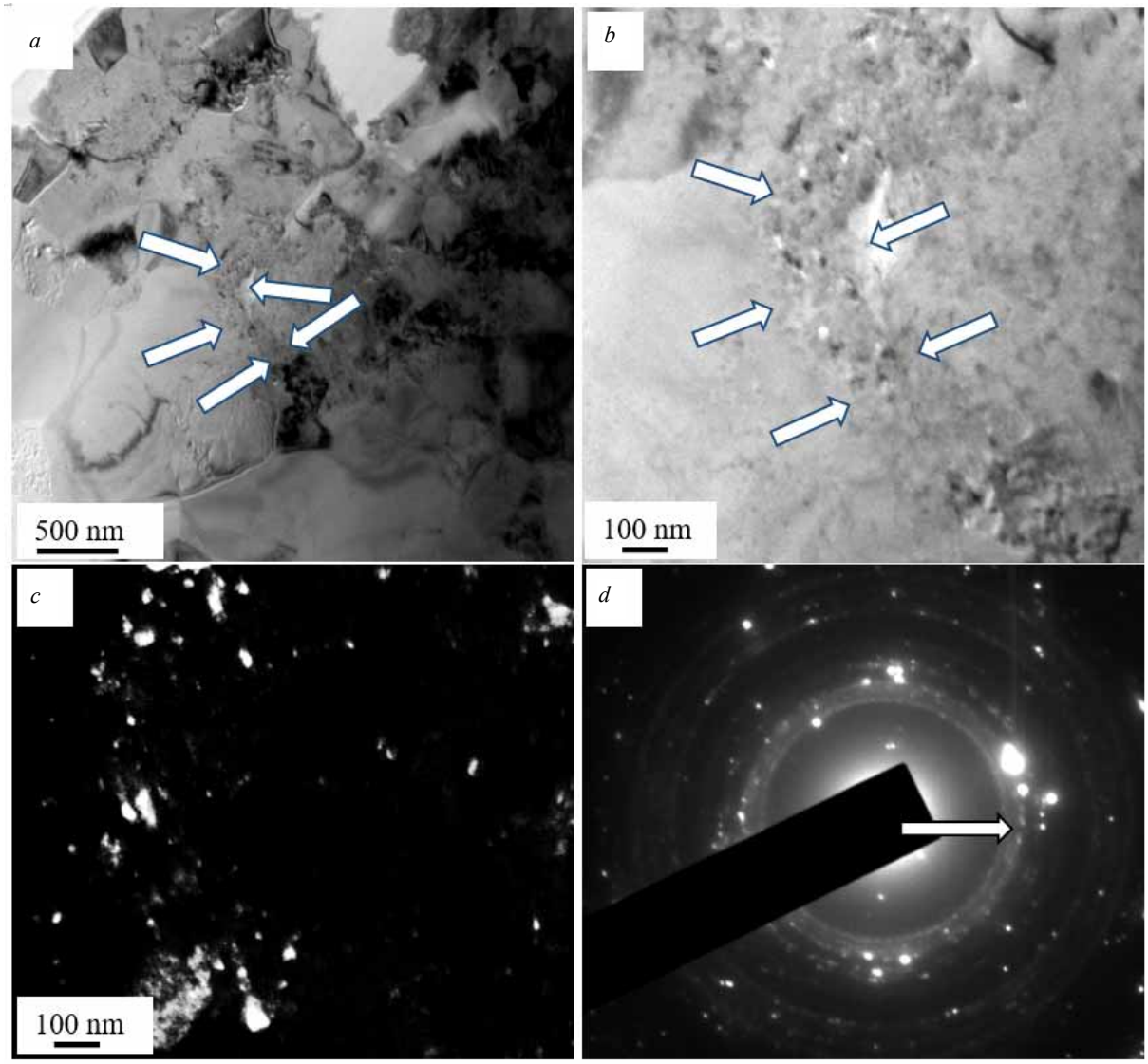

Fig. 4. Electron-microscopic image of the surface layer of technically pure aluminum grade A7, modified by nitriding (540 °C, 8 h) of a surface alloy formed by pulsed melting in a vacuum of the Al-Ti system (20 sputtering / irradiation cycles) with an electron beam with parameters 10 J / cm^2; 50 μs; 10 imp; film thickness of titanium in each cycle (0.5 μm): *a*, *b* – bright-field images; *c* – dark field obtained in the [200] AlN reflex; *d* – microelectron diffraction pattern. The arrows on fig. 4, *a*, *b* indicate aluminum nitride particles located along the boundaries of titanium aluminide; on fig. 4, *g* is the reflex in which the dark-field image was obtained

Рис. 4. Электронно-микроскопическое изображение поверхностного слоя технически чистого алюминия марки А7, модифицированного путем азотирования (540 °С, 8 ч) поверхностного сплава, сформированного импульсным плавлением в вакууме системы Al-Ti (20 циклов «напыления/облучения» электронным пучком с параметрами 10 Дж/см^2; 50 мкс; 10 имп.; толщина пленки титана в каждом цикле 0,5 мкм): *a*, *b* – светлопольные изображения; *c* – темное поле, полученное в рефлексе [200] AlN; *d* – микроэлектронограмма. Стрелками на рис. 4, *a*, *b* указаны частицы нитрида алюминия, расположенные вдоль границ алюминида титана; на рис. 4, *d* – рефлекс, в котором было получено темнопольное изображение

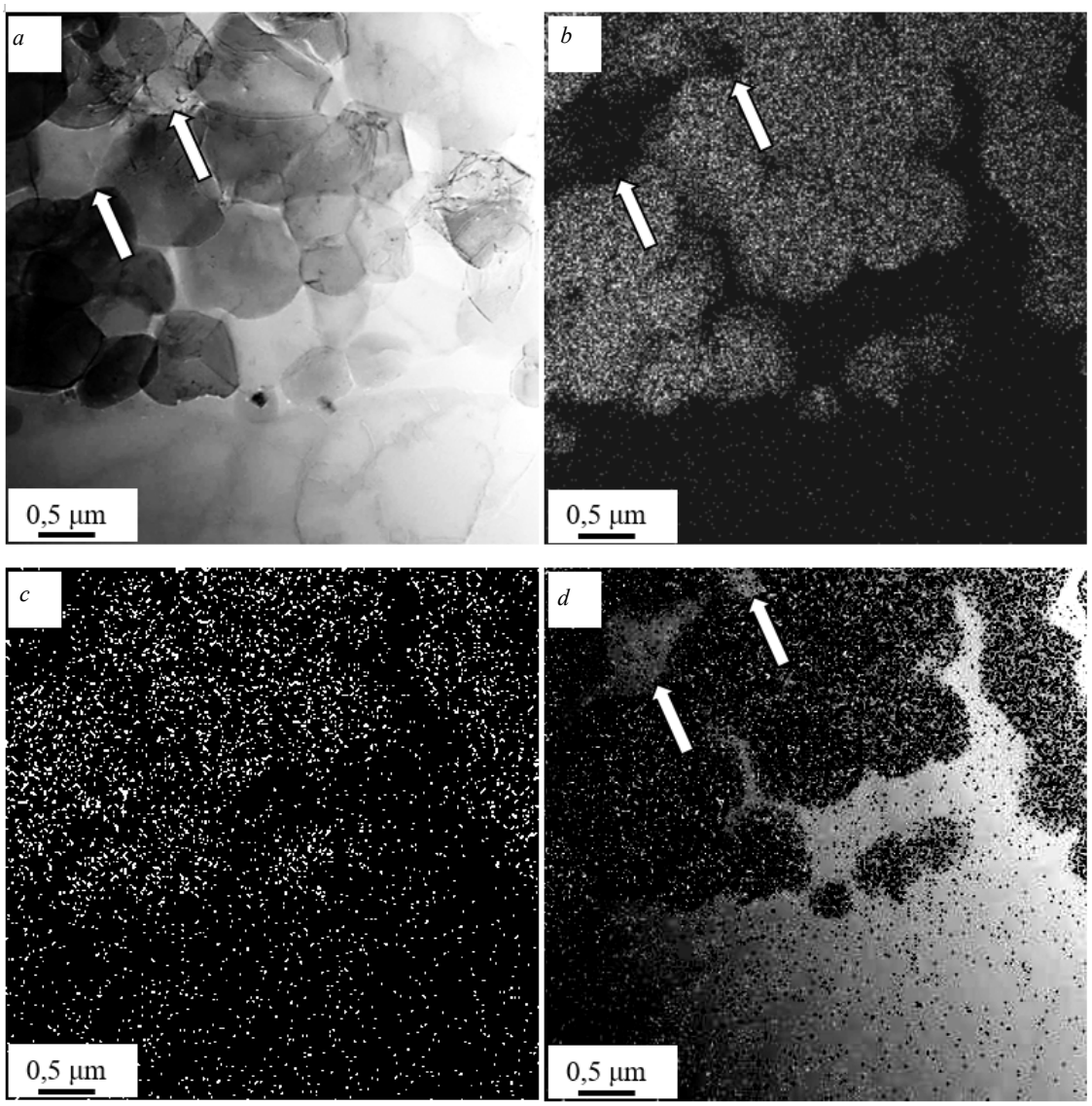

Fig. 5. Electron-microscopic image of the surface layer of technically pure aluminum grade A7 modified by nitriding (540 °C, 8 h) of a surface alloy formed by pulsed melting in a vacuum of the Al-Ti system (20 sputtering / irradiation cycles) with an electron beam with parameters 10 J / cm 2 ; 50 μ s; 10 imp.; film thickness of titanium in each cycle 0.5 μ m) (*a*); image of the foil part (*a*) obtained in the characteristic X-ray radiation of titanium atoms ($Ti_{K\alpha}$) (*b*) and nitrogen ($N_{K\alpha}$) (*c*); *d* – combined image of the foil part (*a*) obtained in the characteristic X-ray radiation of titanium atoms ($Ti_{K\alpha}$) and nitrogen ($N_{K\alpha}$); arrows indicate aluminum grains

Рис. 5. Электронно-микроскопическое изображение поверхностного слоя технически чистого алюминия марки А7, модифицированного путем азотирования (540 °С, 8 ч) поверхностного сплава, сформированного импульсным плавлением в вакууме системы Al-Ti (20 циклов «напыления/облучения» электронным пучком с параметрами 10 Дж/см^2; 50 мкс; 10 имп.; толщина пленки титана в каждом цикле 0,5 мкм) (*a*); изображение участка фольги (*a*), полученное в характеристическом рентгеновском излучении атомов титана ($Ti_{K\alpha}$) (*b*) и азота ($N_{K\alpha}$) (*c*); *d* – совмещенное изображение участка фольги (*a*), полученное в характеристическом рентгеновском излучении атомов титана ($Ti_{K\alpha}$) и азота ($N_{K\alpha}$). Стрелками указаны зерна алюминия

Conclusion. The analysis of binary charts of Al-N, Al-Ti and TIN systems conditions and isothermal section of the threefold AL-TIN system is made. It is shown that under equilibrium conditions in these systems formation of double and threefold compound including the MAX phases of Ti_2AlN и Ti_4AlN_3 structure is observed.

It is established that a complex method of electronic ion-plasma modifying of commercially pure aluminum of A7 brand by nitriding (540 ^{0}C, 8 hours) of the surface alloy formed by pulse melting in an Al-Ti system vacuum (20 cycles “dusting/radiation” an electron beam with the parameters of 10 J/cm^2; 50 microsec; 10 imp.; thickness of a titan film in each cycle equals 0.5 microns) leads to formation of a multiphase multi-element sub-micro nanocrystal surface layer up to 20 microns thick.

Mechanical (micro-hardness) and tribological (wear resistance and friction coefficient) properties of the formed surface layer drastically surpass the properties of initial commercially pure A7 aluminum.

Acknwledgements. The authors are grateful to E. A. Petrikova and O. S. Tolkachev for their active participation in the research of the modified material. The work was partially supported by RFBR grant (project № 19-08-00248).

Благодарности. Авторы выражают благодарность Е. А. Петриковой и О. С. Толкачеву за активное участие в проведении исследований модифицированного материала. Работа выполнена при частичной финансовой поддержке гранта РФФИ (проект № 19-08-00248).

References

1. Belov A. F., Benediktova G. P., Viskov A. S. *Stroyeniye i svoystva aviatsionnykh materialov* [Structure and properties of aviation materials]. Moscow, Metallurgiya Publ., 1989, 368 p.

2. Rakhmankulov M. M. *Metallurgiya strategicheskikh metallov i splavov* [Metallurgy of strategic metals and alloys]. Moscow, Teplotekhnik Publ., 2008, 504 p.

3. Kalachev B. A., Elagin V. I., Livanov V. A. *Metallovedeniye i termicheskaya obrabotka tsvetnykh metallov i splavov* [Metallurgy and heat treatment of non-ferrous metals and alloys]. Moscow, MISiS Publ., 2005, 432 p.

4. Beletskiy V. M., Krivov G. A. *Alyuminiyevyye splavy. Sostav. Svoystva, tekhnologiya, primeneniye* [Aluminum alloy. Composition, properties, technology, application]. Kiyev, KOMINTEKh Publ., 2005, 365 p.

5. Koval N. N., Ivanov Yu. F. *Elektronno-ionno-plazmennaya modifikatsiya poverkhnosti tsvetnykh metallov i splavov* [Electron-ion-plasma modification of the surface of non-ferrous metals and alloys].Tomsk, NTL Publ., 2016, 312 p.

6. Kovaly N. N., Ivanov Yu. F. *Evolyutsiya struktury poverkhnostnogo sloya stali. podvergnutoy elektronno-ionno-plazmennym metodam obrabotki* [Evolution of the structure of the surface layer of steel subjected to electron-ion-plasma treatment]. Tomsk, NTL Publ., 2016, 304 p.

7. Gribkov F. I. Grigoryev. B. A. Kalin V. A. *Perspektivnyye radiatsionno-puchkovyye tekhnologii obrabotki materialov* [Advanced radiation-beam technologies of materials processing]. Moscow, Kruglyy stol Publ., 2001, 528 p.

8. Kadyrzhanov K. K., Komarov F. F., Pogrebnyak A. D. *Ionno-luchevaya i ionno-plazmennaya modifikatsiya materialov* [Ion-beam and ion-plasma modification of materials]. Moscow, MGU Publ., 2005, 640 p.

9. Pout Dzh. M., Foti G., Dzhekobson D. K. *Modifikatsiya i legirovaniye poverkhnosti lazernymi. ionnymi i elektronnymi puchkami* [Modification and alloying of the surface with laser, ion and electron beams]. Moscow, Mashinostroyeniye Publ., 1987, 424 p.

10. Gromov V. E., Ivanov Yu. F. *Struktura, fazovyy sostav i svoystva titana posle kompleksnykh uprochnyayushchikh tekhnologiy* [Structure, phase composition and properties of titanium after complex hardening technologies]. Novokuznetsk, SibGIU Publ., 2015, 304 p.

11. Shulov V. A., Paykin A. G., Novikov A. S. *Silnotochnyye elektronnyye impulsnyye puchki dlya aviatsionnogo dvigatelestroyeniya* [Pulsed high-current electron beams for aircraft engines]. Moscow, Artek Publ., 2012.

12. Uglov V. V., Cherenda N. N., Anishchik V. M., Astashinskiy V. M., Kvasov N. T. *Modifikatsiya materialov kompressionnymi plazmennymi potokami* [Modification of structure and properties of eutectic silumin by electron-ion-plasma treatment]. Minsk, BGU Publ., 2013, 248 p.

13. Laskovnev A. P., Ivanov Yu. F., Petrikova E. A. *Modifikatsiya struktury i svoystv evtekticheskogo silumina elektronno-ionno-plazmennoy obrabotkoy* [Modification of structure and properties of eutectic silumin by electron-ion-plasma treatment]. Minsk, Belaruskaya Navuka Publ., 2013, 287 p.

14. *GOST 11069-2001. Alyuminiy pervichnyy. Marki. Mezhgosudarstvennyy sovet po standartizatsii. metrologii i sertifikatsii* [State Standard Primary aluminum. Brands. Interstate Council for standardization, Metrology and certification]. Minsk, 2001.

15. Lyakishev N. P. *Diagrammy sostoyaniya dvoynykh metallicheskikh system* [State diagrams of double metal systems]. Moscow, Mashinostroyeniye Pabl., 1996, Vol. 1, 992 p.

16. Lyakishev N. P. *Diagrammy sostoyaniya dvoynykh metallicheskikh system* [State diagrams of double metal systems]. Moscow, Mashinostroyeniye Pabl., 2001, Vol. 3, 872 p.

17. Lengauer W., Ettmayer P. The Crystal Structure of a New Phase in the Titanium-Nitrogen System. *J. Less-Common Met*. 1986. Vol. 120, P. 153–159.

18. Rogl P., Schuster J.C. Ti-B-N (Titanium – Boron – Nitrogen) in Phase Diagrams of Ternary Boron Nitride and Silicon Nitride Systems. *Materials Park, Ohio: Materials Informations Soc*. 1992. P. 103–106.

19. Lengauer W. The Crystal Structure of η-Ti_3N_{2-X}: An Additional New Phase in the Ti-N System. *J. Less-Common Met*. 1986, Vol. 125, P.127–134.

20. Durlu N., Gruber U., Pietzka M. A. Phases and Phase Equilibria in the Quaternary System Ti-Cu-Al-N at 850 °C. *Z. Metallkd*. 1997, Vol. 97, P. 390–400.

21. Procopio A. T., El-Raghy T., Barsoum M. W. Synthesis of Ti_4AlN_3 and Phase Equilibria in the Ti-Al-N System. *Metall. Mater. Trans*. 2000, Vol. 31A, P. 373–378.

22. Schuster J. C., Bauer J. The Ternary System Titanium-Aluminium-Nitrogen. *J. Solid State Chem*. 1984, Vol. 53, P. 260–265.

23. Schuster J. C., Bauer J., Nowotny H. Applications to Materials Science of Phase Diagrams and Crystal Structures in the Ternary Systems Transition Metal-Aluminium-Nitrogen. *Rev. Chim. Miner*. 1985, Vol. 22, P. 546–554.

24. Barsoum M. W., Ali M., El-Raghy T. Processing and Characterization of Ti_2AlC, Ti_2AlN and $Ti_2AlC_{0.5}N_{0.5}$. *Metall. Trans*. 2000, Vol. A 31A, P. 1857–1865.

25. Barsoum M. W. Rawn C. J., El-Raghy T., Procopio A. T., Porter W. D., Wang H., Hubbard C. R. Thermal Properties of Ti_4AlN_3. *J. Appl. Phys*. 2000, Vol. 87, P. 8407–8414.

26. Petrov I., Mojab E., Adibi F., Greene J. E., Hultman L., Sundgren J.-E. Interfacial Reactions in Epitaxial Al/$Ti_{1-x}Al_xN$ ($0 \le x \le 0.2$) Model Diffusion-Barrier Structure. *J. Vac. Sci. Technol*. 1993, Vol. A11, P. 11–17.

27. Tanaka Y., Guer T. M., Kelly M., Hagstrom S. B., Ikeda T. Strusture and Properties of $(Ti_{1-x}Al_x)N$ Films Prepared by Reactive Sputtering. *Thin Solid Films*. 1993, Vol. 228, P. 238–241.

28. Ikeda T., Satoh H. Phase Formation and Characterization of Hard Coatings in the Ti-Al-N System Prepared by the Cathodic Arc Ion Platting Method. *Thin Solid Films*. 1991, Vol. 195, P. 99–110.

29. Wu Z. L., Pope D. P., Vitek V. Ti_2NAl in $L1_2$ Al_3Ti-Base Alloys. *Metall. Mater. Trans*. 1995, Vol. A26, P. 521–524.

30. Nowotny H., Jeitschko W., Benesovsky F. Novel Complex Carbides and Nitrides and Their Relation to Phases of Hard Substances. *Planseeber. Pulvermetall*. 1964, Vol. 12, P. 31–43.

31. Mabuchi H., Tsuda H., Nakayama Y. Processing of TiAl-Ti_2AlN Composites and their Compressive Properties. *J. Mater. Res*. 1992, Vol. 7. P. 894–900.

32. Jeitschko W., Nowotny H., Benesovsky F. Ti_2AlN and Nitrogen Containing H-Phase. *Monatsh. Chem*. 1963, Vol. 94, P. 1198–1200.

33. Ivchenko V. I., Lesnaya M. I., Nemchenko V. F., Kosolapova T. Ya. Study of Preparation Conditions and Certain Physical Properties of the Ternary Compound TI_2AlN. *Poroshk. Metall*. 1976, No. 4, P. 60–63.

34. Ivchenko V. I., Kosolapova T. Ya. Investigation of Abrasive Properties of Ternary Compounda in the Systems Ti-Al-C and Ti-Al-N. *Poroshk. Metall.* 1976, No. 8, P. 56–59.

35. Farber L., Levin I., Barsoum M. W., El-Raghy T., Tzenov T. High-Resolution Transmission Electron Microscopy of Some $Ti_{n+1}AX_n$ Compounds (n = 1, 2; A = Al or Si; X = C or N). *J. Appl. Phys*. 1990, Vol. 86, P. 2540–2543.

36. Magnan J., Weatherly G. C., Cheynet M.-C. The Nitriding Behavior of Ti-Al Alloys at 1000 °C. *Metall. Mater. Trans*. *A*. 1999, Vol. 30A, P. 19–29.

37. Gamarnik M. Y., Barsoum M. W., El-Raghy T. Improved X-Ray Powder Diffraction Data for Ti_2AlN. *Powder Diffr*. 2000, Vol. 15, P. 241–242.

38. Barsoum M. W. The MN+1AXN phases: a newclass of solids; thermodinamically stable nanolaminates. *Prog. Solid St. Chem*. 2000, Vol. 28, P. 201–281.

39. Barsoum M. W., El-Raghy T., Radovic M. Ti_3SiC_2: a layered machinable ductile carbide. *Interceram*. 2000, Vol. 49, P. 226–233.

40. Kooi B. J. R., Poppen J., Carvalho N. J. M. Ti_3SiC_2: a damage tolerant ceramic studied with nanoindentations and transmission electron microscopy. *Acta Mater*. 2003, Vol. 51, P. 2859–2872.

41. Palmquist J.-P. Carbide and MAX-phase engineering by thin film synthesis. *Comprehensive Summaries of Uppsala. Dissertations from the Faculty of Science and Technology*. 2004, No. 930, 70 p.

42. Sun Z. M. Progress in research and development on MAX phases: a family of layered ternary Compounds. *International Materials Reviews.* 2011, Vol. 56, P. 143–167.

43. Khirsh P., Khovi A., Nikolson R. *Elektronnaya mikroskopiya tonkikh kristallov* [Electron microscopy of thin crystals]. Moscow, Mir Publ., 1968, 574 p.

44. Koneva N. A., Kozlov E. V. [The nature of substructure hardening]. *Izvestiya VUZov*. *Fizika.* 1982, No. 8, P. 3–14 (In Russ.).

45. Koneva N. A., Kozlov E. V., Trishkina L. I. [The long-range stress fields, curvature-torsion of the crystal lattice and the stage of plastic deformation. The Measurement methods and results]. *Novyye metody v fizike i mekhanike deformiruyemogo tverdogo tela. Sbornik trudov mezhdunarodnoy konferentsii*. Tomsk, TGU Publ., 1990, P. 83–93 (In Russ.).

46. Teplyakova L. A., Ignatenko L. N., Kasatkina N. F. [The Regularities of plastic deformation of steel with the structure of tempered martensite]. *Plasticheskaya deformatsiya splavov. Strukturno-neodnorodnyye materialy*. Tomsk, TGU Publ., 1987, P. 26–51 (In Russ.).

47. Ivanov Yu. F., Gromov V. E., Popova N. A. *Strukturno-fazovyye sostoyaniya i mekhanizmy uprochneniya deformirovannoy stali* [The structural-phase state and strengthening mechanisms of deformed steel]. Novokuznetsk, Poligrafist Publ., 2016, 510 p.

Библиографические ссылки

1. Белов А. Ф., Бенедиктова Г. П., Висков А. С. Строение и свойства авиационных материалов. М. : Металлургия, 1989. 368 с.

2. Рахманкулов М. М. Металлургия стратегических металлов и сплавов. М. : Теплотехник, 2008. 504 с.

3. Калачев Б. А., Елагин В. И., Ливанов В. А. Металловедение и термическая обработка цветных металлов и сплавов. М. : МИСиС, 2005. 432 с.

4. Белецкий В. М., Кривов Г. А. Алюминиевые сплавы. Состав, свойства, технология, применение. Киев : КОМИНТЕХ, 2005. 365 с.

5. Электронно-ионно-плазменная модификация поверхности цветных металлов и сплавов / под ред. Н. Н. Коваля, Ю. Ф. Иванова. Томск : НТЛ, 2016. 312 с.

6. Коваль Н. Н., Иванов Ю. Ф. Эволюция структуры поверхностного слоя стали, подвергнутой электронно-ионно-плазменным методам обработки. Томск : НТЛ, 2016. 304 с.

7. Грибков В. А., Григорьев Ф. И., Калин Б. А. Перспективные радиационно-пучковые технологии обработки материалов. М. : Круглый стол, 2001. 528 с.

8. Кадыржанов К. К., Комаров Ф. Ф., Погребняк А. Д. Ионно-лучевая и ионно-плазменная модификация материалов. М. : МГУ, 2005. 640 с.

9. Поут Дж. М., Фоти Г., Джекобсон Д. К. Модификация и легирование поверхности лазерными, ионными и электронными пучками. М. : Машиностроение, 1987. 424 с.

10. Громов В. Е., Иванов Ю. Ф. Структура, фазовый состав и свойства титана после комплексных упрочняющих технологий. Новокузнецк : СибГИУ, 2015. 304 с.

11. Шулов В. А., Пайкин А. Г., Новиков А. С. Сильноточные электронные импульсные пучки для авиационного двигателестроения. М. : Артек, 2012.

12. Модификация материалов компрессионными плазменными потоками / В. В. Углов [и др.]. Минск : БГУ, 2013. 248 с.

13. Модификация структуры и свойств эвтектического силумина электронно-ионно-плазменной обработкой / А. П. Ласковнев [и др.]. Минск : Беларус. Навука, 2013. 287 с.

14. ГОСТ 11069–2001. Алюминий первичный. Марки. Межгосударственный совет по стандартизации, метрологии и сертификации. Минск, 2001.

15. Лякишев Н. П. Диаграммы состояния двойных металлических систем : справ. В 3 т. М. : Машиностроение. 1996. Т. 1. С. 992.

16. Лякишев Н. П. Диаграммы состояния двойных металлических систем : справ. В 3 т. М. : Машиностроение. 1996. Т. 3. С. 872.

17. Lengauer W., Ettmayer P. The Crystal Structure of a New Phase in the Titanium-Nitrogen System // J. Less-Common Met. 1986. Vol. 120. P. 153–159.

18. Rogl P., Schuster J. C. Ti-B-N (Titanium – Boron – Nitrogen) in Phase Diagrams of Ternary Boron Nitride and Silicon Nitride Systems // Materials Park, Ohio: Materials Informations Soc. 1992. P. 103–106.

19. Lengauer W. The Crystal Structure of η-Ti_3N_{2-X}: An Additional New Phase in the Ti-N System // J. Less-Common Met. 1986. Vol. 125. P. 127–134.

20. Durlu N., Gruber U., Pietzka M. A. Phases and Phase Equilibria in the Quaternary System Ti-Cu-Al-N at 850 °C // Z. Metallkd. 1997. Vol. 97. P. 390–400.

21. Procopio A. T., El-Raghy T., Barsoum M. W. Synthesis of Ti_4AlN_3 and Phase Equilibria in the Ti-Al-N System // Metall. Mater. Trans. 2000.Vol. 31A. P. 373–378.

22. Schuster J. C., Bauer, J. The Ternary System Titanium-Aluminium-Nitrogen // J. Solid State Chem. 1984. Vol. 53. P. 260–265.

23. Schuster J. C., Bauer J., Nowotny H. Applications to Materials Science of Phase Diagrams and Crystal Structures in the Ternary Systems Transition Metal-Aluminium-Nitrogen // Rev. Chim. Miner. 1985. Vol. 22. P. 546–554.

24. Barsoum M. W., Ali M., El-Raghy T. Processing and Characterization of Ti_2AlC, Ti_2AlN and $Ti_2AlC_{0.5}N_{0.5}$ // Metall. Trans. 2000. Vol. A 31A. P. 1857–1865.

25. Barsoum M. W. Rawn C. J., El-Raghy T., Procopio A. T., Porter W. D., Wang H., Hubbard C.R. Thermal Properties of Ti_4AlN_3 // J. Appl. Phys. 2000. Vol. 87. P. 8407–8414.

26. Interfacial Reactions in Epitaxial Al/$Ti_{1-x}Al_xN$ ($0 \le x \le 0.2$) Model Diffusion-Barrier Structure / I. Petrov [et al.] // J. Vac. Sci. Technol. 1993. Vol. A11. P. 11–17.

27. Strusture and Properties of ($Ti_{1-x}Al_x$)N Films Prepared by Reactive Sputtering / Y. Tanaka [et al.] // Thin Solid Films. 1993. Vol. 228. P. 238–241.

28. Ikeda T., Satoh H. Phase Formation and Characterization of Hard Coatings in the Ti-Al-N System Prepared by the Cathodic Arc Ion Platting Method // Thin Solid Films. 1991. Vol. 195. P. 99–110.

29. Wu Z. L., Pope D. P., Vitek V. Ti_2NAl in $L1_2$ Al_3Ti-Base Alloys // Metall. Mater. Trans. 1995. Vol. A26. P. 521–524.

30. Nowotny H., Jeitschko W., Benesovsky F. Novel Complex Carbides and Nitrides and Their Relation to Phases of Hard Substances // Planseeber. Pulvermetall. 1964. Vol. 12. P. 31–43.

31. Mabuchi H., Tsuda H., Nakayama Y. Processing of TiAl-Ti_2AlN Composites and their Compressive Properties // J. Mater. Res. 1992. Vol. 7. P. 894–900.

32. Jeitschko W., Nowotny H., Benesovsky F. Ti_2AlN and Nitrogen Containing H-Phase // Monatsh. Chem. 1963. Vol. 94. P. 1198–1200.

33. Ivchenko V. I., Lesnaya M. I., Nemchenko V. F., Kosolapova T. Ya. Study of Preparation Conditions and Certain Physical Properties of the Ternary Compound TI_2AlN // Poroshk. Metall. 1976. No. 4. P. 60–63.

34. Ivchenko V. I., Kosolapova T. Ya. Investigation of Abrasive Properties of Ternary Compounda in the Systems Ti-Al-C and Ti-Al-N // Poroshk. Metall. 1976. No. 8. P. 56–59.

35. High-Resolution Transmission Electron Microscopy of Some $Ti_{n+1}AX_n$ Compounds (n = 1, 2; A = Al or Si; X = C or N) / L. Farber [et al.] // J. Appl. Phys. 1990. Vol. 86. P. 2540–2543.

36. Magnan J., Weatherly G. C., Cheynet M.-C. The Nitriding Behavior of Ti-Al Alloys at 1000°C // Metall. Mater. Trans. A. 1999. Vol. 30A. P. 19–29.

37. Gamarnik M. Y., Barsoum M. W., El-Raghy T. Improved X-Ray Powder Diffraction Data for Ti2AlN // Powder Diffr. 2000. Vol. 1. P. 241–242.

38. Barsoum M. W. The MN+1AXN phases: a new-class of solids; thermodinamically stable nanolaminates // Prog. Solid St. Chem. 2000. Vol. 28. P. 201–281.

39. Barsoum V. W., El-Raghy T., Radovic M. Ti_3SiC_2: a layered machinable ductile carbide // Interceram. 2000. Vol. 49. P. 226–233.

40. Kooi B. J., Poppen R. J., Carvalho N. J. M. Ti_3SiC_2: a damage tolerant ceramic studied with nanoindentations and transmission electron microscopy // Acta Mater. 2003. Vol. 51. P. 2859–2872.

41. Palmquist J-P. Carbide and MAX-phase engineering by thin film synthesis // Comprehensive Summaries of Uppsala. Dissertations from the Faculty of Science and Technology. 2004. No. 930. 70 p.

42. Sun Z. M. Progress in research and development on MAX phases: a family of layered ternary Compounds // International Materials Reviews. 2011. Vol. 56, No. 3. P. 143–167.

43. Хирш П., Хови А., Николсон Р. Электронная микроскопия тонких кристаллов. М. : Мир, 1968. 574 с.

44. Конева Н. А., Козлов Э. В. Природа субструктурного упрочнения // Известия вузов. Физика. 1982. № 8. С. 3–14.

45. Конева Н. А., Козлов Э. В., Тришкина Л. И. Дальнодействующие поля напряжений, кривизна-кручение кристаллической решетки и стадии пластической деформации. Методы измерений и результаты // Новые методы в физике и механике деформируемого твердого тела : сб. тр. междунар. конф. Томск : ТГУ, 1990. С. 83–93.

46. Теплякова Л. А., Игнатенко Л. Н., Касаткина Н. Ф. Закономерности пластической деформации

стали со структурой отпущенного мартенсита // Пластическая деформация сплавов. Структурно-неоднородные материалы. Томск : ТГУ, 1987. С. 26–51.

47. Иванов Ю. Ф., Громов В. Е., Попова Н. А. Структурно-фазовые состояния и механизмы упрочнения деформированной стали. Новокузнецк : Полиграфист, 2016. 510 с.

Ivanov Yurii Fedorovich – Dr. Sc., assistant professor, senior scientist, Institute of High Current Electronics of the SB RAS. E-mail: yufi55@mail.ru.

Eresko Sergei Pavlovich – Dr. Sc., professor, Corresponding member of Academy of Higher Education of the Russian Federation, honored inventor of the Russian Federation, Department of Fundamentals of machine design, Institute of Mechanical Engineering and Mechatronics, Reshetnev Siberian State University of Science and Technology. E-mail: ereskosp@mail.sibsau.ru, eresko07@mail.ru.

Ahmadeev Yurii Halatovych – Cand. Sc., senior researcher, Institute of High Current Electronics of the SB RAS. E-mail: ahmadeev@opee.hcei.tsc.ru.

Lopatin Ilya Viktorovich – Cand. Sc., scientist, Institute of High Current Electronics of the SB RAS. E-mail: lopatin@opeee.hcei.tsc.ru.

Klopotov Anatoly Anatolyevich – Dr. Sc., professor, Tomsk State University of Architecture and Building. E-mail: klopotovaa@tsuab.ru.

Иванов Юрий Федорович – доктор физико-математических наук, доцент, главный научный сотрудник лаборатории плазменной эмиссионной электроники, Институт сильноточной электроники СО РАН. E-mail: yufi55@mail.ru .

Ереско Сергей Павлович – доктор технических наук, заслуженный изобретатель Российской Федерации, член-корреспондент Академии наук ВШ РФ, профессор, профессор кафедры основ конструирования машин, Сибирский государственный университет науки и технологий имени академика М. Ф. Решетнева. E-mail: eresko07@mail.ru.

Ахмадеев Юрий Халяфович – кандидат технических наук, старший научный сотрудник лаборатории плазменной эмиссионной электроники, Институт сильноточной электроники СО РАН. E-mail: ahmadeev@opee.hcei.tsc.ru.

Лопатин Илья Викторович – кандидат технических наук, научный сотрудник лаборатории плазменной эмиссионной электроники, Институт сильноточной электроники СО РАН. E-mail: lopatin@opeee.hcei.tsc.ru.

Клопотов Анатолий Анатольевич – доктор физико-математических наук, профессор, Томский государственного архитектурно-строительного университета. E-mail: klopotovaa@tsuab.ru.

UDC 543.428
Doi: 10.31772/2587-6066-2019-20-1-99-105

For citation: Igumenov A. Yu., Parshin A. S., Andryushchenko T. A. [Factor analysis of inelastic electron scattering cross section spectra of iron monosilicide FeSi]. *Siberian Journal of Science and Technology.* 2019, Vol. 20, No. 1, P. 99–105. Doi: 10.31772/2587-6066-2019-20-1-99-105

Для цитирования: Игуменов А. Ю., Паршин А. С., Андрющенко Т. А. Факторный анализ спектров сечения неупругого рассеяния электронов силицида FeSi // Сибирский журнал науки и технологий. 2019. Т. 20, № 1. С. 99–105. Doi: 10.31772/2587-6066-2019-20-1-99-105

FACTOR ANALYSIS OF INELASTIC ELECTRON SCATTERING CROSS SECTION SPECTRA OF IRON MONOSILICIDE FeSi

A. Yu. Igumenov*, A. S. Parshin, T. A. Andryushchenko

Reshetnev Siberian State University of Science and Technology
31, Krasnoyarsky Rabochy Av., Krasnoyarsk, 660037, Russian Federation
*E-mail: igumenovau@mail.ru

The inelastic electron scattering cross-section spectra of FeSi silicide were calculated from the experimental reflected electron energy loss spectra as the product of the average inelastic mean free path and the differential cross section of the inelastic electron scattering. To inelastic electron scattering cross-section spectra study, factor analysis was used. This method allowed us to quantitatively separate the surface and bulk contributions to the spectra, and determine the energy of the bulk plasmon more accurately than it is possible using traditional methods.

Inelastic electron scattering cross-section spectra (Kλ-spectra) are the products of the average inelastic mean free path λ and the differential inelastic scattering cross-section K (E_0, $E_0 – E$), where E_0 and E are the energies of the primary and reflected electrons, respectively. The advantage of inelastic electron scattering cross section spectroscopy is that, unlike the reflected electron energy loss spectra, the Kλ-spectra exclude losses due to multiple excitations, and the intensities are determined in absolute units. These spectra are also more sensitive to changes in the energy of the primary electrons and the angle of emission. Inelastic electron scattering cross-section spectroscopy allows to determine the element composition with much greater accuracy than the traditional method of reflected electron energy loss spectroscopy.

In this work, factor analysis is used to study the inelastic electron scattering cross section spectra of the FeSi silicide. This method allowed to solve the actual problem of separating spectra into contributions of a different origin, quantify them and determine the energies of a bulk plasmon more accurately compared with traditional methods. The study of electron energy loss processes by isolating contributions of different origin in the inelastic electron scattering cross section spectra is one of the urgent problems of electron spectroscopy, which can be used to assess the effect of surface excitations in REELS, XPS and AES.

Keywords: inelastic electron scattering cross-section spectra, electron energy loss spectroscopy, factor analysis, iron silicides.

ФАКТОРНЫЙ АНАЛИЗ СПЕКТРОВ СЕЧЕНИЯ НЕУПРУГОГО РАССЕЯНИЯ ЭЛЕКТРОНОВ СИЛИЦИДА FeSi

А. Ю. Игуменов*, А. С. Паршин, Т. А. Андрющенко

Сибирский государственный университет науки и технологий имени академика М. Ф. Решетнева
Российская Федерация, 660037, г. Красноярск, просп. им. газ. «Красноярский рабочий», 31
*E-mail: igumenovau@mail.ru

Спектры сечения неупругого рассеяния электронов силицида FeSi рассчитаны из экспериментальных спектров характеристических потерь энергии отраженных электронов как зависимости произведения средней длины неупругого пробега и дифференциального сечения неупругого рассеяния электронов от потерь энергии электронов. Для исследования спектров сечения неупругого рассеяния электронов применен факторный анализ. Этот метод позволил разделить вклады поверхностной и объемной природы в спектры, количественно их оценить и определить энергию объемного плазмона более точно по сравнению с традиционным методом спектроскопии потерь энергии отраженных электронов.

Спектры сечения неупругого рассеяния электронов (Kλ-спектры) представляют собой произведения средней длины неупругого пробега электронов λ и дифференциального сечения неупругого рассеяния K(E_0, $E_0 – E$),

где E_0 и E – энергии первичных и отраженных электронов, соответственно. Преимущество спектроскопии сечения неупругого рассеяния электронов заключается в том, что, в отличие от спектров характеристических потерь энергии отраженных электронов, в Kλ-спектрах исключены потери на многократные возбуждения, а интенсивности определяются в абсолютных единицах. Эти спектры также более чувствительны к изменению энергии первичных электронов и угла эмиссии. Спектроскопия сечения неупругого рассеяния электронов позволяет определять элементный состав со значительно большей точностью, чем традиционный метод спектроскопии потерь энергии отраженных электронов.

В данной работе для исследования спектров сечения неупругого рассеяния электронов силицида FeSi применен факторный анализ. Этот метод позволил решить актуальную задачу разделения спектров на вклады разной природы, количественно их оценить и определить энергии объемного плазмона более точно по сравнению с традиционными методами. Исследование процессов потерь энергии электронов путем выделения из спектров сечения неупругого рассеяния вкладов разной природы является одной из актуальных задач электронной спектроскопии, которая может быть использована для оценки влияния поверхностных возбуждений на спектры характеристических потерь энергии электронов, рентгеновские фотоэлектронные спектры и Оже-электронные спектры.

Ключевые слова: спектроскопии сечения неупругого рассеяния электронов, спектроскопия характеристических потерь энергии электронов, факторный анализ, силициды железа.

Introduction. The successful development of nanoelectronics, nanophotonics and spintronics devices requires compliance with a number of requirements to the methods of structures synthesis on the basis of silicon and the transitional metals and to the methods of their analysis. For such structures research the greatest distribution gained such electronic spectroscopy methods as Auger-electron Spectroscopy (AES), X-ray photoelectron spectroscopy (XPS) and reflected electron energy loss spectroscopy (REELS). Fe-Si system, is of research interest from the fundamental and applied points of view [1]. However, the elemental analysis of iron silicides using XPS and REELS methods is difficult because the values of photoelectron and plasmon peaks energies for silicides with different structure are close to each other [2].

Inelastic electron scattering cross-section spectra ($K\lambda$-spectra [3]) are the products of the inelastic mean free path λ and the differential cross section for inelastic electron scattering K (E_0, $E_0 - E$), where E_0 and E are the energies of the primary and reflected electrons, respectively. The advantage of inelastic electron scattering cross section spectroscopy is that, unlike the reflected electron energy loss spectra, the $K\lambda$-spectra exclude losses due to multiple excitations, and the intensities are determined in absolute units. These spectra are also more sensitive to changes in the primary electron energy and the emission angle [4–6]. Inelastic electron scattering cross-section spectroscopy allows to determine the element composition with much greater accuracy than the traditional method of reflected electron energy loss spectroscopy [6].

In this work, factor analysis (FA) is used to study the inelastic electron scattering cross section spectra of FeSi silicide. This method allowed to solve the actual problem of spectra separating into different origin contributions, quantify them and determine the energies of a bulk plasmon more accurately compared with traditional methods. The study of electron energy loss processes by isolating contributions of different origin in the inelastic electron scattering cross section spectra is one of the urgent problems of electron spectroscopy, which can be used to assess the effect of surface excitations in REELS, XPS and AES [1–15].

Previously [16–21], we studied Si, Fe and $FeSi_2$, Fe_5Si_3 silicides using an author's technique of spectra decomposition into energy loss peaks.

Experimental technique. The iron silicide FeSi is made by alloying of iron and silicon mixture in atomic ratio 1×1 under high vacuum conditions. The mixture was kept at melting temperature for 15 min. then the alloy was crushed and annealed for 15 min. 1 mm thick washers were cut out from bulk samples and after grinding the spectroscopical research was conducted.

Photoelectron spectra and integrated reflected electron energy loss spectra measurements were carried out on the ultra-high vacuum photoelectron spectrometer SPECS (Germany) at angles between the incidence and detecting electrons and the sample surface normal respectively $\alpha_i = 59°$, $\alpha_d = 0°$. The spectrometer is completed with a spherical energy analyser PHOIBOS MCD9, an *X*-ray tube with the double anode as a source of X-ray radiation, an electronic Microfocus EK-12-M gun (STAIB Instruments) for exaltation of electron energy loss spectra. Surface contamination, protective and oxide layers were removed using argon ions Ar^+ etching (accelerating voltage 2.5 kV, ionic current 15 mA) with the raster ion PU-IQE-12/38 (SPECS) gun immediately in the spectrometer camera before electron spectra registration. The completeness of oxygen and contamination removal was controlled with *X*-ray photoelectron spectra (XPS).

From the experimental reflected electron energy loss spectra using the QUASES^{TM} XS REELS software package (Quantitative Analysis of Surfaces by Electron Spectroscopy cross section determined by REELS) [22], according to the algorithm offered in [23] the inelastic electron scattering cross section spectra – the product of the inelastic mean free path λ and the differential cross section for inelastic electron scattering $K(E_0, E_0 - E)$ are received. Inelastic electron scattering cross section spectra are defined by electron energy loss T probability at single scattering on the inelastic mean free path λ, related to an energy unit. These spectra maxima values determine probabilities of single energy loss on the surface or bulk exitations. Due to absolute values of energy loss intensity

inelastic electron scattering cross-section spectra, in comparison with traditional reflected electron energy loss spectra, allow to carry out comparison and the analysis of different spectra not only on peaks energies, but also on their intensity.

Factor analysis is the statistical method widely used in electron spectroscopy [10]. Application of factor analysis is possible for spectra representing as a linear combination of components which concentration changes during any process. This method is relevant for AES where simple decomposition of spectrum lines on components is impossible as in Auger spectra, besides chemical shift there is also a change of a lines form [11–13]. In electronic Auger spectroscopy FA is used for study the processes of layer-by-layer etching of thin films [12], the processes of adsorption [13; 14].

In [15] XPS method was applied to study chemical changes induced by He^+ bunch influence in a natural crystal of pyrite (FeS_2). It is shown that the routine analysis use together with FA can be a powerful method of elements identification when changes in bond energy and broadening happen simultaneously. Due to the routine analysis and FA of XPS spectra combination the complete signal Fe 2p XPS was analysed.

As noted in [15], the advantage of FA, in comparison with the XPS routine analysis, is that whole set of spectra is used (usually in XPS each spectrum is separately analysed) and FA does not need the preliminary knowledge of XPS peaks form and position, that allows to get these data using only experimental data. On the other hand, the FA disadvantages is noise component existence and nonideality of a components form, in comparison with XPS results.

The inelastic electron scattering cross section spectra received at various primary electron energy or the angles of falling/detecting electrons represent sequences of data in which the relative contributions of surface and bulk loss change systematically depending on the experimental conditions. In [5] the factor analysis is used as a way of inelastic electron scattering cross section spectra decomposition into two contributions (bulk and surface) in Si and SiO_2 research.

Factor analysis is carried out as follows. The matrix which columns are intensity values of energy loss at various primary electron energies is formed. At the first stage the selection of principal factors (components), which provide a spectrum in total, close to the initial, is made. Later, two columns with the greatest intensity – principal abstract factors (principal components) are allocated from the received matrix. Further, these factors conversion is carried out by multiplication to a matrix of rotation R (target rotation):

$$R = \begin{bmatrix} \cos\varphi & \sin\varphi \\ -\sin\varphi & \cos\varphi \end{bmatrix}.$$

Target rotation transforms abstract factors to physical ones by achievement of predetermined criterion of a peak form and the maximum provision. In [5] the Lorentzian peak form corresponding to bulk plasmon exaltation is taken as such criterion and by means of φ angle change the component form, close to the Lorentz peak having a maximum at bulk plasmon energy, is reached. Then the most accurate form of the surface was reached by additional rotation. Further reconstruction of the initial spectrum as a two factors linear combination is carried out.

In this work, unlike [5], the peaks form was not selected close to standard Lorentzian peaks, but to Tougaard peaks form. [24]:

$$\lambda K = \frac{BT}{\left(C - T^2\right)^2 + DT^2}.$$

The B, C, D parameters are adjustable and for each element have defined values [24]. Parameter B defines peak intensity, parameter C defines the position (influences to position, but does not correspond to it in an explicit form), parameter D defines the width and indirectly influences peak position and intensity. The Tougaard functions (universal classes of inelastic electron scattering cross-section) are used for the description of inelastic electron scattering cross-section spectra.

The three-parametrical Tougaard function was transformed to:

$$\lambda K = \frac{BT}{\left(\left(T_p\left(-T_p + \sqrt{4T_p^2 + D}\right)\right) - T^2\right)^2 + DT^2},$$

where T_p parameter corresponds to the position of a peak maximum in absolute units.

In fig. 1, 2 the model spectrum which consists of 2 unsolved peaks is presented.

A set of such spectra at a different peaks amplitude ratio was considered.

By means of the factor analysis 1 and 2 peaks factors are allocated from initial spectra, they coincide with initial peaks. For an example factors at rotation at different angles (fig. 3, 4) are given.

Experimental results. In fig. 5, 6 FeSi silicide spectra at primary electron energies 300 and 3000 eV are presented. The main maximum energy in FeSi inelastic electron scattering cross-section spectra is close to the bulk plasmon energy [16; 25] and possesses the value 20.1 ± 0.6 eV. The low-energy $K\lambda$-spectra area has a weak peak with energy about 3 eV.

These spectra are approximated with the sum of two factors. When receiving actual factors the angle was selected so that the bulk factor was well approximated by the Tougaard peak, similarly for the surface factor, but its form remained irregular, that means the existence of several unsolved peaks of the different origin. In [16; 17] the decomposition of these spectra into the elemental components described by the Tougaard functions was carried out. The method [16–21] allows to allocate a higher quantity of peaks in $K\lambda$-spectra than the factor analysis, including separation the surface origin peaks in low-energy spectrum area.

The bulk and surface factors ratio is close to $\sqrt{2}$ that corresponds to the classic plasmon theory for the free electron gas [26].

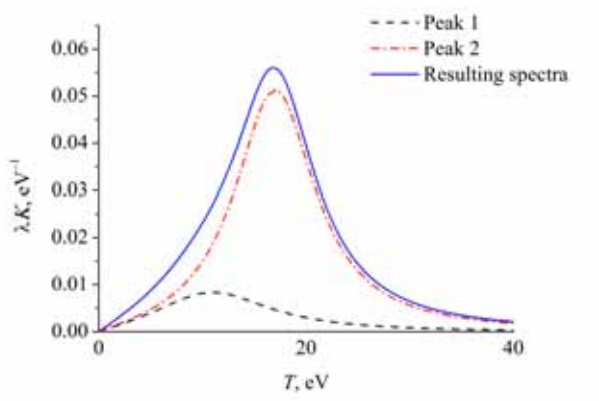

Fig. 1. Model spectrum, peak 1 to peak 2 amplitude ratio 0.2

Рис. 1. Модельный спектр, соотношение амплитуд 1 и 2 пиков 0,2

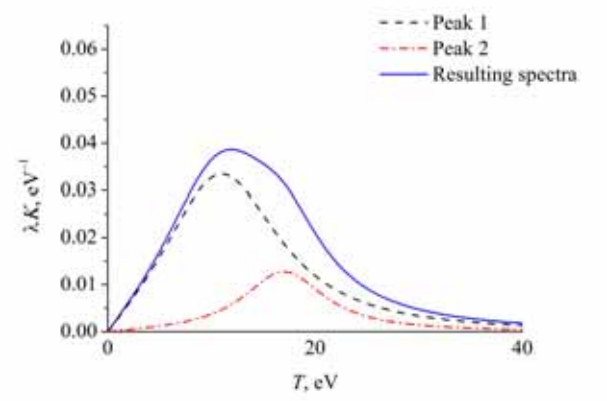

Fig. 2. Model spectrum, peak 1 to peak 2 amplitude ratio 2.6

Рис. 2. Модельный спектр, соотношение амплитуд 1 и 2 пиков 2,6

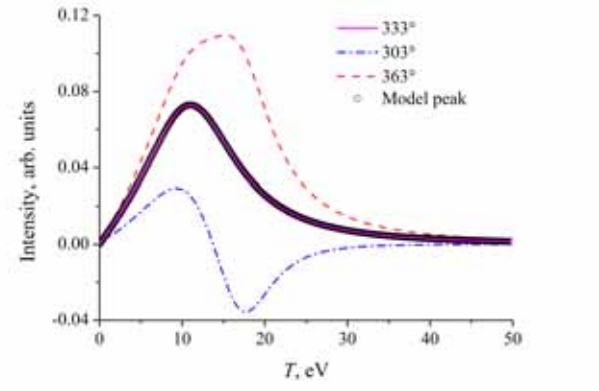

Fig. 3. The peak 1 factor at different angles of rotation

Рис. 3. Фактор пика 1 при разных углах вращения

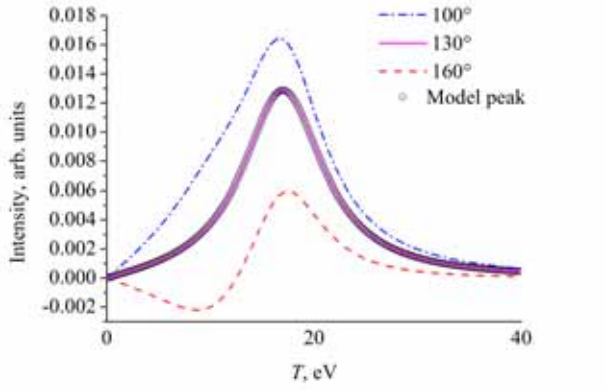

Fig. 4. The peak 2 factor at different angles of rotation

Рис. 4. Фактор пика 2 при разных углах вращения

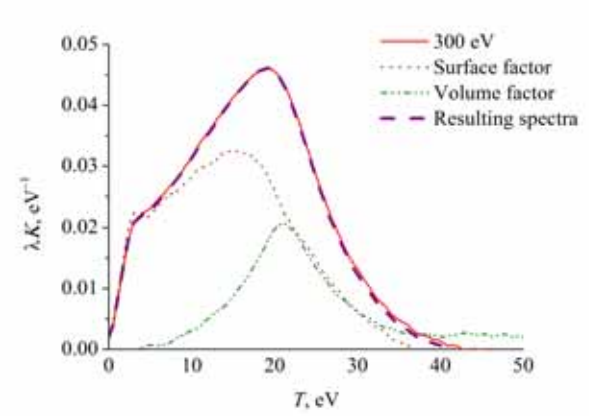

Fig. 5. FeSi spectra at E_0 = 300 eV

Рис. 5. Спектры FeSi при E_0 = 300 эВ

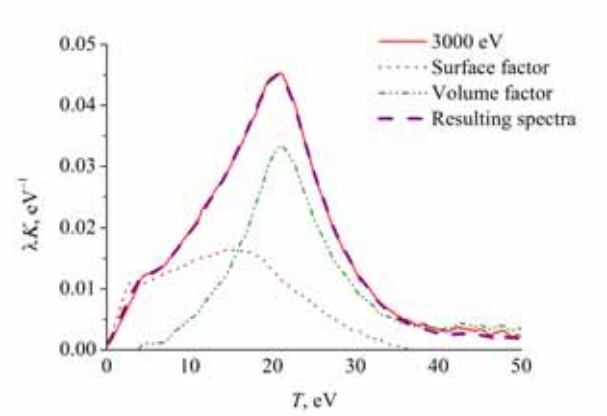

Fig. 6. FeSi spectra at E_0 = 3000 eV

Рис. 6. Спектры FeSi при E_0 = 3000 эВ

In fig. 7 the primary electron energy dependences of factor amplitudes are presented

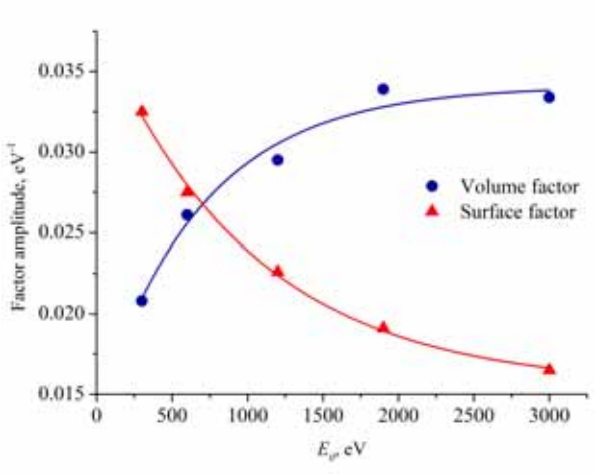

Fig. 7. Primary electron energy dependence of factor amplitudes

Рис. 7. Зависимость амплитуд факторов от энергии первичных электронов

With increasing of primary electron energy the bulk factor amplitude increases, and the surface factor amplitude decreases. This regularity is a confirmation of its origin.

The factor analysis, along with the method of *Kλ*-spectra decomposition on the elemental components described by the Tougaard functions [16–21] can be used for the quantitative assessment of the change of various origin contributions to inelastic electron scattering cross-section spectra.

Conclusion. The applicability of the factor analysis for bulk and surface contributions division in FeSi inelastic electron scattering cross-section spectra has been proved.

The surface and bulk origin contribution separation and quantitative assessment in FeSi inelastic electron scattering cross-section spectra with factor analysis were carried out. Factor amplitudes dependences on primary electron energy reflect their surface and bulk origin.

References

1. Galkin N. G., Polyarnyi V. O., Gouralnik A. S. Self-organization of β-FeSi2 islands on Si(111)7×7. *Thin Solid Films.* 2004, Vol. 464–465, P. 199–203.

2. Ohtsu N., Oku M., Satoh K. Dependence of core-level XPS spectra on iron silicide phase. *Applied Surface Science*. 2013, Vol. 264, P. 219–224.

3. Tougaard S., Chorkendorff. I. Differential inelastic electron scattering cross sections from experimental reflection electron-energy-loss spectra: Application to background removal in electron spectroscopy. *Physical Review B.* 1987, No. 35, 13, P. 6570–6577.

4. Jin H., Yoshikawa H., Iwai H. [et al.] Inelastic Scattering Cross Section of Si Determined from Angular Dependent Reflection Electron Energy Loss Spectra. *Journal of Surface Analysis*. 2009, Vol. 15, No. 3, P. 321–324.

5. Jin H., Shinotsuka H., Yoshikawa H. et al. Measurement of optical constants of Si and SiO_2 from reflection electron energy loss spectra using factor analysis method. *Journal of applied physics*. 2010, No. 107, P. 083709, 1–11.

6. Jin H., Shinotsuka H., Yoshikawa H. et al. Evaluation of robustness to surface conditions of the target factor analysis method for determining the dielectric function from reflection electron energy loss spectra: Application to GaAs. *Surface and Interface Analysis*. 2013, Vol. 45, No. 6, P. 985–992.

7. Gergely G. Elastic backscattering of electrons: determination of physical parameters of electron transport processes by elastic peak electron spectroscopy. *Progress in Surface Science.* 2002, No. 71, P. 31–88.

8. Orosz G. T. Gergely G., Gurban S. et al. Experimental determination of electron inelastic scattering cross-sections in Si, Ge and III–V semiconductors. *Vacuum*. 2003, No. 71, P. 147–152.

9. Tougaard S. Quantitative Analysis of the Inelastic Background in Surface Electron Spectroscopy. *Surface and Interface Analysis*. 1988, No. 11, P. 453–472.

10. Andryushechkin B. V., El'cov K. N., Klimov A. N. [Experimental techniques, methods and methods of work with Halogens on the surface of metals]. *Trudy instituta obshhej fiziki*. Moscow, Nauka Publ., 2003, Vol. 59, P. 23–44 (In Russ.).

11. Malinowski E. R., Howery D. G. Factor Analysis in Chemistry. New York, Wiley, 1980, 207 p.

12. Gaarenstroom S. W. Application of Auger lineshapes and factor-analysis to characterize a metal-ceramic interfacial reaction. *Journal of Vacuum Science and Technology*. 1982, Vol. 20, P. 458–461.

13. Steffen J., Hofmann S. Use of factor analysis with O KLL Auger spectra to distinguish chemisorption and oxide formation on Ni. *Surface Science*. 1988, Vol. 202, P. L607–L611.

14. Hofmann S., Steffen J. Factor analysis and superposition of Auger electron spectra applied to room temperature oxidation of Ni and $NiCr_{21}Fe_{12}$. *Surface And Interface Analysis*. 1989, Vol. 14, P. 59–65.

15. Ruano S., Gustavo D., Pomiro F. Surface chemical reactions induced on pyrite by ion bombardment. *Surface Science*. 2018, Vol. 667, P. 138–147.

16. Parshin A. S., Igumenov A. Yu., Mikhlin Yu. L. et al. [Reflection electron energy loss spectroscopy of iron monosilicide]. *Izvestiya Vysshikh Uchebnykh Zavedenii. Fizika*. 2016, Vol. 59, No. 10, P. 82–86 (In Russ.).

17. Parshin A. S., Igumenov A. Yu., Mikhlin Yu. L. et al. Reflection electron energy loss spectroscopy of structures based on silicon and transition metals. *IOP Conference Series: Materials Science and Engineering. XX International Scientific Conference Reshetnev Readings*-2016. 2017, Vol. 255, P. 012019, 1–7. Doi:10.1088/1757-899X/255/1/012019.

18. Parshin A. S., Igumenov A. Yu., Mikhlin Yu. L. et al. Comparative Analysis of the Characteristic Electron Energy-Loss Spectra and Inelastic Scattering Cross-Section Spectra in Fe. *Physics of the Solid State*. 2016, Vol. 58, No. 5, P. 908–914.

19. Parshin A. S., Igumenov A. Yu., Mikhlin Yu. L. et al. Electron Spectroscopy of Iron Disilicide. *Technical Physic*. 2016, Vol. 61, No. 9, P. 1418–1422.

20. Parshin A. S., Igumenov A. Yu., Mikhlin Yu. L. et al. On the Fine Structure of Spectra of the Inelastic-Electron-Scattering Cross Section and the Si Surface Parameter. *Semiconductors*. 2015, Vol. 49, No. 4, P. 423–427.

21. Igumenov A. Yu., Parshin A. S., Mikhlin Yu. L. et al. [Raschet veroyatnosti generacii poverhnostnyh vozbuzhdenij ehlektronami, otrazhennymi ot poverhnosti Si]. *Vestnik SibGAU*. 2014, No. 4 (56), P. 230–235 (In Russ.).

22. Tougaard S. QUASES – Software packages to characterize surface nano-structures by analysis of electron spectra. Available at: http:// www.quases.com (accessed: 15.10.2018).

23. Tougaard S., Chorkendorff. I. Differential inelastic electron scattering cross sections from experimental reflection electron-energy-loss spectra: Application to background removal in electron spectroscopy. *Physical Review B*. 1987, No. 35, 13, P. 6570–6577.

24. Tougaard S. Universality Classes of Inelastic Electron Scattering Cross-sections. *Surface And Interface Analysis*. 1997, No. 25, P. 137–154.

25. Lifshits V. G., Lunyakov Yu. V. *Spektry KhPEE poverkhnostnykh faz na kremnii* [EELS spectra of surface phases on silicon]. Vladivostok, Dal'nauka Publ., 2004, 315 p.

26. Raether H. Surface Plasmons on Smooth and Rough Surfaces and on Gratings. Berlin, Springer-Verlag, 1988, 140 p.

Библиографические ссылки

1. Galkin N. G., Polyarnyi V. O., Gouralnik A. S. Self-organization of β-FeSi2 islands on Si(111)7×7 // Thin Solid Films. 2004. Vol. 464–465. P. 199–203.

2. Ohtsu N., Oku M., Satoh K. Dependence of core-level XPS spectra on iron silicide phase // Applied Surface Science. 2013. Vol. 264. P. 219–224.

3. Tougaard S., Chorkendorff. I. Differential inelastic electron scattering cross sections from experimental reflection electron-energy-loss spectra: Application to background removal in electron spectroscopy // Physical Review B. 1987. Vol. 35, No. 13. P. 6570–6577.

4. Inelastic Scattering Cross Section of Si Determined from Angular Dependent Reflection Electron Energy Loss Spectra / H. Jin, H. Yoshikawa, H. Iwai [et al.] // Journal of Surface Analysis. 2009. Vol. 15, No. 3. P. 321–324.

5. Measurement of optical constants of Si and SiO_2 from reflection electron energy loss spectra using factor analysis method / H. Jin, H. Shinotsuka, H. Yoshikawa [et al.] // Journal of applied physics. 2010. No. 107. P. 083709, 1–11.

6. Evaluation of robustness to surface conditions of the target factor analysis method for determining the dielectric function from reflection electron energy loss spectra: Application to GaAs / H. Jin, H. Shinotsuka, H. Yoshikawa [et al.] // Surface and Interface Analysis. 2013. Vol. 45, No. 6. P. 985–992.

7. Gergely G. Elastic backscattering of electrons: determination of physical parameters of electron transport processes by elastic peak electron spectroscopy // Progress in Surface Science. 2002. No. 71. P. 31–88.

8. Experimental determination of electron inelastic scattering cross-sections in Si, Ge and III–V semiconductors / Orosz G. T., Gergely G., Gurban S. [et al.] // Vacuum. 2003. No. 71. P. 147–152.

9. Tougaard S. Quantitative Analysis of the Inelastic Background in Surface Electron Spectroscopy // Surface and Interface Analysis. 1988. No. 11. P. 453–472.

10. Андрюшечкин Б. В., Ельцов К. Н., Климов А. Н. Экспериментальная техника, методы и методика работы с галогенами на поверхности металлов // Труды института общей физики. М. : Наука, 2003. Т. 59. С. 23–44.

11. Malinowski E. R., Howery D. G. Factor Analysis in Chemistry. New York, Wiley, 1980. 207 c.

12. Gaarenstroom S. W. Application of Auger lineshapes and factor-analysis to characterize a metal-ceramic interfacial reaction // Journal of Vacuum Science and Technology. 1982. Vol. 20. P. 458–461.

13. Steffen J., Hofmann S. Use of factor analysis with O KLL Auger spectra to distinguish chemisorption and oxide formation on Ni // Surface Science. 1988. Vol. 202. P. L607–L611.

14. Hofmann S., Steffen J. Factor analysis and superposition of Auger electron spectra applied to room temperature oxidation of Ni and $NiCr_{21}Fe_{12}$ // Surface And Interface Analysis. 1989. Vol. 14. P. 59–65.

15. Ruano S., Gustavo D., Pomiro F. Surface chemical reactions induced on pyrite by ion bombardment // Surface Science. 2018. Vol. 667. P. 138–147.

16. Спектроскопия потерь энергии отраженных электронов моносилицида железа / А. С. Паршин, А. Ю. Игуменов, Ю. Л. Михлин [и др.] // Известия высших учебных заведений. Физика. 2016. Т. 59, № 10. С. 82–86.

17. Reflection electron energy loss spectroscopy of structures based on silicon and transition metals / A. S. Parshin, A. Yu. Igumenov, Yu. L. Mikhlin [et al.] // IOP Conference Series: Materials Science and Engineering. XX International Scientific Conference Reshetnev Readings-2016. 2017. Vol. 255. P. 012019, 1–7. Doi:10.1088/1757-899X/255/1/012019.

18. Сравнительный анализ спектров характеристических потерь энергии электронов и спектров сечения неупругого рассеяния в Fe / А. С. Паршин, А. Ю. Игуменов, Ю. Л. Михлин [и др.] // Физика твердого тела. 2016. Т. 58, вып. 5. С. 881–887.

19. Исследование дисилицида железа методами электронной спектроскопии / А. С. Паршин, А. Ю. Игуменов, Ю. Л. Михлин [и др.] // Журнал технической физики. 2016. Т. 86, вып. 9. С. 136–140.

20. Тонкая структура спектров сечения неупругого рассеяния электронов и поверхностный параметр Si / А. С. Паршин, А. Ю. Игуменов, Ю. Л. Михлин [и др.] // Физика и техника полупроводников. 2015. Т. 49, вып. 4. С. 435–439.

21. Расчет вероятности генерации поверхностных возбуждений электронами, отраженными от поверхности Si / А. Ю. Игуменов, А. С. Паршин, Ю. Л. Мих-

лин [и др.] // Вестник СибГАУ. 2014. № 4 (56). С. 230–235.

22. Tougaard S. QUASES – Software packages to characterize surface nano-structures by analysis of electron spectra [Электронный ресурс]. URL: http://www.quases.com (дата обращения: 15.10.2018).

23. Tougaard S., Chorkendorff. I. Differential inelastic electron scattering cross sections from experimental reflection electron-energy-loss spectra: Application to background removal in electron spectroscopy // Physical Review B. 1987. No. 35, 13. P. 6570–6577.

24. Tougaard S. Universality Classes of Inelastic Electron Scattering Cross-sections // Surface And Interface Analysis. 1997. No. 25. P. 137–154.

25. Лифшиц В. Г., Луняков Ю. В. Спектры ХПЭЭ поверхностных фаз на кремнии. Владивосток : Дальнаука, 2004. 315 с.

26. Raether H. Surface Plasmons on Smooth and Rough Surfaces and on Gratings. Berlin : Springer-Verlag, 1988. 140 p.

Igumenov Aleksandr Yurievich – Cand. Sc., Associate Professor; Reshetnev Siberian State University of Science and Technology. E-mail: igumenovau@mail.ru.

Parshin Anatoly Sergeevich – Dr. Sc., Associate Professor, Head of the Technical Physics Department; Reshetnev Siberian State University of Science and Technology. E-mail: aparshin@sibsau.ru.

Andryushchenko Tatyana Aleksandrovna – 3rd year student; Reshetnev Siberian State University of Science and Technology. E-mail: tanya.andryuchshenko@mail.ru.

Игуменов Александр Юрьевич – кандидат физико-математических наук, доцент; Сибирский государственный университет науки и технологий имени академика М. Ф. Решетнева. E-mail: igumenovau@mail.ru.

Паршин Анатолий Сергеевич – доктор физико-математических наук, доцент, заведующий кафедрой технической физики; Сибирский государственный университет науки и технологий имени академика М. Ф. Решетнева. E-mail: aparshin@sibsau.ru.

Андрющенко Татьяна Александровна – студент 3 курса; Сибирский государственный университет науки и технологий имени академика М. Ф. Решетнева. E-mail: tanya.andryuchshenko@mail.ru.

UDC 620.192
Doi: 10.31772/2587-6066-2019-20-1-106-111

For citation: Larchenko A. G., Filippenko N. G., Livshits A. V. [Mathematical modeling of the technological process of improving the quality of polymeric products of machine-building purposes]. *Siberian Journal of Science and Technology*. 2019, Vol. 20, No. 1, P. 106–111. Doi: 10.31772/2587-6066-2019-20-1-106-111

Для цитирования: Ларченко А. Г., Филиппенко Н. Г., Лившиц А. В. Математическое моделирование технологического процесса повышения качества полимерных изделий машиностроительного назначения // Сибирский журнал науки и технологий. 2019. Т. 20, № 1. С. 106–111. Doi: 10.31772/2587-6066-2019-20-1-106-111

MATHEMATICAL MODELING OF THE TECHNOLOGICAL PROCESS OF IMPROVING THE QUALITY OF POLYMERIC PRODUCTS OF MACHINE-BUILDING PURPOSES

A. G. Larchenko*, N. G. Filippenko, A. V. Livshits

Irkutsk State Transport University
15, Chernyshevsky St., Irkutsk, 664074, Russian Federation
*E-mail: Larchenkoa@inbox.ru

In this scientific work, a method of controlling high-frequency products from polymeric composite materials is considered. The authors of the work present the rationale for choosing a method of high-frequency diagnostics as the most suitable for non-destructive testing of products from polymeric materials of machine-building and rocket-space purposes. In the presented article, the primary task of creating and studying a mathematical model of the effect of high-frequency radiation on a polymer product, including those with a "metallic inclusion" defect, has been stated and solved. In addition, the work presents the calculations of diagnostic parameters using the mathematical model developed during the study. The calculation of the dynamics of heating the product and the temperature distribution during the control process is presented. The results of the calculation of specific power are described, the dependence of the instantaneous power consumption on the warm-up time is found. In the study based on a mathematical model, the Aleo-Diagnost software package was developed and registered, which is directly intended to ensure the functioning of the diagnostic devices and the investigation of the monitoring process. In addition, the developed complex allows solving a number of such practical problems as the calculation of the operating voltage depending on the geometrical parameters of the product and the determination of the value of energy consumed for monitoring the product for a specified period of time. This stage was necessary, as the consumed energy is the main output parameter of the diagnosis. In addition, the value of energy consumed is taken as the basis for the organization of the process of non-destructive testing in the automated mode. The solution of the tasks in this work has significantly reduced the cost of preparation of diagnostic operations, as well as improve the quality of control of products on an industrial scale at the stages of manufacture, operation and during repair work. The article also presents practical results, conclusions.

Keywords: control of high frequency currents, device for products diagnosing, polymer products, automated control system, diagnosing products of complex configuration, mathematical model of the diagnostic process, software, non-destructive testing.

МАТЕМАТИЧЕСКОЕ МОДЕЛИРОВАНИЕ ТЕХНОЛОГИЧЕСКОГО ПРОЦЕССА ПОВЫШЕНИЯ КАЧЕСТВА ПОЛИМЕРНЫХ ИЗДЕЛИЙ МАШИНОСТРОИТЕЛЬНОГО НАЗНАЧЕНИЯ

А. Г. Ларченко*, Н. Г. Филиппенко, А. В. Лившиц

Иркутский государственный университет путей сообщения
Российская Федерация, 664074, Иркутск, ул. Чернышевского, 15
*E-mail: Larchenkoa@inbox.ru

Рассматривается метод контроля изделий из полимерных композиционных материалов токами высокой частоты. Приводится обоснование выбора метода высокочастотного диагностирования как наиболее подходящего для проведения неразрушающего контроля изделий из полимерных материалов машиностроительного и ракетно-космического назначения. Поставлена и решена первостепенная задача создания и исследования математической модели воздействия высокочастотного излучения на полимерное изделие, в том числе с дефектом типа «металлическое включение». Приведены расчеты параметров диагностирования с использованием разработанной в ходе исследования математической модели. Представлен расчет динамики разогрева изделия и распределение температуры при осуществлении процесса контроля. Описаны результаты расчета удельной мощности, найдена зависимость мгновенной потребляемой мощности от времени разогрева. На базе математической модели разработан и зарегистрирован программный комплекс Aleo-Diagnost, который непо-

средственно предназначен для обеспечения функционирования устройств диагностирования и исследования процесса контроля. Разработанный комплекс позволяет решать ряд таких практических проблем, как расчет рабочего напряжения в зависимости от геометрических параметров изделия и определение значения потребляемой энергии на контроль изделия за заданный промежуток времени. Данный этап являлся необходимым, так как потребляемая энергия является основным выходным параметром диагностирования. Значение потребляемой энергии принимается за основу при организации процесса неразрушающего контроля в автоматизированном режиме. Решение поставленных задач в данной работе позволило значительно снизить себестоимость подготовки операций диагностирования, а также повысить качество контроля изделий в промышленных масштабах на стадиях изготовления, эксплуатации и в ходе ремонтных работ. В статье приведены практические результаты, сделаны выводы.

Ключевые слова: контроль токами высокой частоты, устройство диагностирования изделий, полимерные изделия, система автоматизированного управления, диагностирование изделий сложной конфигурации, математическая модель процесса диагностики, программное обеспечение, неразрушающий контроль.

Introduction. Intensive development of modern science and technology demands the development and use of structural materials with special physic-mechanical characteristics. In this regard polymeric composite materials got great prospects for application in various branches of mechanical engineering and the rocket industry. With the increasing volume of polymeric products and increased performance requirements, the problems of materials quality improvement and reduction of manufacture costs have become relevant [1–6]. The main means in the solution of the problem of manufactured products quality improvement at various stages of life cycle is the use of non-destructive monitoring. One of such ways of monitoring is the high-frequency method (HF) of diagnosing implemented in industrial conditions on the basis of the UZP 2500 device [7–9]. This method is based on local defects identification mainly in products from polymeric, composites by the impact of an external electric field on the studied object, and further amplitude intensity synthesis of the complex of output, operated diagnostics parameters emergence. HF method allows to carry out high precision monitoring without mechanical influence, to define a type of defect, to restore physic-mechanical properties of a product [10].

Main problems. Research tasks statement. It should be noted that in modern production process a wide range of products and details of complex spatial shape applied in mechanical engineering and space industry creates particular difficulties in the course of diagnosing using the high-frequency radiation method. The conducted theoretical and pilot research results presented in works [11–15] confirm that for the process of complex configuration products monitoring it is necessary to select the mode of high-frequency diagnosing each time, to develop rather complex design devices (electrodes) and the equipment. Taking into account the complexity of industrial equipment manufacture, difficulty of equipment setup and also the selection of diagnostics modes for polymer products, it is obvious that the development and practical use of mathematical model operation of monitoring process, and implementation of the software on the basis of the designed model will allow to reduce considerably the cost of preparation for diagnostic operations and also to increase the quality of monitoring of polymeric composites products on an industrial scale. Proceeding from the aforesaid during the research the primary tasks of the development and research of a mathematical model of high-frequency radiation impact on a polymeric product, including with "metallic inclusion" defect type and also the development of the accompanying software for testing, setting and ensuring diagnostic devices operation were set.

Mathematical model of high-frequency radiation impact on a polymeric product. The mathematical model in the research is necessary for calculation of key parameters of the monitoring process of complex configuration machine-building products both in the manual, and in the automated mode. The calculation was carried out for a sample from 8 mm thickness polyamide-610 material with 30 mm diameter with "metallic inclusion" defect type. The defect of 1 mm thickness, of 4 mm^2 is simulated between two polyamide plates of 3 mm and 4 mm thickness. When designing a mathematical model, the studied sample was considered as a set of three areas: the first area – the polyamide without a defect, the second area – the polyamide located over the defect, the third area – the polyamide located under the defect. The scheme for the studied sample is shown in fig. 1.

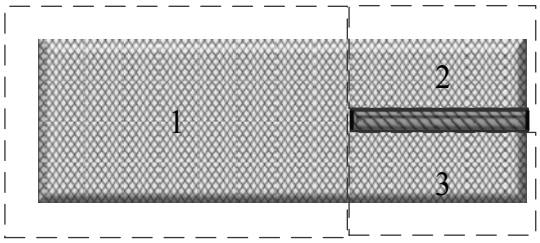

Fig. 1. Scheme of the simulated sample with a defect type "metallic inclusion"

Рис. 1. Схема смоделированного образца с дефектом типа «металлическое включение»

To perform the given tasks there was also a need for the development of high-frequency impact technological scheme shown in fig. 2, which is a set of electrodes, a variable quantity of heat insulators and a product to be heated with the defect.

Taking into account the presented high-frequency impact technological scheme, the calculation of dynamics of warming up in each area and temperature distribution in a multilayered plate are described by a set of equations of transient heat conduction [1; 5]. The area warming up without a metal plate is described by a set of equations (1), and the dynamics of increase in temperature of

areas with metal inclusion is characterized by a set of equations (2).

$$\begin{cases} \dfrac{\partial T_1}{\partial \tau} = \dfrac{\lambda_1}{c_{p_1}(T_1)\rho_1} \cdot \dfrac{\partial^2 T_1}{\partial x^2}; \\ \dfrac{\partial T_2}{\partial \tau} = \dfrac{\lambda_2}{c_{p_2}(T_2)\rho_2} \cdot \dfrac{\partial^2 T_2}{\partial x^2}; \\ \dfrac{\partial T_3}{\partial \tau} = \dfrac{\lambda_3}{c_{p_3}(T_3)\rho_3} \cdot \dfrac{\partial^2 T_3}{\partial x^2} + \dfrac{p_3(\tau)}{c_{p_3}(T_3)\rho_3}; \\ \dfrac{\partial T_4}{\partial \tau} = \dfrac{\lambda_4}{c_{p_4}(T_4)\rho_4} \cdot \dfrac{\partial^2 T_4}{\partial x^2}; \\ \dfrac{\partial T_5}{\partial \tau} = \dfrac{\lambda_5}{c_{p_5}(T_5)\rho_5} \cdot \dfrac{\partial^2 T_5}{\partial x^2}; \end{cases} \quad (1)$$

$$\begin{cases} \dfrac{\partial T_{i_1}}{\partial \tau} = \dfrac{\lambda_{i_1}}{c_{p_{i_1}}(T_{i_1})\rho_{i_1}} \cdot \dfrac{\partial^2 T_{i_1}}{\partial x^2}; \\ \dfrac{\partial T_{i_2}}{\partial \tau} = \dfrac{\lambda_{i_2}}{c_{p_{i2}}(T_{i_2})\rho_{i_2}} \cdot \dfrac{\partial^2 T_{i_2}}{\partial x^2}; \\ \dfrac{\partial T_{i_3}}{\partial \tau} = \dfrac{\lambda_{i_3}}{c_{p_{i3}}(\text{м}_{i_3})\rho_{i_3}} \cdot \dfrac{\partial^2 T_{i_3}}{\partial x^2} + \dfrac{p_{i_3}(\tau)}{c_{p_3}(T_{i_3})\rho_{i_3}}; \\ \dfrac{\partial T_{i_4}}{\partial \tau} = \dfrac{\lambda_{i_4}}{c_{p_{i4}}(T_{i_4})\rho_{i\,4}} \cdot \dfrac{\partial^2 T_{i_4}}{\partial x^2}; \end{cases} \quad (2)$$

where for the second area $i_1 = 12$; $i_2 = 11$; $i_3 = 10$; $i_4 = 9$; for the third area $i_1 = 6$; $i_2 = 7$; $i_3 = 8$; $i_4 = 9$; T_j – local temperature of a layer, C°; x – current thickness of a layer, mm; λ_j – thermal conductivity, W / (m · K); c_{pj} – specific heat, KJ / (kg · K); ρ_j – material density, Pa; p_j – specific power of an internal source of heat of W/m^3; j – layer number: 1, 5, 6, 12 – electrodes; 2, 4, 7, 11 – insulators; 3, 8, 10 – polymer; 9 – metal inclusion.

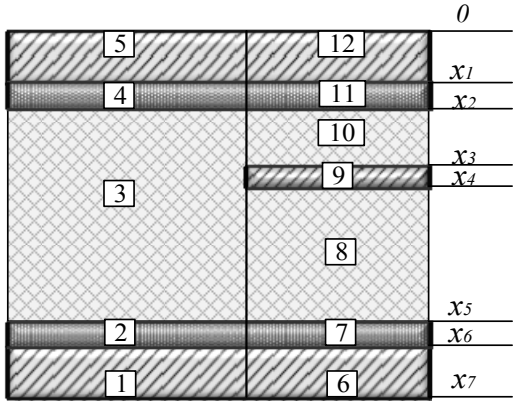

Fig. 2. Technological scheme of high-frequency impact on a product with a defect of the type "metallic inclusion": *1*, *5*, *6*, *12* – electrodes; *2*, *4*, *7*, *11* – insulators; *3*, *8*, *10* – polymer; *9* – metal inclusion

Рис. 2. Технологическая схема высокочастотного воздействия на изделие с дефектом типа «металлическое включение»: *1*, *5*, *6*, *12* – электроды; *2*, *4*, *7*, *11* – изоляторы; *3*, *8*, *10* – полимер; *9* – металлическое включение

Boundary conditions on external borders of electrodes correspond:

$$-\lambda \frac{\partial T_i}{\partial x}\Big|_{x=x_i} = \alpha_i \Delta T_i; (i = 5, 1, 12, 6), \quad (3)$$

where α_i – heat exchange coefficient; ΔT_i – difference of surface temperatures of a body and surrounding medium.

Referring to rather low heating temperatures of the studied polymeric products at implementation of diagnosing and high dynamics of a warming up, heat exchange with its surrounding medium when monitoring the first and single products can be considered negligibly small:

$$-\lambda \frac{\partial T_i}{\partial x}\Big|_{x=x_i} = 0 \quad (4)$$

On borders of layers heat fluxes and temperatures are equal:

$$T_i = T_{i+1}; (j = 1\ldots4; 6\ldots11); \quad (5)$$

$$\lambda_j \frac{\partial T_j}{\partial x} = \lambda_{j+1} \frac{\partial T_{j+1}}{\partial x}; \ (j = 2\ldots4; 6\ldots11); \quad (6)$$

The specific power of P_l is other than zero only for polymer

$$P_l \neq 0; \ (l = 3, 8, 10); \quad (7)$$

The carried out research calculations with the created mathematical model use showed that the sample is heated non-uniformly, the required temperature on areas with metal inclusion is reached in 25 seconds. The analysis of the received results allows to draw a conclusion on a possibility of mathematical model use for calculation of necessary diagnosing time which excess will lead to the material melting and, therefore, to product rejection. The following necessary research phase was finding of the instantaneous power consumption dependence on the heating time $P_{\text{мпм}}(t)$ in each area which chart is presented in fig. 3.

The received dependences of specific power on temperature $P_{\text{мпм1}}(t)$, $P_{\text{мпм2}}(t)$, $P_{\text{мпм3}}(t)$ were approximated in the form of a polynomial function and used when determining the energy spent monitoring a sample with the defect type "metallic inclusion":

$$Э_{\text{потреб}} = \int_0^{25} P_{\text{мпм}}(t) \cdot dt. \quad (8)$$

Compliance check of the model with actual diagnosing processes showed that when monitoring samples of brand 610 polyamide of 8 mm thickness and with a 15 mm radius, the time is 111 sec., and the heating time of the same sizes sample with the defect type "metallic inclusion" of 4 mm^3 in 25 seconds, the deviations on heating time from the pilot research make no more than 2 % that confirms the mathematical model correctness. At the same time the power consumption of a standard sample is 1.3 W · h, and a sample with the defect – 0.35 W · h [1; 9; 12; 13].

On the basis of the given research it is possible to draw a conclusion that the more the amount of metal inclusion in a polymer, the less energy and time is spent on monitoring object heating. The analysis of the results received by means of the created mathematical model allowed to reveal the additional controlled parameter hav-

ing informational content – the consumed energy. Besides, the obtained data confirm the pilot studies presented in works [1; 8].

For the use of a high-frequency control method and diagnosing process control it is necessary to provide a fixed level of power impact when monitoring different materials and products of various configuration. The presented mathematical model allows not only to determine the voltage necessary for specific power control preservation but also provides the opportunity for electrothermal equipment input data determination at automated control of high-frequency diagnosing process, differing in the established by mathematical dependence of operating voltage supply on the form and sizes of the controlled product [1; 4].

The Aleo-Diagnost software package. Calculations of productive parameters diagnosing were carried out for the particular sample of a specific form and size. The instantaneous power consumption directly depends on two components – the volume of a monitoring object and specific power. For implementation of the developed mathematical model of various forms and sizes products monitoring it is necessary to keep a condition of the dependence of the instantaneous power consumption invariance on time. For adaptation of calculations of diagnosing process necessary parameters with the high-frequency radiation method, the Aleo-Diagnost software was developed and registered [1]. The package interface implemented in the programming language C++ is shown in fig. 4.

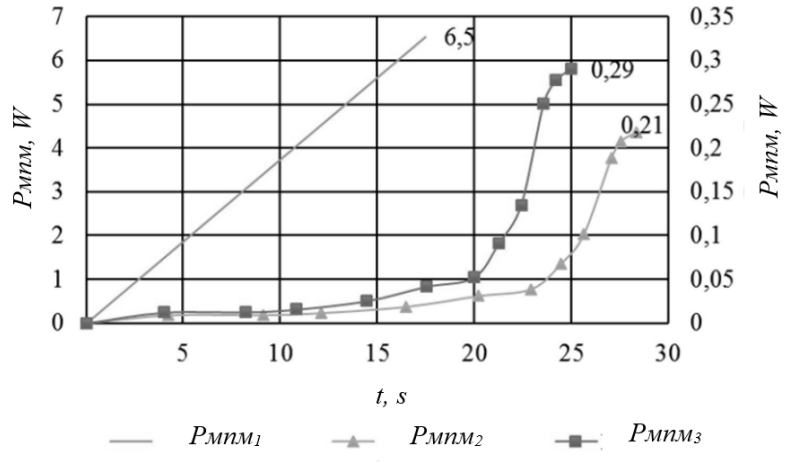

Fig. 3. The dependence of the instantaneous power consumption in the areas of polyamide 610 from the heating time

Рис. 3. Зависимость мгновенной потребляемой мощности на участках полиамида 610 от времени разогрева

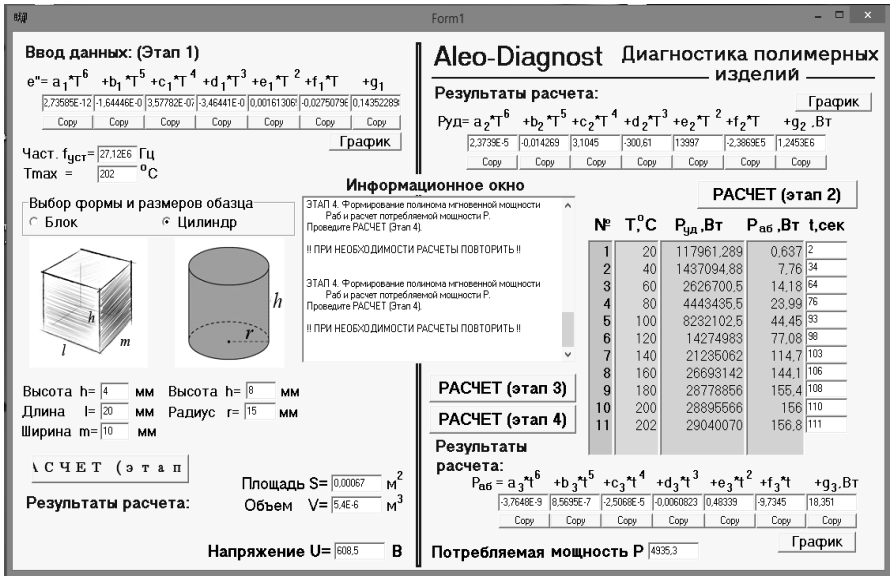

Fig. 4. Interface of the Aleo-Diagnost software package

Рис. 4. Интерфейс программного комплекса Aleo-Diagnost

The executable file contains the main libraries, forms of input and output. Calculation is conducted in 4 stages. The process of calculations with recommendations and explanations on the corresponding stages is displayed in "Information window".

When calculating the heating time the Aleo-HFH software package version 2.0 [5; 15] is used. After completion of calculations of products from polyamide materials heating time the software package displays key parameters of calculation for descriptive reasons in the form of tables with the intermediate values of specific and instantaneous power consumption depending on temperature and the time of heating at high-frequency radiation impact. The software package has an opportunity to send calculation results to the text file for their convenient transfer in the approximation module. For reduction of the obtained tabular data to a polynomial form a convenient to use program-approximator is installed in the package allowing to obtain coefficients of polynomical function of the instantaneous power consumption dependence on time for carrying out further research and calculations. There is a module of the consumed energy calculation on a heating sample which results are displayed in the bottom right corner of the program window in the program. Besides, the Aleo-Diagnost allows to solve a number of such practical problems as calculation of operating voltage depending on geometrical parameters of a product for process realization and also the calculation of the energy consumed on diagnostics of a product for the given time period. The solution of these problems was a necessary stage as the consumed energy is the key output parameter of diagnosing. This parameter is assumed as the basis at non-destructive monitoring process organization in the automated mode.

Conclusion. In conclusion, it should be noted once again that the created mathematical model of high-frequency radiation impact on a polymeric product and the software on the basis of the designed model practical use significantly reduces the cost not only of diagnosing operations preparation, but also of the monitoring process. The results of the presented research allow to reduce the time and improve the quality of products non-destructive monitoring in the conditions of production, operation and repair work. Besides, during the research the sensitivity of diagnosing was defined. The developed method allows to reveal the "metallic inclusion" defects type of total volume 0.0017 % that allows to use this method commercially in machine-building and rocket-space industries. At the moment the software package on the basis of the created mathematical model is used in the scientific, educational and production purposes.

References

1. Larchenko A. G. *Sistema avtomatizirovannogo upravleniya vysokochastotnym diagnostirovaniyem pri proizvodstve i ekspluatatsii izdeliy iz polimernykh materialov. Kand. Diss.* [Automated control system for high-frequency diagnostics in the production and operation of products from polymeric materials. Cand. Diss.]. Irkutsk, 2014, 164 p.

2. La Mantia F. *Vtorichnaya pererabotka plastmass*. [Recycling plastics]. St.Petersburg, Profession Publ., 2006, 400 p.

3. Rabek J. *Eksperimental'nyye metody v khimii polimerov* [Experimental methods in chemistry of polymers], Moscow, Mir Publ., 1983, 480 p.

4. Filippenko N. G. *Avtomatizatsiya upravleniya protsessom vysokochastotnoy obrabotki polimernykh materialov. Kand. Diss.* [Automation of the process control of high-frequency processing of polymer materials. Cand. Diss.]. Irkutsk, 2012, 160 p.

5. Popov S. I. *Avtomatizatsiya upravleniya tekhnologicheskimi protsessami vosstanovleniya ekspluatatsionnykh svoystv polimerov. Kand. Diss.* [Automation of Control of Technological Processes for Restoration of Polymer Operational Properties. Cand. Diss.], Irkutsk, 2013, 120 p.

6. Popov S. I., Livshits A. V., Filippenko N. G. [Experimental studies of the possibility of restoring products from polymeric materials]. *Transportnaya infrastruktura Sibirskogo regiona: Materialy tret'yey vserossiyskoy nauchno–prakticheskoy konferentsii s mezhdunarodnym uchastiyem* [Siberian Transport Infrastructure: Materials of the third all-Russian scientific-practical conference with international participation]. Irkutsk, IrGUPS, 2013, P. 430–437 (In Russ.).

7. Larchenko A. G., Filippenko N. G., Livshits A. V. [Diagnostic device for polyamide separators by high-frequency radiation method]. *Covremennyye tekhnologii. Sovremennyy analiz. Modelirovaniye.* 2014, No. 4, P. 162–168 (In Russ.).

8. Larchenko A. G., Livshits A. V., Popov S. I., Filippenko N. G. *Ustroystvo diagnostiki detaley iz poliamidnykh materialov* [Device for diagnostics of parts from polyamide materials]. Patent RF, No. 132209, 2013.

9. Larchenko A. G. [Automated detection of defects in products made of polyamide materials by the method of high-frequency radiation]. *Covremennyye tekhnologii. Sovremennyy analiz. Modelirovaniye*. 2014, No. 41, P. 160–165 (In Russ.).

10. Filipenko N. G., Larchenko A. G., Livshits A. V. [Innovative method for diagnosing products from polymeric materials]. *Sbornik nauchnykh trudov. Transportnaya infrastruktura Sibirskogo regiona.* [Proc. Transport infrastructure of the Siberian region]. 2013, No. 2, P. 437–440 (In Russ.).

11. Larchenko A. G., Filippenko N. G., Popov S. I., Livshits A. V. [Investigation of the influence of the dielectric elements of a working capacitor in a high-frequency electrothermal installation on the processing of polymeric materials]. *Covremennyye tekhnologii. Sovremennyy analiz. Modelirovaniye*. 2013, No. 3, P. 270–275 (In Russ.).

12. Larchenko A. G. [Automated Device for Diagnosing Polymeric Products of Complex Configuration by the Method of High-Frequency Radiation]. *Kontrol'. Diagnostika*. 2016, No. 2, P. 61–65 (In Russ.).

13. Larchenko A. G. [Automated control system for high-frequency diagnostics of articles made of polymeric materials]. *Avtomatizatsiya. Sovremennyye tekhnologii.* 2015, No. 8, P. 3–8 (In Russ.).

14. Filipenko N. G Livshits A. V, Mashovich A. Ya. [Automation of the process of high-frequency heating of materials at an industrial unit UZP 2500]. *Covremennyye tekhnologii. Sovremennyy analiz. Modelirovaniye.* 2011, No. 2 (30), P. 193–198 (In Russ.).

15. Livshits A. V. Mathematical modeling of the processes of the high-frequency heating of thermoplasts and quality improvement of welded polymeric items. *JP Journal of Heat and Mass Transfer.* Pushpa Publishing House, Allahabad, India, 2017.

Библиографические ссылки

1. Ларченко А. Г. Система автоматизированного управления высокочастотным диагностированием при производстве и эксплуатации изделий из полимерных материалов : дис. … канд. техн. наук. Иркутск, 2014. 164 с.

2. Ла Мантиа Ф. Вторичная переработка пластмасс / пер. с анг. Г. Е. Заикова. СПб. : Профессия, 2006. 400 с.

3. Рабек Я. Экспериментальные методы в химии полимеров / пер. с англ. В. В. Коршака. М. : Мир, 1983. 480 с.

4. Филиппенко Н. Г. Автоматизация управления процессом высокочастотной обработки полимерных материалов : дис. … канд. техн. наук. Иркутск, 2012. 160 с.

5. Попов С. И. Автоматизация управления технологическими процессами восстановления эксплуатационных свойств полимеров : дис. … канд. техн. наук. Иркутск, 2013. 120 с.

6. Попов С. И., Лившиц А. В., Филиппенко Н. Г. Экспериментальные исследования возможности восстановления изделий из полимерных материалов // Транспортная инфраструктура Сибирского региона : материалы 3 Всеросс. науч.-практич. конф. с междунар. участием. 13–17 мая 2013. Иркутск : ИрГУПС, 2013. С. 430–437.

7. Ларченко А. Г., Филиппенко Н. Г., Лившиц А. В. Устройство диагностики полиамидных сепараторов методом высокочастотного излучения // Современные технологии. Современный анализ. Моделирование. 2014. № 4. С. 162–168.

8. Пат. 132209 РФ МПК G01N29/04. Устройство диагностики деталей из полиамидных материалов / А. Г. Ларченко, А. В. Лившиц, С. И. Попов, Н. Г. Филиппенко. Заяв. 10.09.2013. № 132209.

9. Ларченко А. Г. Автоматизированное выявление дефектов в изделиях из полиамидных материалов методом высокочастотного излучения // Современные технологии. Системный анализ. Моделирование. 2014. № 41. С. 160–165.

10. Филиппенко Н. Г., Ларченко А. Г., Лившиц А. В. Инновационный метод диагностики изделий из полимерных материалов // Транспортная инфраструктура Сибирского региона : сб. науч. тр. 2013. № 2. С. 437–440.

11. Исследование влияния диэлектрических элементов рабочего конденсатора в высокочастотной электротермической установке на процесс обработки полимерных материалов / А. Г. Ларченко, Н. Г. Филиппенко, С. И. Попов, А. В. Лившиц // Современные технологии. Системный анализ. Моделирование. 2013. № 3. С. 270–275.

12. Ларченко А. Г. Автоматизированное устройство диагностирования полимерных изделий сложной конфигурации методом высокочастотного излучения // Контроль. Диагностика. 2016. № 2. С. 61–65.

13. Ларченко А. Г. Система автоматизированного управления высокочастотным диагностированием изделий из полимерных материалов // Автоматизация. Современные технологии. 2015. № 8. С. 3–8.

14. Филиппенко Н. Г., Лившиц А. В., Машович А. Я. Автоматизация процесса высокочастотного нагрева материалов на промышленной установке УЗП 2500 // Современные технологии. Системный анализ. Моделирование. 2011. № 2 (30). С. 193–198.

15. Livshits A. V. Mathematical modeling of the processes of the high-frequency heating of thermoplasts and quality improvement of welded polymeric items // JP Journal of Heat and Mass Transfer. 2017. Pushpa Publishing House, Allahabad, India.

Larchenko Anastasia Gennadyevna – Cand. Sc., Associate Professor of the Department “Automation of Production Processes”, Irkutsk State Transport University. E-mail: Larchenkoa@inbox.ru.

Filippenko Nikolay Grigorievich – Cand. Sc., Associate Professor of the Department “Automation of Production Processes”, Irkutsk State Transport University. E-mail: Pentagon@mail.ru.

Livshits Alexander Valerievich – Dr. Sc., Vice-Rector for Research, Irkutsk State Transport University. E-mail: livshic_av@irgups.ru.

Ларченко Анастасия Геннадьевна – кандидат технических наук, доцент кафедры автоматизации производственных процессов; Иркутский государственный университет путей сообщения. E-mail: Larchenkoa@inbox.ru.

Филиппенко Николай Григорьевич – кандидат технических наук, доцент, доцент кафедры автоматизации производственных процессов; Иркутский государственный университет путей сообщения. E-mail: Pentagon@mail.ru.

Лившиц Александр Валерьевич – доктор технических наук, проректор по научной работе; Иркутский государственный университет путей сообщения. E-mail: livshic_av@irgups.ru.

UDC 539.21:537.86
Doi: 10.31772/2587-6066-2019-20-1-112-118

For citation: Masyugin A. N., Fisenko O. B., Rybina U. I., Filippson G. Yu. [Interaction of magnetic and dielectric subsystes in a bismuth nodymic ferrite-granate]. *Siberian Journal of Science and Technology*. 2019, Vol. 20, No. 1, P. 112–118. Doi: 10.31772/2587-6066-2019-20-1-112-118

Для цитирования: Масюгин А. Н., Фисенко О. Б., Рыбина У. И., Филиппсон Г. Ю. Взаимодействие магнитной и диэлектрической подсистем в висмут-неодимовом феррите-гранате // Сибирский журнал науки и технологий. 2019. Т. 20, № 1. С. 112–118. Doi: 10.31772/2587-6066-2019-20-1-112-118

INTERACTION OF MAGNETIC AND DIELECTRIC SUBSYSTES IN A BISMUTH NODYMIC FERRITE-GRANATE

A. N. Masyugin*, O. B. Fisenko, U. I. Rybina, G. Yu. Filippson

Reshetnev Siberian State University of Science and Technology
31, Krasnoyarsky Rabochy Av., Krasnoyarsk, 660037, Russian Federation
* E-mail fisenko_o@mail.ru

Bismuth-substituted ferrite garnets possess magneto-optical (MO) properties and are used as spatial light modulators and indicators. The paper studies the influence of magnetic and electric fields on the structural characteristics of thin epitaxial films of bismuth-neodymium ferrite garnet (Bi: NIG) deposited on glass and gallium gadolinium garnet (GGG) substrates. Dynamic properties of polarization, relaxation in a magnetic and electric field are considered, which is an important task for getting a deep insight into the mechanisms of electromagnetic phenomena in solids.

Dependence of the magnetostriction coefficient on the magnetic field and dependence of a relative change in the length of the film on the electric field at different temperatures are obtained. A change in the sign of magnetostriction constants with respect to temperature was found. The electric polarization in a periodically applied electric field of 400 V / cm with a frequency of 10 MHz is determined for various magnetic field orientations of 12 kOe and in the absence of a magnetic field. Anisotropy of polarization in a magnetic field and a functional dependence of the polarization relaxation on time are found. These materials can be used as sensors of the magnetic field in a spacecraft.

Keywords: bismuth ferrite films, magneto elastic interaction, electric polarization, relaxation.

ВЗАИМОДЕЙСТВИЕ МАГНИТНОЙ И ДИЭЛЕКТРИЧЕСКОЙ ПОДСИСТЕМ В ВИСМУТ-НЕОДИМОВОМ ФЕРРИТЕ-ГРАНАТЕ

А. Н. Масюгин*, О. Б. Фисенко, У. И. Рыбина, Г. Ю. Филиппсон

Сибирский государственный университет науки и технологий имени академика М. Ф. Решетнева
Российская Федерация, 660037, просп. им. газ. «Красноярский рабочий», 31
* E-mail fisenko_o@mail.ru

Висмут замещенные ферриты-гранаты обладают магнитооптическими (МО) свойствами и применяются в качестве пространственных модуляторов света, индикаторов. В работе исследуется влияние магнитного и электрического полей на структурные характеристики тонких эпитаксиальных пленок висмут-неодимового феррита-граната (Bi:NIG), нанесенных на подложки из стекла и галлий-гадолиниевого граната (GGG). Рассматриваются динамические свойства поляризации, релаксация в магнитном и электрическом полях, что является важной задачей для детального понимания механизмов электромагнитных явлений в твердых телах.

Получены зависимости коэффициента магнитострикции от магнитного поля и величины относительного изменения длины пленки от электрического поля при разных температурах. Найдена смена знака констант магнитострикции по температуре. Определена электрическая поляризация в периодически прикладываемом электрическом поле 400 В/см с частотой 10 мГц при различных ориентациях магнитного поля величиной 12 kOe и в отсутствии магнитного поля. Обнаружена анизотропия поляризации в магнитном поле и функциональная зависимость релаксации поляризации от времени. Данные материалы могут использоваться в качестве сенсоров магнитного поля в космических аппаратах.

Ключевые слова: пленки феррита висмута, магнитоупругое взаимодействие, электрическая поляризация, релаксация.

Introduction. Multiferroics attract interest both from the practical, and from the fundamental point of research of interaction mechanisms between magnetic and electric subsystems [1–5].

Unique combination of magnetic, optical and magneto-optical properties makes bismuth ferrite garnets an attractive material both for theoretical researches and for technological applications. These materials can be used as sensors of the magnetic field in spacecrafts and in writer-reader devices resistant to radioactive effects.

Bismuth-substituted ferrite garnets possess magneto-optical (MO) properties and are used as spatial modulators of light, indicators and also other MO of devices in the field of visible light [6–9]. It is established that the increase in replacement of bismuth leads to an increase of MO effects. Thus, for completely substituted Bi3Fe5O12 (BIG) the Faraday spinning effect reaches 25 °/micron for 530 nanometers of the light wavelength. Thereof the garnets substituted with a large amount of bismuth become an attractive material for MO applications. Magnetic anisotropy of films depends on a substrate, the constant of film grating has 0.2 % change when filming on a Gd3Ga5O12 substrate in directions (111) and (100) [10]. Also, in Bi:NIG films Seebeck spin effect was found [11] which can be used in new thermoelectric devices applying the spin current generated by a temperature gradient.

In $Bi_3Fe_5O_{12}$ applying the method of ferromagnetic resonance with the electric field modulation linear magneto-electric effect with maximum under 450 K was found, mechanism of which has not been determined, however, it has a direct connection with bismuth ions presence [12]. In this regard, the research of interrelation between magnetic and electric properties, having been carried out earlier in a number of connections, [13–16] is relevant for bismuth ferrite garnets as well.

Materials and research methods.

Epitaxial films $Nd_1Bi_2Fe_5O_{12}$ (450 nm)/$Nd_2Bi_1Fe_4Ga_1O_{12}$ (90 nm) were examined on the glass substrate and $Nd_{0.5}Bi_{2.5}Fe_5O_{12}$ (450 nm) – on single-crystalline substrate GGG, grown in crystallographic direction (111). Films were produced applying the method of metal-organic compound decomposition of solution (MOD) [17] at the Technological University of Nagaoka (Japan). The process of film formation consisted of the following stages: applying solution on the metal-organic compounds blended so as to meet Stoichiometry requirements to a film structure on the centrifuge at 3000 rot/min within 60 sec. → drying under 100 °C within 10 minutes → preburning under 450 °C within 10 minutes in the open air → repeating the processes from putting metal-organic solution on the centrifuge before preliminary burning so as to obtain the required film thickness → burning at 650°C for 1 hour in the open air. As a buffer layer on a non-directional glass substrate the film $Nd_2Bi_1Fe_4Ga_1O_{12}$ was formed in advance with 90 nm thickness. Schematic diagram of the process MOD is shown in fig. 1.

Values of constants electro- and magnet- strictions were defined as a relative film deformation under the influence of electric and magnetic fields dL = (R (H;E) – R (H = 0; E = 0)) / R (H = 0; E = 0)), where R (H;E) – strain gage resistance in electric or magnetic field, R (H = 0; E = 0) – strain gage resistance without external fields. The ZFLA-3-11 strain gage was used. Polarization was defined as a pyroelectric charge (Q) divided into the area of contact (A) P = Q/A. Charge was measured applying the Keithley 6517B electrometer.

Results and discussions. Interaction of a magnetic and elastic subsystem can be implemented as a result of the single-ion mechanism, spin-orbit interaction and deformation dependence of exchange on the distance. The latter mechanism is found in the field of magnetic phase transition. Film magnetostriction constants on glass and GGG depending on the external magnetic field directed perpendicular to a film are measured. In fig. 2 and 3 temperature dependences of magnetostriction coefficient in magnetic field of 12 kOe for two films applied on different substrates are presented.

For a film on glass in the range of room temperatures the nonlinear dependence λ is observed (N). Lower than 310 K a magnetostriction constant in magnetic field of H = 12 kOe changes the sign. At a temperature of 200 K the maximum film compression is observed. When cooling from 200 K the constant magnetostriction value decreases and at 80K falls dramatically. A small anisotropy of magnetostriction is observed, so that film lengthening in the magnetic field, perpendicularly applied to a film, exceeds the film lengthening in the direction of the field. Under the film rotation relative magnetic field film lengthening reaches a maximum at coal 24 °. Lower than 280 K a minimum and a maximum of magnetostriction is reached at 30 ° respectively and perpendicular to the film.

The film on GGG substrate at $T > 300$ K linearly expands in magnetic field and contracts below room temperature. With the temperature decrease magnetostriction changes the sign, passes through a minimum at $T = 160$ K and similarly to glass practically does not depend on temperature at further cooling (fig. 3). Change of magnetic field orientation hardly influences the magnetostriction constant.

The film electrostriction value Bi: NIGNA on a glass substrate was measured in electric field up to 400 V / cm. The film slightly expands in the external electric field at $T = 80$ K. Above $T = 120$ K the film contracts not linearly and reaches the maximum size of compression in fields of 300–400 V/cm at $T > 200$ K. At temperatures above room there are two competing mechanisms: the first is connected with the film contraction, the second - with expansion. Magnetostriction in this area of temperatures changes the sign. Film deformation does not depend on the electric field sign. Electrostriction under absolute value increases at temperature rise, passes through a maximum at 200 K and decreases under a further temperature rise up to 360 K.

Polarization of Bi:NIG films is measured in the electric field of 400 V/cm amplitude with a frequency of 10 MHz in the form of a rectangular impulse under various magnetic field orientations. In fig. 4 and 5 dependences of polarization on time are represented at different temperatures for both films.

Over time electric polarization of the film on glass smoothly grows in external electric field. At switching off the field, polarization falls abruptly and changes the sign from positive value to negative below room temperature.

At temperatures over 300 K residual polarization coincides with external electric field by sign (fig. 4).

The time dependence of film polarization on garnet qualitatively differs from films on glass (fig. 5). Under switched off electric field residual polarization remains positive and smoothly increases over time.

Observed effects are explained by charged defects on the film-substrate interface which are compensated by the shift of oxygen ions along certain directions in crystal. External electric field removes degeneration in the direction of polarization, leads to turning of the local dipolar moments across the field and to the formation of residual polarization. In films on glass there are two interfaces and double electric layer is formed causing the polarization sign change after switching off the field.

In films on glass and on garnets the anisotropy of electric polarization in magnetic field which is caused by magnetoelectric effect is observed.

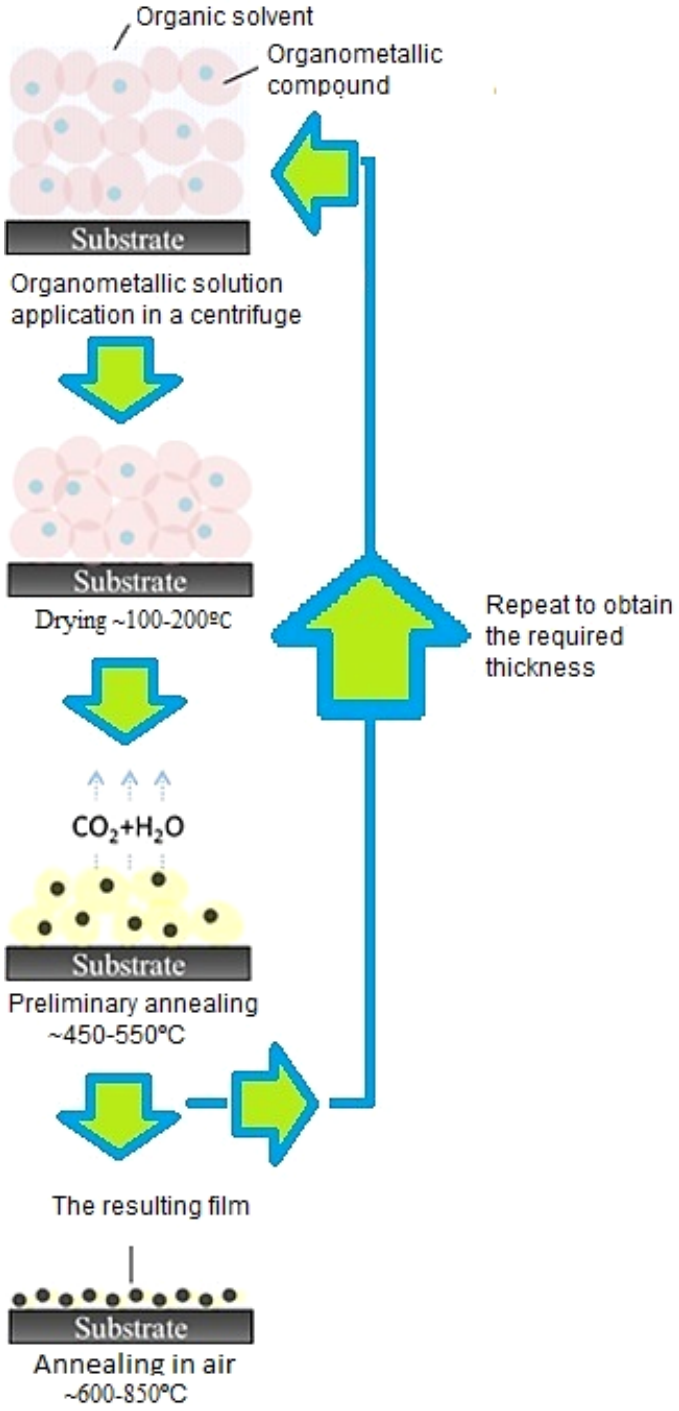

Fig. 1. Sketch flowchart MOD

Рис. 1. Эскизная схема технологического процесса MOD

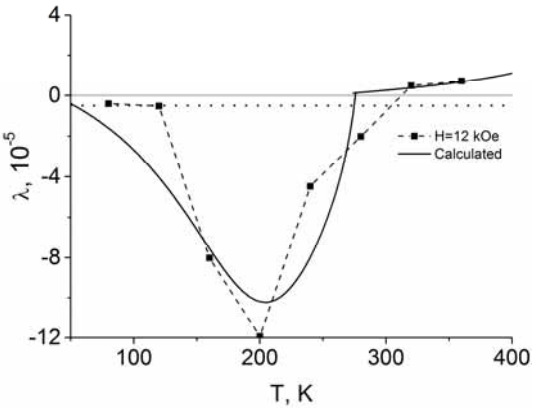

Fig. 2. Dependence of the magnetostriction coefficient on temperature in Bi: NIG on a glass substrate

Рис. 2. Зависимость коэффициента магнитострикции от температуры в Bi:NIG на подложке из стекла

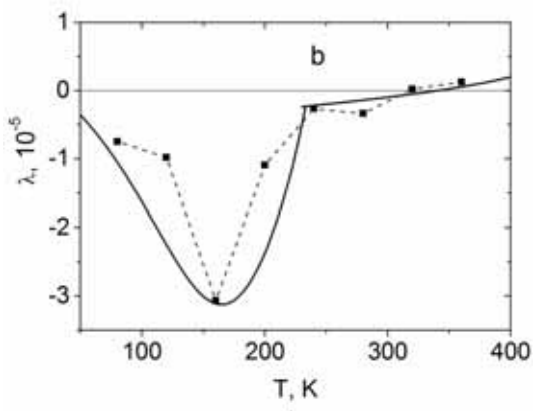

Fig. 3. Dependence of the magnetostriction coefficient on temperature in Bi: NIG on a GGG substrate

Рис. 3. Зависимость коэффициента магнитострикции от температуры в Bi:NIG на подложке из GGG

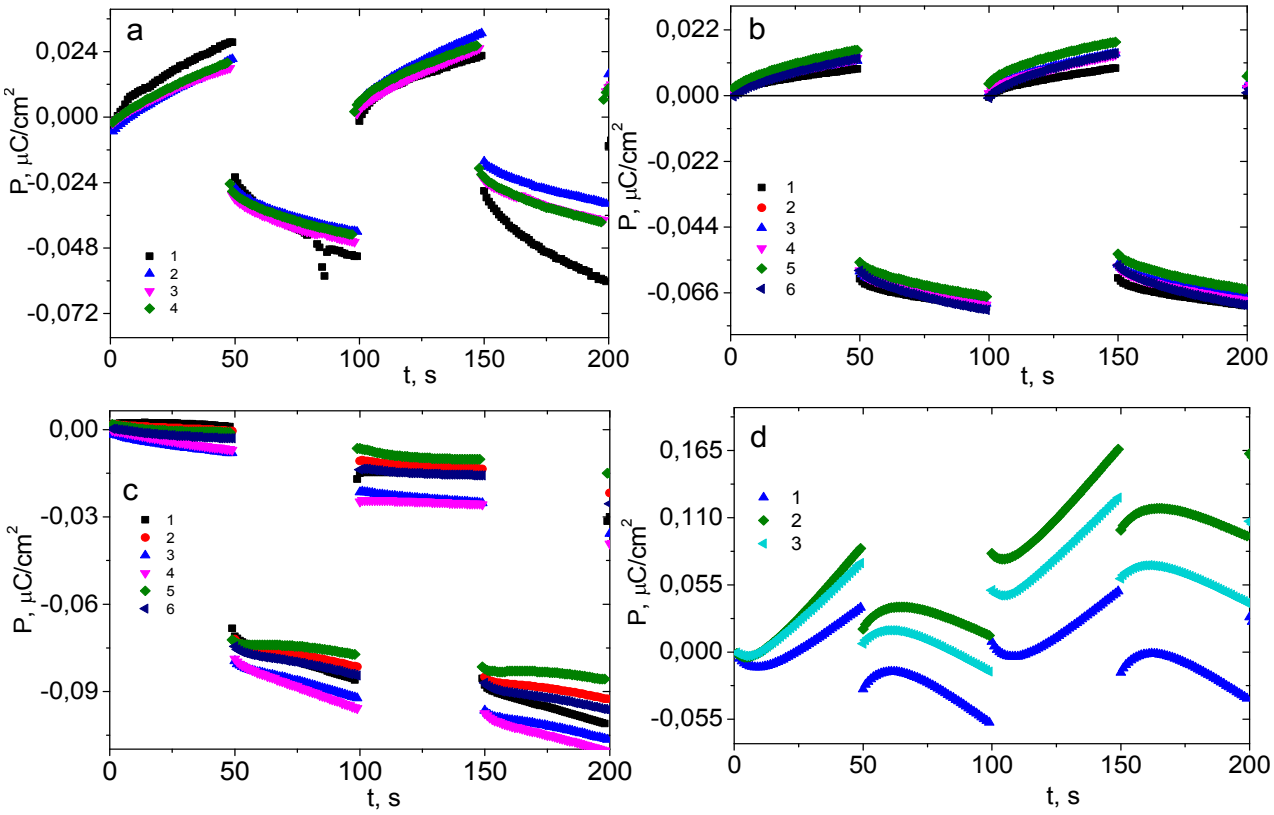

Fig. 4. Polarization of Bi: NIG film on glass over time:
a – at temperatures *t* = 120º KH = 0 (1), in magnetic fields *H* = 12 kOe when the magnetic field is oriented relative to the surface normal at angles φ = 90º (2), φ = 180º (3), φ = 360º (4); *b* – at temperatures *t* = 200º KH = 0 (1, 6), in magnetic fields *H* = 12 kOe when the magnetic field is oriented relative to the surface normal at angles φ = 0º (2), φ = 90º (3), φ = 180º (4), φ = 360º (5); *c* – at temperatures *t* = 280º KH = 0 (1, 6), in magnetic fields *H* = 12 kOe when the magnetic field is oriented relative to the surface normal at angles φ = 0º (2), φ = 90º (3), φ = 180º (4), φ = 360º (5); *d* – at temperatures *t* = 360º K H = 0 (3), in magnetic fields *H* = 12 kOe when the magnetic field is oriented relative to the surface normal at angles φ = 90º (1), φ = 360º (2)

Рис. 4. Поляризация пленки Bi:NIG на стекле от времени:
a – при температурах *t* = 120º KH = 0 (1), в магнитных полях *H* = 12 кЭ при ориентации магнитного поля относительно нормали поверхности при углах φ = 90º (2), φ = 180º (3), φ = 360º (4); *b* – при температурах *t* = 200º KH = 0 (1, 6), в магнитных полях *H* = 12 кЭ при ориентации магнитного поля относительно нормали поверхности при углах φ = 0º (2), φ = 90º (3), φ = 180º (4), φ = 360º (5); *c* – при температурах *t* = 280º KH = 0 (1, 6), в магнитных полях *H* = 12 кЭ при ориентации магнитного поля относительно нормали поверхности при углах φ = 0º (2), φ = 90º (3), φ = 180º (4), φ = 360º (5); *d* – при температурах *t* = 360º KH = 0 (3), в магнитных полях *H* = 12 кЭ при ориентации магнитного поля относительно нормали поверхности при углах φ = 90º (1), φ = 360º (2)

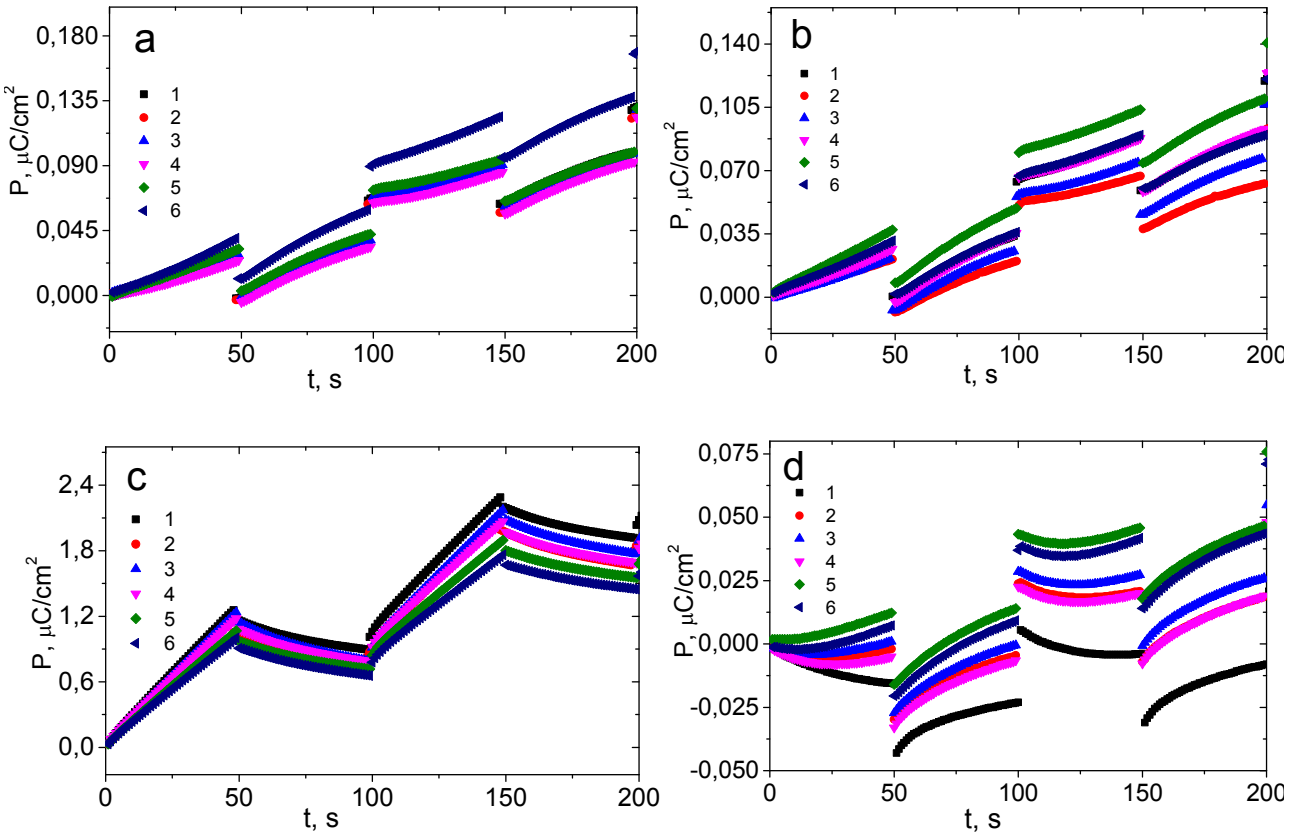

Fig. 5. Polarization of Bi: NIG film on GGG over time:
a – at temperatures *t* = 120º KH = 0 (1, 6), in magnetic fields *H* = 12 kO when the magnetic field is oriented relative to the surface normal at angles φ = 0º (2), φ = 90º (3), φ = 180º (4), φ = 360º (5); *b* – at temperatures *t* = 160º KH = 0 (1, 6), in magnetic fields *H* = 12 kO when the magnetic field is oriented relative to the surface normal at angles φ = 0º (2), φ = 90º (3), φ = 180º (4), φ = 360º (5); *c* – at temperatures *t* = 280º KH = 0 (1, 6), in magnetic fields *H* = 12 kOe when the magnetic field is oriented relative to the surface normal at angles φ = 0º (2), φ = 90º (3), φ = 180º (4), φ = 360º (5); *d* – at temperatures *t* = 320º KH = 0 (1, 6), in magnetic fields *H* = 12 kOe when the magnetic field is oriented relative to the surface normal at angles φ = 0º (2), φ = 90º (3), φ = 180º (4), φ = 360º (5)

Рис. 5. Поляризация пленки Bi:NIG на GGG от времени:
a – при температурах *t* = 120º KH = 0 (1, 6), в магнитных полях *H* = 12 кЭ при ориентации магнитного поля относительно нормали поверхности при углах φ = 0º (2), φ = 90º (3), φ = 180º (4), φ = 360º (5); *b* – при температурах *t* = 160º KH = 0 (1, 6), в магнитных полях *H* = 12 кЭ при ориентации магнитного поля относительно нормали поверхности при углах φ = 0º (2), φ = 90º (3), φ = 180º (4), φ = 360º (5); *c* – при температурах *t* = 280º KH = 0 (1, 6), в магнитных полях *H* = 12 кЭ при ориентации магнитного поля относительно нормали поверхности при углах φ = 0º (2), φ = 90º (3), φ = 180º (4), φ = 360º (5); *d* – при температурах *t* = 320º KH = 0 (1, 6), в магнитных полях *H* = 12 кЭ при ориентации магнитного поля относительно нормали поверхности при углах φ = 0º (2), φ = 90º (3), φ = 180º (4), φ = 360º (5)

Magnetic field orientation angle is defined relative to a film surface normal. Dependence of polarization relaxation on time cannot be described by one functional dependence like an exponent, a logarithm or a power function. Change of electric polarization in magnetic field, under switching on and off electric field of *E* = 400 V/cm, reaches 40 % and depends on the direction of magnetic field relative to the film

Conclusion. Contraction of films below room temperature has been found in magnetic and electric fields. Magnetostriction sign change under temperature rise in films on glass and on garnet has been revealed. Residual electric polarization after external electric field switching off has been observed. The anisotropy of polarization in external magnetic field has been found which indicates magnetoelectric interaction in bismuth ferrite films.

Acknowledgments. The study was carried out with the financial support of the Russian Foundation for Basic Research, the Government of the Krasnoyarsk Territory, the Krasnoyarsk Regional Science Foundation under the scientific project No. 18-42-240001: “Inversion of the sign of the components of the magnetoelectric tensor on the temperature in bismuth-filled garnet ferrite films replaced by neodymium financial support number 18-32-00079 mol_a.

Благодарности. Исследование выполнено при финансовой поддержке Российского фонда фундаментальных исследований, Правительства Красноярского края, Красноярского краевого фонда науки в рамках научного проекта № 18-42-240001: «Инверсия знака компонент магнитоэлектрического тензора по температуре в пленках висмутового феррита-граната, замещенного неодимом». Работа частично выполнена при финансовой поддержке № 18-32-00079 mol_a.

References

1. Udod L. V., Aplesnin S. S., Sitnikov M. N., Molokeev M. S. Dielectric and electrical properties of polymorphic bismuth pyrostanate $Bi_2Sn_2O_7$. *Physics of the Solid State.* 2014, Vol. 56, Iss. 7, P. 1315–1319.

2. Aplesnin S. S., Sitnikov M. N. Magnetotransport effects in a paramagnetic state in $Gd_xMn_{1-x}S$. *JETP Letters*. 2014, Vol. 100, Iss. 2, P. 95–101.

3. Aplesnin S. S., Ostapenko A. A. Kretinin V. V. et al. [Dielectric Properties of $Bi_{1-x}La_xFeO_3$ Thin Films]. *Vestnik SibGAU.* 2014, No. 3 (55), P. 192–197 (In Russ.).

4. Aplesnin S. S., Udod L. V., Sitnikov M. N. et al. $Bi_2(Sn_{0.95}Cr_{0.05})2O_7$: Structure, IR specture, and dielectric properties. *Ceramics International.* 2016, Vol. 42, P. 5177–5183.

5. Aplesnin S. S., Sitnikov M. N. Magneto capacitive effect in $Gd_xMn_{1-x}S$. *Physics of the Solid State.* 2016, Vol. 58, Iss. 6, P. 1112–1117.

6. Yamakita J., Lou G., Nishikawa M., Kato T., Iwata S., Ishibashi T. Magnetic properties of bismuth-substituted neodymium iron garnet films on $Gd_3Ga_5O_{12}(100)$ substrates determined by ferromagnetic resonance measurements. *Japanese Journal of Applied Physics*. 2018, Vol. 57, P. 09TC01. Doi: 10.7567/JJAP.57.09TC01.

7. Veis M., Lišková E., Antoš R. et al. Polar and longitudinal magneto-optical spectroscopy of bismuth substituted yttrium iron garnet films grown by pulsed laser deposition. *Thin Solid Films*. 2011, Vol. 519, Iss. 22, P. 8041–8046. Doi: 10.1016/j.tsf.2011.06.007.

8. Chern M.-Y., Liaw J.-S. Study of $Bi_xY_{3\ x}Fe_5O_{12}$ Thin Films Grown by Pulsed Laser Deposition. *Japanese Journal of Applied Physics*. 1997, Vol. 36, Part 1, No. 3A, P. 1049–1053. Doi: 10.1143/JJAP.36.1049.

9. Aplesnin S. S., Khar'kov A. M. Magnetic and Dynamic Properties of $Sm_xMn_{1-x}S$ Solid Solutions. *Physics of the Solid State*. 2013, Vol. 55, No. 1, P. 81–87.

10. Michimasa Sasaki, Gengjian Lou, Qi Liu. $Nd_{0.5}Bi_{2.5}Fe_{5-\ y}Ga_yO_{12}$ thin films on $Gd_3Ga_5O_{12}$ substrates prepared by metal–organic decomposition. *Japanese Journal of Applied Physics.* 2016, Vol. 55, P. 055501.

11. Asada H., Kuwahara A., Sueyasu K. et al. Longitudinal Spin Seebeck Effect in Bi-substituted Neodymium Iron Garnet on Gadolinium Gallium Garnet Substrate Prepared by MOD Method. *Physics Procedia.* 2015, Vol. 75, P. 932–938. Doi: 10.1016/j.phpro.2015.12.128.

12. Popova E., Shengelaya A., Daraselia D. et al. Bismuth iron garnet $Bi_3Fe_5O_{12}$: A room temperature magnetoelectric material. *Applied Physics Letters.* 2017, Vol. 110, P. 142404.

13. Aplesnin S. S., Sitnikov M. N., Romanova O. B., Pichugin A. Yu. Magnetoelectric and magnetoresistive properties of the $Ce_xMn_{1-x}S_{semiconductors}$. *Physica Status Solidi(B).* 2016, Vol. 253, Iss. 9, P. 1771–1781.

14. Aplesnin S. S., Sitnicov M. N., Panasevich A. M., Galyas A. I., Demidenko O. V., Yanushkevich K. I. Magnetic and Magnetoresistive Properties of $Gd_xMn_{1-\ x}Se_{Selenides}$. *Bulletin of the Russian Academy of Sciences: Physics*. 2016, Vol. 80, No. 11, P. 1306–1309.

15. Aplesnin S. S., Kretinin V. V., Panasevich A. M., Yanushkevich K. I. Magnetic capacitance of the $Gd_xBi_{1-x}FeO_3$ thin films. *Physics of the Solid State.* 2017, No. 59(4), P. 667–673. Doi: 10.21883 / FTT.2017.04.44265.094.

16. Aplesnin S. S., Udod L. V., Sitnikov M. N. et al. Magnetic, Dielectric and Transport Properties of bismuth pyrostanate $Bi_2(Sn_{0.9}Mn_{0.1})2O_7$. *Physics of the Solid State.* 2017, Vol. 59, No. 11, P. 2268–2273.

17. Ishibashi T., Mizusawa A., Nagai M. et al. Characterization of epitaxial $(Y,Bi)_3(Fe,Ga)_5O_{12}$ thin films grown by metal-organic decomposition method. *Japanese Journal of Applied Physics*. 2005, Vol. 97, Iss. 1, P. 013516. Doi: 10.1063/1.1827339.

Библиографические ссылки

1. Диэлектрические и электрические свойства полиморфного пиростаната висмута $Bi_2Sn_2O_7$ / Л. В. Удод, С. С. Аплеснин, М. Н. Ситников [и др.] // Физика твердого тела. 2014. Т. 56, вып. 7. С. 1267–1271.

2. Аплеснин С. С., Ситников М. Н. Магнитотранспортные эффекты в парамагнитном состоянии в $Gd_xMn_{1-x}S$ // Письма в ЖЭТФ. 2014. Т. 100, вып. 2. С. 104–110.

3. Диэлектрические свойства тонких пленок $Bi_{1-x}La_xFeO_3$ / С. С. Аплеснин, А. А. Остапенко, В. В. Кретинин [и др.] // Вестник СибГАУ. 2014. № 3 (55). С. 192–197.

4. $Bi_2(Sn_{0.95}Cr_{0.05})2O_7$: Structure, IRspecture, and dielectric properties / S. S. Aplesnin, L.V. Udod, M. N. Sitnikov [et al.] // Ceramics International. 2016. Vol. 42. P. 5177–5183.

5. Аплеснин С. С., Ситников М. Н. Магнитоемкостный эффект в $Gd_xMn_{1-x}S$ // Физика твердого тела. 2016. Т. 58, вып. 6. С. 1112–1117.

6. Magnetic properties of bismuth-substituted neodymium iron garnet films on $Gd_3Ga_5O_{12}(100)$ substrates determined by ferromagnetic resonance measurements / J. Yamakita, G. Lou, M. Nishikawa [et at.] // Japanese Journal of Applied Physics. 2018. Vol. 57. P. 09TC01. Doi: 10.7567/JJAP.57.09TC01.

7. Polar and longitudinal magneto-optical spectroscopy of bismuth substituted yttrium iron garnet films grown by pulsed laser deposition / M. Veis, E. Lišková, R. Antoš [et al.] // Thin Solid Films. 2011. Vol. 519, Iss. 22. P. 8041–8046. Doi:10.1016/j.tsf.2011.06.007.

8. Chern M.-Y., Liaw J.-S.. Study of $Bi_xY_{3\ x}Fe_5O_{12}$ Thin Films Grown by Pulsed Laser Deposition // Japanese Journal of Applied Physics. 1997. Vol. 36, Part 1, No. 3A. P. 1049–1053. Doi: 10.1143/JJAP.36.1049.

9. Аплеснин С. С., Харьков А. М. Магнитные и динамические свойства твердых растворов $Sm_xMn_{1-x}S$ // Физика твердого тела. 2003. Т. 59, вып. 1. С. 69–74.

10. Sasaki M., Lou G., Liu Q. $Nd_{0.5}Bi_{2.5}Fe_{5-\ y}Ga_yO_{12}$ thin films on $Gd_3Ga_5O_{12}$ substrates prepared by metal–organic decomposition // Japanese Journal of Applied Physics. 2016. Vol. 55. P. 055501.

11. Longitudinal Spin Seebeck Effect in Bi-substituted Neodymium Iron Garnet on Gadolinium Gallium Garnet Substrate Prepared by MOD Method / H. Asada, A. Kuwahara, K. Sueyasu [et al.] // Physics Procedia. 2015. Vol. 75. P. 932–938. Doi: 10.1016/j.phpro.2015.12.128.

12. Bismuth iron garnet $Bi_3Fe_5O_{12}$: A room temperature magnetoelectric material / E. Popova, A. Shengelaya, D. Daraselia [et al.] // Appl. Phys. Lett. 2017. Vol. 110. P. 142404.

13. Magnetoelectric and magnetoresistiveproperties of the $Ce_xMn_{1-x}S_{semiconductors}$ / S. S. Aplesnin, M. N. Sitnikov [et al.] // Physica Status Solidi (B). 2016. Vol. 253, Iss. 9. P. 1771–1781.

14. Magnetic and Magnetoresistive Properties of $Gd_xMn_{1-x}Se_{Selenides}$ / S. S. Aplesnin, M. N. Sitnikov [et al.] // Bulletin of the Russian Academy of Sciences: Physics. 2016. Vol. 80, No. 11. P. 1306–1309.

15. Магнитоемкость тонких пленок $Gd_xBi_{1-x}FeO_3$ / С. С. Аплеснин, В. В. Кретинин, А. М. Панасевич [и др.] // Физика твердого тела. 2017. №. 4. С. 653–659, Doi: 10.21883/FTT.2017.04.44265.094.

16. Магнитные, Диэлектрические и транспортные свойства пиростаната висмута $Bi_2(Sn_{0.9}Mn_{0.1})2O_7$ / С. С. Аплеснин, Л. В. Удод, М. Н. Ситников [и др.] // Физика твердого тела. 2017. Т. 59, вып. 11. С. 2246–2251.

17. Characterization of epitaxial $(Y,Bi)_3(Fe,Ga)_5O_{12}$ thin films grown by metal-organic decomposition method / T. Ishibashi, A. Mizusawa, M. Nagai [et al.] // Japanese Journal of Applied Physics. 2005. Vol. 97, Iss.1. P. 013516. Doi: 10.1063/1.1827339.

Masyugin Albert Nikolaevich – graduate student; Reshetnev Siberian State University of Science and Technology. E-mail: albert.masyugin@mail.ru.

Fisenko Olga Borisovna – graduate student; Reshetnev Siberian State University of Science and Technology. E-mail: fisenko_o@mail.ru.

Rybina Ulyana Ilinishna – a student of the Institute of Space Technology, group A17-01; Reshetnev Siberian State University of Science and Technology. E-mail: rybinau@mail.ru.

Filippson Gleb Yuryevich – a student of the Institute of Space Technology, group A17-01; Reshetnev Siberian State University of Science and Technology. E-mail: filippson@mail.ru.

Масюгин Альберт Николаевич – аспирант; Сибирский государственный университет науки и технологий имени академика М. Ф. Решетнева. E-mail: albert.masyugin@mail.ru.

Фисенко Ольга Борисовна – аспирант; Сибирский государственный университет науки и технологий имени академика М. Ф. Решетнева. E-mail: fisenko_o@mail.ru.

Рыбина Ульяна Ильинишна – студент института космической техники, группа А17-01; Сибирский государственный университет науки и технологий имени академика М. Ф. Решетнева. E-mail: mail: rybinau@mail.ru.

Филиппсон Глеб Юрьевич – студент института космической техники, группа А17-01; Сибирский государственный университет науки и технологий имени академика М. Ф. Решетнева. E-mail: filippson@mail.ru.

UDC 663.63.0
Doi: 10.31772/2587-6066-2019-20-1-119-125

For citation: Pshenko E. B., Shestakov I. Ya., Shestakov V. I. [Features of electroactivated water production at a coaxial electrode location]. *Siberian Journal of Science and Technology*. 2019, Vol. 20, No. 1, P. 119–125. Doi: 10.31772/2587-6066-2019-20-1-119-125

Для цитирования: Пшенко Е. Б., Шестаков И. Я., Шестаков В. И. Особенности получения электроактивированной воды при коаксиальном расположении электродов // Сибирский журнал науки и технологий. 2019. Т. 20, № 1. С. 119–125. Doi: 10.31772/2587-6066-2019-20-1-119-125

FEATURES OF ELECTROACTIVATED WATER PRODUCTION AT A COAXIAL ELECTRODE LOCATION

E. B. Pshenko*, I. Ya. Shestakov, V. I. Shestakov

Reshetnev Siberian State University of Science and Technology
31, Krasnoyarsky Rabochy Av., Krasnoyarsk, 660037, Russian Federation
*E-mail: pshenko-64@mail.ru

Important characteristics of any product are quality and reliability. One of the factors affecting product reliability is the surface cleanliness provided by flushing with liquids. Electroactivated water and aqueous solutions can be used as liquids. On the basis of domestic and foreign experience, leading experts have developed methodological instructions for the widespread implementation of electro-activated water and aqueous solutions in instrument-making and mechanical engineering. For the production of electrochemically activated water and solutions, non-flowing and flow-through modular elements, as well as universal installations, have been developed. Analysis of the structures of these devices has shown that flat metal plates are used as electrodes, therefore there are volumes of water that are subjected to uneven electrical effects. As a result, the specific energy consumption for obtaining activated water is significant. The purpose of the work is to reduce the specific energy consumption in the production of activated water and aqueous solutions. Coaxial arrangement of the electrodes leads to reduction in energy consumption. The study of the electroactivator of water with a coaxial arrangement of electrodes allowed us to establish the optimal ratio between the volumes of anolyte and catholyte and the time of electrolysis of water and an aqueous solution of sodium chloride. A new indicator of efficiency (the specific energy consumption per unit of change in the pH of water or an aqueous solution) objectively reflects the perfection of the design of electroactivators. The research results can be used in instrument and mechanical engineering.

Keywords: water, electrochemical activator, anolyte, catholyte.

ОСОБЕННОСТИ ПОЛУЧЕНИЯ ЭЛЕКТРОАКТИВИРОВАННОЙ ВОДЫ ПРИ КОАКСИАЛЬНОМ РАСПОЛОЖЕНИИ ЭЛЕКТРОДОВ

Е. Б. Пшенко*, И. Я. Шестаков, В. И. Шестаков

Сибирский государственный университет науки и технологии имени академика М. Ф. Решетнева
Российская Федерация, 660037, Красноярск, просп. им. газ. «Красноярский рабочий», 31
*E-mail: pshenko-64@mail.ru

Важной характеристикой любого изделия является качество и надежность. Одним из факторов, влияющих на надежность изделий, является чистота поверхности, которая обеспечивается промывкой жидкостями. В качестве жидкости могут быть использованы электроактивированная вода и водные растворы. На основе отечественного и зарубежного опыта ведущими специалистами разработаны методические инструкции по широкому применению и использованию электроактивированных воды и водных растворов в приборо- и машиностроении. Для получения электрохимически активированной воды и растворов разработаны непроточные и проточные модульные элементы, а также универсальные установки. Анализ конструкций этих устройств показал, что в качестве электродов применяются плоские металлические пластины, поэтому имеются объемы воды, которые подвергаются неравномерному электрическому воздействию. В результате этого удельные энергозатраты на получение активированной воды значительны. Целью работы явилось снижение удельных энергозатрат при получении активированной воды и водных растворов. Коаксиальное расположение электродов приводит к снижению энергозатрат. Исследование электроактиватора воды с коаксиальным расположением электродов позволило установить оптимальное соотношение между объемами анолита и католита и временем электролиза воды и водного раствора хлорида натрия. Новый показатель эффективности (удельные энергозатраты на единицу изменения водородного показателя воды или водного раствора)

объективно отражает совершенство конструкции электроактиваторов. Результаты исследования могут быть использованы в приборо- и машиностроении.

Ключевые слова: вода, электрохимический активатор, анолит, католит.

Introduction. The amazing properties of water obtained by electrolysis were discovered in different countries independently. The unusual properties of the electroactivated water were discovered by chance, not by the doctors, but by the gas workers, not in the laboratory, but on the drilling test towers of the Institute SredAzNIIGaz. This institute was located in Tashkent and was engaged in gas production in the Kyzyl Kum desert. The scientists of this institute came up with an original installation: on the basis of electrolysis, two solutions were obtained from ordinary water. One of them, catholyte, was used to produce drilling mud with high physical and chemical indices. Another solution – anolyte – was used for coagulation of excess clay phase.

The study and use of electroactivated water solutions began in 1978 in the organization "Sreda-3 NIIgaz", where S. A. Alekhin, V. M. Bakhir, N. A. Mariam-Polsky, U. D. Mamadzhanov et al. worked [1–3].

Three international symposiums were held on the electrochemical activation of water and aqueous solutions [4–6]. In the introductory report at the first symposium the President of the Academy of Medical and Technical Sciences of Russia, Doctor of Technical Sciences, Professor. B. I. Leonov noted that "electrochemical activation of water and water solutions is the technology of the future, which will allow creating an ecologically clean future for the Earth and other planets". Further work confirms the conclusion of the scientist [7–9].

The widespread use of activated water is presented in article [10]. Water with pH 2–3 was introduced into a solution of ferric chloride for etching printed circuit boards [11]. The etching rate has increased, the consumption of chemicals has decreased, the process of industrial waste regeneration has been simplified. For cleaning printed circuit boards, a composition consisting of electroactivated water (pH 12–14) and caustic soda has been developed [12]. The cleaning time is reduced several times. When cutting metals, the redox potential of the emulsion was measured at the time of chip removal. As soon as the cutting began, the redox potential became negative. Having added electroactivated water (catholyte) with redox potential from minus 300 to minus 800 mV to the emulsion, a new coolant-lubricant was obtained [13]. Working on the process of industrial waste utilization, the authors improved the previously developed coolant-lubricant. The activator was close to the metalworking machine. At the same time, the catholyte was directed to the cutting zone, and the anolyte was mixed with the spent emulsion. The effect of increasing the cutting tool durability was obtained, the emulsion stability increased 1.5 times, and the used coolant did not require additional treatment for utilization [14].

For washing printed circuit boards, various liquids are used. In the study [15] electroactivated water was used for this purpose, which led to a reduction in the consumption of chemicals.

To obtain electrochemically activated water and solutions such devices are used as: STEL installations, Aquachlor, Izumrud; flow modular elements PEM-3, PEM-7, PEM-9; universal MB-11, MB-26, etc. With a small consumption of activated water, a large variety of electroactivators are offered: Iva-1, Melesta, AP-1, Aqualife and others (fig. 1).

Analysis of the structures of these devices showed that flat metal plates are used as electrodes, therefore there are volumes of water that are exposed to uneven electrochemical effects. In addition, due to the small surface area of the electrodes, the current density increases, which, according to the Tafel equation, leads to an increased overvoltage of electrochemical processes. As a result of this, the specific energy consumption for obtaining activated water is significant and amounts to 15÷30 W · h / l. The calculation is made on the basis of passport data.

In the Espero-1 electroactivator shown in fig. 2, the anode is made in the form of a graphite rod of square section, the cathode is made of thin-sheet steel in the form of a cylindrical shell. The electrodes are mounted coaxially to each other. The anode is in the center, the cathode is in the periphery. As a result, all the water in the activator is subjected to electrochemical exposure, which leads to a significant reduction of energy consumption to 2÷3 W · h / l (when dissolving table salt in water 10 g/l). On the side surface of the anode, due to the right angle, the electric field strength and current density are increased, which adversely affects the efficiency of the electroactivator.

Methods and equipment of research. To study the activator with a coaxial arrangement of electrodes, a device with a graphite rod of circular cross-section was manufactured [16]. Fig. 3 shows an experimental electroactivator.

Tarpaulin cloth is used as the diaphragm. The anode is a graphite rod, the cathode is a hollow stainless steel cylinder. Fig. 4 shows the assembled electroactivator, power supply, multimeter and pH meter.

Methods of conducting experiments in the study of electroactivator with a coaxial arrangement of electrodes:

1. Filling the glass tank with cold tap water.
2. Settling water with the lid open for at least 8–10 hours at room temperature.
3. Control the pH of the source water.
4. Filling the anodic and cathodic spaces of the activator with water.
5. Installation of the electrode in the anode space.
6. Pause from 3 to 5 minutes to level the water levels in the cathode and anode spaces.
7. Electrochemical effect on water by passing a current.
8. Current control.
9. After disconnecting the voltage, the anolyte is discharged into a separate container.
10. Control of pH of the anolyte (pHA) and the catholyte (pHK).

Fig. 1. Electric water activators: Iva-1, Melesta, AP-1

Рис. 1. Электроактиваторы воды: Ива-1, Мелеста, АП-1

Fig. 2. Electroactivator “Espero-1”

Рис. 2. Электроактиватор «Эсперо-1»

Fig. 3. Experimental electroactivator

Рис. 3. Экспериментальный электроактиватор

Fig. 4. Used equipment

Рис. 4. Используемое оборудование

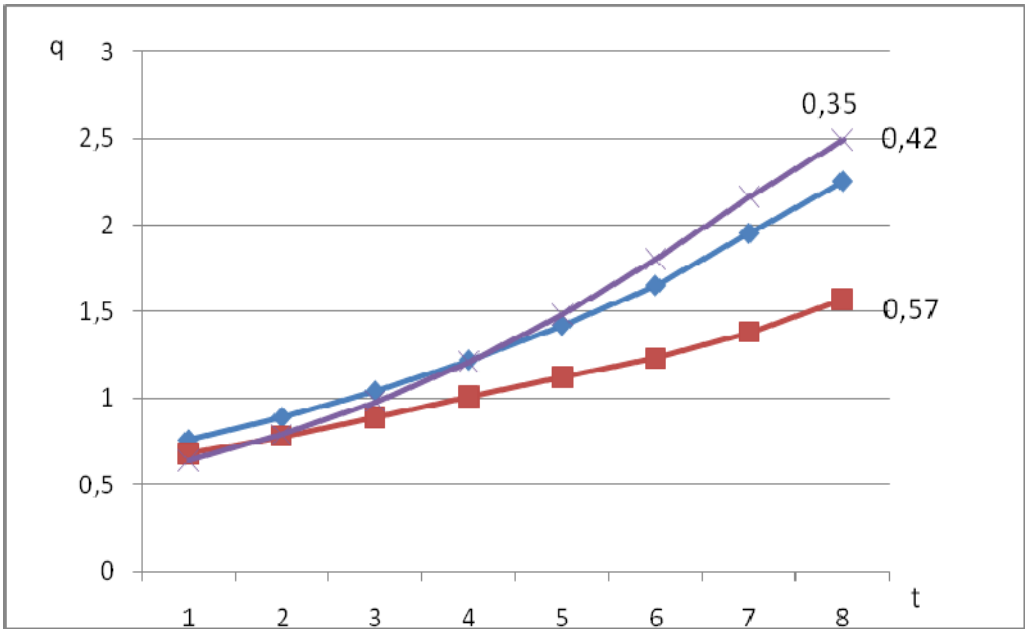

Fig. 5. The change in pH of anolyte and catholyte from the time of activation of tap water

Рис. 5. Изменение pH анолита и католита от времени активирования водопроводной воды

Specific energy consumption is determined by the formula:

$$Q = I \cdot U \cdot \tau / 60 \cdot V, \quad (1)$$

where U is the voltage on the electrodes, V; V is the volume of activated water, l; I is the amperage, A; τ is the time of water activation, min.

We believe that the specific energy consumption does not reflect the efficiency of the electroactivator. It is proposed to evaluate the operation of the device according to the following indicator:

$$q = Q/\Delta\text{pH}, \quad (2)$$

where q is the specific energy consumption per unit of change in the pH of water or an aqueous solution; ΔpH = pHK – pHA is the difference in pH values of catholyte and anolyte.

The experiments were conducted at a different ratio of the volumes of anolyte and catholyte from 0.35 to 1.72.

Results. Experiments have shown (fig. 5) that the minimum value of specific energy consumption per unit of pH change is typical for a volume ratio of 0.57, there-

fore, further experiments were carried out with this ratio. It can be seen from the figure that with electrolysis time from 3.5 to 7 minutes specific energy consumption for the specified ratio of volumes is 15–20 % less than for other values.

Fig. 6 shows the changes in the pH of anolyte and catholyte from the time of water activation. It follows from the graph that the maximum change in the hydrogen index (pH) occurs in 7 minutes of electrochemical activation of water.

For the experiments an aqueous solution of sodium chloride (0.9 % physiological solution widely used in medicine and in everyday life – the Espero activator) was used. The results are presented in fig. 7, 8.

The nature of the change in the pH of the solution and the specific energy consumption does not change with the activation time.

However, the specific energy consumption is an order of magnitude less and the maximum change in the pH value occurs in 3 minutes.

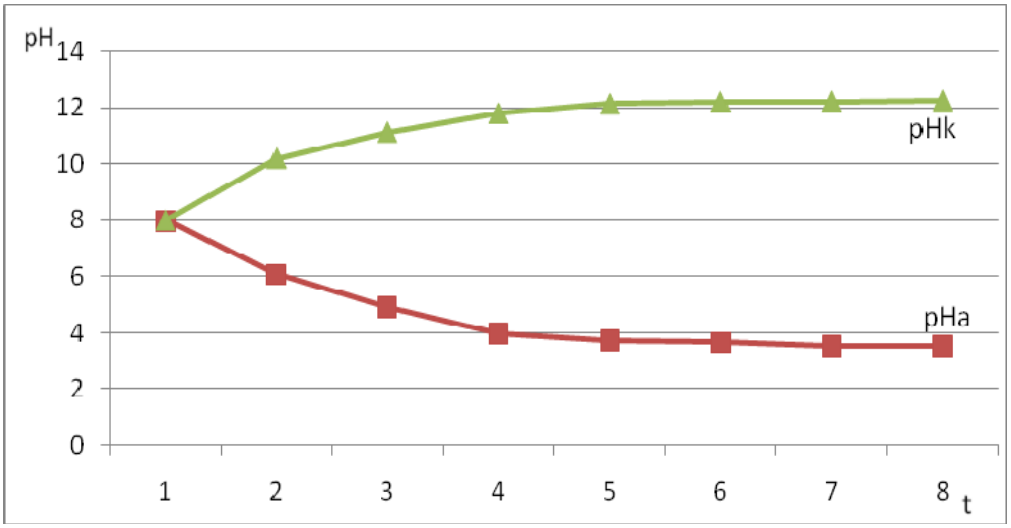

Fig. 6. The change in pH of anolyte and catholyte from the time of water activation

Рис. 6. Изменение pH анолита и католита от времени активации воды

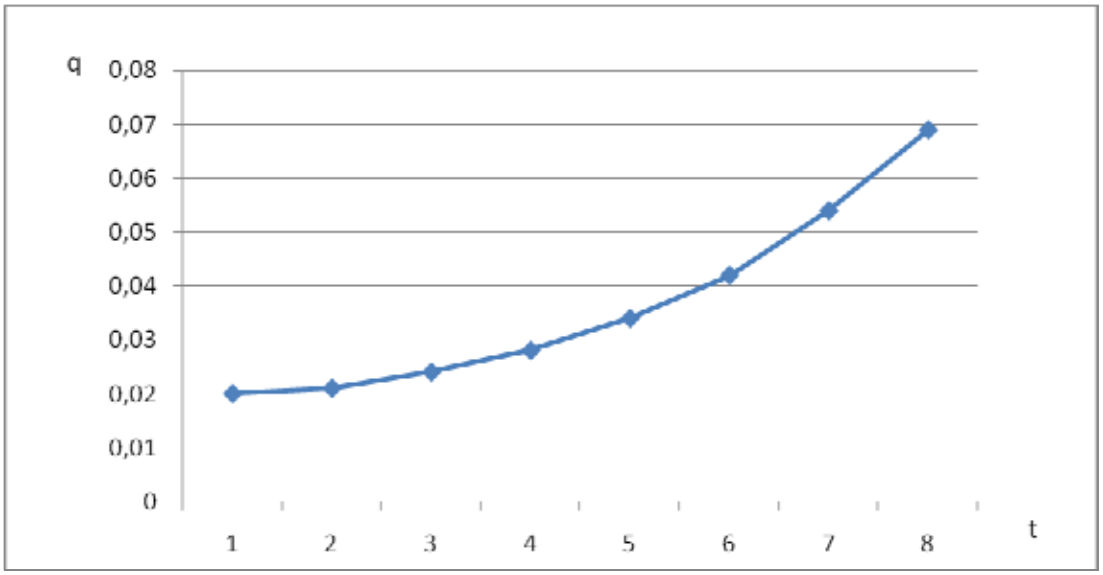

Fig. 7. Specific energy consumption per unit of change using an aqueous solution of sodium chloride (0.9 % physiological solution)

Рис. 7. Удельные энергозатраты на единицу изменения с использованием водного раствора хлорида натрия (0,9 % физиологический раствор)

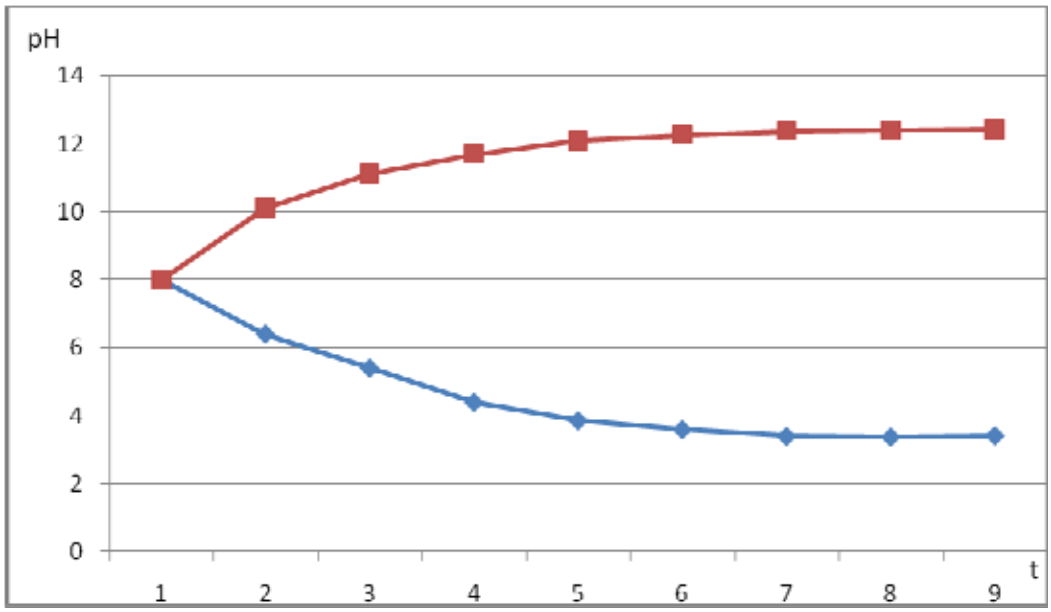

Fig. 8. The change in the pH of the anolyte and catholyte from the time of activation of water using an aqueous solution of sodium chloride (0.9 % physiological solution)

Рис. 8. Изменение pH анолита и католита от времени активации воды с использованием водного раствора хлорида натрия (0,9 % физиологический раствор)

Specific energy consumption per unit of change in the water pH

Model	Ratio V_A/V_k	Specific energy consumption q
Melesta	0.6	2.86
AP-1	0.33	2.77
IVA-1	0.75	2.96
Aqualife	0.11	2.76
Espero-1	0.2	1.5
Electroactivator under study	0.57	1.25

The results of the calculations of the specific energy consumption per unit of change in the water pH are shown in the table. It follows from the table that the electrical activator has the minimum value of specific energy consumption per unit of change in the pH value.

Conclusion. Existing devices for the electrochemical activation of water and aqueous solutions have design flaws, and therefore have increased specific energy consumption. The developed electroactivator with a coaxial arrangement of the electrodes has the lowest specific energy consumption per unit of change in the pH value, which is very important at the present time.

References

1. Bahir V. M., Liakumovich A. G., Kirpichnikov P. A., Spektor L. E., Mamadzhanov U. D. [The physical nature of the phenomena of activation of substances]. *Izv. AN UzSSR. Ser.tekhn. nauk.* 1983, No. 1, P. 60–64 (In Russ.).

2. Kirpichnikov P. A., Bakhir V. M., Gamer P. U., Dobrenkov G. A., Liakumovich A. G., Fridman B. S., Agadzhanyan S. I. [On the nature of electrochemical activation of media]. *Dokl. AN SSSR.* 1986, No. 286 (3), P. 663–666 (In Russ.).

3. Prilutsky V. I., Bakhir V. M. *Elektrokhimicheski aktivirovannaya voda: anomal'nye svoystva, mekhanizm biologicheskogo deystviya* [Electrochemically activated water: anomalous properties, mechanism of biological action]. Moscow, VNIIIMT, 1997, 228 p.

4. [Electrochemical activation in medicine, agriculture, industry]. *First International Symposium Coll. Report*. Moscow, Ekran Publ., 1997, 248 p. (In Russ.).

5. Alekhin S. A. [Electrochemical activation]. *Second International Symposium. Abstracts and short messages*. Part 1. Moscow, VNIIMT, MIS-RT Publ., 1999, 210 p. (In Russ.).

6. Bahir V. M. [Electrochemical activation]. *Third International Symposium. Abstracts and brief messages*. Moscow, VNIIMT Publ., 2001, 293 p. (In Russ.).

7. Shestakov V. I. [Electroactivator of water]. *Actual problems of aviation and cosmonautics: theses IX Vseros. scientific-practical conf. creative youth*. Krasnoyarsk, SibSAU Publ., 2013, Vol. 1, P. 504 (In Russ.).

8. Tachikawa H., Takada T. [Proton transfer rates in ionized water clusters (H 2 O) n (n = 2–4]. *RSC Advances*. 2015, Vol. 5, No. 9, P. 6945–6953.

9. Herr J. D., Talbot J., Steele R. P. [Structural progression in clusters of ionized water, (H2O) n = 1–5 +].

The Journal of Physical Chemistry A. 2015, Vol. 119, No. 4, P. 752–766.

10. Kozlov A. F. [From printed circuit boards to air purification]. *Second International Symposium. Electrochemical activation in medicine, agriculture, industry. Part 2."MIS-RT"*. 1999, No. 21-1, P. 34–36 (In Russ.).

11. Afanasov V. M. *Etching solution for printed circuit boards* [Etching solution for printed circuit boards]. A.S. No. 1018266 USSR, No. 3324018, 2003.

12. Afanasov V. M. *Composition for cleaning printed circuit boards* [Composition for cleaning printed circuit boards]. A.S. No. 1018267 USSR, No. 3323368, 1983.

13. Kozlov A. F., Bolotsky E. N., Teveleva S. I. et al. *Lubricating fluid for mechanical processing of metals* [Lubricating fluid for mechanical processing of metals]. A.S. No. 1119340, 1982.

14. *A method of producing cutting fluid for cutting metals* [A method of producing cutting fluid for cutting metals]. A.S. No. 1336552, 1986.

15. Medvedev A. [Installation fluxes. Flush or not flush]. *Komponenty i tekhnologii*. 2001, No. 4, P. 96–98 (In Russ.).

16. Shestakov I. Ya., Shestakov V. I. *Elektroaktivator* [Electrical activator]. Patent RF, No. 147543, 2014.

Библиографические ссылки

1. Физическая природа явлений активации веществ / В. М. Бахир, А. Г. Лиакумович, П. А. Кирпичников [и др.] // Изв. АН УзССР. Сер. техн. науки. 1983. № 1. С. 60–64.

2. О природе электрохимической активации сред / П. А. Кирпичников, В. М. Бахир, П. У. Гамер [и др.] // Докл. АН СССР. 1986. № 286(3). С. 663–666.

3. Прилуцкий В. И., Бахир В. М. Электрохимически активированная вода: аномальные свойства, механизм биологического действия. М. : ВНИИИМТ, 1997. 228 с.

4. Электрохимическая активация в медицине, сельском хозяйстве, промышленности // I Междунар. симп. : сб. докл. М. : ВНИИМТ ; АО НПО "Экран", 1997. 248 с.

5. Алёхин С. А. Электрохимическая активация // II Междунар. симп. : тез. докл. и краткие сообщения. М. : ВНИИМТ ; МИС-РТ, 1999. Ч. 1. 210 с.

6. Бахир В. М. Электрохимическая активация // III Междунар. симп. : тез. докл. и краткие сообщения. М. : ВНИИМТ, 2001. 293 с.

7. Шестаков В. И. Электроактиватор воды // Актуальные проблемы авиации и космонавтики : тез. IX Всеросс. науч.-практ. конф. творческой молодёжи / СибГАУ. Красноярск, 2013. Т. 1. 504 с.

8. Tachikawa H., Takada T. Proton transfer rates in ionized water clusters (H 2 O) n (n= 2–4) // RSC Advances. 2015. Vol. 5, No. 9, P. 6945–6953.

9. Herr J. D., Talbot J., Steele R. P. Structural progression in clusters of ionized water,(H2O) n = 1–5+ // The Journal of Physical Chemistry A. 2015. Vol. 119, No. 4. P. 752–766.

10. Козлов А. Ф. От печатных плат до очистки воздуха // Электрохимическая активация в медицине, сельском хозяйстве, промышленности : II Междунар. симп. Ч. 2: "МИС-РТ". 1999. № 21-1. С. 34–36.

11. А. с. 1018266. Раствор для травления печатных плат / В. М. Афанасов. № 3324018/18-21 ; заявл. 20.07.81 ; опубл. 15.05.83, Бюл. 18.

12. А. с. 1018267. Состав для очистки печатных плат / В. М. Афанасов. № 3323368/18-21 ; заявл. 20.07.81 ; опубл. 15.05.83, Бюл.18.

13. А. с. 1119340. Смазочно-охлаждающая жидкость для механической обработки металлов / А. Ф. Козлов, Е. Н. Болотский, С. И. Тевелёва [и др.]. 1982.

14. А. с. 1336552. Способ получения смазочно-охлаждающей жидкости для резания металлов. 1986.

15. Медведев А. Монтажные флюсы. Смывать или не смывать // Компоненты и технологии. 2001, № 4. С. 96–98.

16. Патент на полезную модель. Электроактиватор / И. Я. Шестаков, В. И. Шестаков. № 147543 ; Опубл. 10.11.2014, Бюл. № 31.

Pshenko Elena Borisovna – Cand. Sc., Associate Professor at the Department of Mechanical Engineering Technology, Reshetnev Siberian State University of Science and Technology. E-mail: pshenko-64@mail.ru.

Shestakov Ivan Yakovlevich – Dr. Sc., associate professor, professor; Reshetnev Siberian State University of Science and Technology. E-mail: yakovlevish@mail.ru

Shestakov Vladislav Ivanovich – student, Reshetnev Siberian State University of Science and Technology.

Пшенко Елена Борисовна – кандидат технических наук, доцент кафедры технологии машиностроения; Сибирский государственный университет науки и технологий имени академика М. Ф. Решетнёва. E-mail: pshenko-64@mail.ru.

Шестаков Иван Яковлевич – доктор технических наук, доцент, профессор, Сибирский государственный университет науки и технологий имени академика М. Ф. Решетнёва. E-mail: yakovlevish@mail.ru

Шестаков Владислав Иванович – студент, Сибирский государственный университет науки и технологий имени академика М. Ф. Решетнёва.